LIGAND EFFECTS IN ALLYL, CYCLOPENTADIENYL, AND RELATED COMPLEXES OF THE TRANSITION AND MAIN GROUP METALS

By

Keith Thomas Quisenberry

Dissertation

Submitted to the Faculty of the

Graduate School of Vanderbilt University

in partial fulfillment of the requirements

for the degree of

DOCTOR OF PHILOSOPHY

in

Chemistry

December, 2005

Nashville, Tennessee

Approved:

Professor Timothy P. Hanusa

Professor Piotr Kaszynski

Professor Chuck M. Lukehart

Professor David W. Wright

To my loving parents, Larry and Clara, for providing me with opportunities that they themselves never had

ACKNOWLEDGMENTS

When thinking about my scholastic career, I realize that I have had a large support network of colleagues, friends, and family for whom I am grateful. Several teachers at Muhlenberg South High, including Denise Baker, Rick Carver, Doug Haskins, Dianne Jernigan, Cara Meadows, Carolyn Mitchell, and Joyce Walker had made positive impacts on my study habits and career goals. Joyce, in particular, awakened my love for reading, which is still a relaxing hobby for me.

I owe a great deal to the science faculty at Kentucky Wesleyan College: Dr. Henry Connor, Prof. Donald Davenport, Adj. Prof. Nancy Flachskam, Dr. Robert Flachskam, Dr Robert Kingsolver, Dr. W. L. Magnuson, and Dr. David Oetinger. They helped shape me into the researcher that I am today. Working as a general chemistry student teaching assistant ignited my desire to pursue a career in chemistry over medicine. Dr. Ben Xue, at the University of Tennessee, Knoxville, is responsible for directing my interest in chemistry to synthetic inorganic research, and for that I would like to acknowledge him.

I would also like to thank my academic research monitoring committee at Vanderbilt: Dr. Timothy P. Hanusa, Dr. Piotr Kaszynski, Dr. Charles M. Lukehart, and Dr. David W. Wright. Although my ARM meetings may not have always seemed pleasurable, my committee was teaching me (through their questions) how to approach problems in research. They challenged me to think critically about my work, and to ask the "right" questions when conducting research. I would also like to thank Dr. Wright for his input with respect to my possible career choices.

Of the entire faculty from whom I have had the pleasure to learn, no one professor has been such a positive influence on me more than my advisor at

Vanderbilt, Dr. Timothy P. Hanusa. I have been very fortunate to have such a caring boss. He armed me with the laboratory skills and background in chemistry that I need to succeed in my future endeavors. I have always felt welcomed in his office, no matter the time of day, and he is continually forthcoming with advice and help. He truly gives new meaning to phrase “open door policy”. I will miss our discussions on a variety of topics from chemistry to history and religion.

I would also like to acknowledge sources of funding during my graduate career: the National Science Foundation, the Petroleum Research Fund, and Vanderbilt University for GAANN fellowships and a University Fellowship. Only funded research can be pursued, and only employed graduate students can afford to continue their educations.

Friendships are important to the overall quality of life, which can be reflected in the quality of work done. There are several friends who I would like to acknowledge. I would like to thank Dr. Brett M. Meredith for being such a good friend. He was with me when I took all of my classes and he worked in Dr. Hanusa’s laboratory. I could always count on Brett for his valuable input both inside and outside of our laboratory. He has been a life mentor of sorts who got me looking beyond my “four walls and a ceiling”. His advice has given me the level perspective that I sometimes haven’t possessed within myself. I would also like to thank Dr. Lisa M. Sullivan. In addition to helping me with characterization techniques (e.g., powder XRD, TGA) and dissertation formatting advice, she has been a close friend and, along with Eric Mowles, was a late night researcher buddy. Our dinner dates and discussions of personal lives were most enjoyable. Eric Mowles was also a good friend to me at Vanderbilt. He was one of the few people with whom I spent time away from the lab. Rosemary White deserves thanks for

introducing me to methods of polymerization studies. I would also like to thank Dr. Melanie J. Harvey for helping me get started in the Hanusa lab, and the past and present Hanusa group members for their help and camaraderie over the years. Aren Gerdon, Matt Wellons, Mike Warnament, and Ryan Rutledge also provided me with a sense of respite from my studies.

Finally, there are several people to whom I am indebted, for they have been true pillars of support in my life. I much appreciate the love and friendship Ana Petrovic´ has shown me over the years. She has a very strong work ethic and kept me on task throughout my writing. She also listened to all my aggravations during my last year at Vanderbilt without reproach. I am very fortunate that she has been a part of my life. I would also like to thank Jason Best. He has been a close friend for many years, and I have confided in him for just as long. I would also like to thank Kevin Quisenberry; he is my twin and closest friend. Nothing more needs to be said. Finally, I would to thank Larry and Clara Quisenberry, my parents. They have been ever loving and very supportive in all aspects of my life. My parents have always been interested in seeing me succeed, but never to the point of pressuring me. They have instilled their values into me and I am better off for it. My father has taught me the importance of hard work, truthfulness, and dependability by his example, and I admire him for that. I have long known that I can depend on him to be true to his word and I strive to do the same in life. My mother is one of the kindest persons I know and she has inspired me to show people the same love and respect that she exhibits everyday. Because of the opportunities provided to me by Larry and Clara, my career will never be a strenuous as his has been. My list of acknowledgements may be large, but I am very thankful that that is the case.

TABLE OF CONTENTS

LIST OF TABLES

LIST OF FIGURES

CHAPTER I

TRIMETHYLSILYLATED ALLYL COMPLEXES OF NICKEL. THE STABILIZED BIS(π-ALLYL)NICKEL COMPLEX $[\eta^3\text{-}1,3\text{-}(SiMe_3)_2C_3H_3]_2Ni$ AND ITS MONO(π-ALLYL)NiX (X = Br, I) DERIVATIVES

Introduction

Bis(allyl)nickel, $(C_3H_5)_2Ni$, was the first homoleptic transition metal allyl complex to be isolated,[1] and it is still the archetypal example of its class. A variety of both homoleptic and heteroleptic (allyl)nickel complexes have been prepared and studied in the ensuing 40 years,[2-6] and many of them have found uses in homogeneous catalysis and organic synthesis.[7-10] Stoichiometric reactions of homoleptic $(allyl)_2Ni$ complexes with phosphines,[5] halogens[11] and carbon dioxide[12] have also been examined in detail.[4,6-10,13] Such studies have been conducted despite the low oxidative and thermal stability of many bis(allyl)nickel complexes (e.g., the parent $(C_3H_5)_2Ni$ is pyrophoric and decomposes above 20 °C). Even physical characterization of these (allyl)nickel compounds can be problematic, and has often relied heavily on solution NMR studies[5,14] or theoretical investigations.[15-17] The instability of the compounds has made the use of other methods, such as photoelectron spectroscopy,[18] electrochemistry, and in some cases even crystallography[19] problematic.

Sterically bulky cyclopentadienyl rings (e.g., C_5Me_5, $C_5H_3(SiMe_3)_2$) are frequently used to synthesize compounds of greater diversity and stability than is possible with Cp alone,[20-22] and a similar approach has recently been found effective with the allyl ligand. In some instances, allyl compounds with ligands substituted by trimethylsilyl and dimethyl(*tert*-butyl)silyl[23] groups represent new classes of metal complexes. Among these are the thermally stable, electron-deficient bis(allyl) compounds $[1,3\text{-}(SiMe_3)_2C_3H_3]_2M$ (M = Cr, 12-e$^-$;[24] Fe, 14-e$^-$;[25] Co, 15-e$^-$[26]); they have no monomeric counterparts with unsubstituted ligands. Various lanthanide containing species have also been isolated that have no analogues containing the parent allyl anion (e.g., the neutral monomeric tris(allyl) complexes $[1,3\text{-}(SiMe_3)_2C_3H_3]_3Ln(thf)$ (Ln = Ce, Nd, Tb)[27] and the tetrametallic salt $(K(thf)_2Sm[1,3\text{-}(SiMe_3)_2C_3H_3]_3)_2$[28]). In other cases, substituted allyl ligands can provide versions of known compounds that are more robust and easily studied than the unsubstituted species. This situation occurs, for instance, with the homoleptic thorium complexes $[(SiMe_3)_nC_3H_{5-n}]_4Th$ (n = 1, 2).[29] In contrast to $(C_3H_5)_4Th$, which decomposes at 0 °C, the trimethylsilylated derivatives are stable up to 90 °C, and their structural authentications were the first for neutral $[R_nC_3H_{5-n}]_4M$ species.

The chemistry already known for (allyl)nickel complexes suggests that the study of their derivatives with bulky allyl ligands should be particularly informative. Previous use of substituted allyl ligands in nickel complexes has been limited to groups such as methyl (e.g., the crotyl anion), ethyl, or phenyl,[30] and some of these

compounds have been used as catalysts.[31-33] Modest improvements in thermal stability are observed in several cases (for example, $(2\text{-}MeC_3H_4)_2Ni$ decomposes at 33 °C, and the heavily substituted bis(1,1´,3,3´-tetraphenylallyl)nickel is stable at room temperature[34]). The good solubility in hydrocarbons and the typically high thermal stability of known complexes containing trimethylsilylated allyl ligands suggests that nickel species could benefit considerably from their use.

We report here our investigation of the effects of the 1,3-bis(trimethylsilyl)allyl ligand on the synthesis, structure, and reactions of bis(allyl)nickel complexes. As part of this research, we investigated the related heteroleptic nickel complexes (1,3-bis(trimethylsilyl)allyl)NiX (X = Br, I), and compared their properties with the parent $(C_3H_5)NiX$ species.[35] Reactions of the homoleptic $(1,3\text{-bis(trimethylsilyl)allyl})_2Ni$ with phosphines were also studied. As this project was a continuation and completion of initial work by Dr. J. Dominic Smith, any data from his work used in this dissertation will be attributed as such.

Experimental Section

General Considerations. All manipulations were performed with the rigorous exclusion of air and moisture using high vacuum, Schlenk, or glovebox techniques. Proton, carbon (^{13}C), and phosphorus (^{31}P) NMR spectra were obtained on a Bruker DPX–300 spectrometer at 300, 75.5, and 121 MHz, respectively, and were referenced to the residual proton and ^{13}C resonances of

C_6D_6 (δ 7.15 and 128.0) or to external H_3PO_4 (δ 0.0). NOESY, COSY, and HMQC NMR spectra were recorded on a Bruker DPX–400 spectrometer and were similarly referenced. HSQC NMR spectra were recorded on a Bruker Avance 500 instrument. All NMR data were processed using Bruker XWINNMR 3.5 software on an Octane workstation (Silicon Graphics, Mountain View, CA).

UV-vis and IR spectra, presented in this section, were first reported by Dr. J. Dominic Smith. UV–vis spectra were obtained on a Cary 50 spectrometer. Infrared data were obtained on an ATI Mattson–Genesis FT–IR spectrometer either neat or as KBr pellets prepared as previously described.[36] GC–MS data were obtained with a Hewlett–Packard 5890 Series II gas chromatograph/mass spectrometer with a 5971 Series mass selective detector. Melting points were determined on a Laboratory Devices Mel–Temp apparatus in sealed capillaries. A Cryocool series immersion cooler with Cryotrol thermocouple was used for reactions run at –40 °C. Metal analyses were obtained from complexometric titration;[37] combustion analyses were performed by Desert Analytics, Tuscon, AZ.

^{31}P decoupled HSQC experiments. The phase sensitive ^{1}H–^{13}C HSQC experiments used the following parameters: 1024 data points; a spectral width of 5000 Hz in the acquisition dimension and 1006 Hz in the indirect dimension; an acquisition time of 102 ms with GARP decoupling of the carbons; and two scans for each of the 1024 increments. An echo-antiecho acquisition scheme was employed. Phosphorus decoupling was achieved through an additional 180° hard pulse on the

phosphorus resonance using a third channel. All other parameters were kept constant. The data was zero-filled and a square sinebell apodization was applied in both dimensions.

Materials. 1-$(SiMe_3)C_3H_5$ and $(C_6H_5COO)_2$ were purchased from Acros, $(COD)_2Ni$ was obtained from Strem, and $NiCl_2$, $NiBr_2$, $NiBr_2$(dme), NiI_2, and $[AgI{\bullet}PMe_3]_4$ were purchased from Aldrich; all were used as received. 1,3-$(SiMe_3)_2C_3H_4$ and Li[1,3-$(SiMe_3)_2C_3H_3$] were synthesized according to literature procedures.[38] K[1,3-$(SiMe_3)_2C_3H_3$] was prepared by transmetallation of Li[1,3-$(SiMe_3)_2C_3H_3$] with potassium *t*-butoxide in hexanes solution. THF, toluene, and hexanes were distilled under nitrogen from potassium benzophenone ketyl.[39] $Ni(PMe_3)_4$ was prepared according to a literature procedure,[40] using $[AgI{\bullet}PMe_3]_4$ in place of neat PMe_3. Deuterated solvents were vacuum distilled from Na/K (22/78) alloy prior to use.

Attempted synthesis of [1,3-$(SiMe_3)_2C_3H_3]_2Ni$ from $NiCl_2$ and K[1,3-$(SiMe_3)_2C_3H_3$]. Formation of 1,3,4,6-tetrakis(trimethylsilyl)-1,5-hexadiene. A 125 mL Schlenk flask containing a magnetic stirring bar and fitted with an addition funnel was charged with $NiCl_2$ (0.288 g; 2.22 mmol) in 10 mL of THF. K[1,3-$(SiMe_3)_2C_3H_3$] (1.00 g; 4.45 mmol) dissolved in 15 mL of THF was placed in the addition funnel. The apparatus was cooled to –78 °C using a dry ice/acetone bath. The THF solution of K[1,3-$(SiMe_3)_2C_3H_3$] was added dropwise with stirring over the course of 30 min. The solution was allowed to warm to room temperature

overnight, after which the THF was removed under vacuum. The residue was extracted with hexanes, and the extract was filtered over a medium porosity glass frit. Removal of the hexanes under vacuum afforded a dark oil. Under reduced pressure (10^{-3} Torr) at 55 °C, a white, waxy solid (mp 44–46 °C) sublimed from the oil; it was identified as 1,3,4,6-tetrakis(trimethylsilyl)-1,5-hexadiene (0.192 g, 23% yield). The product could be obtained as colorless crystals from hexanes. Anal. Calcd for $C_{18}H_{42}Si_4$: C, 58.29; H, 11.41. Found: C, 58.44; H, 11.74. MS (*m/e*) 370 (M^+), 355 (M^+ – Me), 297 (M^+ – $SiMe_3$), 73 ($SiMe_3$). Principle IR bands (KBr, cm^{-1}): 2959 (s), 2898 (m), 2390 (w), 1600 (w), 1449 (m), 1250 (s), 1248 (s), 1082 (s), 1028 (s), 850 (s), 803 (s), 734 (w), 687 (m), 402 (m). Two diastereomers were identified in NMR spectra; their ratios varied somewhat from reaction to reaction, but the same one was always present in larger amounts. Major product diastereomer: ^{1}H NMR (300 MHz, C_6D_6, 298 K): δ 0.14 (s, 36H, $SiMe_3$); 2.01 (mult, 2H, $C_{(3,4)}$–H); 5.47 (d, 2H, J = 18.3 Hz, $C_{(1,6)}$–H); 5.90 (mult, 2H, $C_{(2,5)}$–H). ^{13}C NMR (75 MHz, C_6D_6, 298 K): δ –1.05 ($SiMe_3$); –0.88 ($SiMe_3$); 39.89 ($C_{(3,4)}$); 127.20 ($C_{(2,5)}$); 149.38 ($C_{(1,6)}$). Minor product diastereomer: ^{1}H NMR (300 MHz, C_6D_6, 298 K): δ 0.068 (s, 18H, $SiMe_3$); 0.084 (s, 18H, $SiMe_3$); 2.01 (mult, 2H, $C_{(3,4)}$–H); 5.60 (d, 2H, J = 18.3 Hz, $C_{(1,6)}$–H); 6.37 (dd, 2H, J = 18.3 Hz, J = 9.9 Hz, $C_{(2,5)}$–H). ^{13}C NMR (75 MHz, C_6D_6, 298 K): δ –2.16 ($SiMe_3$); –1.05 ($SiMe_3$); 39.50 ($C_{(3,4)}$); 128.76 ($C_{(2,5)}$); 146.88 ($C_{(1,6)}$).

Attempted synthesis of [1,3-$(SiMe_3)_2C_3H_3]_2Ni$ (1) from $NiBr_2$. A 125 mL Schlenk flask containing a magnetic stirring bar and fitted with an addition funnel was charged with $NiBr_2$ (0.500 g; 2.29 mmol) in 10 mL THF. K[1,3-$(SiMe_3)_2C_3H_3$] (1.027 g; 4.58 mmol) dissolved in 15 mL THF was added to the addition funnel. The apparatus was cooled to –78 °C using a dry ice/acetone bath. The THF solution of K[1,3-$(SiMe_3)_2C_3H_3$] was added dropwise with stirring over the course of 30 min. The solution was allowed to warm to room temperature overnight. THF was removed under vacuum, and the residue was extracted with hexanes. The extract was filtered over a medium porosity glass frit, and the hexanes was removed under vacuum to afford a dark, yellow–brown oil. The oil crystallized upon standing for a few days and was identified as 1,3,4,6-tetrakis(trimethylsilyl)-1,5-hexadiene (0.661 g) in 78% yield, by its proton NMR spectrum.

Attempted synthesis of [1,3-$(SiMe_3)_2C_3H_3]_2Ni$ (1) from NiI_2. A 125 mL Schlenk flask containing a magnetic stirring bar and fitted with an addition funnel was charged with NiI_2 (0.835 g; 2.67 mmol) in 10 mL THF. K[1,3-$(SiMe_3)_2C_3H_3$] (1.200 g; 5.35 mmol) dissolved in 15 mL THF was added to the addition funnel. The apparatus was cooled to –78 °C using a dry ice/acetone bath. The THF solution of K[1,3-$(SiMe_3)_2C_3H_3$] was added dropwise with stirring over the course of 30 min. The solution was allowed to warm to room temperature overnight. THF was removed under vacuum, and the residue was extracted with hexanes. The extract was filtered over a medium porosity glass frit, and the hexanes was removed under

vacuum to afford a dark oil that crystallized over a few days (0.383 g) in 39% yield. The oil was identified as 1,3,4,6-tetrakis(trimethylsilyl)-1,5-hexadiene by its proton NMR spectrum.

Synthesis of $[1,3\text{-}(SiMe_3)_2C_3H_3]_2Ni$ (1). A 125 mL Schlenk flask containing a magnetic stirring bar and fitted with an addition funnel was charged with $NiBr_2$•DME (1.002 g; 3.224 mmol) in 10 mL of THF. $K[1,3\text{-}(SiMe_3)_2C_3H_3]$ (1.457 g; 6.490 mmol), dissolved in 15 mL of THF, was added to the addition funnel. The apparatus was cooled to –78 °C using a dry ice/acetone bath. The THF solution of $K[1,3\text{-}(SiMe_3)_2C_3H_3]$ was added dropwise with stirring over the course of 30 min. The solution was allowed to warm to room temperature overnight. THF was removed under vacuum, and the residue was extracted with hexanes. The extract was filtered over a medium porosity glass frit, and the hexanes was removed under vacuum to afford a nearly black oil that appeared dark red when transilluminated. Over a period of days, orange needles grew (1.00 g, 72% yield), mp 64–66 °C. The compound sublimes at 0.01 torr and 45 °C. Anal. Calcd for $C_{18}H_{42}NiSi_4$: C, 50.33; H, 9.85; Ni, 13.7. Found: C, 49.24; H, 9.85; Ni (complexometric), 13.4. Principle IR bands (KBr, cm^{-1}): 2959 (s), 2898 (m), 2390 (w), 1600 (w), 1449 (m), 1250 (s), 1248 (s), 1082 (s), 1028 (s), 850 (s), 803 (s), 734 (w), 687 (m), 402 (m). UV–vis (THF): 318 nm ($\varepsilon = 4100$), 330 nm ($\varepsilon = 2500$), 411 nm ($\varepsilon = 540$). Magnetic susceptibility measurements (toluene–d_8) indicate that the compound is diamagnetic. Two diastereomers (in variable ratio) were identified in

NMR spectra. Major product diastereomer (**1a**): ^{1}H NMR (300 MHz, C_6D_6, 298 K): δ 0.151 ppm (s, 18H, $SiMe_3$); 0.156 (s, 18H, $SiMe_3$); 2.67 (d, J = 16.0 Hz, 2H, *anti* C–H); 3.60 (d, J = 10.4 Hz, 2H, *syn* C–H); 4.96 (dd, J = 16.0 Hz, J = 10.4 Hz, 2H, $C_{(2)}$–H). ^{13}C NMR (75 MHz, C_6D_6, 298 K): δ 0.41 ppm ($SiMe_3$); 1.88 ($SiMe_3$); 63.67 (*anti* C–H); 67.02 (*syn* C–H); 125.60 ($C_{(2)}$). Minor product diastereomer (**1b**): ^{1}H NMR (300 MHz, C_6D_6, 298 K): δ –0.055 ppm (s, 18H, $SiMe_3$); 0.29 (s, 18H, $SiMe_3$); 2.07 (d, J = 16.4 Hz, 2H, *anti* C–H); 3.63 (d, J = 10.0 Hz, 2H, *syn* C–H); 5.62 (dd, J = 16.4 Hz, J = 10.0 Hz, 2H, $C_{(2)}$–H). ^{13}C NMR (75 MHz, C_6D_6, 298 K): δ 1.06 ppm ($SiMe_3$); 1.27 ($SiMe_3$); 63.14 (*anti* C–H); 63.49 (*syn* C–H); 123.79 ($C_{(2)}$).

Reaction of 1 with PMe_3. In a 125 mL Schlenk flask, a solution of **1** (60% **1a**) (0.064 g; 0.15 mmol) in hexanes (10 mL) was cooled to –78 °C in a dry ice/acetone bath. The flask was connected to a glass tube containing $[AgI{\bullet}PMe_3]_4$ (0.190 g; 0.153 mmol). The glass tube was heated with a heat gun; after the PMe_3 was released, the initial dark red solution turned yellow–brown. The reaction was filtered, and the hexanes was removed under vacuum leaving an orange oil that crystallized and was identified with NMR data as containing staggered $[1,3\text{-}(SiMe_3)_2C_3H_3]_2Ni$ (>95% **1b**). Several crystals obtained from the concentrated reaction mixtures were examined with X-ray diffraction, and were found to have unit cells matching only **1 b**. The organophosphorus compound tetramethyltetraphosphane was also detected in the oil. For it, ^{1}H NMR (300 MHz, C_6D_6, 298 K): δ 1.15 (s). ^{13}C NMR (75 MHz, C_6D_6, 298 K): δ 25.1 (apparent

quintet, $J \approx 10.1$ Hz). ^{1}H–^{13}C HSQC {^{1}H,^{31}P} NMR (C_6D_6, 298 K): δ 25.1 (s). ^{31}P NMR (121 MHz, C_6D_6, 298 K): δ –21.6 (s). The same products were detected when the reaction was repeated with a 1 : 0.25 ratio of **1** and $[AgI{\bullet}PMe_3]_4$ (i.e., a 1 : 1 ratio of **1** to PMe_3).

Synthesis of $(C_3H_5)_2Ni$. A three-neck 250 mL round bottom flask, fitted with a gas inlet, an addition funnel, and a Schlenk tube containing $[AgI{\bullet}PMe_3]_4$ (2.224 g; 1.79 mmol), was charged with $NiBr_2$ (0.389 g; 1.78 mmol) and diethyl ether (35 mL). $(C_3H_5)_2MgBr$ (3.56 mL; 3.56 mmol) dispersed in 15 mL Et_2O was added to the addition funnel. The apparatus was cooled to –40 °C using a Cryocool Series immersion cooler. The Et_2O solution of $(C_3H_5)_2MgBr$ was added dropwise over the course of 30 min. The resultant yellow solution was allowed to stir overnight at –40 °C and kept at that temperature until its use.

Reaction of $(C_3H_5)_2Ni$ with 4 PMe_3. In a three-neck 250 mL round bottom flask, fitted with a gas inlet, an addition funnel, and a Schlenk tube containing $[AgI{\bullet}PMe_3]_4$ (2.224 g; 1.79 mmol), the solution of the as-synthesized $(C_3H_5)_2Ni$ in diethyl ether (50 mL) was kept cooled to –40 °C using a Cryocool Series immersion cooler. The glass Schlenk tube was heated with a heat gun; after the PMe_3 was released, the initial yellow solution turned orange-red. The solution was stirred for one hour, allowed to warm to –25 °C, and diethyl ether was then removed under vacuum. The organophosphorus compound tetramethyltetraphosphane was detected as a product. ^{1}H NMR (300 MHz, C_6D_6,

298 K): δ 1.15 (s). ^{13}C NMR (75 MHz, C_6D_6, 298 K): δ 25.0 (apparent quintet, $J \approx$ 10.1 Hz). ^{31}P NMR (121 MHz, C_6D_6, 298 K): δ –21.3 (s).

Synthesis of 1,3-$(SiMe_3)_2C_3H_3Br$. A 500 mL Schlenk flask containing a magnetic stirring bar and fitted with a reflux condenser was charged with 1,3-$(SiMe_3)_2C_3H_4$ (7.01 g; 37.6 mmol) and NBS (6.60 g; 37.1 mmol) in 200 mL of CCl_4. The solution turned pale yellow upon mixing. Benzoyl peroxide, $(C_6H_5COO)_2$, (0.104 g; 0.429 mmol) was added, and the solution was refluxed overnight. The resulting dark yellow solution was cooled to room temperature, and then it was filtered to remove NHS. Removal of CCl_4 under vacuum afforded a dark yellow oil, which upon vacuum distillation (200 mTorr) at 40 °C afforded 1,3-$(SiMe_3)_2C_3H_3Br$ as a colorless liquid (6.98 g) in 70% yield. Anal. Calcd for $C_9H_{21}BrSi_2$: C, 40.74; H, 7.98. Found: C, 40.60; H, 7.76. MS (m/e) 266/264 (M^+), 251/249 (M^+ – Me), 178/176 (M^+ – $SiMe_3$, – Me), 139/137 (HC(Si(Me)H_2)Br), 97 (C(C)$SiMe_3$), 73 ($SiMe_3$). Principle IR bands (neat, cm^{-1}): 3059 (m), 2957 (s), 2898 (m), 2484 (w), 2263 (w), 1697 (m), 1604 (m), 1409 (m), 1287 (m), 1250 (s), 1138 (m), 991 (m), 908 (m), 840 (s), 752 (m), 694 (m), 475 (m), 409 (m). ^{1}H NMR (300 MHz, C_6D_6, 298 K): δ 0.025 (s, 9H, vinylic $SiMe_3$); 0.044 (s, 9H, $SiMe_3$); 3.65 (d, J= 8.8 Hz, 1H, sp^3-C–H); 5.71 (d, J= 18.0 Hz, 1H, *anti* C–H); 6.26 (dd, J= 18.0 Hz, J= 8.8 Hz, 1H, ($C_{(2)}$–H). ^{13}C NMR (75 MHz, C_6D_6, 298 K): δ –3.28 (vinylic $SiMe_3$); –1.29 ($SiMe_3$); 45.83 (sp^3-C); 131.13 (*anti* C–H); 143.78 ($C_{(2)}$).

Synthesis of [1,3-$(SiMe_3)_2C_3H_3$]NiBr (2a) from 1,3-$(SiMe_3)_2C_3H_3$Br and Ni(COD)$_2$. A 125 mL Schlenk flask containing a magnetic stirring bar and fitted with a septum was charged with Ni(COD)$_2$ (2.00 g; 7.27 mmol) in 30 mL of toluene. The apparatus was cooled to –78 °C using a dry ice/acetone bath. To the stirred solution, 1,3-$(SiMe_3)_2C_3H_3$Br (1.99 g; 7.50 mmol) was delivered with a syringe. The solution was allowed to warm to room temperature overnight and became deep red-purple upon warming. Toluene was removed under vacuum, and the residue was extracted with hexanes. The reaction was filtered, and the hexanes was removed under vacuum to afford a deep purple solid (1.94 g, 82% yield). Purple plates could be obtained on recrystallization from hexanes. Anal. Calcd for $C_9H_{21}BrNiSi_2$: Ni, 18.1. Found: Ni (complexometric), 17.4. Principle IR bands (KBr, cm^{-1}): 2960 (s), 2898 (m), 2358 (w), 2341 (w), 1600 (w), 1260 (s), 1099 (s), 1086 (s), 1019 (s), 850 (s), 801 (s), 693 (m), 424 (m). Magnetic susceptibility measurements (toluene–d_8) indicate the compound is diamagnetic. ^{1}H NMR (300 MHz, C_6D_6, 298 K): δ 0.22 (s, 18H, $SiMe_3$); 1.93 (d, J = 14.4 Hz, 2H, *anti* C–H); 5.27 (t, J = 14.4 Hz, 1H, $C_{(2)}$–H). ^{13}C NMR (75 MHz, C_6D_6, 298 K): δ –0.53 ($SiMe_3$); 68.70 ($C_{(1,3)}$); 114.65 ($C_{(2)}$).

Synthesis of [1,3-$(SiMe_3)_2C_3H_3$]NiBr (2b) from [1,3-$(SiMe_3)_2C_3H_3$]$_2$Ni and Br$_2$. A 125 mL Schlenk flask containing a magnetic stirring bar and fitted with an addition funnel was charged with [1,3-$(SiMe_3)_2C_3H_3$]$_2$Ni (0.302 g; 0.703 mmol) in 15 mL of benzene. Bromine (0.112 g; 0.701 mmol) and benzene (15 mL) were

added to the addition funnel. The apparatus was cooled to 0 °C using an ice bath. The bromine solution was added dropwise with stirring over a period of 30 min, and the reaction was stirred at room temperature overnight. The mixture was then filtered, and benzene was removed from the filtrate under vacuum to yield a red-purple solid (0.21 g, 92%). Two isomers (2:1 ratio) were identified in NMR spectra. Major product isomer: ^{1}H NMR (300 MHz, C_6D_6, 298 K): δ 0.067 (s, 9H, $SiMe_3$); 0.13 (s, 9H, $SiMe_3$); 2.00 (d, J = 10.0 Hz, 1H, *syn* C–H); 5.58 (d, J = 18.4 Hz, 1H, *anti* C–H); 6.34 (dd, J = 18.4 Hz, J = 10.0 Hz, 1H, $C_{(2)}$–H). ^{13}C NMR (75 MHz, C_6D_6, 298 K): δ –2.11 ($SiMe_3$); –0.98 ($SiMe_3$); 39.52 (*syn* C–H); 128.77 (*anti* C–H); 146.88 ($C_{(2)}$). Minor product isomer: ^{1}H NMR (300 MHz, C_6D_6, 298 K): δ 0.023 (s, 9H, $SiMe_3$); 0.044 (s, 9H, $SiMe_3$); 2.96 (d, J = 9 Hz, 1H, *syn* C–H); 5.46 (d, J = 18.4 Hz, 1H, *anti* C–H); 6.10 (dd, J = 18.4 Hz, J = 9 Hz, 1H, $C_{(2)}$–H). ^{13}C NMR (75 MHz, C_6D_6, 298 K): δ –3.23 ($SiMe_3$); –1.24 ($SiMe_3$); 30.48 (*syn* C–H); 131.52 (*anti* C–H); 145.70 ($C_{(2)}$).

Attempted synthesis of [1,3-$(SiMe_3)_2C_3H_3$]NiBr from $NiBr_2$(dme) and K[1,3-$(SiMe_3)_2C_3H_3$]. A three-neck flask containing a magnetic stirring bar and fitted with a stopper, gas inlet, and addition funnel was charged with $NiBr_2$(dme) (1.236 g; 4.004 mmol) in 50 mL of THF. K[1,3-$(SiMe_3)_2C_3H_3$] (0.900 g; 4.00 mmol) was added in 10 mL of THF to the addition funnel. The apparatus was cooled to –78 °C using a dry ice/acetone bath. The THF solution of K[1,3-$(SiMe_3)_2C_3H_3$] was added dropwise with stirring over the course of 30 min. The solution was allowed to

warm to room temperature overnight. THF was removed under vacuum, and the residue was extracted with hexanes. The extract was filtered over a medium porosity glass frit, and the hexanes was removed under vacuum to afford a nearly black solid. The solid was identified as $[1,3\text{-}(SiMe_3)_2C_3H_3]_2Ni$ (**1**) from its NMR data and melting point.

Attempted synthesis of $[1,3\text{-}(SiMe_3)_2C_3H_3]NiBr$ from $NiBr_2$(dme) and $Li[1,3\text{-}(SiMe_3)_2C_3H_3]$. A 125 mL Schlenk flask containing a magnetic stirring bar and fitted with an addition funnel was charged with $NiBr_2$•DME (0.999 g; 3.24 mmol) in 10 mL toluene. $Li[1,3\text{-}(SiMe_3)_2C_3H_3]$ (0.624 g; 3.24 mmol) dissolved in 15 mL toluene was added to the addition funnel. The apparatus was cooled to –78 °C using a dry ice/acetone bath. The toluene solution of $Li[1,3\text{-}(SiMe_3)_2C_3H_3]$ was added dropwise with stirring over the course of 30 min. The solution was allowed to warm to room temperature overnight. The toluene was removed under vacuum, and the residue was extracted with hexanes. The extract was filtered over a medium porosity glass frit, and the hexanes was removed under vacuum to afford a nearly black oil that appeared dark red when transilluminated. The oil crystallized upon standing for a few days and was identified as $[1,3\text{-}(SiMe_3)_2C_3H_3]_2Ni$, (0.506 g) in 73% yield, by its mp and NMR spectra.

Synthesis of $[1,3\text{-}(SiMe_3)_2C_3H_3]NiI$ (3). A 125 mL Erlenmeyer flask containing a magnetic stirring bar and fitted with a septum was charged with $[1,3\text{-}(SiMe_3)_2C_3H_3]_2Ni$ (0.335 g; 0.780 mmol) in 20 mL of hexanes. Iodine (0.098 g; 0.78

mmol) in hexanes (20 mL) was cannulated into the stirred solution at room temperature. The color of the solution changed from red to dark red–purple with the addition of the iodine solution. After being stirred overnight, the hexanes was removed under vacuum to yield a red–purple solid (0.205 g) in 71% yield. Recrystallization from hexanes afforded dark red blocks. The compound decomposes at 130 °C, giving off purple vapor (presumably I_2). Anal. Calcd for $C_9H_{21}INiSi_2$: C, 29.13; H, 5.70. Found: C, 30.19; H, 5.60. Principle IR bands (KBr, cm^{-1}): 2956 (s), 2897 (m), 2390 (w), 1600 (w), 1470 (w), 1259 (s), 1250 (s), 1099 (s), 1087 (s), 1021 (s), 854 (s), 808 (s), 742 (w), 693 (m), 420 (m). Two isomers (1.6:1 ratio) were identified in NMR spectra. Isomer 1: ^{1}H NMR (300 MHz, C_6D_6, 298 K): δ 0.011 (s, 9H, $SiMe_3$); 0.060 (s, 9H, $SiMe_3$); 3.60 (d, J = 10.0 Hz, 1H, *syn* C–H); 5.57 (d, J = 18.0 Hz, 1H, *anti* C–H); 6.09 (dd, J = 18.0 Hz, J = 10.0 Hz, 1H, $C_{(2)}$–H). ^{13}C NMR (75 MHz, C_6D_6, 298 K): δ –2.47 ($SiMe_3$); –1.33 ($SiMe_3$); 23.12 (*syn* C–H); 131.20 (*anti* C–H); 145.30 ($C_{(2)}$).

Isomer 2: ^{1}H NMR (300 MHz, C_6D_6, 298 K): δ 0.078 (s, 9H, $SiMe_3$); 0.13 (s, 9H, $SiMe_3$); 2.01 (d, J = 10.0 Hz, 1H, *syn* C–H); 5.59 (d, J = 18.0 Hz, 1H, *anti* C–H); 6.36 (dd, J = 18.0 Hz, J = 10.0 Hz, 1H, $C_{(2)}$–H). ^{13}C NMR (75 MHz, C_6D_6, 298 K): δ –2.14 ($SiMe_3$); –1.02 ($SiMe_3$); 39.51 (*syn* C–H); 128.77 (*anti* C–H); 146.88 ($C_{(2)}$).

General Procedures for X–Ray Crystallography. Data collection and structure solution were conducted at the X–Ray Crystallographic Laboratory at the University of Minnesota. All calculations were performed using the current

SHELXTL[41] suite of programs. Suitable crystals were located and attached to the tip of a glass capillary and mounted on a Siemens SMART Platform CCD diffractometer for data collection at 173(2) K. A preliminary set of cell constants was calculated from reflections harvested from three sets of 20 frames. These initial sets of frames were oriented such that orthogonal wedges of reciprocal space were surveyed. Data collection of a randomly oriented region of reciprocal space was carried out using MoKα radiation (graphite monochromator). Final cell constants were calculated from the *xyz* centroids of strong reflections from the actual data collection after integration. Relevant crystal and collection data parameters can be found in Table 1.

Table 1. Crystal data and summary of X–ray data collection.

compound	$[1,3\text{-}(SiMe_3)_2C_3H_3]_2Ni$ (eclipsed) (**1a**)	$[1,3\text{-}(SiMe_3)_2C_3H_3]_2Ni$ (staggered) (**1b**)	$[1,3\text{-}(SiMe_3)_2C_3H_3NiBr]_2$ (**2a**)	$[1,3\text{-}(SiMe_3)_2C_3H_3NiI]_2$ (**3**)
formula	$C_{18}H_{42}NiSi_4$	$C_{18}H_{42}NiSi_4$	$C_{18}H_{42}Br_2Ni_2Si_4$	$C_{18}H_{42}I_2Ni_2Si_4$
formula weight	429.59	429.59	648.12	742.10
color of cryst	orange	yellow	purple	dark red
cryst dimens, mm	0.32 x 0.12 x 0.08	0.29 x 0.21 x 0.14	0.24 x 0.14 x 0.04	0.24 x 0.16 x 0.12
space group	$C2/c$	$C2/c$	$C2/c$	$C222_1$
cell dimens				
a, Å	16.537(5)	10.969(1)	14.819(7)	16.448(4)
b, Å	12.438(4)	19.144(2)	23.37(1)	19.038(4)
c, Å	12.723(4)	12.491(2)	11.251(5)	19.669(4)
β, deg	90.1555(5)	103.151(2)	130.197(8)	90.000
volume, $Å^3$	2617.0(14)	2554.1(5)	2976(2)	6159(2)
Z	4	4	4	8
calcd density, Mg/m^3	1.090	1.117	1.447	1.601
abs coeff, mm^{-1}	0.924	0.946	4.115	3.387
$F(000)$	936	936	1328	2944
limits of data	$1.60° \leq \theta \leq 25.06°$	$2.13° \leq \theta \leq 27.53°$	$1.74° \leq \theta \leq 25.05°$	$1.94° \leq \theta \leq 25.05°$

Table 1 continued

compound	$[1,3\text{-}(SiMe_3)_2C_3H_3]_2Ni$ (eclipsed) (**1a**)	$[1,3\text{-}(SiMe_3)_2C_3H_3]_2Ni$ (staggered) (**1b**)	$[1,3\text{-}(SiMe_3)_2C_3H_3NiBr]_2$ (**2a**)	$[1,3\text{-}(SiMe_3)_2C_3H_3NiI]_2$ (**3**)
index ranges	$-19 \leq h \leq 19$, $-13 \leq k \leq 14$, $-15 \leq l \leq 15$	$-14 \leq h \leq 14$, $-24 \leq k \leq 24$, $-16 \leq l \leq 16$	$-17 \leq h \leq 13$, $0 \leq k \leq 27$, $0 \leq l \leq 13$	$-19 \leq h \leq 19$, $-15 \leq k \leq 22$, $-22 \leq l \leq 23$
total reflcns collected	8667	11,447	6593	15,491
unique reflcns	2315 ($R_{int} = 0.0311$)	2939 ($R_{int} = 0.0519$)	2604 ($R_{int} = 0.0727$)	5389 ($R_{int} = 0.0597$)
transmission factors	1.000–0.787	0.8789–0.7709	0.8527–0.4384	1.000–0.600
data/restraints/param	2315 / 10 / 136	2939 / 1 / 123	2604 / 0 / 131	5389 / 0 / 248
R indices ($I>2s(I)$)	$R = 0.0285$, $R_w = 0.0727$	$R = 0.0377$, $R_w = 0.0924$	$R = 0.0520$, $R_w = 0.1132$	$R = 0.0485$, $R_w = 0.1222$
R indices (all data)	$R = 0.0307$, $R_w = 0.0738$	$R = 0.0480$, $R_w = 0.0971$	$R = 0.1025$, $R_w = 0.1286$	$R = 0.0594$, $R_w = 0.1274$
goodness of fit on F^2	1.033	1.008	1.013	1.027
max/min peak in final diff map, e–/Å^3	0.463/–0.263	0.710/–0.269	0.769/–0.486	2.046/–0.447
Absolute structure parameter				0.16(3)

Computational Details. Geometry optimization calculations were performed using the GAUSSIAN 03W suite of programs.[42] Both the B3LYP functional, which incorporates Becke's three–parameter exchange functional[43] and the correlation functional of Lee, Yang, and Parr,[44,45] as well as the B3PW91 functional, which employs the 1991 gradient–corrected correlation functional of Perdew and Wang, were used.[46] The DFT-optimized double zeta polarized basis sets DGDZVP2 and DGDZVP (for Br, I) of Godbout[47] were used for geometry optimizations and energy calculations of the allyl complexes. The standard Pople basis sets 6-311G(d,p) and 6-311+G(2d,p) were used for other calculations.[48] Stationary points were characterized by the calculation of vibrational frequencies, and unless otherwise noted, all geometries were found to be minima ($N_{imag} = 0$).

Results and Discussion

Synthesis of a trimethylsilylated bis(allyl)nickel complex. In a reaction modeled after that used for preparing the substituted chromium, iron, and cobalt complexes,[24-26] an attempt was made to synthesize a trimethylsilylated bis(allyl)nickel complex from the reaction of $NiCl_2$ and the substituted potassium allyl K[1,3-$(SiMe_3)_2C_3H_3$] in THF. On workup of the reaction mixture, however, the dimerized ligand (1,3,4,6-tetrakis(trimethylsilyl)-1,5-hexadiene) (Figure 1) was isolated instead (eq 1).

$$NiCl_2 + 2\ K[1,3\text{-}(SiMe_3)_2C_3H_3] \rightarrow [(SiMe_3)_2C_3H_3]_2 + 2\ KCl + \text{nickel byproducts} \quad (1)$$

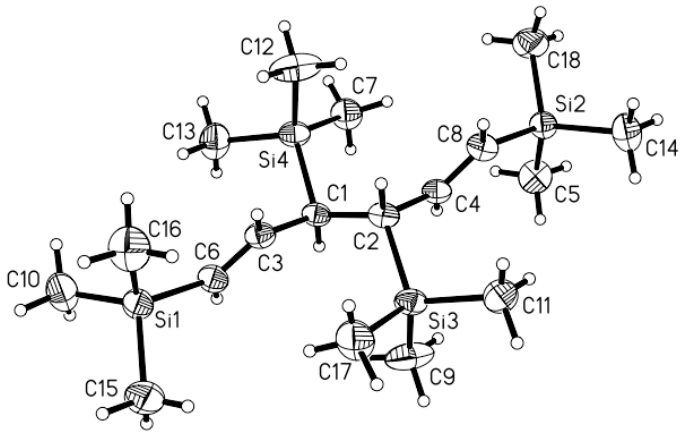

Figure 1. ORTEP of $[(SiMe_3)_2C_3H_3]_2$.

Similar attempts to synthesize the bis(allyl)nickel complex from the reaction of $NiBr_2$ or NiI_2 with $K[1,3\text{-}(SiMe_3)_2C_3H_3]$ also resulted in the formation of the trimethylsilylated hexadiene. Coupling of allyl ligands on a nickel center is well-documented,[5] and it may be that oxidative coupling of the allyl anion is occurring at the surface of these relatively insoluble nickel starting materials.

NMR studies indicate that the hexadiene is found in two forms with an average ratio of 1.7:1, although it ranges from 1.3:1 to 2.5:1. The patterns in the NMR spectra are consistent with two diastereomers of C_i (*meso*) and C_2 (*rac*) symmetry (Figure 2). DFT calculations (B3PW91/6-311G(d,p)) indicate that the C_i dimer is more thermodynamically stable by 3.7 kcal mol^{-1} ($\Delta H°$; 5.3 kcal mol^{-1} for

$\Delta G°$). Steric congestion from the adjacent $SiMe_3$ groups (closest Me···Me´ contact = 3.89 Å) possibly raises the energy of the C_2 form. As the diastereomer ratio reflects kinetic factors during coupling rather than thermodynamic effects (the two forms are not in equilibrium), it cannot automatically be assumed that the more abundant form is the one with C_i symmetry. Attempts using NOESY experiments to assign the resonances to their diastereomeric forms were not conclusive. Although the compound is crystalline, a single crystal X-ray structure was severely disordered;[49] multiple forms appear to be incorporated in the unit cell.

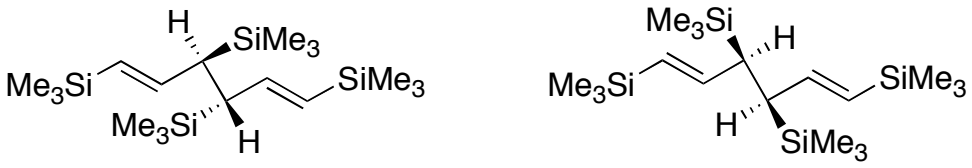

Figure 2. Proposed diastereomeric forms of the trimethylsilylated hexadiene, with C_i (*meso*)(left) and C_2 (*rac*)(right) symmetry.

In an attempt to avoid the coupling reactions, the more soluble nickel halide $NiBr_2$(dme) was used as a reagent. Reaction of two equivalents of K[1,3-$(SiMe_3)_2C_3H_3$] with $NiBr_2$(dme) in THF at –78 °C affords the bis(allyl)nickel complex (**1**) in 72% yield (eq 2):

$$NiBr_2(dme) + 2\ K[1,3\text{-}(SiMe_3)_2C_3H_3] \rightarrow [1,3\text{-}(SiMe_3)_2C_3H_3]_2Ni\ (\mathbf{1}) + 2\ KBr\downarrow \quad (2)$$

The complex is initially isolated as an oil that crystallizes to an orange solid after several days at room temperature. It is soluble in a wide range of solvents, from THF to hexanes, and readily sublimes under vacuum. It melts at 64 °C and decomposes only above 100 °C. In the solid state, finely divided, sublimed **1** will survive for several hours in the air before noticeable decomposition begins, but larger, oily crystals can last several days in air. A hexanes solution of **1** can be layered on top of water, where no change is observed for several hours. The increase in oxidative and thermal stability compared to the pyrophoric, thermally sensitive (dec. above 20 °C) parent compound $(C_3H_5)_2Ni$ is striking.[1] The electrochemistry of **1** was briefly investigated with voltammetry and electrolysis in a nitrogen-filled drybox. In THF containing 0.1 M $[N(n\text{-}Bu_4)][PF_6]$ and dichloromethane containing 0.05 M $[N(n\text{-}Bu_4)][B(C_6F_5)_4]$, an irreversible, one-electron oxidation was observed (0.81 V in THF, 0.92 V in dichloromethane, potentials vs ferrocene / ferrocenium); cyclic voltametry scan rates of 0.1 V/s to 0.5 V/s (Pt or glassy carbon electrodes) were used. There was no evidence for electroactive oxidation products.

Like the parent complex $(C_3H_5)_2Ni$, **1** is diamagnetic, and both ^1H and ^{13}C NMR spectra of the substituted compound display two forms in solution, identified as eclipsed (*cis*) (**1a**) and staggered (*trans*) (**1b**). Each form exhibits two resonances for their trimethylsilyl groups, which is consistent with the syn, anti arrangement of $SiMe_3$ groups observed in their solid-state structures (below). This $SiMe_3$

arrangement is different from the syn, syn arrangement found for the potassium salt.[50]

The relative amounts of the eclipsed and staggered conformers change with temperature for both $(C_3H_5)_2Ni$ and **1**, although not in the same way. For $(C_3H_5)_2Ni$, the staggered form is always predominant, and a 1:7.8 ratio of eclipsed to staggered isomers is observed at –75 °C (^{1}H NMR). At higher temperatures more of the eclipsed form is present, and once room temperature is reached, for example, the eclipsed to staggered ratio is 1:3.[14] Higher temperatures produce even more of the eclipsed form, but the two conformers remain interconvertible, and the eclipsed:staggered ratio reverts to 1:3 on cooling to room temperature.[51]

In contrast, the reaction represented in eq 2 generates a mixture of **1a** and **1b** in varying proportions, but the eclipsed **1a** is in excess (up to a **1a:1b** ratio of approximately 9:1) when the reaction is conducted at –78 °C. Excess **1a** is only observed when the reaction is performed at low temperature; if the reaction to form **1** is conducted at room temperature, **1b** is found to be predominant, with a **1a:1b** ratio of 2:3. A sample of **1** in solution will display essentially the same **1a:1b** ratio for weeks if room temperature is maintained, but the proportion of **1b** in the sample irreversibly increases if the temperature is raised. In a variable temperature ^{1}H NMR experiment, conversion of the eclipsed to staggered form was first noticeable at 358 K, and essentially complete conversion of **1a** to **1b** occurred by the time the

sample was heated to 380 K (approximately 50 minutes total time). Conversion back to **1a** did not occur on cooling.

The steric bulk of the trimethylsilyl substituents on the allyl ligands directs the formation of the kinetically stabilized eclipsed bis(allyl′)Ni product over the slightly thermodynamically favored staggered one. The kinetic stabilization of one form over another one has been seen in other substituted allyl nickel systems. In the case of the substituted $(2\text{-MeC}_3H_4)_2Ni$, the eclipsed form predominates 2:1 at low (–75 °C) temperatures, but the staggered form is preferred over the eclipsed one by 2.3:1 at room temperature.[13]

Reactions of 1 with phosphines. The reactivity of **1** was explored with several phosphines and halogens. As a point of reference, tertiary phosphines PR_3 (R = Me, Et, Ph, C_6H_{11}) form adducts with $(C_3H_5)_2Ni$ at low temperature, but they are unstable at room temperature. With one equivalent of PMe_3, an air- and moisture-sensitive 1:1 adduct has been isolated and crystallized at –78 °C (eq 3).[5]

$$(C_3H_5)_2Ni + PMe_3 \xrightarrow{-78\ ^\circ C} (C_3H_5)_2Ni + PMe_3 \qquad (3)$$

The X-ray crystal structure reveals eclipsed allyl ligands with a Ni–P distance of 2.218(1) Å (Figure 3). In solution, coupling is observed between the phosphorus and hydrogen atoms of the allyl ligands, but the coupling is lost above –40 °C; this has been taken as an indication that PMe_3 dissociation is occurring.

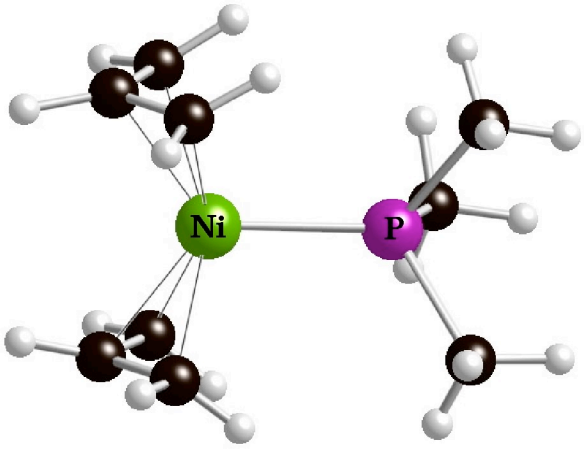

Figure 3. Solid-state structure of $(C_3H_5)_2NiPMe_3$.

Reaction of **1** (a mixture of **1a** and **1b**) with four equivalents of PMe_3 in hexanes at room temperature yields two products: the staggered bis(allyl)nickel complex **1b** and an organophosphorus compound characterized with multinuclear NMR spectroscopy. Similar results were found with either one or eight equivalents of PMe_3. Regardless of the starting **1a**:**1b** ratio, almost no **1a** ($< 5\%$) is identifiable in NMR spectra of the products, and X-ray crystallography was used to confirm that several crystals obtained from the concentrated reaction mixtures had unit cells matching only **1b**. The organophosphorus compound was not free PMe_3, as a broadened singlet (δ 1.15) in the ^1H NMR spectrum and a singlet (δ –21.6) in the ^{31}P NMR spectrum do not match that of PMe_3 in C_6D_6 (for it, we have measured $^1H = 0.814$ ppm (d, $J = 1.6$ Hz); ^{31}P NMR = –62.4 ppm; ^{13}C NMR = 16.4 ppm (d, $J = 10.7$ Hz)). This was substantiated by the $^{13}C\{^1H\}$ NMR spectrum, which

contains an apparent quintet at δ 25.1 ($J \approx$ 10.1 Hz; cf. δ 16.43 ($J =$ 10.7 Hz) for PMe_3).

A two-dimensional HSQC (heteronuclear single quantum correlation) experiment correlates the chemical shift of a nucleus (e.g., ^1H) with the chemical shift of a directly bonded nucleus (e.g., ^{13}C). The ^1H–^{13}C HSQC[52] coupled and phosphorus-decoupled data collected for the reaction product were used to confirm that carbon–phosphorus splitting was responsible for the multiplet in the ^{13}C spectrum. The HSQC experiment {^1H,^{31}P} demonstrates that the quintet collapses to a singlet upon ^{31}P decoupling (Figure 4). Such an A_4X spin system restricts the possible P_4-containing products, the most reasonable of which is the cyclic tetramethyltetraphosphane, $(MeP)_4$. The singlets in the ^1H and ^{31}P spectra reflect the likely D_{2d} symmetry of the compound (Figure 5), as exists in structurally characterized analogues such as $(PhP)_4$[53] and $[(i\text{-Pr})P]_4$[54]. Attempts to separate the product from the accompanying **1b** have not been successful. Despite the various ratios of **1** and PMe_3 used, only a single phosphorus-containing species was evident in the ^{31}P NMR spectrum within the limit of detection. A larger ring such as $(MeP)_5$ has a chemical shift of 17.3 ppm, thus ruling out the possibility of chemical shift overlap.

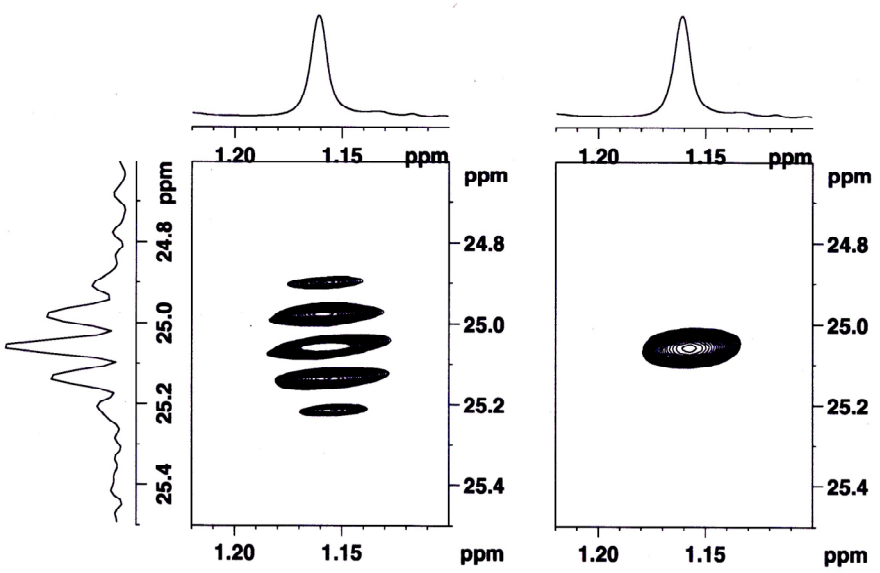

Figure 4. ^{1}H–^{13}C HSQC spectrum {^{1}H} (left) exhibits collapse of ^{13}C quintet upon ^{31}P decoupling {^{1}H,^{31}P} (right).

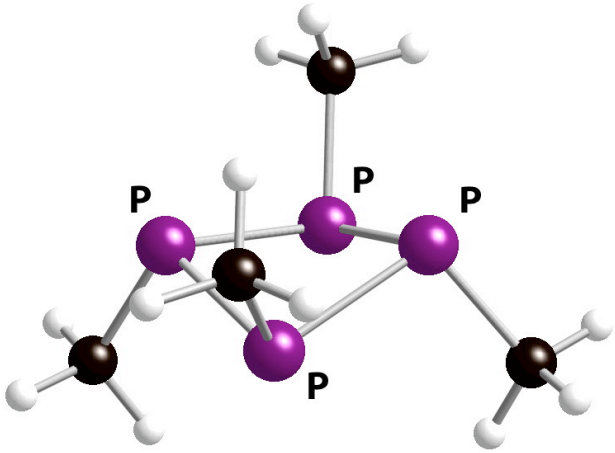

Figure 5. Calculated D_{2d} structure of $(MeP)_4$.

Tetramethyltetraphosphane has been described as a product in equilibrium with molten $(MeP)_5$, which served as the solvent.[55] The sole characterization for $(MeP)_4$ was a singlet in the ^{31}P NMR spectrum at –67.7 ppm, a value recorded at 160 °C; no ^{1}H or ^{13}C NMR data were reported. Although the ^{31}P chemical shift is reasonable (a variety of cyclotetraphosphanes have ^{31}P NMR chemical shifts in the range from –50 to –80 ppm[56,57]), it is not definitive for $(RP)_4$ rings, as evidenced by the considerably more deshielded values displayed by $[(C_5Me_5)P]_4$ (–39.0 ppm)[58] and $\{[(SiMe_3)_2CH]P\}_4$ (–14.6 ppm).[59]

The energetics of the transformation of PMe_3 to $(MeP)_4$ are reasonable. The decomposition of trimethylphosphines to tetramethyltetraphosphane and ethane is exothermic by –2.7 kcal mol^{-1} ($\Delta H°$; –10.3 kcal mol^{-1} in $\Delta G°$) (B3LYP/DGDZVP2 level) (eq 4).

$$4\ PMe_3 \rightarrow (MeP)_4 + 4\ CH_3CH_3 \qquad (4)$$

With the larger 6-311+G(2d,p) basis set, the energetics are slightly more favored with $\Delta H° = -7.9$ kcal mol^{-1} and $\Delta G° = -16.1$ kcal mol^{-1}. For both functional/basis set combinations, $(MeP)_4$ was optimized under D_{2d} symmetry, and it was a minimum on the potential energy surface ($N_{imag} = 0$).

Initially, a different phosphorus containing species, $Ni(PMe_3)_4$, (Figure 6) was considered as a possible product of the reaction of **1** and PMe_3 because of

similiarites seen in the NMR data of the product of this reaction and $Ni(PMe_3)_4$. However, the product could not be $Ni(PMe_3)_4$, for several reasons.

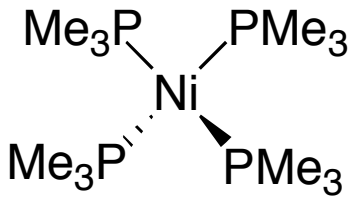

Figure 6. Structure of $Ni(PMe_3)_4$.

First of all, the nickel center in $Ni(PMe_3)_4$ is zero-valent. A Ni(0) source (e.g., bis(cyclooctadiene)nickel), in the presence of the free trimethylphosphine, results in the formation of tetrakis(trimethylphosphine)nickel(0), $Ni(PMe_3)_4$ (eq 5).[2]

$$Ni(COD)_2 + 4\ PMe_3 \rightarrow Ni(PMe_3)_4 + 2\ COD \qquad (5)$$

A zero-valent nickel source is not directly provided in the nickel allyl case.

Similar to the reaction involving PMe_3, bulkier phosphines such as PPh_3 and $P(C_6H_{11})_3$ form adducts with $(C_3H_5)_2Ni$ at low temperature. However, the phosphines dissociate at low temperatures, and coupling of the allyl ligands occurs on further warming (at 0 °C with PPh_3; at –20 °C with $P(C_6H_{11})_3$),[5] leaving zero-valent (hexadiene)nickel(0) phosphine complexes (eq 6).

$$(C_3H_5)_2Ni + PR_3 \rightarrow (C_3H_5)_2Ni(PR_3) \rightarrow$$ 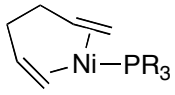 (6)

It is also known that trimethylphosphine dissociates from $(C_3H_5)_2NiPMe_3$, and $(C_3H_5)_2Ni$ decomposes by oxidative coupling of the allyl ligands to hexadiene above room temperature.[5] At this point, a zero-valent nickel source has been produced in the presence of PMe_3, which can conceivably react with PMe_3 to form $Ni(PMe_3)_4$ (eq 7). Thus, $Ni(PMe_3)_4$ is potentially a thermal decomposition product of $(C_3H_5)_2NiPMe_3$.

$$(\eta^3\text{-}C_3H_5)_2NiPMe_3 \xrightarrow[-40\ ^\circ C]{\Delta} (\eta^3\text{-}C_3H_5)_2Ni + PMe_3 \xrightarrow[20\ ^\circ C]{\Delta}$$

$$1,5\text{-hexadiene} + Ni(PMe_3)_4 \qquad (7)$$

For the reaction of **1** and PMe_3 to have resulted in the formation of $Ni(PMe_3)_4$, **1** would have to be reduced to Ni(0) upon oxidative coupling of the substituted allyl anions, forming $[(SiMe_3)_2C_3H_3]_2$. Experimental NMR data (^1H, ^{13}C) have shown that none of the distinctive resonances of $[(SiMe_3)_2C_3H_3]_2$ were present, and more importantly, that resonances corresponding to *trans*-[1,3-$(SiMe_3)_2C_3H_3]_2Ni$ (**1b**) were detected. In addition, crystals collected from the reaction filtrate were found to be those of **1b**. Furthermore, as previously mentioned, the reaction of PMe_3 with mixtures of **1a** and **1b** results in conversion of

1a to **1b** with a **1a**:**1b** ratio of 95:5. Obviously, this reaction occurs with no decomposition of the bis(allyl´)Ni starting material to Ni(0). With no Ni(0) source present, there is no chemical mechanism for the formation of $Ni(PMe_3)_4$, thus obviating the need to further consider $Ni(PMe_3)_4$ as a possible product in this reaction.

However, the similarities of ^{13}C NMR spectra between $Ni(PMe_3)_4$ and $(MeP)_4$ can be explained in terms of virtual coupling. Virtual coupling has been used to describe ^{13}C ABX systems that look like false AA´X systems for many transition metal complexes with two phosphines ligands.[60] In these systems (where A = ^{31}P, A´ = ^{31}P´, and X = ^{13}C), virtual coupling occurs when $J_{AA'}$ is much larger than J_{AX} and $J_{AX} > J_{A'X}$, where $J_{A'X} \approx 0$. The result is a ^{13}C resonance that is split into an apparent triplet by seemingly equivalent ^{31}P nuclei. In other words, two strongly coupled nuclei form effectively a nuclear triplet or singlet state analogous to an electronic triple or singlet state with quantum numbers of 1, 0, –1 or 0, respectively.[61]

It has been established that virtual coupling arises in the ^{13}C NMR spectrum of $Ni(PMe_3)_4$, resulting in an apparent quintet at 25.2 ppm with $J_{CP} \approx 8.67$ Hz.[62] With virtual coupling of ^{13}C nuclei to ^{31}P nuclei through the nickel center being detected in $Ni(PMe_3)_4$, it is no surprise that $(MeP)_4$ also exhibits virtual coupling of ^{13}C nuclei to ^{31}P nuclei in its ^{13}C NMR spectrum (apparent quintet at 25.1 ppm and $J_{CP} \approx 10.1$ Hz). Although similarities seem to exist in the ^{1}H, ^{13}C, and ^{31}P

NMR data for $Ni(PMe_3)_4$ and $(MeP)_4$, they are evidently coincidental, as seen in the ^{13}C NMR spectra with respect to virtual coupling.

As definitive proof for the case against the formation of $Ni(PMe_3)_4$, a closer inspection of all possible NMR data is warranted. Along with the differences in coupling constants, the peak heights of the apparent quintets found in the ^{13}C NMR data of both $Ni(PMe_3)_4$ and $(MeP)_4$ are different (i.e., 1:5.2:9.5:5.2:1 in $Ni(PMe_3)_4$ vs 1:3.4:6.5:3.4:1 in $(MeP)_4$).

^{61}Ni is an NMR active nucleus (I = 3/2) although it has low natural abundance (1.13%). Therefore, ^{61}Ni should split the ^{31}P NMR resonance of $Ni(PMe_3)_4$ into a quartet, and this splitting has been reported.[62] Tetrakis(trimethylphosphine)nickel(0) was synthesized following a literature procedure[40] and its ^{31}P and ^{61}Ni NMR spectra were measured for comparison to those of the reaction product of **1** and PMe_3.

In an extended run (276 scans) of the ^{31}P NMR experiment for a concentrated sample (57 mg) of $Ni(PMe_3)_4$, a quartet splitting pattern (J = 285 Hz) is seen due to splitting by ^{61}Ni (Figure 7). In a more concentrated sample (of the product of **1** and PMe_3; 79 mg), however, ^{31}P NMR data (601 scans) reveal that no ^{61}Ni satellites are present in ^{31}P NMR spectrum (Figure 8). Much like the absence of coupled allyl dimer in the reaction of **1** and PMe_3 indicates that there is no formation of Ni(0), thereby discrediting the possibility of $Ni(PMe_3)_4$ as a product, the lack of ^{31}P resonance splitting (quartet) of the P_n conaining product (by ^{61}Ni)

proves that there is no nickel–phosphorus interaction present in this compound; providing further evidence for the absence of $Ni(PMe_3)_4$ as a product of the reaction of **1** and PMe_3.

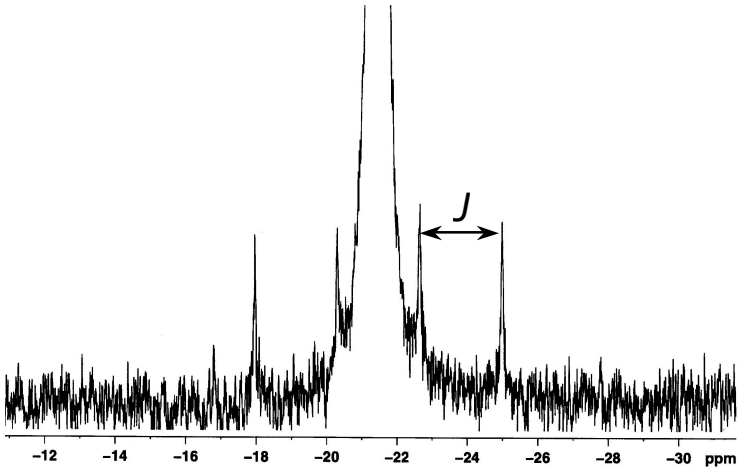

Figure 7. ^{31}P NMR spectrum of $Ni(PMe_3)_4$ exhibiting $J_{^{31}P-^{61}Ni}$ satellites (285 Hz) after 276 scans at 121 MHz.

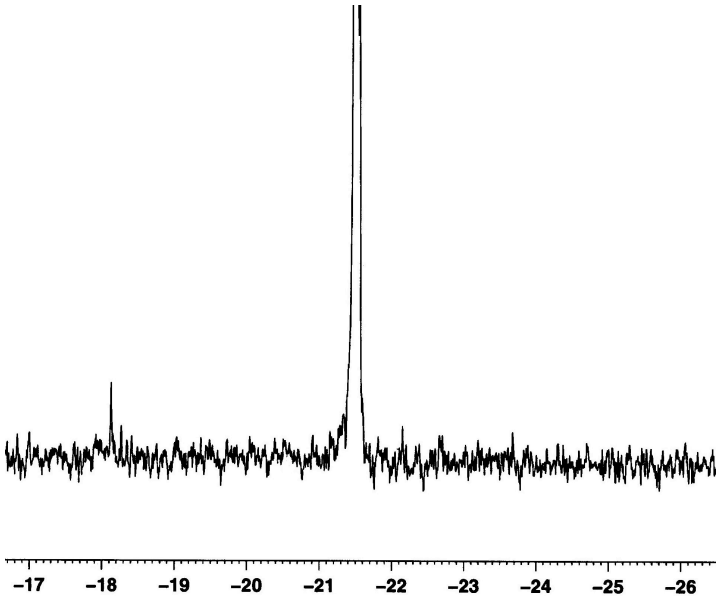

Figure 8. ^{31}P NMR spectrum of product of **1** and PMe_3 exhibiting no $J_{^{61}Ni-^{31}P}$ satellites after 601 scans at 121 MHz. The peak at ~18 ppm is an impurity.

As further conformation for the absence of $Ni(PMe_3)_4$ as a reaction product, ^{61}Ni NMR experiments were run for the independently synthesized $Ni(PMe_3)_4$ and for the putative $(MeP)_4$. ^{61}Ni (1.13 %) has a nuclear spin of 3/2 with a relative sensitivity (^{1}H = 1.00) of 3.57x10^{-3} (c.f. 0.0159 for ^{13}C) and receptivity (^{13}C = 1.00) of 0.242.[63] Its high quadrupolar moment (0.16 x 10^{-28} m^2), coupled with its low sensitivity and receptivity, renders this nucleus difficult to study with NMR; however, highly symmetrical structures (e.g., T_d or D_{4h}) can minimize the quadrupolar effect of the ^{61}Ni nucleus, making NMR experiments feasible.[63] Tetracarbonylnickel(0) has been used as a calibration standard for ^{61}Ni NMR, but due to its toxicity, an absolute resonance frequency of ^{61}Ni in $Ni(CO)_4$ at

8.936050MHz (relative to the resonance of protons in $Si(CH_3)_4$ at 100 MHz) is currently employed.[62] For these experiments, the probe was tuned to the absolute frequency of 35.722 Mhz, and no $Ni(CO)_4$ reference was used.

Tetrakis(trimethylphosphine)nickel(0) was prepared following a literature procedure.[40] Although it has been reported that as little as 20 mg of sample will provide a good ^{61}Ni NMR spectrum,[62] a more concentrated sample (57 mg) was used to lessen the time required for the experiment. A quintet was evident in spectrum after 16422 scans (Figure 9) although the outer peaks were just barely distinguishable from the baseline noise; the low resonance frequency leads to severe ringing effects and thus, rolling baselines. As expected, a *J* coupling constant value of 285 Hz was seen in the ^{61}Ni spectrum due to splitting by the four equivalent ^{31}P nuclei (Figure 10). This multiplet was calibrated to 40 ppm.

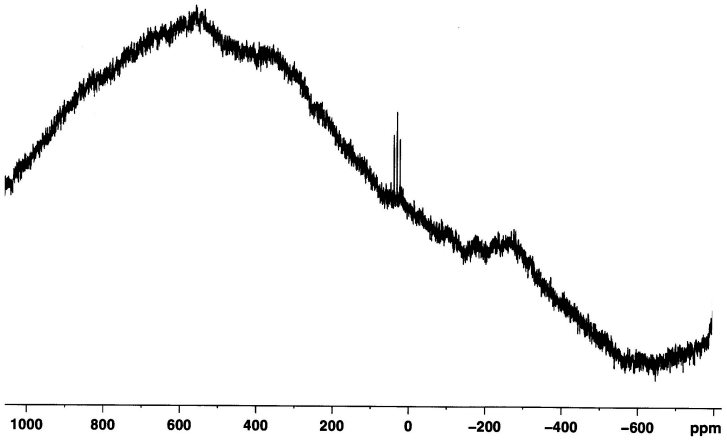

Figure 9. ^{61}Ni NMR spectrum of Ni(PMe$_3$)$_4$ exhibiting a quintet after 16,422 scans at 35.7 MHz. Rolling baseline due to ringing effect.

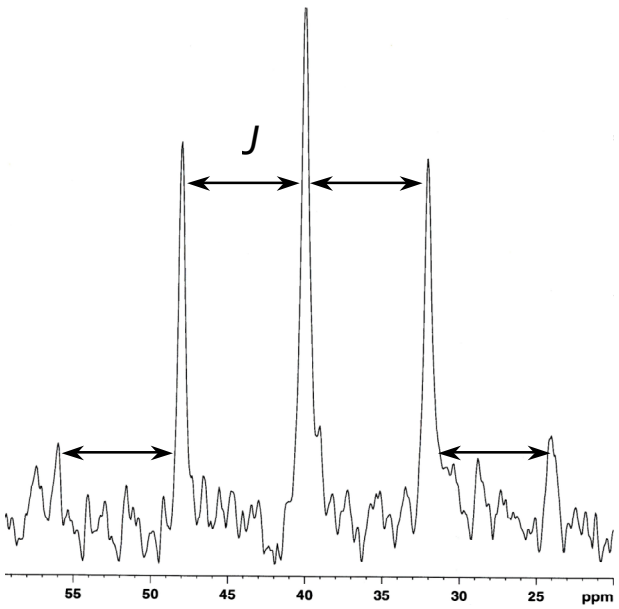

Figure 10. A closeup view of the quintet in the ^{61}Ni NMR spectrum of Ni(PMe$_3$)$_4$ exhibiting $J_{^{61}\mathrm{Ni}-^{31}\mathrm{P}}$ coupling (285 Hz) after 16,422 scans at 35.7 MHz.

An NMR sample was prepared from the products of the reaction of **1** and PMe_3. Since two products were expected, the bis(allyl´)Ni complex and $(MeP)_4$, the concentration of the sample was increased (79 mg) to ensure that a signal for ^{61}Ni would be detected if $Ni(PMe_3)_4$ were actually present. If the sample contained $Ni(PMe_3)_4$, the resultant quintet should be seen at 40 ppm, whereas no signal would be expected at 40 ppm for $[1,3\text{-}(SiMe_3)_2C_3H_3]_2Ni$ and $(MeP)_4$. No peaks were seen in the 2000 ppm range that was used in this experiment even after 82,582 scans, demonstrating that tetrakis(trimethylphosphine)nickel(0) is indeed not a product of the reaction of $[1,3\text{-}(SiMe_3)_2C_3H_3]_2Ni$ and trimethylphosphine.

It is doubtful that a ^{61}Ni NMR spectrum could be obtained for $[1,3\text{-}(SiMe_3)_2C_3H_3]_2Ni$. Only highly symmetrical zerovalent nickel species have had ^{61}Ni NMR spectra recorded. It is not clear what ppm range should be considered, and more likely, the low symmetry of $[1,3\text{-}(SiMe_3)_2C_3H_3]_2Ni$ may preclude any investigation due to inverse relationship of a complex's symmetry and its quadrupolar coupling.[63]

In order for $(MeP)_4$ to be the product of the reaction of **1** with PMe_3, multiple steps involving demethylation and P–P formation must be involved. Why such a transformation should occur with **1** but has not been reported with the unsubstituted $(C_3H_5)_2Ni$ may be related to the relatively unencumbered coordination environment of the latter. In the PMe_3 adduct of $(C_3H_5)_2Ni$, the allyl ligation to the metal is unchanged (η^3), as seen in the following reaction (eq 8).

$$(\eta^3\text{-}C_3H_5)_2Ni + PMe_3 \rightarrow (\eta^3\text{-}C_3H_5)_2Ni\text{–}PMe_3 \quad (8)$$

This reaction is predicted to be to be exothermic by –4.4 kcal mol^{-1} ($\Delta H°$) (+6.0 kcal mol^{-1} for $\Delta G°$) (B3LYP/DGDZVP2 level).

Preliminary computational studies suggest that the addition of trimethylphosphine to **1a** to form a PMe_3 adduct of **1a** similar to the parent compound, would not be favorable ($\Delta H° = +10.3$ kcal mol^{-1}; $\Delta G° = +24.1$ kcal mol^{-1}); the resulting complex is only a transition structure ($N_{imag} = 1$) (eq 9).

$$[1,3\text{-}(SiMe_3)_2C_3H_3]_2Ni\ \mathbf{(1a)} + PMe_3 \rightarrow (\eta^3\text{-allyl}^-)_2Ni\text{–}PMe_3\ (N_{imag} = 1) \quad (9)$$

For steric reasons, coordination of PMe_3 to $1,3\text{-}(SiMe_3)_2C_3H_3]_2Ni$ cannot occur to form a stable complex when both allyls are η^3-bound; slippage of an allyl ligand from η^3 to η^1 would probably be required for phosphine binding. The $\eta^3 \rightarrow \eta^1$ conversion of one of the allyl ligands may allow more than one phosphine adduct to bind to the nickel center. Subsequent additions of PMe_3 might then occur as the phosphine begins to demethylate, and P–P bond formation ensues. The final release of the cyclotetraphosphane would be accompanied by the rearrangement of the allyl ligands to the thermodynamically preferred staggered form (Figure 11). The

formation of larger rings may be energetically prohibitive; steric crowding may limit access of additional PMe_3 to the already formed five-membered metallacycle.

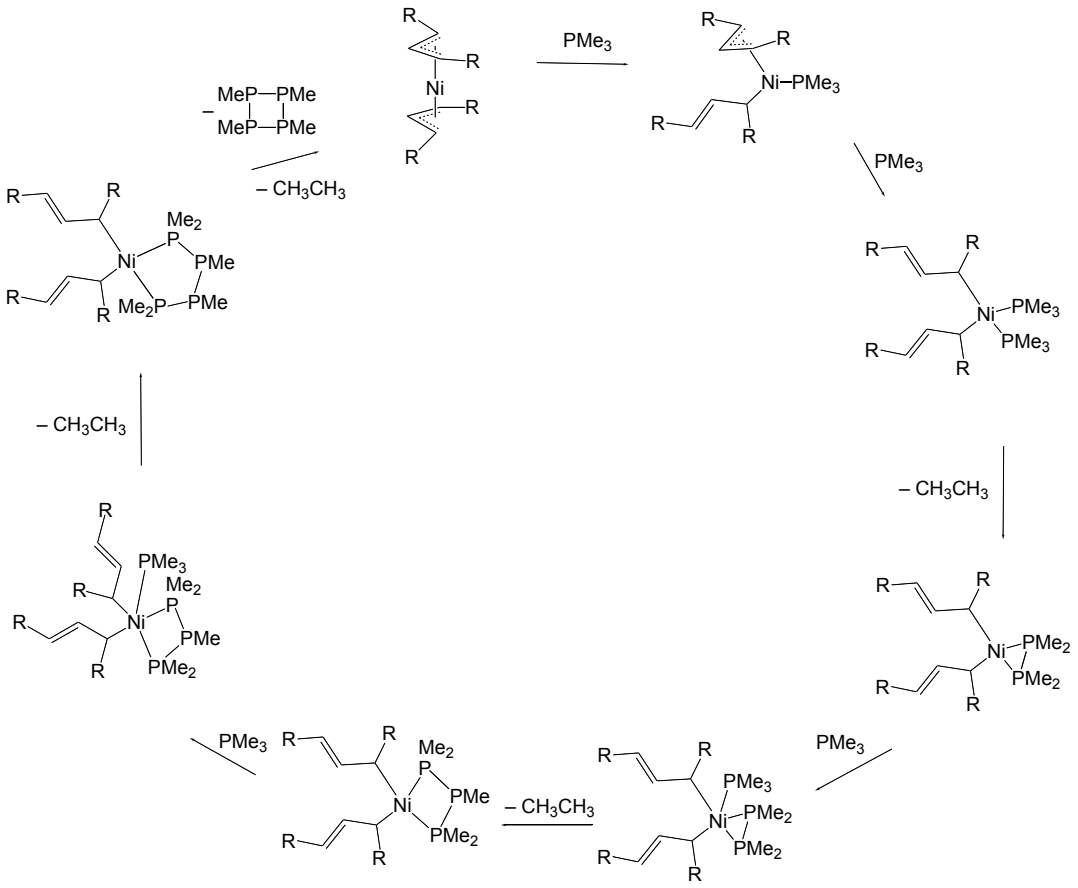

Figure 11. Proposed mechanistic cycle for synthesis of $(MeP)_4$.

The amount of $(MeP)_4$ synthesized depends on the stoichiometry of the starting materials for the reaction of **1** and PMe_3. However, although it is known that a trimethylphosphine adduct of $(C_3H_5)_2Ni$ forms at low temperature,[5] reactions of $(C_3H_5)_2Ni$ and PMe_3 in ratios other than 1:1 have not been reported.

It was hypothesized that there would be no formation of $Ni(PMe_3)_4$ as long as $(C_3H_5)_2Ni$ was not allowed to decompose to zero-valent nickel and hexadiene in the presence of PMe_3. Therefore, the experimental design involved the synthesis of $(C_3H_5)_2Ni$ in-situ, and the introduction of four equivalents of PMe_3, while keeping the reaction temperature (–40 °C) well below the decomposition temperature of $(C_3H_5)_2Ni$. Solvent was removed under vacuum at –25 °C, and the reaction mixture was allowed to warm to room temperature because $(MeP)_4$, once formed, is a stable species, so the subsequent decomposition of $(C_3H_5)_2Ni$ would not affect the product outcome.

An NMR sample was prepared from the reaction product. The NMR data collected for the reaction product of $(C_3H_5)_2Ni$ and four equivalents of PMe_3 were almost identical to the organophosphorus product obtained from the reaction of **1** and PMe_3 (Table 2). Moreover, both the coupling constant ($J \approx 10.1$ Hz) of the apparent quintet in the ^{13}C spectrum and the peak heights of the quintet (1:3.6:6.4:3.6:1) are nearly indistinguishable for both reactions (c.f., 1:3.4:6.5:3.4:1 for **1** and PMe_3).

Table 2. NMR data of organophosphorus compound from reactions of bis(allyl′)Ni and four equivalents of PMe_3 (allyl′ = $C_3H_5^-$, $[1,3\text{-}(SiMe_3)_2C_3H_3]^-$).

	NMR data of organophosphorus product (Reaction of $(C_3H_5)_2Ni$ and 4 PMe_3)	NMR data of organophosphorus product (Reaction of **1** and 4 PMe_3)
^1H NMR (300 MHz, C_6D_6, 298 K)	δ 1.15 (s)	δ 1.15 (s)
^{13}C NMR (75 MHz, C_6D_6, 298 K)	δ 25.0 (apparent quintet, $J \approx 10.1$ Hz)	δ 25.1 (apparent quintet, $J \approx 10.1$ Hz)
^{31}P NMR (121 MHz, C_6D_6, 298 K)	δ –21.3 (s)	δ –21.6 (s)

A concentrated NMR sample was used for an extended ^{31}P NMR experiment (1892 scans) of the product of $(C_3H_5)_2Ni$ and four PMe_3. Analogous to the results with the trimethylsilyl-substituted nickel complex, no ^{61}Ni satellites are present in the ^{31}P NMR spectrum for this sample (Figure 12). Since it has been determined that ^{31}P–^{61}Ni coupling is present in both ^{31}P and ^{61}Ni NMR spectra if coupling is present at all, it was deemed unnecessary to run a ^{61}Ni NMR experiment.

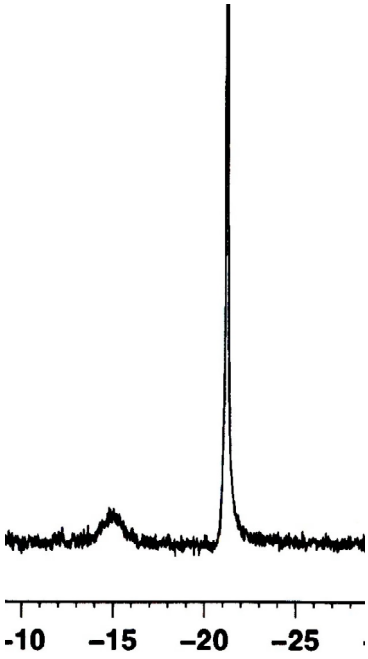

Figure 12. ^{31}P NMR spectrum of product of $(C_3H_5)_2Ni$ and PMe_3 exhibiting no $J_{^{61}Ni-^{31}P}$ satellites after 1,892 scans at 121 MHz. The peak at –15 ppm represents an impurity.

As previously mentioned, the bulkier phosphines PPh_3 and $P(C_6H_{11})_3$ form adducts with $(C_3H_5)_2Ni$ at low temperature, but coupling of the allyl ligands occurs on warming,[5] and (hexadiene)nickel(0) phosphine complexes have been isolated from the reactions. As seen in the analogous reaction with $(C_3H_5)_2Ni$ and PMe_3, the addition of bulky phosphines to $(C_3H_5)_2Ni$ produces phosphine adducted complexes; however, the thermodynamic instability of $(C_3H_5)_2Ni$ results in zero-valent nickel phosphine products when the reaction temperatures rise above the decomposition temperature of $(C_3H_5)_2Ni$.

In contrast, after being stirred with triphenylphosphine in hexanes overnight, **1** is recovered with no change in the **1a:1b** ratio, and NMR data (^{1}H, ^{13}C, ^{31}P) indicate that free triphenylphosphine is in solution. The lack of reactivity likely indicates that the steric bulk of the trimethylsilyl groups prevents the phosphine from gaining access to the metal center. In this regard, **1** is like [1,3-$(SiMe_3)_2C_3H_3]_2M$ (M = Cr, Fe), neither of which displays reactivity with PPh_3.[24,25]

Synthesis of trimethylsilyl-substituted (allyl)nickel halides. In order to gain more insight into the similarities and differences between complexes of the parent allyl $C_3H_5^-$ and the substituted $C_3(SiMe_3)_2H_3^-$, mono(allyl)nickel bromide and iodide derivatives were synthesized and characterized.

(Allyl)nickel bromides are red to red-purple, air- and moisture-sensitive compounds that can be prepared in several ways. One is by an oxidative addition reaction between an allyl bromide and a source of Ni(0), such as $Ni(CO)_4$ or bis(cyclooctadiene)nickel (e.g., eq 10).[64]

$$C_3H_5Br + (COD)_2Ni \rightarrow (C_3H_5)NiBr + 2\,COD \qquad (10)$$

The reaction between bis(allyl)nickel and elemental bromine in an aromatic solvent also generates (allyl)nickel bromide (eq 11).[11]

$$(C_3H_5)_2Ni + Br_2 \rightarrow C_3H_5Br + (C_3H_5)NiBr \quad (11)$$

The allyl halide complex is a dimer in aromatic hydrocarbons (i.e., $[(C_3H_5)NiBr]_2$), but a Schlenk equilibrium is established if the compound is dissolved in a coordinating donor solvent such as DMF or HMPA (i.e., eq 12).[9]

$$2\ (C_3H_5)NiBr \rightleftharpoons (C_3H_5)_2Ni + NiBr_2 \quad (12)$$

In aromatic solvents, (allyl)nickel bromide does not react with organic halides, but it does react in polar solvents by a radical chain mechanism that is initiated by heat, light or reducing agents (e.g., sodium naphthalenide).[7,9]

The oxidative addition method of (allyl)nickel halide preparation was investigated with trimethylsilylated ligands by preparing the previously unknown 3-bromo-1,3-(trimethylsilyl)propene (eq 13).[65]

$$C_3(SiMe_3)_2H_4 + NBS \xrightarrow[CCl_4]{(C_6H_5COO)_2} C_3(SiMe_3)_2H_3Br + NHS\downarrow \quad (13)$$

The reaction is refluxed under nitrogen for three hours, after which the solution is filtered, the solvent is removed under vacuum, and the product is vacuum distilled as a colorless liquid in 70% yield.

The bis(trimethylsilyl)allyl bromide reacts with $(COD)_2Ni$ in toluene to afford the substituted (allyl)nickel bromide (**2a**) (eq 14).

$$C_3(SiMe_3)_2H_3Br + (COD)_2Ni \rightarrow \textit{syn, syn}\text{-}[1,3\text{-}(SiMe_3)_2C_3H_3]NiBr + 2\ COD \quad (14)$$

Compound **2a** is an air- and moisture-sensitive red-purple solid. Its ^1H NMR spectrum indicates that the trimethylsilyl groups are equivalent, and hence in a syn, syn arrangement. This is also the arrangement found in the solid state (see below).

The direct reaction of **1** with elemental bromine in benzene at 0 °C can be used to form **2b** (eq 15).

$$[1,3\text{-}(SiMe_3)_2C_3H_3]_2Ni + Br_2 \xrightarrow{0\ ^\circ C} \textit{syn, anti}\text{-}[1,3\text{-}(SiMe_3)_2C_3H_3]NiBr + C_3(SiMe_3)_2H_3Br \quad (15)$$

The ^1H NMR spectrum of **2b** indicates the presence of two diastereomers with inequivalent trimethylsilyl groups; thus the $SiMe_3$ arrangement is syn, anti for both conformers. Interestingly, the mono(allyl) derivative has preserved the syn, anti configuration of the starting material **1**.

An attempted alternative synthetic route for the preparation of the trimethylsilyl-substituted (allyl)nickel bromide involved the 1:1 reaction of K[1,3-$(SiMe_3)_2C_3H_3$] with $NiBr_2$(dme) in THF at low temperature (eq 16).

$$K[1,3\text{-}(SiMe_3)_2C_3H_3] + NiBr_2(dme) \not\longrightarrow [1,3\text{-}(SiMe_3)_2C_3H_3]NiBr + KBr\downarrow + dme \quad (16)$$

However, the only organometallic product isolated from the reaction was **1**, which was also the case when the reactions were attempted in toluene with one equivalent of Li[1,3-$(SiMe_3)_2C_3H_3$]. After its formation, **1** evidently does not react further with the nickel bromide that is still present in solution; i.e., as in eq 17.

$$[1,3\text{-}(SiMe_3)_2C_3H_3]_2Ni + NiBr_2 \not\longrightarrow 2\,[1,3\text{-}(SiMe_3)_2C_3H_3]NiBr \quad (17)$$

As is obvious from eq 15, no reaction is observed between **2** and $C_3(SiMe_3)_2H_3Br$ in an aromatic solvent. This is also true when **2** and $C_3(SiMe_3)_2H_3Br$ were mixed in the donor solvent THF. In addition, **2** is stable to rearrangement in THF; i.e., there is no NMR evidence for the formation of [1,3-$(SiMe_3)_2C_3H_3]_2Ni$.

Bis(allyl)nickel reacts with I_2 in diethyl ether to yield the synthetically useful $(C_3H_5)NiI$ (eq 18).[11]

$$(C_3H_5)_2Ni + I_2 \rightarrow (C_3H_5)NiI + C_3H_5I \quad (18)$$

In a parallel fashion, iodine reacts smoothly with **1** in hexanes to yield a red-purple solid that can be recrystallized from hexanes as dark red blocks (eq 19).

$$[1,3\text{-}(SiMe_3)_2C_3H_3]_2Ni + I_2 \rightarrow$$

$$\textit{syn, anti}\text{-}[1,3\text{-}(SiMe_3)_2C_3H_3]NiI + C_3(SiMe_3)_2H_3I \quad (19)$$

The complex was characterized as $[1,3\text{-}(SiMe_3)_2C_3H_3]NiI$ (**3**) with elemental analysis, NMR spectral data, and X-ray crystallography. The NMR data are complex, as not only are inequivalent trimethylsilyl groups evident, indicative of a syn, anti arrangement of trimethylsilyl groups, but two diastereomers are also present. These sets of resonances correspond to the staggered and eclipsed conformers found in the solid state (see below). In THF, **3** is stable to rearrangement in donor solvents, and as with **2**, no reaction is observed between **3** and $C_3(SiMe_3)_2H_3Br$ in THF.

Crystallographic Results

Solid state structure of 1a. The structure determination of **1a** was obtained from orange crystals grown in hexanes solution over several days. The Ni atom lies on a crystallographic two-fold axis, so that only half of the molecule is unique. One of the $SiMe_3$ groups is modeled as disordered over two positions (66:34). An ORTEP view of the complex is displayed as Figure 13. Selected bond distances and angles for the structure are listed in Table 3.

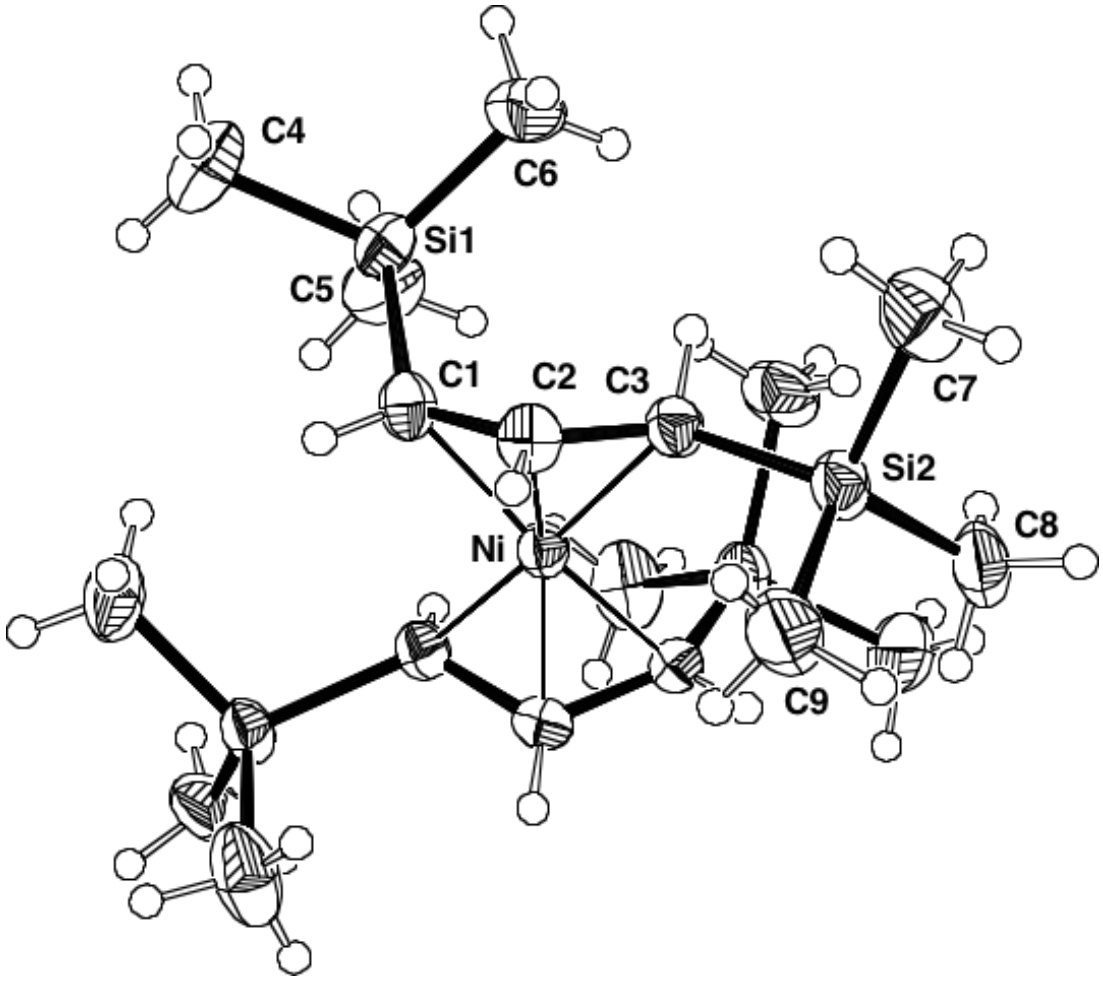

Figure 13. ORTEP of **1a**, giving the numbering scheme used in the text. Displacement ellipsoids are shown at the 50% level.

Table 3. Observed and calculated structural parameters for bis(π-allyl)nickel complexes.[a]

	$(C_3H_5)_2Ni$			$[1,3\text{-}(SiH_3)_2C_3H_3]_2Ni$		$[1,3\text{-}(SiMe_3)_2C_3H_3]_2Ni$			
	Staggered	Eclipsed	Experimental (staggered)	Staggered	Eclipsed	Staggered	Experimental (**1b**)	Eclipsed	Experimental (**1a**)
Ni–C_{mid}[b]	1.986	1.985	1.980(1)	1.994	1.990	1.994	1.972(2)	1.985	1.944(3)
Ni–C_{syn}[c]	2.028	2.029	2.029 (av)	2.076	2.038	2.105	2.070(2)	2.069	2.037(3)
Ni–C_{anti}[d]	2.028	2.029	2.029 (av)	2.028	2.054	2.026	2.016(2)	2.050	2.029(3)
C_{syn} C_{mid}	1.417	1.416	1.416 (av)	1.419	1.424	1.416	1.404(3)	1.420	1.416(4)
C_{mid}–C_{anti}	1.417	1.416	1.416 (av)	1.424	1.420	1.425	1.414(3)	1.423	1.418(4)
C_{syn} Ni–C_{anti}	74.8	74.7	74.6(1)	74.7	75.0	74.5	74.86(8)	74.6	75.6(1)
C_{syn} C_{mid}–C_{anti}	120.7	120.8	120.5(1)	122.4	122.2	123.3	123.7(2)	122.8	123.1(2)
Angle between allyl planes	0.0	59.8	0.0	4.4	56.7	2.9	4.6	47.5	49.1
Displacement of *anti*-substituent	0.57 Å	0.57 Å	0.54 (av) Å	0.96 Å	1.01 Å	1.07 Å	0.97 Å	1.14 Å	1.11 Å
Displacement of *syn*-substituent	0.18 Å	0.18 Å	0.17 (av) Å	0.20 Å	0.32 Å	0.06 Å	0.13 Å	0.21 Å	0.10 Å
Relative energy (ΔH°)	0.0	+1.5		0.0	+0.6	0.0		+1.5	

[a] B3LYP/DGDZVP2. Relative energy is in ΔH°, kcal mol^{-1}; [b] C_{syn} is the carbon adjacent to the *syn*-substituent (either SiH_3 or $SiMe_3$)

The complex has an eclipsed (*cis*) (η^3-allyl′)$_2$M geometry, with Ni–C bonds varying from 1.944(3) to 2.037(3) Å. The $SiMe_3$ groups in **1a** are arranged in a *syn*, *anti* configuration; the *syn* Si atoms, Si(2) and Si(2A), are near to the C_3 plane (their 0.10 Å displacement is reflected in the nearly linear C1–C2–C3–Si2 torsion angle of 176.5(7)°), whereas the *anti* Si atoms, Si(1) and Si(1A), are considerably shifted out of the allyl plane (by 1.11 Å, with a Si1–C1–C2–C3 angle of 47.8(4)°). Complex **1a** is the first structurally authenticated (η^3-allyl′)$_2$Ni complex with an eclipsed conformation, and only the second example reported for any metal. Like the eclipsed [1,3-$(SiMe_3)_2C_3H_3]_2Fe$,[25] the C_3 planes are sharply canted to each other (49.1°; cf. 52.7° in the iron complex). As with other first-row trimethylsilyl substituted bis(allyl)metal complexes ($[(SiMe_3)_nC_3H_{5-n}]_2Cr$ (n = 1–3),[24] [1,3-$(SiMe_3)_2C_3H_3]_2Fe$[25]), there is no evidence for agostic bonding involving H atoms of the ligand.

Solid state structure of 1b. For comparison to the eclipsed structure, the solid state structure of **1b**, which was first determined by J. Dominic Smith, will be discussed; the unit cell of crystals that I sent for structural determination matched the unit cell for the structure described herein. Two polymorphs of **1b** with different spacegroups ($P2_1/c$ and $C2/c$) were identified in separate crystallographic studies at 173 K. The unit cell volume is 3% larger for the $P2_1/c$ polymorph, and the symmetry of the molecule is approximately C_2. In the $C2/c$ polymorph, exact crystallographic C_2 symmetry is imposed on the molecule. It is not certain what

conditions produce the different forms, as the crystals of both polymorphs were grown from hexanes at room temperature; it is possible that the rate of growth was slower in one case. The molecules are closely similar, and only the more symmetric structure is discussed here. An ORTEP view of the complex is displayed as Figure 14. Selected bond distances and angles for the structure are listed in Table 3.

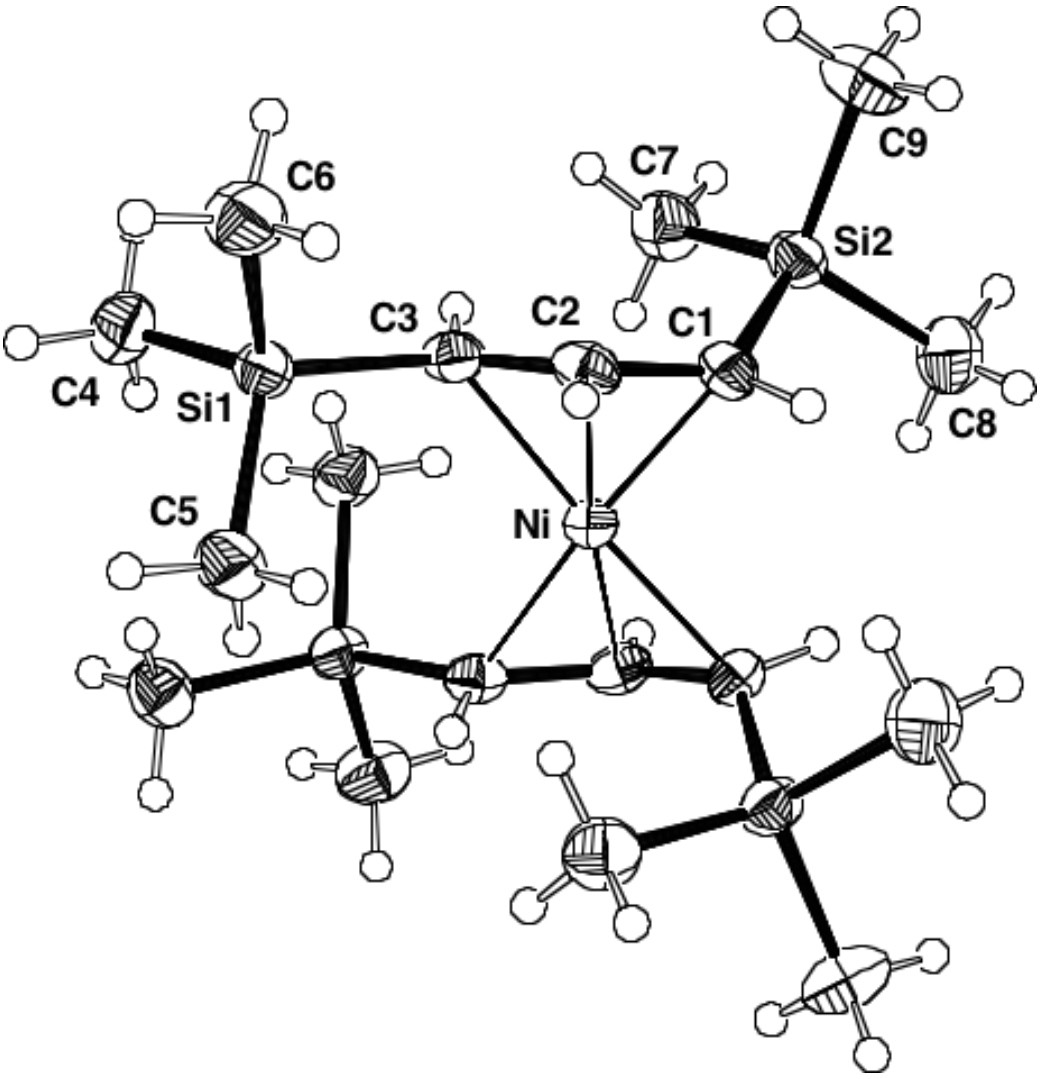

Figure 14. ORTEP drawing of **1b**, giving the numbering scheme used in the text. Displacement ellipsoids are shown at the 50% level.

The complex has a classic staggered (*trans*) (η^3-allyl′)$_2$M geometry, and as with **1a**, the $SiMe_3$ groups are arranged in a syn, anti configuration. The syn Si atoms, Si1 and Si1′, lie close to the C_3 plane (0.13 Å displacement, with a C1–C2–C3–Si1 torsion angle of 175.2(1)°), whereas the anti Si atoms, Si2 and Si2′, are substantially displaced out of the allyl plane (by 0.97 Å; the Si2–C1–C2–C3 torsion angle is 42.5(3)°). As is typical with π-bound allyls, the shortest Ni–C distance (1.972(2) Å) is to the central carbon of the allyl ligand. The carbon bearing the anti $SiMe_3$ group (C1) is slightly closer to the nickel (2.016(2) Å) than that with the syn $SiMe_3$ group (C3, at 2.070(2) Å). This lateral displacement ($\Delta = 0.054$ Å) is somewhat more than that displayed by **1a**, for which $\Delta = 0.008$ Å. A space-filling drawing of **1b** suggests the extent to which the metal center is encapsulated by the bulky allyl ligands (Figure 15).

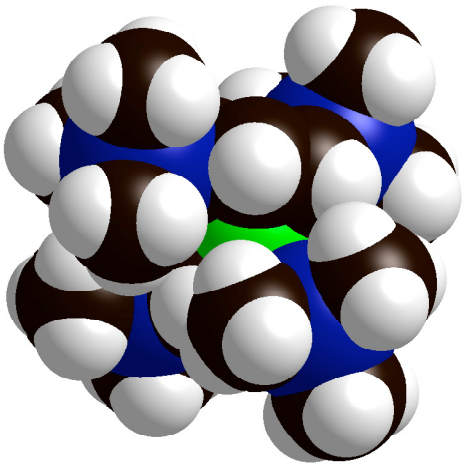

Figure 15. Space-filling drawing of **1b**; the nickel is the green atom in the center.

The Ni–C bond lengths in **1b** are similar to the Ni–C bond lengths in the parent $(C_3H_5)_2Ni$ (1.980(1) to 2.031(1) Å),[19] as are the interplanar C_3 angles (4.6° in **1b**, 0.0° in $(C_3H_5)_2Ni$). The positions of the $SiMe_3$ groups on the ligands mimic the out-of-plane distortions present in the hydrogen atoms in $(C_3H_5)_2Ni$ (e.g., the displacements of the anti hydrogens away from the nickel).

Solid state structure of 2a. For comparison to the iodide-bridged structure, the solid state structure of **1b**, which was first determined by J. Dominic Smith, will be discussed. The complex crystallizes from hexanes as a bromide-bridged dimer. The molecule lies on a crystallographic two-fold axis; thus, only one half of the molecule is unique. Whereas Br2 lies on the two-fold axis, Br1 lies slightly off the axis and was modeled as disordered over it (50:50). An ORTEP view of the complex is displayed as Figure 16. Selected bond distances and angles for the structure are listed in Table 4.

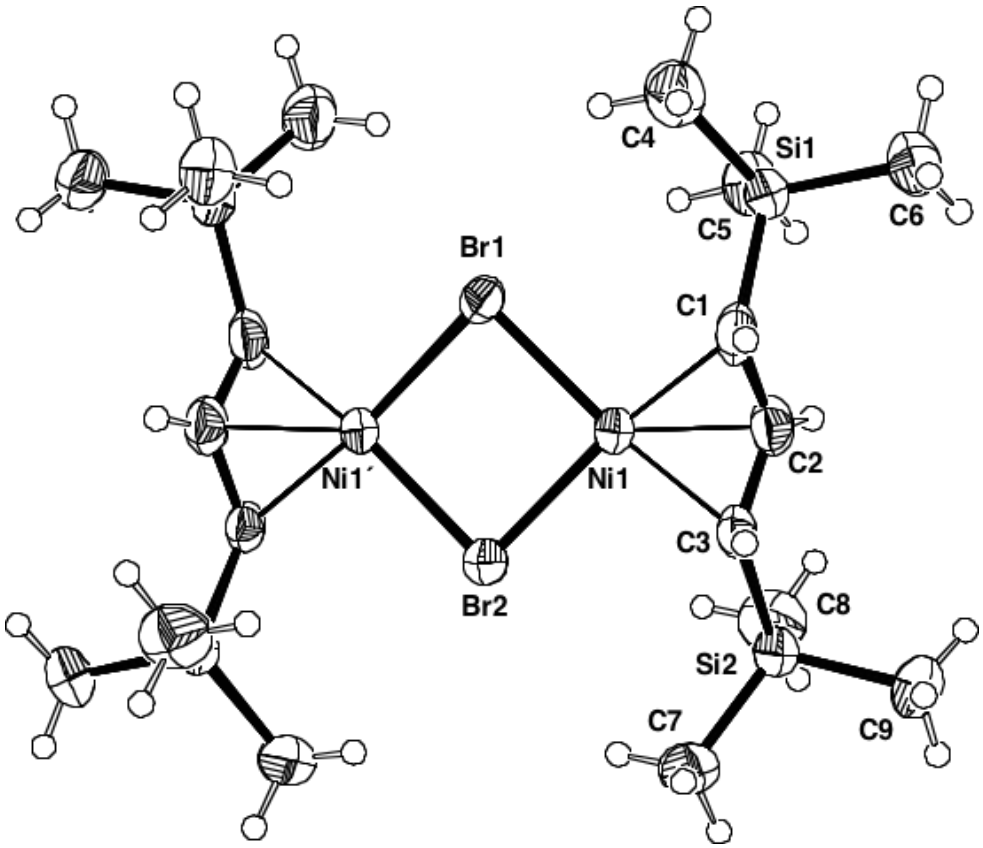

Figure 16. ORTEP drawing of **2a**, giving the numbering scheme used in the text. Displacement ellipsoids are shown at the 50% level.

Table 4. Selected bond distances (Å) and angles (deg) for **2a**.

atoms	distance	atoms	angle
Ni–Br1	2.362(10)	Br1–Ni1–Br2	89.6(2)
Ni–Br2	2.365(1)	Ni1–Br1–Ni1	90.35(8)
Ni–C1	2.062(7)	Ni1–Br2–Ni1	90.32(6)
Ni–C2	1.978(6)	C1–C2–C3	120.0(7)
Ni–C3	2.039(6)		
C1–C2	1.385(9)		
C2–C3	1.457(9)		

The Ni–C bond lengths range from 1.978(6) to 2.062(7) Å, which are within 0.08 Å of those in **1b**. Although not required to be so by symmetry, the Ni–Br1 and Ni–Br2 bond lengths are identical within error (2.362(10) and 2.365(1) Å). The Ni···Ni′ separation is 3.35 Å, too long to represent any significant interaction (cf. the 2.49 Å distance in nickel metal[66]). The angle between the C_3 plane and $(NiBr)_2$ plane is 117.7°. The dimeric structure of **2a** joins a family of bridged π-allyl nickel species (Table 5), but the most directly comparable structure is the dimeric (2-

carboxyethylallyl)nickel bromide, $\{[2\text{-}(CO_2C_2H_5)C_3H_4]NiBr\}_2$, which has Ni–C bond lengths ranging from 1.90(2) to 2.06(2) Å, and Ni–Br bonds of 2.334(5) and 2.378(5) Å.[67] Despite the differences in the substitution on the allyl ligands, the metrics for the listed complexes are quite similar to those in **2a**.

Table 5. Selected structural data for bridged (π-allyl)nickel dimers (distances in Å).

Compound	Ni–X, X´	Ni···Ni´	Ni–C (range)	Allyl substituents	ref.
$\{[1,3\text{-}(SiMe_3)_2C_3H_3]NiBr\}_2$ (**2**)	2.362, 2.365	3.35	1.978–2.062	*syn, syn*	this work
$\{[1,3\text{-}(SiMe_3)_2C_3H_3]NiI\}_2$ (**3a; 3b**)	2.513, 2.539; 2.521, 2.528	3.49	1.973–2.049; 1.979–2.041	*syn, anti*	this work
$\{[2\text{-}(CO_2C_2H_5)C_3H_4]NiBr\}_2$	2.334, 2.378	3.24	1.90–2.06	N/A	[67]
$\{[2\text{-}PhC_3H_4]Ni(O_2CCF_3)\}_2$	1.924, 1.924	3.10	1.971–1.980	N/A	[68]
$\{[2\text{-}(SiMe_3)C_3H_4]Ni(O_2CCF_3)\}_2$	1.918, 1.929	2.98	1.927–1.991	N/A	[68]

Table 5. continued.

{[1-PhC_3H_4]Ni(O_2CCF_3)}$_2$	1.876, 1.973	2.93	1.890–2.052	*syn*	[68]
{[1-Me-3-($OSiMe_3$)C_3H_3]NiCl}$_2$	2.234, 2.263	3.04	1.957–2.043	*syn, syn*	[69]
{[C_3H_5]Ni(OSi(O-*t*-Bu)$_3$)}$_2$	1.917, 2.049	2.67	1.915–1.920	N/A	[70]
{[2-MeC_3H_4]Ni(O_2CCF_3)}$_2$	1.927, 1.934	3.04	1.973–1.987	N/A	[71]
{[1,3-$Me_2C_3H_3$]Ni(CH_3)}$_2$	2.044, 2.067	2.37	1.953–2.039	*syn, syn*	[72]
{[2-MeC_3H_4]Ni($O_2CC_6H_4$(-*o*-NPh_2))}$_2$	1.905–1.920	2.95	1.955–1.991	N/A	[73]

* The average value is listed.

Unlike the arrangement found in **1a** or **1b**, the $SiMe_3$ groups in **2a** are in a syn, syn configuration; the Si atoms Si1 and Si2 lie close to the C_3 plane (0.13 Å and 0.10 Å, respectively; the Si1–C1–C2–C3 torsion angle is –175.1(5)°; the C1–C2–C3–Si2 torsion angle is 176.5(5)°. The syn, syn configuration has been observed before in other bridged allyl dimers of nickel, such as $\{(1,3\text{-}Me_2C_3H_3)Ni(\mu\text{-}Me)\}_2$[72] and $\{[1\text{-}Me\text{-}3\text{-}(OSiMe_3)C_3H_3]NiCl\}_2$[69] (Table 4). The arrangement in **2a** is the first time it has been observed in a neutral transition metal complex containing trimethylsilylated allyl ligands, however.

Solid state structure of 3. Like **2a**, complex **3** crystallizes as a halide-bridged dimer with crystallographically imposed symmetry. In the case of **3**, however, there are two independent half-molecules in the asymmetric unit. The molecule with atom Ni2 (**3a**) is fully generated by a two-fold axis parallel to the *a*-axis and perpendicular to the diamond core; the molecule with atom Ni1 (**3b**) is completely generated by a two-fold axis parallel to the *b*-axis that contains both bridging iodide atoms. Both structures are similar except for the orientation of the ligands; structure **3a** has an eclipsed orientation while structure **3b** has a staggered orientation. Both are discussed together here. An ORTEP view of **3a** is displayed as Figure 17; **3b** is shown in Figure 18. Selected bond distances and angles for the structures are listed in Table 6.

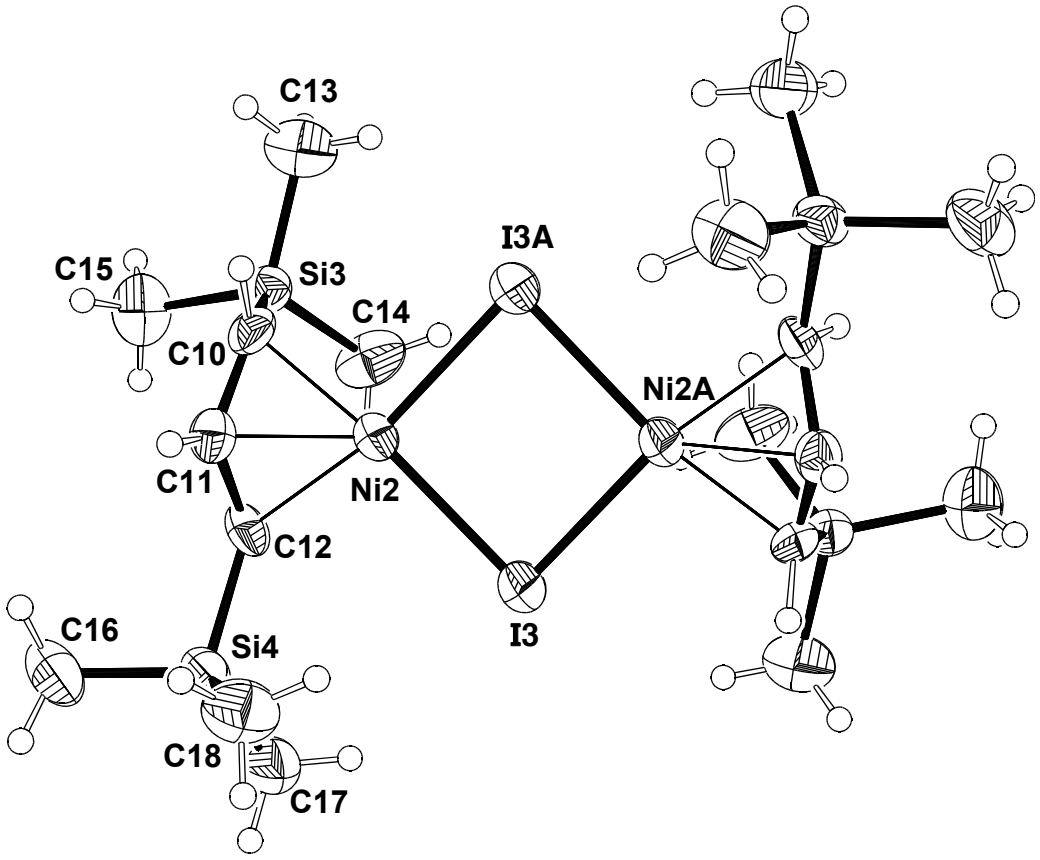

Figure 17. ORTEP drawing of **3a**, giving the numbering scheme used in the text. Displacement ellipsoids are shown at the 50% level.

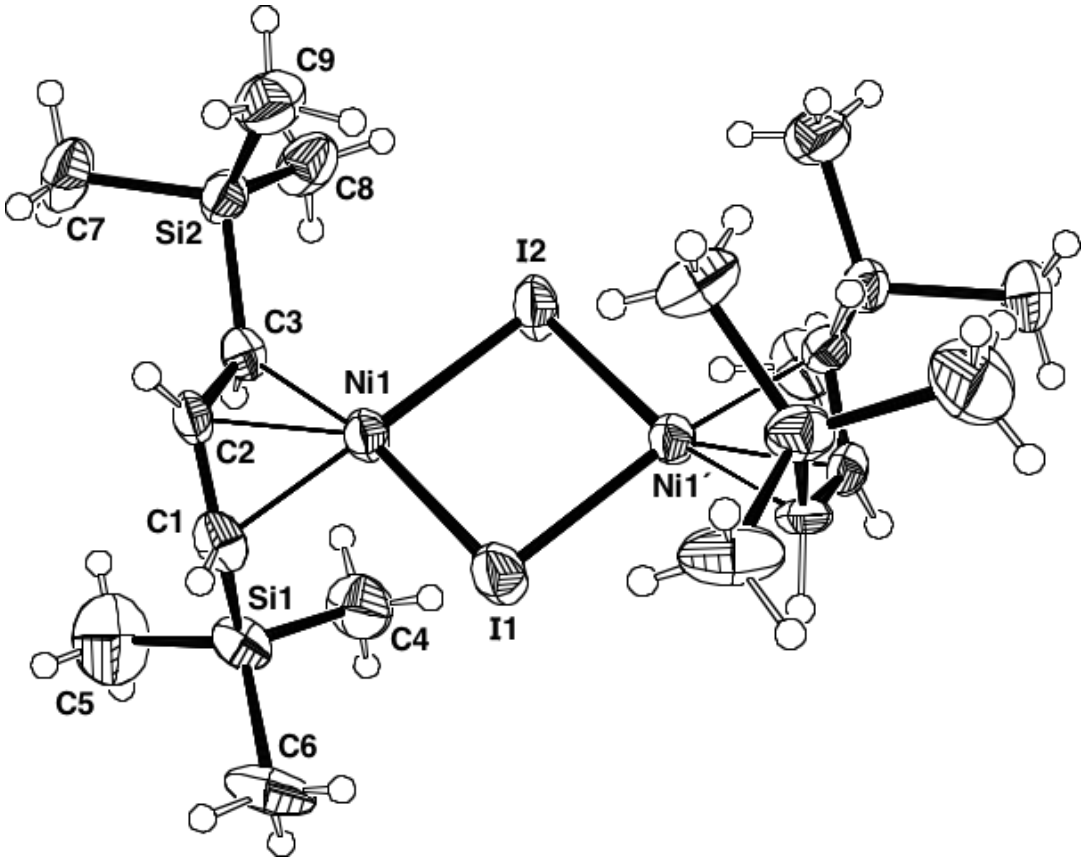

Figure 18. ORTEP drawing of **3b**, giving the numbering scheme used in the text. Displacement ellipsoids are shown at the 50% level.

Table 6. Selected bond distances (Å) and angles (deg) for **3a** (top table) and **3b** (bottom table).

atoms	distance	atoms	angle
Ni2–I3	2.513(1)	I3–Ni2–I3´	92.61(4)
Ni2–I3´	2.539(1)	Ni2–I1–Ni2´	87.35(4)
Ni2–C10	2.020(8)	C10–C11–C12	120.3(7)
Ni2–C11	1.973(8)		
Ni2–C12	2.049(7)		
C10–C11	1.422(11)		
C11–C12	1.402(11)		

atoms	distance	atoms	angle
Ni1–I1	2.528(1)	I1–Ni1–I2	92.43(4)
Ni1–I2	2.521(1)	Ni1–I1–Ni1´	87.42(5)
Ni1–C1	2.041(7)	Ni1–I2–Ni1´	87.73(5)
Ni1–C2	1.979(7)	C1–C2–C3	119.1(7)
Ni1–C3	2.038(8)		
C1–C2	1.436(12)		
C2–C3	1.404(11)		

The Ni–C bond lengths in **3a** range from 1.973(8) to 2.049(7) Å (1.979(9) to 2.041(7) Å in **3b**), which like those in **2a**, are similar to those in the bis(allyl) complexes **1a** and **1b**. The Ni–I bond lengths are only slightly different in **3a** (2.513(1) and 2.539(1) Å), and are nearly equal in **3b** (2.521(1) and 2.528(1) Å). The Ni···Ni´ separation of 3.49 Å (the same in **3a** and **3b**) precludes any metal–metal interaction. This compound represents the first structurally authenticated LNi(μ-$I)_2$NiL dimer, and there are few other iodide-bridged nickel centers available for comparison. The nickel-iodide bond distances in **3a/3b** are somewhat shorter than the 2.62 Å (av) distance found in the carbamoyl cluster (μ-$OCNEt_2)_4Ni_2$(μ-$I)_2$Ni($NHEt_2$),[74] for example, but weak metal-metal bonding exists between the the nickel centers in the latter (Ni···Ni´ separation of 2.67 Å), which complicates a direct comparison.

In contrast to the arrangement found in **2a**, the $SiMe_3$ groups in **3a/3b** are in syn, anti relationships. As is typical for such configurations, the syn Si atoms (Si4 in **3a**; Si2 in **3b**) are close to the C_3 plane (0.14 Å and 0.10 Å, respectively), whereas the anti Si atoms (Si3 in **3a**; Si1 in **3b**) are considerably displaced from the allyl plane (1.02 Å and 0.90 Å, respectively); similar values are found in **2a**.

Computational Results

$(C_3H_5)_2Ni$. The electronic structure of bis(allyl)nickel has been investigated repeatedly at various levels of sophistication.[15-17,75,76] For ease of comparison with the substituted derivatives, the staggered and eclipsed forms of $(C_3H_5)_2Ni$ were reexamined at the B3LYP/DGDZVP2 level of theory under C_2 symmetry (nearly identical results were obtained with the crystallographically observed C_i symmetry). The agreement of the staggered geometry with the single crystal neutron diffraction structure[19] is quite good; the calculated Ni–C(1,3) and Ni–C2 distances of 2.028 Å and 1.986 Å can be compared with the average Ni–C(1,3) and Ni–C2 distances observed at 2.029(1) and 1.980(1) Å, and the calculated C–C–C angle (120.7°) in the ligand essentially matches the observed angle of 120.5(1)°. The bond distances and angles in the calculated structure of the eclipsed form (Ni–C(1,3) = 2.029 Å; Ni–C2 = 1.985 Å; C–C–C = 120.8°) are almost the same as in the staggered conformation. The angle between the C_3 planes is markedly different in the two conformations, however: parallel (0.0°) in the staggered form, 59.8° in the eclipsed. The solid state structure of $(C_3H_5)_2Ni$ has parallel ligands.

Most calculations have identified the staggered form of $(C_3H_5)Ni$ as slightly lower in energy than the eclipsed conformation, and that is found to be the case with the B3LYP/DGDZVP2 combination (1.5 kcal mol^{-1} for both $\Delta H°$ and $\Delta G°$). Recently, Casarin found that quasi-relativistic DFT calculations indicated that the two forms were virtually identical in energy (0.1 kcal mol^{-1} in favor of the eclipsed

conformation, although with the use of a triple zeta quality basis set on all atoms (instead of on nickel only), the preference shifted to 0.13 kcal mol^{-1} in favor of the staggered form).[17] It should be noted that in solution at room temperature, both conformers are present in an eclipsed to staggered ratio of 1:3,[14] and only the staggered form has been identified in the solid state.[19]

As a more realistic model for **1a/1b**, the molecule $[1,3\text{-}(SiH_3)_2C_3H_3]_2Ni$ was optimized using the B3LYP/DGDZVP2 method under C_2 symmetry, the highest possible with *syn*, *anti* silyl groups. Some asymmetry is now evident in the binding of the allyl ligand; in the staggered conformation, the distance from Ni to C1, which bears the *syn* SiH_3 group, is 2.076 Å, and Si1 is relatively close to the C_3 plane (0.20 Å). The corresponding Ni–C3 distance is 2.028 Å, and Si3 is displaced by 0.96 Å from the allyl plane. The Ni–C2 distance (1.994 Å) is only slightly longer than that calculated for unsubstituted $(C_3H_5)_2Ni$, and the calculated C–C–C angle has widened slightly to 122.4°; the C_3 allyl planes now form an angle of 4.4°. These values closely model features in **1b**, including the longer Ni–C(*syn*-TMS) vs Ni–C(*anti*-TMS) distance (2.070(2) and 2.016(2) Å, respectively), the difference in silyl group displacements (close to the allyl plane for the *syn*-groups, markedly displaced for the *anti*-groups), and the interplanar C_3 angle (4.4° in the model; 4.6° in **1b**).

Calculations on the eclipsed version of $[1,3\text{-}(SiH_3)_2C_3H_3]_2Ni$ under C_2 symmetry were found to reproduce the structure of **1a** to a reasonable degree. The

similarities include the slightly more symmetrical bonding of the allyl ligand (2.038 Å to the carbon with the anti $SiMe_3$ group and 2.054 Å to the carbon with the syn $SiMe_3$ group) and the tilting of the C_3 ligand planes (calculated at 56.7°; experimentally found in **1a** at 49.1°). It is apparent that the inclusion of SiH_3 groups is sufficient to reproduce the major features of both the staggered and eclipsed forms of $[1,3\text{-}(SiMe_3)_2C_3H_3]_2Ni$. The staggered conformer continues to be the more stable, although by even less than in the case of the unsubstituted complex (0.6 kcal mol^{-1} in $\Delta H°$, 1.3 kcal mol^{-1} in $\Delta G°$).

As an additional check on the possible steric influence of the trimethylsilyl groups, the structures of $[1,3\text{-}(SiMe_3)_2C_3H_3]_2Ni$ were optimized with the B3LYP/DGDZVP2 combination using the crystal structures of **1a** and **1b** as starting geometries; C_2 symmetry was used throughout. As in the SiH_3 substituted model, the calculated values for the trimethylsilyl-substituted models closely match those of the experimental $[1,3\text{-}(SiMe_3)_2C_3H_3]_2Ni$ structures (see Table 3).

Of particular interest is the C_3 interplanar angle calculated for the eclipsed structure; it has decreased from 56.7° in the SiH_3 substituted model to 47.5° with the inclusion of trimethylsilyl groups. The latter angle is close to the experimentally found value of 49.1°. This suggests that this structural feature is controlled by steric interactions among the $SiMe_3$ groups; with a smaller tilt angle, there are no Me···Me´ contacts of less than 4.0 Å, the sum of the van der Waals' radii for two methyl groups.[77]

Although it has not been observed in the bis(allyl)nickel structures, the geometry of staggered [1,3-$(SiMe_3)_2C_3H_3]_2Ni$ was calculated under C_2 symmetry with both trimethylsilyl substituents in *syn*, *syn* arrangements. The optimized structure was a minimum ($N_{imag} = 0$), with Ni–C distances ranging from 1.999 to 2.089 Å. It is distinctly higher in energy than the staggered form with *syn*, *anti* substituents (by 4.1 kcal mol^{-1} in $\Delta H°$, 3.7 kcal mol^{-1} in $\Delta G°$).

It is interesting to note that the energetic difference between the eclipsed and staggered conformers is small and coincidentally matches the value for the unsubstituted versions (1.5 kcal/mol). The irreversible conversion of eclipsed to staggered structure at high temperature seems inconsistent with this small energy difference. There may be important differences between the solution and solid-state structures or solvent interactions present that are responsible the apparent discrepancy.

Conclusion

Trimethylsilyl substituents affect the properties of allyl nickel complexes in ways ranging from subtle to substantial. It is possible to identify several categories of similarities and differences, as summarized below.

(1) *Structure and thermodynamics.* The crystal structures of $(C_3H_5)_2Ni$ and **1b** are remarkably similar in the core features of the metal-ligand geometry. The

nickel–carbon bond lengths are within 0.04 Å of each other, and the angles between the C_3 planes differ by less than 5°, even though DFT calculations suggest that the potential energy surface for the interplanar angle is nearly flat, and hence easily perturbable. Although the trimethylsilyl groups cause substantial changes in other attributes of the complexes, they exert little effect on the framework Ni–C distances.

Consistent with this finding, the DFT calculations on the eclipsed and staggered conformations of $(C_3H_5)_2Ni$, $[1,3\text{-}(SiH_3)_2C_3H_3]_2Ni$, and $[1,3\text{-}(SiMe_3)_2C_3H_3]_2Ni$ indicate that successively greater substitution does not change the relative stability of the two forms (Table 3). The staggered form is always preferred, but not by more than 1.5 kcal mol^{-1}. The consistency of the preference energy indicates that the trimethylsilyl groups do not exert a major effect on the relative thermodynamic stability of the molecules.

(2) *Kinetic stability*. Probably the most obvious difference between the properties of $(C_3H_5)_2Ni$ and **1** is the considerably improved oxidative and thermal stability of the latter. Although $(C_3H_5)_2Ni$ is pyrophoric, **1** can survive in air for hours (as a powder) to days (as large crystals). Steric shielding of the metal center is undoubtedly the source of this kinetic stability (see Figure 14).

The enhanced thermal stability of **1** (dec. over 100 °C) may also be a kinetic phenomenon. The decomposition of $(C_3H_5)_2Ni$ is accompanied by the coupling of the allyl ligands,[5] but a similar process may be more difficult with the sterically bulky trimethylsilylated analogue.

The kinetic influence of the substituted allyl ligands is also evident in the difference in the solution behavior of **1** and $(C_3H_5)_2Ni$. The eclipsed and staggered conformations of the latter are in dynamic equilibrium, and the ratio is adjustable by a variation in the temperature.[14] Orbital symmetry arguments indicate that the interconversion of the two conformations cannot be accomplished by a simple rotation of the allyl ligands,[78] and likely involves a sequence of $\pi-\sigma-\pi$ rearrangements of the binding modes. In contrast, the eclipsed (**1a**) and the staggered (**1b**) forms of **1** are not in detectable equilibrium. Their relative ratios in solution are constant until a temperature of 85 °C is reached, at which point *irreversible* conversion of **1a** to **1b** occurs. Although the enthalpic difference between the two forms is small (~1.5 kcal mol^{-1}), the set of ligand rearrangements that would be required to convert **1b** back to **1a** must be more difficult for the bulky trimethylsilyated ligands than for the parent anion.

(3) *Reactions with phosphines and halides.* Given the apparent thermodynamic similarities between $(C_3H_5)_2Ni$ and **1**, their different reactions with nucleophiles, like their susceptibility to oxidation, probably stem largely from the kinetic differences arising from the bulky trimethylsilylated ligands. This is apparent in the reactions of the two compounds with phosphines. All phosphines do not react in the same way with $(C_3H_5)_2Ni$, and this is also true with **1**. With $(C_3H_5)_2Ni$, an unstable adduct is formed with PPh_3 (and other bulky phosphines such as $(C_6H_{11})_3P$ and $(i\text{-}Pr)_3P$), which decomposes with the formation of a nickel hexadiene complex. The

lack of any detectable interaction between **1** and PPh_3 is probably a direct consequence of the shielding of the metal center by the bulky allyl groups. With the smaller PMe_3, however, the roles are partially reversed; i.e., $(C_3H_5)_2Ni$ forms a thermally unstable 18-e$^-$ adduct that can be characterized at low temperature, but which dissociates at room temperature without affecting the nickel complex. In contrast, on reaction with a mixture of **1a/1b**, trimethylphosphine is converted to tetramethyltetraphosphane, $(MeP)_4$, leaving behind the thermodynamically more stable staggered **1b**. The full mechanism of this transformation must be complex and is under investigation.

The reaction of **1** with halogens is similar to that of $(C_3H_5)_2Ni$, in that both bis(allyl) complexes will lose an allyl ligand when treated with Br_2 or I_2 to form (allyl´)NiX species. The extra kinetic stabilization imparted by the bulky allyl ligands results in some differences, however, such as the resistance to Schlenk rearrangements in donor solvents.

A subtle effect can be recognized in the derivatives of **1** that does not exist with $(C_3H_5)_2Ni$, namely, the variable occurrence of *syn, syn* and *syn, anti* ligand substituents. *Syn, syn* arrangements are uniformly observed in bis(trimethylsilyl)allyl complexes of the s- and f-block metals; i.e., in those cases in which a largely ionic allyl-metal interaction can be presumed.[27-29,79,80] *Syn, anti* conformations have to date only been observed in d-block transition metal complexes, where they are the rule for the first row series $[1,3\text{-}(SiMe_3)_2C_3H_3]_2M$; M = Cr, Fe, Co, Ni). The observation

of both *syn, syn* and *syn, anti* versions of the mono(allyl)nickel species **2** indicates that the $SiMe_3$ arrangement is a conserved feature of the bis(allyl) starting materials; i.e., the *syn*, *anti* version of **2** and the **3** were both derived directly from **1**, which contains *syn*, *anti* groups. The *syn, syn* version of **2** was derived from 1,3-$(SiMe_3)_2C_3H_4Br$, to which the *syn* and *anti* distinction does not apply. The fact that the bis(allyl)metal species are derived from alkali metal salts (Li+, K+) with *syn, syn* substituents suggests that this arrangement is not conserved on transfer of the ligands to transition metal centers.

The chemistry of $(C_3H_5)_2Ni$ and that of the trimethylsilylated derivatives described here differ in various ways, both in degree and kind. We anticipate that greater use of such substituted ligands will lead to new and unexpected elaborations in stoichiometric and catalytic nickel allyl chemistry.

CHAPTER II

REACTIONS OF $[\eta^3$-1,3-$(SiMe_3)_2C_3H_3]_2M$ (M = Fe, Co, Ni) COMPLEXES WITH SMALL MOLECULES INCLUDING CARBONYL, PHOSPHINES, AND HALOGENS

Introduction

Wilke prepared the first homoleptic (π-allyl)transition metal complex, $(C_3H_5)_2Ni$,[1] in 1961, and many other examples of these complexes have been subsequently synthesized.[3] The $C_3H_5^-$ allyl anion is sterically compact, and when used as the sole ligand in organometallic complexes, results in coordinatively unsaturated metal centers, and thus highly reactive complexes. These attributes make (π-allyl) metal complexes useful as reagents in organic and materials chemistry[81-83] and catalysis,[84-89] and numerous examples have been synthesized for these purposes.

Despite their uses in numerous applications, first-row transition metal allyls have low-energy decomposition pathways, resulting in low thermal stabilities, regardless of electron count or number of coordinated allyl ligands. This is certainly the case for the late-transition metals of the first row. For example, bis(allyl)Ni decomposes at 20 °C,[1] and although bis(allyl)M (M = Fe, Co) complexes are not known, tri(allyl)iron and tri(allyl)cobalt are both unstable at low temperatures in inert atmospheres.[3] Although these transition metal allyl complexes are unstable and subsequently difficult to handle, there has been interest in the study of the reactions of (allyl)transition metal complexes with small molecules such as σ-donors

(e.g., phosphines),[90,91] π-acceptors (e.g., carbon monoxide),[92,93] and oxidizing agents (e.g., halogens).[94,95]

The addition of donor ligands provides little improvement to the stability of homoleptic allyl complexes of first-row transition metals. For example, 18-electron complexes of the type $(C_3H_5)_2Fe(PR_3)_2$ exhibit low stability (dec. ~0 °C) even though the iron(II) center is electronically saturated.[96] Carbon monoxide, the quintessential π-acceptor ligand,[97] has been used to synthesize (π-allyl)transition metal carbonyl complexes[98-100] although there are few such complexes described for bis(allyl) species. Although $(C_3H_5)_2Fe(CO)_2$ has been synthesized and studied via NMR and infrared spectroscopy,[101] it is unstable and must be stored at low temperature under an inert atmosphere.[102] There is only one report of a bis(allyl´)NiCO species in the literature (it decomposes at –30 °C),[92] and there are no reports of bis(allyl)Co(II) carbonyl monomers.

The instability associated with the homoleptic (π-allyl)transition metal complexes is also found in heteroleptic (π-allyl)transition metal halide complexes. It has been shown that the parent bis(allyl)Ni reacts with bromine and iodine to form the heteroleptic (allyl)nickel halide species (eq 20) (see Chapter 1).[2]

$$(C_3H_5)_2Ni + X_2\ (X = Br, I) \rightarrow C_3H_5X + (C_3H_5)NiX \qquad (20)$$

In addition to possessing low thermal stability, $(C_3H_5)NiX$ (X = Br, I) complexes undergo ligand redistribution in donor solvents (eq 21).[9]

$$2\ (C_3H_5)NiX\ (X = Br,\ I) \rightleftharpoons (C_3H_5)_2Ni\ +\ NiX_2 \qquad (21)$$

In a similar low-temperature reaction, $(C_3H_5)_3Co$ and iodine react to form $(C_3H_5)_2CoI$ (eq22).[103] Like the (allyl)nickel halide complexes, this species is presumed to be dimeric in solution.

$$(C_3H_5)_3Co + I_2 \rightarrow C_3H_5I + (C_3H_5)_2CoI \qquad (22)$$

It has been shown that the addition of sterically bulky substituents to cyclopentadienyl ligands results in organometallic complexes that are stabilized relative to their unsubstituted analogs.[20,104-106] In a similar effort to increase the stability of transition metal allyl complexes, sterically bulky substituents have been added to the allyl carbon backbone. Moderate success has been achieved by simply adding a methyl group to the allyl ligand for use in the synthesis of iron(II) allyl complexes.[96] For example, the bis(2-$MeC_3H_4)_2Fe(PMe_3)_2$[107] complex decomposes at ~20 °C (cf., 0 °C for the parent analog).[96] It is thought that the methyl groups on the allyl ligands provide kinetic stability to the resultant complex by blocking a decomposition pathway.

More recently, the much bulkier $[1,3\text{-}(SiMe_3)_2C_3H_3]^-$ ligand[38] has been used to synthesize bis(allyl′)M complexes (M = Cr,[24] Fe,[25] Co,[26] Ni[108]). These complexes show marked improvement in stability when compared to their unsubstituted conformers with metal centers in the +2 oxidation state (i.e., $(C_3H_5)_2Cr$,[84,109] $(C_3H_5)_2Ni$[1]). In the cases of Fe(II) and Co(II), the bulky allyl ligands allow the synthesis and characterization of homoleptic bis(allyl′) species.

In this chapter, $[1,3\text{-}(SiMe_3)_2C_3H_3]_2M$ (M = Fe, Co, Ni) complexes will be studied with respect to reactions with phosphines, carbon monoxide and halogens. A portion of this research involving the use of Ni(II) metal center has been described in Chapter 1, but will be noted here for comparative purposes.

Experimental Section

General Considerations. All manipulations were performed with the rigorous exclusion of air and moisture using high vacuum, Schlenk, or glovebox techniques. Proton and carbon (^{13}C) NMR spectra were obtained on a Bruker DPX–300 spectrometer at 300 and 75.5 MHz, respectively, and were referenced to the residual proton (δ 7.15 ppm) and ^{13}C resonances (δ 128.0 ppm) of C_6D_6. COSY, and HMQC NMR spectra were recorded on a Bruker DPX–400 spectrometer and were similarly referenced. All NMR data were processed using Bruker XWINNMR 3.5 software on an Octane workstation (Silicon Graphics, Mountain View, CA).

Infrared data were obtained on an ATI Mattson–Genesis FT–IR spectrometer as KBr pellets prepared as previously described.[36] Melting points were determined on a Laboratory Devices Mel–Temp apparatus in sealed capillaries. Combustion analyses were performed by Desert Analytics, Tuscon, AZ. Magnetic susceptibility data were obtained on a Bruker DRX-400 spectrometer using Evans' method[110-112] with a small sample (8-15 mg) placed in a 1.0 mL volumetric flask and diluted with toluene-d_8. After complete mixing, approximately 0.5 mL was transferred into an NMR tube with a sealed capillary containing toluene-d_8. The NMR tube was capped, and the ^1H NMR spectrum was collected.

Materials. 1-$(SiMe_3)C_3H_5$ and *n*-BuLi (2.5 M in hexanes) were purchased from Acros, and $FeCl_2$, $CoCl_2$, $NiBr_2$(dme), and *t*-BuOK were purchased from Aldrich; all were used as received. Carbon monoxide (CP grade) was purchased in a pressurized cylinder from A–L Compressed Gases and passed through a drying column (anh. $CaSO_4$) before use. A Schlenk-line adapted needle, which was purged with CO for several minutes, was used to introduce CO to $[1,3\text{-}(SiMe_3)_2C_3H_3]_2M$ (M = Fe,Co,Ni) solutions. $1,3\text{-}(SiMe_3)_2C_3H_4$ and $Li[1,3\text{-}(SiMe_3)_2C_3H_3]$ were synthesized according to literature procedures.[38] $K[1,3\text{-}(SiMe_3)_2C_3H_3]$ was prepared by transmetallation of $Li[1,3\text{-}(SiMe_3)_2C_3H_3]$ with potassium *t*-butoxide in hexanes solution. The potassium allyl salt undergoes halide metathesis reactions with $FeCl_2$,[25] $CoCl_2$,[26] or $NiBr_2$(dme)[108] in THF to produce the corresponding $[1,3\text{-}(SiMe_3)_2C_3H_3]_2M$ compounds in good yields. The synthetic methods described here for these compounds are variations of the literature preparations. THF, toluene, and hexanes were distilled under nitrogen from potassium benzophenone ketyl.[39] Deuterated solvents were vacuum distilled from Na/K (22/78) alloy prior to use.

Synthesis of $[1,3\text{-}(SiMe_3)_2C_3H_3]_2Fe$. A 125 mL Schlenk flask containing a stirring bar was charged with $FeCl_2$ (0.500 g, 3.94 mmol) and 10 mL of THF. The flask was then fitted with a 25 mL addition funnel containing $K[1,3\text{-}(SiMe_3)_2C_3H_3]$ (1.769 g, 7.880 mmol) dissolved in 15 mL of THF. The apparatus was attached to a Schlenk line and then cooled to –78 °C using a dry ice/acetone bath. The $K[1,3\text{-}(SiMe_3)_2C_3H_3]$ solution was added dropwise with stirring over the course of 30 min. The reaction was allowed to slowly warm to room temperature overnight. The THF was removed from the reaction mixture under vacuum, and the dark brown residue

was extracted with small portions (5 mL) of hexanes. The extract was filtered over a medium porosity glass frit to remove KCl and any unreacted starting material, leaving a dark red filtrate. The hexanes was removed under vacuum to afford an orange crystalline solid (1.49 g, 3.48 mmol; 88% yield). Bis(1,3-bis(trimethylsilyl)allyl)iron is an air- and moisture-sensitive orange solid that is thermally stable under an inert atmosphere (m.p. 72–75 °C). The compound sublimes at 48 °C under reduced pressure (10^{-2} Torr) and is soluble in ethers and aromatic and aliphatic hydrocarbons. Principle IR bands (KBr, cm^{-1}): 2953 (s), 2896 (s), 2363 (w), 1600 (s), 1430 (s), 1260 (s), 1090 (s), 870 (s), 800 (s), 690 (m), 480 (m). Magnetic susceptibility (toluene–d_8): $corr_\mu = 2.9$ BM at 303 K and $corr_\mu = 3.0$ BM at 203 K, consistent with 2 unpaired electrons.[113]

Reaction of [1,3-$(SiMe_3)_2C_3H_3]_2$Fe and CO. A 125 mL Schlenk flask containing a stirring bar was charged with [1,3-$(SiMe_3)_2C_3H_3]_2$Fe (0.123 g, 0.309 mmol) and 20 mL of hexanes. A needle was submerged in the solution of [1,3-$(SiMe_3)_2C_3H_3]_2$Fe, and CO was briskly added for six minutes. The solution was then degassed using the freeze-pump-thaw method. The solution was filtered, and hexanes was removed under reduced pressure leaving a yellow-orange oil (0.130 g; 87% yield) that could be distilled at 35 °C (10^{-2} Torr). Anal. Calcd for $C_{20}H_{42}FeO_2Si_4$: C, 49.76; H, 8.77; Fe, 11.57. Found: C, 50.20; H, 8.74; Fe, 11.32. Principle IR bands (KBr pellet, cm^{-1}): 2953 (s), 2898 (s), 1986 (s), 1931 (s), 1697 (m), 1606 (w), 1603 (w), 1477 (m), 1415 (m), 1249 (s), 1204 (m), 1101 (m), 1019 (m), 852 (s), 732 (m), 688 (m), 601 (m), 563 (m). ^{1}H NMR (300 MHz, C_6D_6, 298 K): δ 0.18 ppm (s, 18H, $Si(CH_3)_3$); 0.30 (s, 18H, $Si(CH_3)_3$); 1.15 (d, J = 13.5 Hz, 2H, *anti* C–H); 3.02 (d, J = 13.5 Hz, 2H, *syn* C–H); 5.29 (dd, J = 13.5 Hz, J = 13.5 Hz, 2H,

$C_{(2)}$–H). ^{13}C NMR (75 MHz, C_6D_6, 298 K): δ –0.22 ppm ($Si(CH_3)_3$); –0.016 ($Si(CH_3)_3$); 47.20 (*syn* C–H); 69.30 (*anti* C–H); 106.85 ($C_{(2)}$); 216.84 (CO).

Reaction of $[1,3\text{-}(SiMe_3)_2C_3H_3]_2Fe$ and I_2. A 125 mL Erlenmeyer flask containing a stirring bar was charged with $[1,3\text{-}(SiMe_3)_2C_3H_3]_2Fe$ (0.401 g, 0.941 mmol) and 30 mL of hexanes. Iodine (0.239 g, 0.941 mmol) was added, and the reaction was stirred overnight. Although no immediate change was observed upon the addition of iodine, the solution eventually turned light yellow with stirring, and a fine suspension of black precipitate was noted. The solution was decanted, and hexanes was removed under reduced pressure leaving a yellow liquid that was identified as 1,3,4,6-tetrakis(trimethylsilyl)-1,5-hexadiene (0.280 g; 80% yield) by its ^1H NMR data.

Reaction of $[1,3\text{-}(SiMe_3)_2C_3H_3]_2Fe$ with PMe_3. In a 125 mL Schlenk flask, $[1,3\text{-}(SiMe_3)_2C_3H_3]_2Fe$ (0.250 g; 0.587 mmol) was dissolved in hexanes (10 mL). The flask was connected to a glass tube containing $[AgI{\bullet}PMe_3]_4$ (0.744 g; 0.598 mmol). The iron(II) solution was cooled to –78 °C in a dry ice/acetone bath. The glass tube was heated with a heat gun; after the PMe_3 was released, the orange-red solution turned darker orange-red. The reaction was filtered, and hexanes was removed under vacuum leaving an orange oil. The oil could not be identified with NMR data (^1H and ^{31}P), as the sample is paramagnetic, and only rolling baselines were seen in the spectra.

Reaction of $[1,3\text{-}(SiMe_3)_2C_3H_3]_2Fe$ with $P(C_6H_5)_3$. In a 125 mL Erlenmeyer flask, $[1,3\text{-}(SiMe_3)_2C_3H_3]_2Fe$ (0.050 g; 0.12 mmol) was dissolved in 20 mL of hexanes. Triphenylphosphine (0.031 g; 12 mmol) was added to the orange $[1,3\text{-}(SiMe_3)_2C_3H_3]_2Fe$ solution. The reaction was stirred overnight. No color

change was noted upon addition. Hexanes was removed under vaccum to afford a mixture of a white precipitate and an orange oil.

Synthesis of [1,3-$(SiMe_3)_2C_3H_3]_2Co$. A 125 mL Schlenk flask containing a stirring bar was charged with $CoCl_2$ (0.500g, 3.85 mmol) and 10 mL of THF. The flask was then fitted with a 25 mL addition funnel containing K[1,3-$(SiMe_3)_2C_3H_3$] (1.725 g, 7.684 mmol) dissolved in 15 mL of THF. The apparatus was attached to a Schlenk line and then cooled to –78 °C using a dry ice/acetone bath. The K[1,3-$(SiMe_3)_2C_3H_3$] solution was added dropwise with stirring over the course of 30 min. The reaction was allowed to slowly warm to room temperature overnight. The THF was removed from the reaction mixture under vacuum, and the dark red residue was extracted with small portions (5 mL) of hexanes. The extract was filtered over a medium porosity glass frit to remove KCl and any unreacted starting material, leaving a dark red filtrate. The hexanes was removed under vacuum to afford a nearly black oil that appeared dark red when transilluminated. Over a period of days, yellow-orange, needle-like crystals grew (1.23 g, 2.86 mmol; 75% yield). Bis(1,3-bis(trimethylsilyl)allyl)cobalt is an air- and moisture-sensitive yellow-orange solid that is thermally stable under an inert atmosphere (m.p. 73 °C). The compound sublimes at 50 °C under reduced pressure (10^{-2} Torr) and is soluble in ethers and aromatic and aliphatic hydrocarbons. *Anal.* Calcd. for $C_{18}H_{42}CoSi_4$: C, 50.30; H, 9.84. Found: C, 50.30; H, 9.81. Principle IR bands (KBr): 2955 (s), 2899 (m), 2366 (w), 1698 (w), 1449 (m), 1400 (w), 1248 (s), 1028 (s), 1009 (s), 843 (s), 800 (s), 715 (w), 549 (w), 478 cm^{-1} (br, w). Magnetic susceptibility (toluene–d_8): $corr_\mu$ = 1.8 BM at 298 K, consistent with one unpaired electron.[113]

Reaction of $CoCl_2$ and Li[1,3-$(SiMe_3)_2C_3H_3$]. A 125 mL Schlenk flask containing a stirring bar was charged with $CoCl_2$ (0.516 g, 3.97 mmol) and 10 mL of toluene. The flask was then fitted with a 25 mL addition funnel containing Li[1,3-$(SiMe_3)_2C_3H_3$] (0.740 g, 3.85 mmol) dissolved in 15 mL of toluene. The apparatus was attached to a Schlenk line and then cooled to –78 °C using a dry ice/acetone bath. The Li[1,3-$(SiMe_3)_2C_3H_3$] solution was added dropwise with stirring. The reaction was allowed to slowly warm to room temperature overnight. The toluene was removed from the reaction mixture under vacuum, and the dark red residue was extracted with hexanes. The extract was filtered over a medium porosity glass frit to remove KCl and any unreacted starting material, leaving a dark red filtrate. The hexanes was removed under vacuum to afford a dark red oil. Over a period of days, yellow-orange, needle-like crystals grew. The unit cell of the crystals matched that of bis(1,3-bis(trimethylsilyl)allyl)cobalt.

Reaction of [1,3-$(SiMe_3)_2C_3H_3]_2Co$ and CO. A 125 mL Schlenk flask containing a stirring bar was charged with [1,3-$(SiMe_3)_2C_3H_3]_2Co$ (0.140g, 0.326 mmol) and 20 mL of hexanes. A needle was submerged in the solution of [1,3-$(SiMe_3)_2C_3H_3]_2Co$, and CO was briskly added for six minutes. The solution was then degassed using the freeze-pump-thaw method. The solution was filtered, and hexanes was removed under reduced pressure leaving an orange oil that distilled at 28 °C (10^{-2} Torr). Colorless crystals grew over a period of days and were structurally determined to be 1,3,4,6-tetrakis(trimethylsilyl)-1,5-hexadiene, $[(SiMe_3)_2C_3H_3]_2$. Two other products were detected in NMR spectra. Principle IR bands (KBr pellet, cm^{-1}): 2954 (s), 2898 (m), 2360 (w), 2344 (w), 2053 (s), 1984 (s, br), 1697 (w), 1599 (m), 1492 (w), 1444 (w), 1247 (s), 994 (m), 838 (s, br), 742 (m),

689 (m), 559 (m), 517 (m). ^{1}H NMR (300 MHz, C_6D_6, 298 K): **Product 1**: δ 0.002 ppm (s, 9H, $Si(CH_3)_3$); 0.082 (s, 9H, $Si(CH_3)_3$); 2.30 (d, J = 12.9 Hz, 1H, *anti* C–H); 3.10 (d, J = 8.7 Hz, 1H, *syn* C–H); 4.89 (dd, J = 12.9 Hz, J = 8.7 Hz, 1H, $C_{(2)}$–H). ^{13}C NMR (75 MHz, C_6D_6, 298 K): δ –1.27 ppm ($Si(CH_3)_3$); 0.55 ($Si(CH_3)_3$); 63.48 (*anti* C–H); 67.92 (*syn* C–H); 96.06 ($C_{(2)}$); 204.51 (CO). **Product 2**: δ 0.10 ppm (s, 18H, $Si(CH_3)_3$); 1.97 (d, J = 12.3 Hz, 2H, $C_{(1,3)}$–H); 4.70 (t, J = 12.3 Hz, 1H, $C_{(2)}$–H). ^{13}C NMR (75 MHz, C_6D_6, 298 K): δ –1.13 ppm ($Si(CH_3)_3$); 67.30 ($C_{(1,3)}$); 94.20 ($C_{(2)}$); 204.51 (CO).

Reaction of [1,3-$(SiMe_3)_2C_3H_3$]$_2$Co and I_2. A 125 mL Erlenmeyer flask containing a stirring bar was charged with [1,3-$(SiMe_3)_2C_3H_3$]$_2$Co (0.415 g, 0.966 mmol) and 30 mL of hexanes. Iodine (0.247 g, 0.973 mmol) was added and the reaction was stirred overnight. Although no immediate change was observed upon the addition of iodine, the solution eventually turned light yellow with stirring, and a fine suspension of black precipitate was noted. The solution was decanted, and hexanes was removed under reduced pressure leaving a yellow liquid that was identified as 1,3,4,6-tetrakis(trimethylsilyl)-1,5-hexadiene (0.270 g; 76 % yield) by its ^{1}H NMR data.

Reaction of [1,3-$(SiMe_3)_2C_3H_3$]$_2$Co with PMe_3. In a 125 mL Schlenk flask, [1,3-$(SiMe_3)_2C_3H_3$]$_2$Co (0.250 g; 0.586 mmol) was dissolved in hexanes (10 mL). The flask was connected to a glass tube containing [AgI•PMe_3]$_4$ (0.728 g; 0.586 mmol). The cobalt(II) solution was cooled to –78 °C in a dry ice/acetone bath. The glass tube was heated with a heat gun; after the PMe_3 was released, the solution changed in color from a dark orange solution to a dark-red solution. The reaction

was filtered, and hexanes was removed under vacuum leaving a red oil. The oil could not be identified with NMR data (^{1}H and ^{31}P), as the sample is paramagnetic, and only rolling baselines were seen in the spectra.

Reaction of $[1,3\text{-}(SiMe_3)_2C_3H_3]_2Co$ with $P(C_6H_5)_3$. In a 125 mL Erlenmeyer flask, $[1,3\text{-}(SiMe_3)_2C_3H_3]_2Co$ (0.054 g; 0.13 mmol) was dissolved in 20 mL of hexanes. Triphenylphosphine (0.033 g; 13 mmol) was added to the orange $[1,3\text{-}(SiMe_3)_2C_3H_3]_2Co$ solution. The reaction was stirred overnight. No color change was noted upon addition. Hexanes was removed under vaccum to afford a mixture of a white precipitate and an orange oil. Orange crystals grew from the oil and were crystallographically characterized as $[1,3\text{-}(SiMe_3)_2C_3H_3]_2Co$.

Reaction of $[1,3\text{-}(SiMe_3)_2C_3H_3]_2Ni$ and CO. A 125 mL Schlenk flask containing a stirring bar was charged with $[1,3\text{-}(SiMe_3)_2C_3H_3]_2Ni$ (0.147g, 0.342 mmol) and 20 mL of hexanes. A needle was submerged in the solution of $[1,3\text{-}(SiMe_3)_2C_3H_3]_2Ni$, and CO was briskly added for six minutes. The solution was then degassed using freeze-pump-thaw method. The solution was filtered, and hexanes was removed under reduced pressure leaving a red-orange oil (0.144 g; 92% yield) that distilled at 46 °C (10^{-2} Torr). Principle IR bands (KBr pellet, cm^{-1}): 2955 (s), 2898 (m), 2005 (m), 1655 (m), 1619 (s), 1597 (s), 1404 (m), 1341 (m), 1247 (s), 1210 (m), 1099 (s), 1020 (s), 945 (m), 908 (m), 840 (s, br), 753 (m), 690 (m), 637 (m). ^{1}H NMR (300 MHz, C_6D_6, 298 K): δ 0.09 ppm (s, 18H, $Si(CH_3)_3$); 0.099 (s, 18H, $Si(CH_3)_3$); 3.19 (d, $J = 9.6$ Hz, 2H, *syn* C–H); 5.49 (d, $J = 18.9$ Hz, 2H, *anti* C–H); 6.70 (dd, $J = 18.9$ Hz, $J = 9.6$ Hz, 2H, $C_{(2)}$–H). ^{13}C NMR (75 MHz, C_6D_6, 298 K): δ –2.50 ppm ($Si(CH_3)_3$); –1.00 ($Si(CH_3)_3$); 61.10 (*syn* C–H); 128.62 (*anti* C–H); 143.01 ($C_{(2)}$); 204.14 (CO).

Computational Details. Geometry optimization calculations were performed using the GAUSSIAN 03W suite of programs.[42] Both the B3LYP functional, which incorporates Becke's three–parameter exchange functional[43] and the correlation functional of Lee, Yang, and Parr,[44,45] as well as the PW91PW91 functional, which employs the 1991 gradient–corrected functional of Perdew and Wang for both correlation and exchange,[46] were used. The DFT-optimized double zeta polarized basis set DGDZVP2 of Godbout[47] was used for geometry optimizations and energy calculations of the bis(allyl) complexes. The standard Pople basis set 6-31+G(d,p) was used for other calculations.[48] Stationary points were characterized by the calculation of vibrational frequencies, and unless otherwise noted, all geometries were found to be minima ($N_{imag} = 0$).

Use of the PW91PW91 functional in conjunction with the 6-31 + G(d,p) basis set has been shown to predict C–O stretching frequencies of molecules with good accuracy although the predicted values are generally lower than experimental ones by 15–25cm $^{-1}$. This functional/basis set combination was used to calculate ν(CO) for several complexes in this study. Table 7 compares experimental C–O stretching frequencies with calculated ones using PW91PW91/6-31 + G(d,p):

Table 7. Experimental vs. calculated ν(CO) values.

Compound	Experimental ν(CO) (cm^{-1})	Calculated ν(CO) (cm^{-1})
CO	2143	2124
$Fe(CO)_5$	2013, 2034	2007, 2024
$Co_2(CO)_8$	2048, 2076 (terminal)	2036, 2061 (terminal)
$Ni(CO)_4$	2057	2041

Results and Discussion

Reactions of $[1,3\text{-}(SiMe_3)_2C_3H_3]_2M$ (M = Fe, Co, Ni) and CO

The trimethylsilyl-substituted bis(allyl)iron complex, $[1,3\text{-}(SiMe_3)_2C_3H_3]_2Fe$, is the first homoleptic (π-allyl)iron(II) complex to be reported.[25] There have been some mention of carbonyl and phosphine adducts of bis(allyl)iron,[96,114] but no donor-free sample has ever been obtained. In contrast to the unstable $(C_3H_5)_2FeL_2$ species, the thermodynamically stable $[1,3\text{-}(SiMe_3)_2C_3H_3]_2Fe$ has a melting point range of 72–75 °C and can even be sublimed (48 °C/10^{-2} Torr). This 14-electron complex is paramagnetic, with $\mu_{eff} = 2.9–3.0$ BM (210–303 K) and S = 1.[113]

As carbon monoxide was added to the orange solution of $[1,3\text{-}(SiMe_3)_2C_3H_3]_2Fe$, the solution immediately turned dark red. After a few seconds, the solution color quickly progressed from red to yellow. Removal of solvent results in a yellow oil characterized by elemental analysis as $[1,3\text{-}(SiMe_3)_2C_3H_3]_2Fe(CO)_2$. The oil does not crystallize upon standing for weeks at room temperature or low temperature (one week, –40 °C). Although the product oil is stable under a nitrogen

atmosphere, it quickly decomposes in air. Some decomposition is noted in hexanes overnight; a small amount of black precipitate is seen.

In contrast to the 14-electron $[1,3\text{-}(SiMe_3)_2C_3H_3]_2Fe$, the reaction product of $[1,3\text{-}(SiMe_3)_2C_3H_3]_2Fe$ and carbon monoxide is diamagnetic. Several facts can be determined from NMR spectroscopy of the product. First of all, there is none of the coupled allyl dimer in the NMR spectra of this reaction product. It has been shown that (allyl´)metal complexes may undergo decomposition by way of oxidative addition of the allyl´ ligands with reduction of the metal centers.[115,116] The absence of 1,3,4,6-tetrakis(trimethylsilyl)-1,5-hexadiene in the NMR spectra not only proves that this product is thermally stable, but also that the bis(allyl´)iron carbonyl product contains iron in the +2 oxidation state. Two carbonyls must be bound to the iron(II) metal center in order for the resulting complex to be diamagnetic (eq 23).

$$[1,3\text{-}(SiMe_3)_2C_3H_3]_2Fe + CO_{(xs)} \rightarrow [1,3\text{-}(SiMe_3)_2C_3H_3]_2Fe(CO)_2 \qquad (23)$$

Only one set of resonances is seen in the proton NMR spectrum for $[1,3\text{-}(SiMe_3)_2C_3H_3]_2Fe(CO)_2$, which means that there is only one orientation of the allyl ligands (i.e., eclipsed or staggered). The proton NMR spectral pattern (s, s, d, d, dd) is indicative of a syn, anti arrangement of trimethylsilyl groups on the allyl ligands, as observed in the crystallographically characterized $[1,3\text{-}(SiMe_3)_2C_3H_3]_2Fe$.[25] The retention of the syn, anti arrangement of trimethylsilyl moieties is not unusual for reactions of bis(allyl´)metal complexes of first row transition metals. For example, reactions of $[1,3\text{-}(SiMe_3)_2C_3H_3]_2Ni$ with halogens and phosphines result in syn, anti allyl products.[108]

Because there is no parent iron allyl complex that can be used as a reference, a comparison of the NMR data in relation to $[1,3\text{-}(SiMe_3)_2C_3H_3]_2Ni$ and $K[1,3\text{-}(SiMe_3)_2C_3H_3]$ was necessary in order to identify the syn and anti protons and carbons in the NMR spectra of $[1,3\text{-}(SiMe_3)_2C_3H_3]_2Fe(CO)_2$. In $K[1,3\text{-}(SiMe_3)_2C_3H_3]$, the trimethylsilyl substituents are in syn, syn orientations, resulting in a singlet, doublet, triplet pattern in the proton NMR spectrum. The *J* coupling constant for the doublet and triplet is 16 Hz in THF-d_8. The protons on the terminal allyl carbons are anti with respect to the central proton (Figure 19). The value of the *J* coupling constant is an important marker for identifying the anti protons in complexes containing syn, anti allyl ligands.

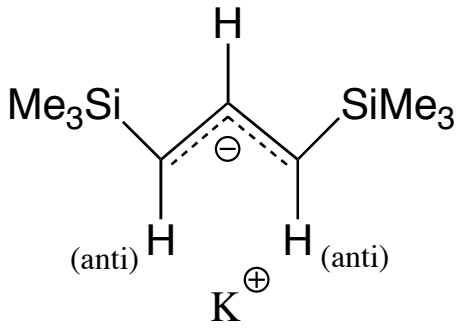

Figure 19. Diagram of $[1,3\text{-}(SiMe_3)_2C_3H_3]K$ depicting anti protons relative to $C_{(2)}$–H.

In the case of $[1,3\text{-}(SiMe_3)_2C_3H_3]_2Ni$ (Figure 20), the allyl ligands have syn, anti trimethylsilyl substituents (see Chapter 1), and the resulting proton NMR spectral pattern is similar to that of $[1,3\text{-}(SiMe_3)_2C_3H_3]_2Fe(CO)_2$ (i.e., s, s, d, d, dd). The terminal allyl protons are syn and anti in correlation to the central proton with the upfield doublet exhibiting the larger *J* coupling constant at 16 Hz (cf., 10 Hz for

downfield doublet). The larger coupling constant corresponds to the anti proton of the allyl ligand. The difference in chemical shifts of the syn and anti protons are reflected in the ^{13}C NMR spectrum for $[1,3\text{-}(SiMe_3)_2C_3H_3]_2Ni$, with the anti proton-bearing allyl carbon positioned upfield from its syn counterpart (correlated using HMQC NMR data).

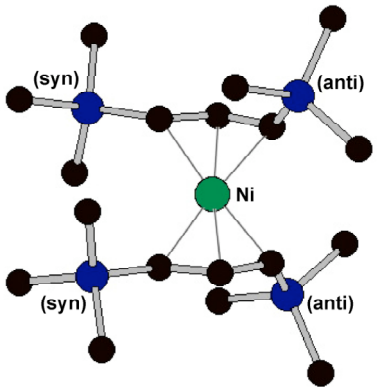

Figure 20. Schematic of $[1,3\text{-}(SiMe_3)_2C_3H_3]_2Ni$ (staggered form shown) depicting syn and anti trimethylsilyl substituents.

The *J* coupling contstants for the two doublets in the proton NMR spectrum of $[1,3\text{-}(SiMe_3)_2C_3H_3]_2Fe(CO)_2$ are both 14 Hz, so the syn and anti protons could not be discerned on the basis of the magnitudes of the *J* values. As this sample is a CO adduct, it may not necessarily mimic the NMR shift trend seen in the bis(allyl′)Ni case (i.e., the upfield anti proton chemical shift positioning relative to the syn proton shift), and it indeed does not (*vide infra*).

Although it may be assumed that the upfield doublet corresponds to the anti protons of the allyl ligands in $[1,3\text{-}(SiMe_3)_2C_3H_3]_2Fe(CO)_2$, the carbon resonance associated with this upfield proton doublet is downfield from the carbon resonance

that is coupled to the downfield syn proton resonance. It is not readily understood why the chemical shifts of the protons and the carbons to which they are attached are conversely positioned relative to each other. There is only one peak in the ^{13}C NMR spectrum for CO (216.84 ppm). Therefore, the two carbonyls in [1,3-$(SiMe_3)_2C_3H_3]_2Fe(CO)_2$ are equivalent on the NMR timescale.

The FT-IR data for the product of [1,3-$(SiMe_3)_2C_3H_3]_2Fe$ and CO is consistent with [1,3-$(SiMe_3)_2C_3H_3]_2Fe(CO)_2$. There are two CO stretching peaks present at 1931 cm^{-1} and 1986 cm^{-1} (Figure 21). Given that the two carbonyls are equivalent according to the ^{13}C NMR data, the two carbonyl peaks in the FT-IR spectrum correspond to asymmetric and symmetric stretching frequencies. These values fall within the limits accepted as terminal carbonyls on transition metals (2150–1850 cm^{-1}) (c.f. 1850–1720 cm^{-1}, doubly bridging; 1720–1600 cm^{-1}, triply bridging).[97]

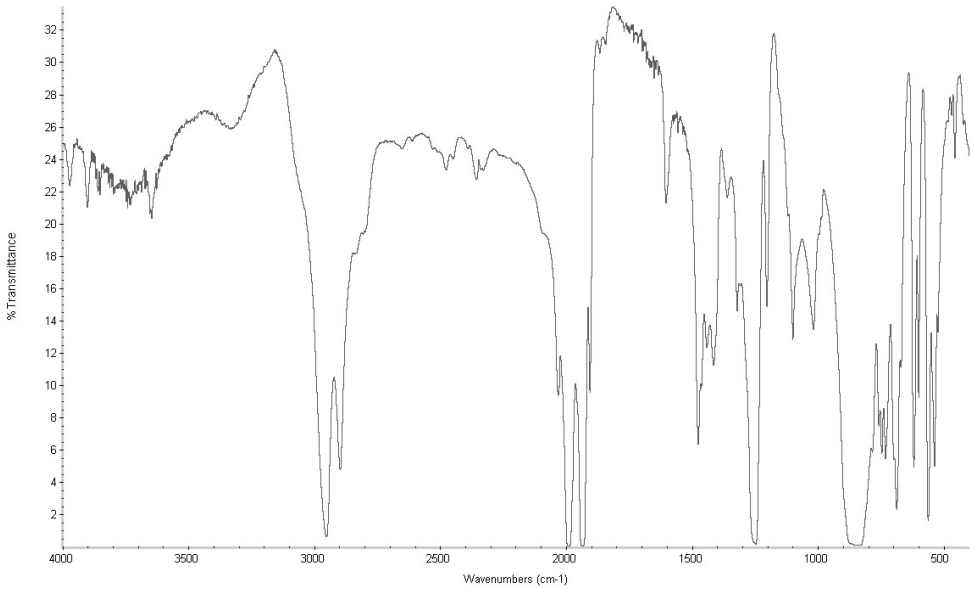

Figure 21. FT-IR spectrum of $[1,3\text{-}(SiMe_3)_2C_3H_3]_2Fe(CO)_2$ with CO stretching frequencies (1931 cm^{-1} and 1986 cm^{-1}).

When discussing the possible allyl bonding motif in $[1,3\text{-}(SiMe_3)_2C_3H_3]_2Fe(CO)_2$, it is important to note that $[1,3\text{-}(SiMe_3)_2C_3H_3]_2Fe$ has been structurally characterized as an eclipsed structure, as this conformation may affect the structure in the resulting carbonyl adduct. Consequently, $[1,3\text{-}(SiMe_3)_2C_3H_3]_2Fe$ is one of only two known eclipsed bis(allyl´) transition metal species (cf. eclipsed $[1,3\text{-}(SiMe_3)_2C_3H_3]_2Ni$).[108] Whereas the nickel analog has both eclipsed and staggered structures (see Chapter 1), the iron complex has no known staggered conformer. However, this does not necessarily mean that a staggered $[1,3\text{-}(SiMe_3)_2C_3H_3]_2Fe$ cannot form; it may just mean that crystals of this conformation have not been isolated and structurally characterized. DFT calculations (B3LYP/DGDZVP2) were run on a staggered confomation for comparison to the known eclipsed one (Figure 22).

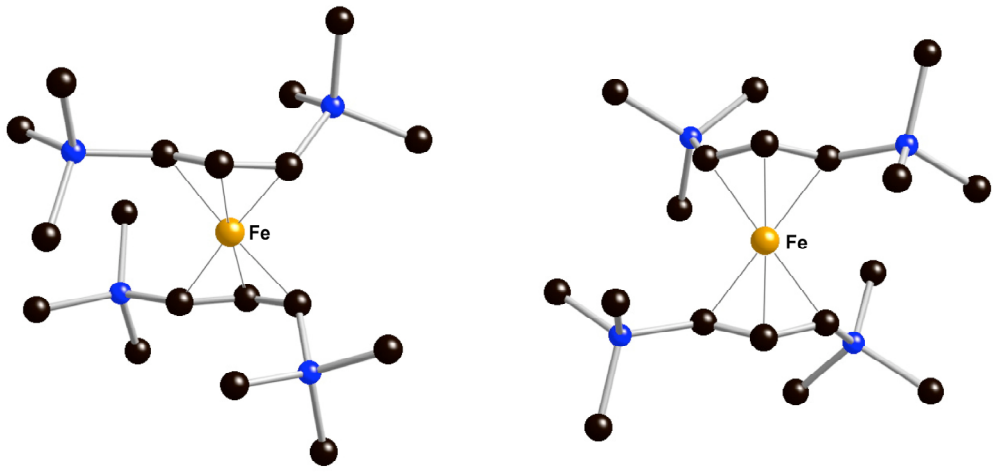

Figure 22. Calculated structures of both staggered (left) and eclipsed (right) $[1,3\text{-}(SiMe_3)_2C_3H_3]_2Fe$.

The eclipsed conformer is only slightly preferred over the staggered one by 1.1 kcal/mol in ΔG° (2.3 kcal/mol in ΔH°). The calculated eclipsed structure (based on the starting geometry of the crystal structure) has Fe–C bonds ranging 2.026–2.118 Å, and an allyl plane angle of 49.6°. These values are close to those reported for the crystal structure (Fe–C = 1.998(2)–2.084(2) Å; allyl plane angle = 52.7°).[25] The calculated staggered $[1,3\text{-}(SiMe_3)_2C_3H_3]_2Fe$ structure has slightly longer Fe–C bonds ranging 2.058–2.152 Å, and an allyl plane angle of 6.2°. This calculated allyl plane angle fits a trend of decreasing values for the experimental allyl plane angles in staggered $[1,3\text{-}(SiMe_3)_2C_3H_3]_2M$ (M = Co,Ni) complexes (cf. 5.5° for Co;[26] 4.6° for Ni).[108]

Because either allyl conformation (eclipsed or staggered) may be plausible for a bis(allyl˙)Fe complex based on DFT calculations, both eclipsed and staggered $(C_3H_5)_2Fe(CO)_2$ complexes (Figure 23) were studied using DFT (PW91PW91/6-

31+G(d,p)). The DFT calculation of eclipsed $(C_3H_5)_2Fe(CO)_2$ shows that it has zero imaginary frequencies, indicating the structure is at least a local minimum on the potential energy surface.[117] The calculated CO stretching frequencies of 1958 cm^{-1} (asymmetric) and 1999 cm^{-1} (symmetric) are within the range of terminal CO values (2150–1850 cm^{-1}).[97] These calculated values are close to the experimental CO stetching frequencies (1965, 2020 cm^{-1}) reported for $(C_3H_5)_2Fe(CO)_2$.

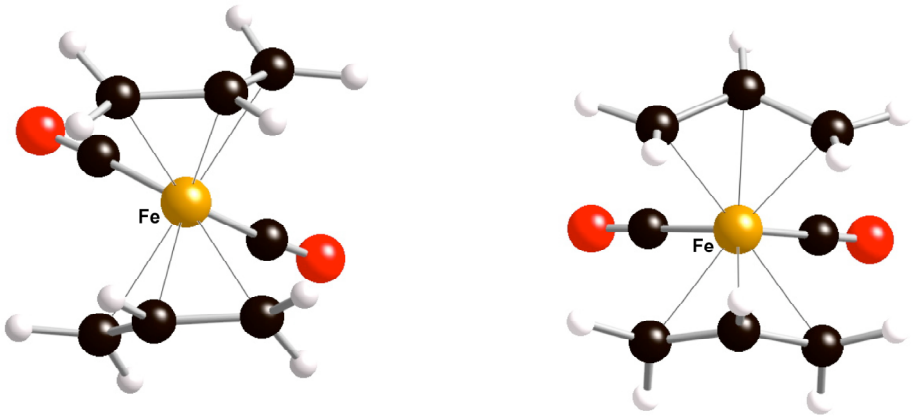

Figure 23. Calculated structures of eclipsed (left) and staggered (right) $(C_3H_5)_2Fe(CO)_2$.

The calculated Fe–C(allyl) bond lengths range from 2.055–2.177 Å, and the Fe–CO bond length is 1.763 Å (cf. Fe–CO bond length in $Fe(CO)_5$ is 1.82 Å (av)).[118] The Fe–C bond lengths are slightly longer than those reported for $[1,3\text{-}(SiMe_3)_2C_3H_3]_2Fe$ due to the extra steric crowding around the iron(II) center. The allyl bending angle is 7.9°, however the allyl ligands have rotated by 64.5° relative to each other. The two CO ligands are also twisted relative to the allyl plane by 31.0°. All of this rearrangement serves to maximize ligand–iron bonding while minimizing unfavorable intramolecular contacts.

Since the calculated eclipsed structure was somewhat twisted from its initial geometry, a more symmetrical eclipsed structure (C_s symmetry) was also computationally studied (Figure 24). Unlike the twisted eclipsed monomer, this structure had one imaginary frequency (–101 cm^{-1}), identifying it as a transition state structure. As expected, this structure has two CO stretching frequencies (1952 cm^{-1}, asymmetric; 1997 cm^{-1}, symmetric) in the terminal CO stretching range. The Fe–C(allyl) bond lengths (2.047–2.135 Å) and the Fe–CO bond length (1.761 Å) are shorter than those of the twisted eclipsed structure, but the angle between the allyl planes (25.5°) is larger. The C_s-symmetric eclipsed structure is higher in energy than the C_1-symmetric structure by 10.7 kcal/mol in ΔG° (by 9.6 kcal/mol in ΔH°), consistent with it representing a transition state geometry.

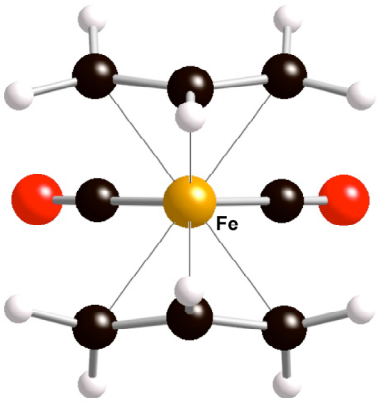

Figure 24. Calculated structure of eclipsed $(C_3H_5)_2Fe(CO)_2$ (C_s symm; $N_{imag} = 1$).

The calculated staggered $(C_3H_5)_2Fe(CO)_2$ also has one imaginary frequency (–95 cm^{-1}), meaning that this structure also represents a transition state. The two CO stretching frequencies, 1950 cm^{-1} (asymmetric) and 1999 cm^{-1} (symmetric), in

this structure are nearly identical with those of the twisted eclipsed form. The Fe–C(allyl) bond lengths (2.026–2.140 Å) are shorter than those of the twisted eclipsed structure, but the Fe–CO bond length (1.775 Å) is slightly longer; the angle between the allyl planes is 65.7°. The calculated staggered conformer is higher in energy the the twisted eclipsed one by 10.3 kcal/mol in ΔG° (by 9.4 kcal/mol in ΔH°). Interestingly, the calculated staggered structure and the C_s-symmetric eclipsed structure are nearly identical in energies.

Based on NMR data, FT-IR data, and the fact that the proposed staggered $(C_3H_5)_2Fe(CO)_2$ conformer was calculated to be a transition state structure, the proposed structure for $[1,3\text{-}(SiMe_3)_2C_3H_3]_2Fe(CO)_2$ is one of eclipsed allyl ligands with syn, anti $SiMe_3$ groups (Figure 25). The carbonyls are attached to the iron(II) metal center at the 'open face' of the complex; the 'open face' orientation of carbonyls, positioned distal in relation to carbon 2, allows the allyl ligands to bend in a way that reduces steric congestion around the metal center while accepting CO adduction.

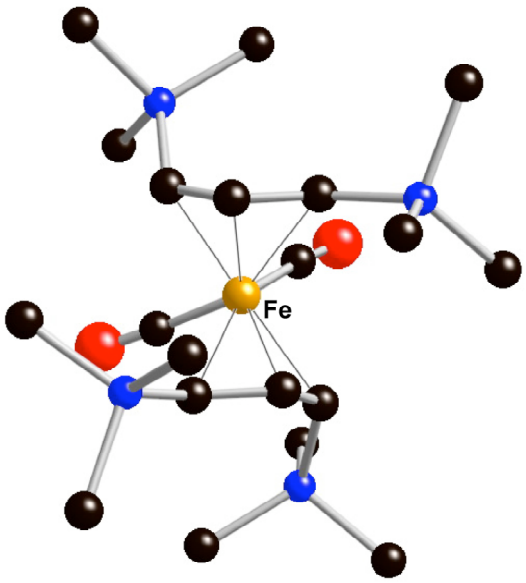

Figure 25. Calculated structure of $[1,3\text{-}(SiMe_3)_2C_3H_3]_2Fe(CO)_2$.

A DFT calculation (PW91PW91/6-31+G(d,p) of the eclipsed $[1,3\text{-}(SiMe_3)_2C_3H_3]_2Fe(CO)_2$ shows that it, like the calculated parent analog, has zero imaginary frequencies, indicating the structure is at least a local minimum on the potential energy surface. The calculated CO stretching frequencies of 1939 cm^{-1} (asymmetric) and 1977 cm^{-1} (symmetric) are somewhat lower than those calculated for the parent structure, but still within the range of terminal CO values. The lower values for the CO stretching frequencies point to increased electron donation from the allyl ligands to the iron center in the substituted case, which results in better π-donation to the CO ligands. These values are close to the experimental values of the CO stretching frequencies (1931, 1987 cm^{-1}) for $[1,3\text{-}(SiMe_3)_2C_3H_3]_2Fe(CO)_2$.

The calculated Fe–C(allyl) bond length lengths (2.069–2.260 Å) are slightly longer than those calculated for the parent, and this serves to relieve steric crowding between the allyls. These values are also longer than those seen in the solid state-structure of $[1,3\text{-}(SiMe_3)_2C_3H_3]_2Fe$[25] (Fe–C(allyl) = 1.998(2)–2.084(2) Å), because of the more coordinatively saturated metal center in the carbonyl adduct. The calculated Fe–CO bond length is shortened to 1.756 Å, which is close to the values reported for $(C_3H_5)Fe(CO)_3Br$ (av Fe–CO = 1.79 Å).[119] Again, this shortening may be ascribed to increased π-donation from the iron center in $[1,3\text{-}(SiMe_3)_2C_3H_3]_2Fe(CO)_2$ relative to $(C_3H_5)Fe(CO)_3Br$. The allyl bending angle (25.0°) is larger than that seen for the calculated parent structure, but smaller than that of $[1,3\text{-}(SiMe_3)_2C_3H_3]_2Fe$ (52.7°); however, the allyl ligands have rotated by 52.6° relative to each other, and the two CO ligands are twisted relative to the allyl plane by 26.0°. Both of these values are smaller for the trimethylsilyl-substituted allyl complex than for the parent allyl complex. These differences are consequences of the difference in ligand size and steric hindrance among the complexes.

There have been no reports for the synthesis of a homoleptic $(C_3H_5)_2Co$ complex, although the tris(allyl) species, $(C_3H_5)_3Co$, is known.[120] Tris(allyl)cobalt is an 18-electron complex that is thermodymically unstable, decomposing at –40°C. Even though $(C_3H_5)_3Co$ is not robust, it has found use in dehydrogenation reactions[3] and polymerization reactions of alkenes[89,121] and butadienes.[122,123] The bulky $[1,3\text{-}(SiMe_3)_2C_3H_3]_2Co$ was first discovered by the Hanusa group. The addition of one or two equivalents of $K[1,3\text{-}(SiMe_3)_2C_3H_3]$ to CoI_2 results in its formation; this tendency to form bis(allyl)species regardless of reaction stoichiometry has also been seen using other metal halides.[124] This 15-electron

species (μ_{eff} = 1.8 BM (298 K); S = 1/2) was found to be stable at room temperature,[26] has a melting point of 73 °C, and can be sublimed (50 °C, 10^{-2} Torr). In contrast to the high catalytic activity of $(C_3H_5)_3Co$, $[1,3\text{-}(SiMe_3)_2C_3H_3]_2Co$ shows low catalytic behavior for polymerization reactions (e.g., norbornene polymerization).[87]

As carbon monoxide was added to the orange solution of $[1,3\text{-}(SiMe_3)_2C_3H_3]_2Co$, the solution immediately turned dark red and then progressed from red to orange after several seconds. Removal of solvent results in an orange oil, from which colorless crystals grew over several days at room temperature. These crystals were crystallographically determined to be 1,3,4,6-tetrakis(trimethylsilyl)-1,5-hexadiene. As observed in the case of $[1,3\text{-}(SiMe_3)_2C_3H_3]_2Fe(CO)_2$, the cobalt product is stable under a nitrogen atmosphere although it quickly decomposes in air. Like $[1,3\text{-}(SiMe_3)_2C_3H_3]_2Fe(CO)_2$, some decomposition is noted in solution overnight, as a small amount of black precipitate is present.

The reaction product is diamagnetic, and the NMR data of this reaction product is informative. In contrast to the reaction of $[1,3\text{-}(SiMe_3)_2C_3H_3]_2Fe$ and CO (see eq 23), the formation of the coupled allyl dimer 1,3,4,6-tetrakis(trimethylsilyl)-1,5-hexadiene is noted in addition to the cobalt allyl species in the proton and ^{13}C NMR spectra (approx. 1:1 ratio). The presence of coupled allyl dimer signifies that an oxidation state change has occurred on the cobalt metal center. The cobalt center has been reduced to Co(I) as the allyl ligands oxidatively couple. Since the cobalt product is diamagnetic, three carbonyls must to be present on the metal center (eq24).

$$[1,3\text{-}(SiMe_3)_2C_3H_3]_2Co + CO_{(xs)} \rightarrow [1,3\text{-}(SiMe_3)_2C_3H_3]Co(CO)_3 + 1/2\ [(SiMe_3)_2C_3H_3]_2 \quad (24)$$

The mechanism of cobalt(II) reduction to cobalt(I) is presumed to be intermolecular, as an intramolecular mechanism would result in the formation of cobalt(0), and there is no evidence for its formation.

There is precedent for the oxidative coupling of allyl ligands in the presence of carbon monoxide in the literature.[1,2] Although an excess of donor ligand can result in insertion reactions, coupling of the allyl fragments along with metal reduction is usually observed (e.g., $(C_3H_5)_2Ni$, [92] $(C_3H_5)_3Co$[116] (eqs25 and 26).

$$(C_3H_5)_2Ni + 4L \rightarrow \text{hexadiene} + NiL_4 \quad (25)$$

$$(C_3H_5)_3Co + 3L \rightarrow \text{hexadiene} + (C_3H_5)CoL_3 \quad (26)$$

Although $(C_3H_5)Co(CO)_3$ is reported to be a stable oil at room temperature, tris(allyl)cobalt is stable only at low temperature (< –50 °C).[116] In the case of $[1,3\text{-}(SiMe_3)_2C_3H_3]_2Co$, the reduction of Co(II) is incomplete, resulting in an (allyl)cobalt(I) carbonyl complex (see eq 24).

Interestingly, there are two different cobalt(I) allyl species present that can be identified from the NMR data. One of the species has the typical proton NMR spectral pattern associated with trimethylsilyl groups in syn and anti positions on the allyl ligands (i.e., s, s, d, d, dd). The two sets of doublets at 2.30 ppm and 3.10 ppm have *J*coupling constants of 12.9 and 8.7 Hz, respectively. As observed in the

proton NMR spectrum of [1,3-$(SiMe_3)_2C_3H_3]_2Ni$, the upfield doublet resonance, with its larger *J* value, is considered to reflect the anti proton position, while the downfield one is associated with the syn protons. The corresponding carbons coupled to the syn and anti protons in the Co(I) species also follow this trend in the ^{13}C NMR spectrum.

The other cobalt(I) allyl species present has an NMR spectral pattern typical of allyl ligands with trimethylsilyl substituents in syn, syn positions (i.e., s, d, t). The *J* coupling constant of 12.3 Hz, for the doublet and triplet resonances is smaller than that either for K[1,3-$(SiMe_3)_2C_3H_3$] (15.6 Hz) or for the anti proton *J* value for [1,3-$(SiMe_3)_2C_3H_3]_2Ni$ (16 Hz), but is similar to the anti proton *J* value for the syn, anti cobalt(I) allyl species. The ratio of the syn, syn species to the syn, anti species in the proton NMR spectra is variable from sample to sample, with the syn, syn one being the major product (note that the syn form is also the major one in (crotyl)$Co(CO)_3$).[116] It is not readily understood what factors affect the formation of one form over the other. DFT calculations have been run in order to better understand the energetic differences of the two systems (see below).

The ^{13}C NMR spectrum shows one broad peak at 204.51 ppm that corresponds to coordinated CO. The fact that there is one broad peak indicates that the CO ligands are in fast exchange, and the CO environments of the two cobalt(I) allyl species are nearly equivalent.

The FT-IR data for this sample exhibits carbonyl peaks at 1984 and 2053 cm^{-1} (Figure 26). The carbonyl resonances are not symmetrical in shape, as the peak at 1984 cm^{-1} is much broader than the sharp peak at 2053 cm^{-1}. The broad

CO peak may be the result of two closely spaced peaks that are unresolved in the FT-IR spectrum of [1,3-$(SiMe_3)_2C_3H_3$]$Co(CO)_3$.

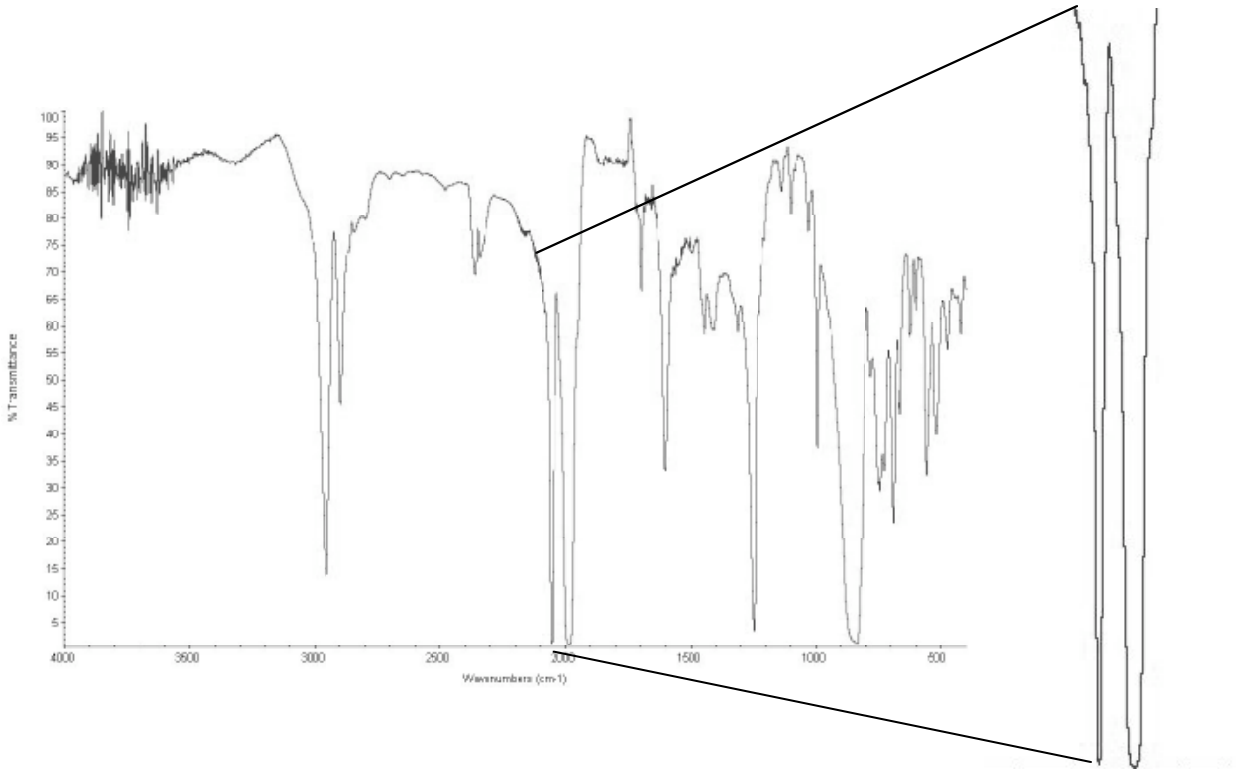

Figure 26. FT-IR spectrum of [1,3-$(SiMe_3)_2C_3H_3$]$Co(CO)_3$ with CO stretching frequencies (1984 cm^{-1} and 2053 cm^{-1}). CO stretching peaks are expanded for clarity.

DFT calculations (PW91PW91/6-31+G(d,p)) were performed on both the syn, syn and syn, anti [1,3-$(SiMe_3)_2C_3H_3$]$Co(CO)_3$ proposed structures; in the case of the syn, syn conformer, a C_s-symmetric structure and one with no symmetry (C_1) were compared. The syn, syn trimethylsilyl-substituted allyl cobalt(I) tricarbonyl bearing a mirror plane is a transition state structure ($N_{imag} = 1$) and is slightly higher in energy than the one with C_1 symmetry (Figure 27) by 2.0 kcal/mol in ΔG°

although it is 0.47 kcal/mol lower in ΔH°. However, the three calculated CO stretching frequencies for these two structures are identical at 1979 (asymmetric), 1987 (asymmetric), and 2038 cm^{-1} (symmetric). These calculated values are close to the experimental CO stretching frequencies in $[1,3\text{-}(SiMe_3)_2C_3H_3]Co(CO)_3$ (1984 cm^{-1} and 2053 cm^{-1}), taking into account that the two asymmetric stretching frequencies may be overlapping to produce the observed broad peak at 1984 cm^{-1}.

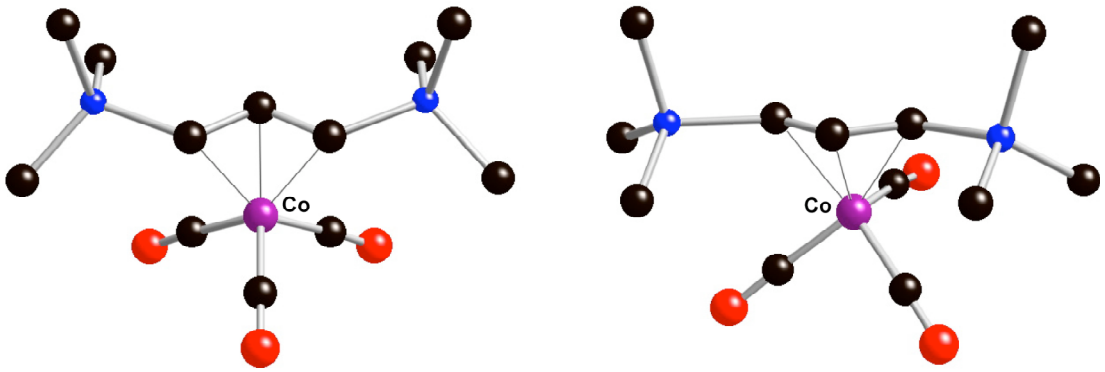

Figure 27. Calculated structures of syn, syn $[1,3\text{-}(SiMe_3)_2C_3H_3]Co(CO)_3$ (left, C_s; right C_1).

In comparison, the experimental C–O stretching frequencies for $(C_3H_5)Co(CO)_3$ are 1998 cm^{-1} (asymmetric) and 2065 cm-1 (symmetric).[125] These frequencies are larger than those of the trimethylsilyl-substituted analog because less π-donation to the π* orbital of CO occurs in $(C_3H_5)Co(CO)_3$, resulting in stronger C–O bonds and larger ν(CO) values. A DFT calculation (PW91PW91/6-31+G(d,p)) of $(C_3H_5)Co(CO)_3$ predicts the C–O stretching frequencies of 1996 cm^{-1}

(asymmetric), 1998 cm^{-1} (asymmetric), and 2053 cm^{-1} (symmetric). This example also shows that three calculated ν(CO) values can be obtained for two experimental ν(CO) values.

The Co–C(allyl) bond lengths range from 2.026–2.164 Å in the C_s structure and 2.028–2.181 Å in the C_1 structure; both ranges are longer than that of the solid-state structure of [1,3-$(SiMe_3)_2C_3H_3$]Co (cf. 1.996(3)–2.096(3) Å).[26] The Co–CO bond lengths are also nearly identical in both calculated structures (1.766–1.806 Å in the C_s structure; 1.762–1.802 Å in the C_1 structure). These values are typical for Co(I)–CO bond lengths, as seen in $(CO)_3Co[(CH_2)_2CCH_2]_2$, for which Co–CO bond lengths range from 1.69(1) Å to 1.815(2) Å[100] (cf. the terminal Co–CO bond length range for $Co_2(CO)_8$ is 1.815(2)–1.836(2) Å).[126] The Co–CO bond length difference in (allyl)cobalt carbonyl complexes is proposed to be a consequence of π-bonding between the metal center and allyl ligand.[127,128]

The calculated syn, anti [1,3-$(SiMe_3)_2C_3H_3$]$Co(CO)_3$ structure (Figure 28) is higher in energy than the lowest energy syn, syn structure (C_1) by 1.79 kcal/mol in ΔG° and 0.25 kcal/mol in ΔH°. These values make the syn, anti structure nearly equienergetic with the syn, syn structure of C_s symmetry. The syn, anti [1,3-$(SiMe_3)_2C_3H_3$]$Co(CO)_3$ has three C–O stretching frequencies at 1978 cm^{-1} (asymmetric), 1985 cm^{-1} (asymmetric), and 2038 cm-1 (symmetric) (Table 8). The fact that all syn, anti calculated structures have nearly exactly the same C–O stretching frequencies is not surprising considering the steric bulk of the allyl ligands are the same for all the structures. The Co–C(allyl) bond length range in the syn, anti structure is 2.027–2.149 Å and the Co–CO bond lengths are 1.763–1.800 Å, making them only slightly shorter than those calculated for the syn, syn structures.

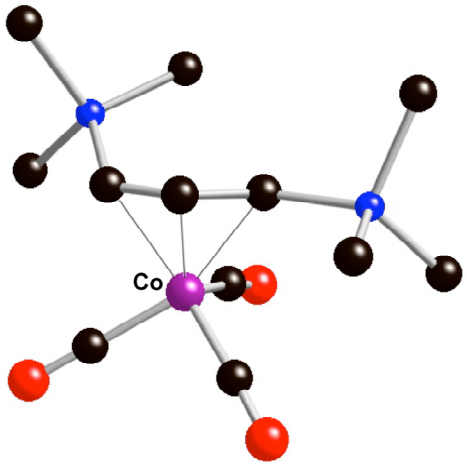

Figure 28. Calculated structure of syn, anti [1,3-$(SiMe_3)_2C_3H_3$]Co$(CO)_3$.

Table 8. Calculated thermodynamic values and ν(CO) for [1,3-$(SiMe_3)_2C_3H_3$]Co$(CO)_3$ conformers.

[1,3-$(SiMe_3)_2C_3H_3$]Co$(CO)_3$	ΔH° (kcal/mol)	ΔG° (kcal/mol)	calc. ν(CO) (cm^{-1})
syn, syn confomer (C_1)	0.00	0.0	1979,1987,2038
syn, syn confomer* (C_s)	–0.5	2.0	1979,1987,2038
syn, anti confomer (C_1)	0.2	1.8	1978,1985,2038

* $N_{imag} = 1$

The diamagnetic starting material [1,3-$(SiMe_3)_2C_3H_3]_2$Ni is described in Chapter 1 and will not be discussed here. As carbon monoxide was added to the dark red solution of [1,3-$(SiMe_3)_2C_3H_3]_2$Ni, the solution lightened in color to yellow-brown. Removal of solvent results in a brown oil that solidifies over a period of days. The nickel product is stable under a nitrogen atmosphere although it

decomposes in air. Unlike the iron and cobalt carbonyl species, no decomposition is noted for the nickel carbonyl product in solution overnight.

The product is diamagnetic with a set of resonances that are indicative of trimethylsilyl substituents on the allyl ligands in syn, anti positions (i.e., s, s, d, d, dd). Only one set of resonances is seen in the NMR data, which means that there is only one isomer present. The absence of any coupled allyl dimer peaks in the NMR data points to the retention of the Ni(II) oxidation state and the stability of this complex.

In the proton NMR spectrum, the two sets of doublets at 3.19 ppm and 5.49 ppm have *J* coupling constants of 9.6 Hz and 18.9 Hz, respectively. Since the proton resonance for the allyl framework's anti proton of $[1,3\text{-}(SiMe_3)_2C_3H_3]_2Ni$ has been associated with a larger *J* value than the one of its syn proton, the proton resonance at 5.49 is assigned to the anti proton in $[1,3\text{-}(SiMe_3)_2C_3H_3]_2NiCO$. Interestingly, this peak position is downfield from the resonance for the syn proton in this sample, making the relative positions of the peaks opposite of what is reported for $[1,3\text{-}(SiMe_3)_2C_3H_3]_2Ni$.[108]

The ^{13}C NMR peaks that are coupled to the corresponding proton peaks also follow the trend of upfield syn and downfield anti positions for the bis(allyl´)nickel carbonyl product. There is one peak in the ^{13}C NMR spectrum that corresponds to CO. Although one CO peak in the ^{13}C NMR spectra signified equivalent CO adducts in the cases of the iron and cobalt allyl complexes, one peak represents one CO in the case of the nickel complex; $[1,3\text{-}(SiMe_3)_2C_3H_3]_2Ni$ is a 16-electron species, and the addition of two or more CO ligands would be electronically unfavorable.

The FT-IR data for $[1,3\text{-}(SiMe_3)_2C_3H_3]_2NiCO$ contains one CO stretching frequency at 2005 cm^{-1} (Figure 29). This value is within the range of terminal CO ligands. The fact that there is only one CO stretch further corroborates the conclusion that only one CO is present on the Ni(II) metal center.

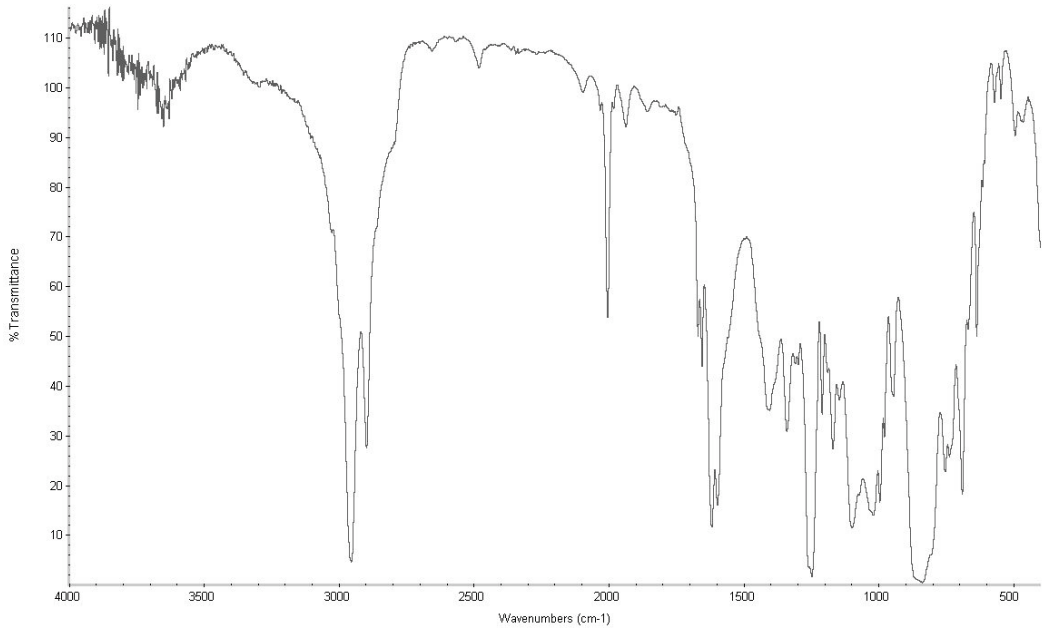

Figure 29. FT-IR spectrum of $[1,3\text{-}(SiMe_3)_2C_3H_3]_2NiCO$ with CO stretching frequency (2005 cm^{-1}).

DFT calculations (PW91PW91/6-31+G(d,p)) on an eclipsed and staggered $(C_3H_5)_2NiCO$ were run to see how favorable the eclipsed allyl bonding motif is over the staggered one for a bis(allyl′)Ni carbonyl complex. The eclipsed bonding motif of $(C_3H_5)_2NiCO$ has been seen in the structurally characterized $(C_3H_5)_2NiPMe_3$ complex (Figure 30),[5] so this motif is expected for a carbonyl adduct. For the $(C_3H_5)_2NiPMe_3$ complex, the eclipsed allyl ligands exhibit a

bending angle of 3.6° and a Ni–C bonding range of 1.998(5)–2.092(5) Å (cf. the allyl bending angle of 49.1° and Ni–C bonding range of 1.994(3)–2.037(3) Å is seen in the eclipsed $[1,3\text{-}(SiMe_3)_2C_3H_3]_2Ni$).[108]

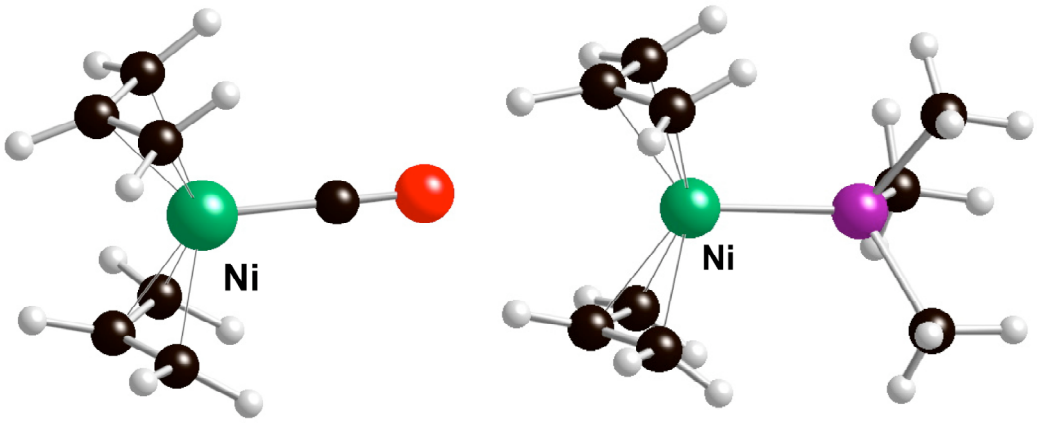

Figure 30. Eclipsed allyl bonding motif seen in the calculated structure $(C_3H_5)_2NiCO$ (left) and the crystal structure of $(C_3H_5)_2NiPMe_3$ (right).

The DFT calculation of eclipsed $(C_3H_5)_2NiCO$ shows that the eclipsed structure has zero imaginary frequencies, indicating the structure is at least a local minimum on the potential energy surface.[117] The calculated C–O stretching frequency of 2002 cm^{-1} is within the normal range of terminal CO values (2150–1850 cm^{-1}).[97] The calculated Ni–C(allyl) distances range from 2.012–2.091 Å, the Ni–CO bond length is 1.790 Å, and the allyl bending angle is 7.9°.

The Ni–C(allyl) bond lengths and allyl bending angle are close to those of the trimethylphosphine adduct of bis(allyl)nickel. The reduction in the allyl bending angles observed in the calculation of the CO-adducted complex (and observed in the structurally authenticated $(C_3H_5)_2NiPMe_3$) versus that calculated for the parent

eclipsed bis(allyl)nickel (59.8°)[108] may be a consequence of orbital mixing. As the square planar bis(allyl)nickel becomes a square pyramidal donor adduct complex, the allyl ligands may shift to improve the bonding with the nickel metal center, thus altering the angle of the allyl planes.

Like the DFT calculation of the eclipsed $(C_3H_5)_2NiCO$, the DFT calculation of the staggered conformer (Figure 31) also results in a structure with no imaginary frequencies, indicating the structure is an energy minimum. The calculated CO stretching frequency of 1995 cm^{-1} is lower than that calculated for the eclipsed structure, but is still within the range of terminal CO values. The Ni–C(allyl) bond range for the calculated staggered structure is 1.986–2.108 Å, which is similar to that of the solid-state structure of $(C_3H_5)_2Ni$ (1.980(1)–2.031(1) Å).[19] The Ni–CO bond length is 1.813 Å, and the angle of the allyl planes is 54.4°. The eclipsed form is slightly more stable than the staggered one by 3.5 kcal/mol in ΔG° (by 4.0 kcal/mol in ΔH°).

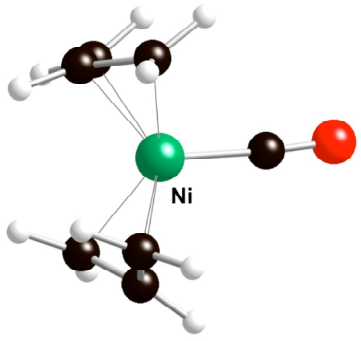

Figure 31. Calculated structure of staggered $(C_3H_5)_2NiCO$.

A DFT calculation (PW91PW91/6-31+G(d,p)) was run on the eclipsed $[1,3\text{-}(SiMe_3)_2C_3H_3]_2NiCO$ (Figure 32). The calculated CO stretching frequency of 1980

cm^{-1}, like its calculated parent analog, is within the range of terminal CO values, albeit lower in value due to better π-donation in the substituted species. This calculated value is close to the experimental C–O stretching frequency measured for $[1,3\text{-}(SiMe_3)_2C_3H_3]_2NiCO$ (2002 cm^{-1}). The only other bis(allyl)NiCO complex reported in the literature displays C–O stretching frequency of 2000 cm^{-1}.[92]

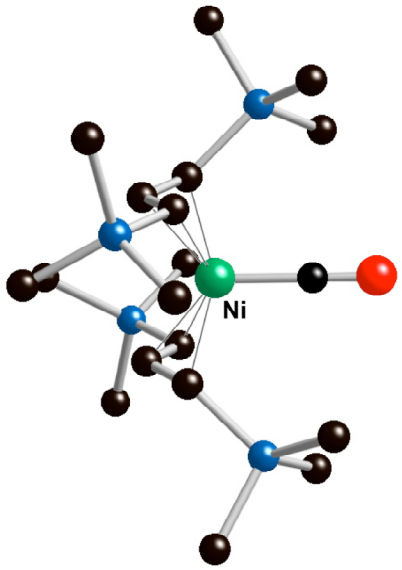

Figure 32. Calculated structure of eclipsed $[1,3\text{-}(SiMe_3)_2C_3H_3]_2NiCO$.

The calculated Ni–C(allyl) bonding range (2.026–2.176 Å) and the allyl bending angle (12.2°) are somewhat larger than those calculated for the parent species; this increase in values reflects the increased steric strain imparted by the trimethylsilyl-substituted allyl ligands. The calculated bond lengths are also longer than those of the solid-state structure of $[1,3\text{-}(SiMe_3)_2C_3H_3]_2Ni$ (1.944(3)–2.037(3) Å), although the calculated allyl bending angle (12.2°) is smaller (cf. 49.1° in [1,3-

$(SiMe_3)_2C_3H_3]_2Ni$ (exp.)).[108] However, the Ni–CO bond length is 1.785 Å for this species, which is nearly identical with that of the calculated parent structure and shorter than that of $Ni(CO)_4$ (1.84 Å).[118]

The Ni–CO bond is shorter in $[1,3\text{-}(SiMe_3)_2C_3H_3]_2NiCO$ because of the increased π-donation to the CO ligands from the metal center in this complex. Since π-donation from the metal center to CO puts electron density into a π* CO orbital,[118] the C–O bond itself is weakened in $[1,3\text{-}(SiMe_3)_2C_3H_3]_2NiCO$ relative to $Ni(CO)_4$, as seen in the ν(CO) values (i.e., 2002 cm^{-1} and 2057 cm^{-1}, respectively).

A DFT calculation (PW91PW91/6-31+G(d,p)) was also run on the staggered $[1,3\text{-}(SiMe_3)_2C_3H_3]_2NiCO$ (Figure 33). This calculated structure has one imaginary frequency (–21 cm^{-1}) and is higher in energy than the eclipsed one by 11 kcal/mol in ΔG° and 10 kcal/mol in ΔH°. The calculated staggered form has one CO stretching frequency at 1980 cm^{-1} ; this value is identical to the one of the eclipsed form. The Ni–C(allyl) bond lengths are 1.998–2.231 Å and the Ni–CO bond length is 1.817 Å, making them only slightly longer than those calculated for the eclipsed structure.

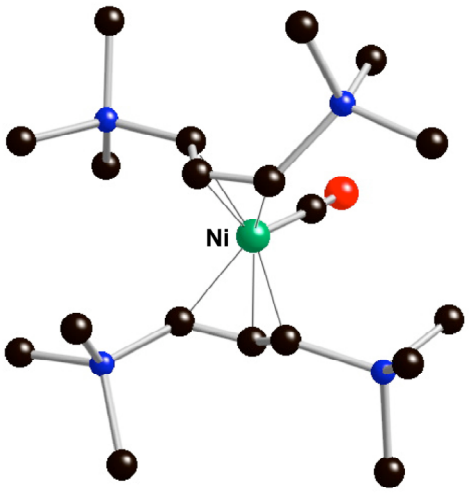

Figure 33. Calculated structure of the staggered [1,3-$(SiMe_3)_2C_3H_3]_2NiCO$.

Based on NMR data, FT-IR data, and calculations, the proposed structure of [1,3-$(SiMe_3)_2C_3H_3]_2NiCO$ is the eclipsed form (see Figure 32), where the CO ligand is bound on the 'open face' side, as seen in the previous donor-adduct examples. The 'open face' binding of CO may be a result of reduced steric strain imparted by the allyl ligands adopting an eclipsed geometry with the CO ligand bound to the metal center distal to the apices of the allyl ligand.

Reactions of [1,3-$(SiMe_3)_2C_3H_3]_2M$ (M = Fe, Co, Ni) and I_2

Halogen addition[6] (eq 27) has been proven to be a good way to synthesize heteroleptic (π-allyl)nickel species.

$$(C_3H_5)_2Ni + X_2 \ \ (X = I, Br) \rightarrow \ C_3H_5X + (C_3H_5)NiX \qquad (27)$$

These reaction products are purportedly dimers in solution; in agreement with this, the reaction of $[1,3\text{-}(SiMe_3)_2C_3H_3]_2Ni$ with iodine (or bromine) leads to the formation of the structurally characterized $[[1,3\text{-}(SiMe_3)_2C_3H_3]NiX]_2$ (X = I, Br)[108] (see Chapter 1). It was thought that similar reactions with $[1,3\text{-}(SiMe_3)_2C_3H_3]_2M$ (M = Fe, Co) would also lead to heteroleptic complexes. However, the addition of I_2 to either the bis(allyl´)iron(II) or bis(allyl´)cobalt(II) (eq 28) results in the formation of the coupled allyl dimer, 1,3,4,6-tetrakis(trimethylsilyl)-1,5-hexadiene and insoluble black precipitates, presumably FeI_2 and CoI_2, respectively.

$$[1,3\text{-}(SiMe_3)_2C_3H_3]_2M\ (M = Fe, Co) + I_2 \rightarrow [1,3\text{-}(SiMe_3)_2C_3H_3]_2 + MI_2 \quad (28)$$

The synthesis of the trimethylsilylated coupled allyl dimer has also been observed in the reaction of electrophiles such as iodine with $[1,3\text{-}(SiMe_3)_2C_3H_3]_2Ca$.[124] Since there is no report of the addition of iodine to $(C_3H_5)_3Fe$ in the literature (and $(C_3H_5)_2Fe$ itself has never been synthesized), there are no examples for comparison to the reaction of $[1,3\text{-}(SiMe_3)_2C_3H_3]_2Fe$ and iodine. However, it is not clear why the addition of iodine induces the bis(allyl´)cobalt(II) species to undergo oxidative allyl coupling because it has been reported that the addition of iodine to $(C_3H_5)_3Co$ forms $(C_3H_5)_2CoI$ (eq 29).[129]

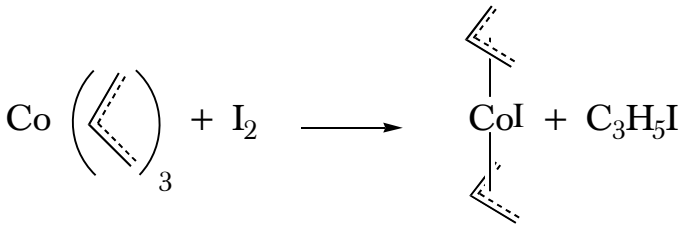

(29)

The bis(allyl)cobalt halide products can also be obtained by addition of HX (X = Cl, Br, I) to tris(allyl)cobalt.[103] These Co(III) complexes, which would be 16-electron monomers, would have 18-electron counts if dimeric; their low solubility has been cited in support of dimeric structures. Even though $(C_3H_5)_3Co$ and $(C_3H_5)_2CoI$ are stable at low temperatures, they are thermally unstable with respect to metal reduction and oxidative allyl coupling.

It is possible that the low electron counts of the iron(II) and cobalt(II) centers are responsible for the formation of decomposition products in the reactions of the bis(allyl′)metal and iodine. Although $[1,3\text{-}(SiMe_3)_2C_3H_3]_2Fe$ is a 14-electron complex and $[1,3\text{-}(SiMe_3)_2C_3H_3]_2Co$ is a 15-electron complex, reactions with iodine would form 12-electron and 13-electron species, respectively. These monomers could conceivably dimerize, but it may be thermodymically preferred to simply remove the allyl ligand (via oxidative coupling) and form the stable metal halides. It is not known whether the oxidative coupling is intermolecular (upon formation of an (allyl)metal halide intermediate) or intramolecular, but no $1,3\text{-}(SiMe_3)_2C_3H_3I$ is observed spectroscopically in the NMR data, suggesting that the mechanism is more likely an intramolecular one.

Reactions of $[1,3\text{-}(SiMe_3)_2C_3H_3]_2M$ (M = Fe, Co, Ni) and phosphines

It was noted above that no reaction occurred upon the addition of triphenylphosphine to $[1,3\text{-}(SiMe_3)_2C_3H_3]_2Ni$; the products were spectroscopically determined to be a mixture of starting materials by comparison of NMR spectra (see chapter 1). It was proposed that the steric bulk of the allyl ligands, which imparts great thermodymic stability to the bis(allyl′)nickel complex, is also responsible for its lack of reactivity with respect to triphenylphoshine. In brief, the phosphine is too bulky itself to get close enough to the nickel center to bind as a donor.

Since the atomic radii of four-coordinate iron(II), cobalt(II), and nickel(II) are similar,[130] it was thought that no reaction would occur with the iron(II) or cobalt(II) analogs of $[1,3\text{-}(SiMe_3)_2C_3H_3]_2Ni$ and triphenylphosphine. The reactions were run under the same conditions as the nickel experiment. No color changes were seen upon addition of triphenylphosphine, and mixtures of white crystalline solid and colored oils were collected. The paramagnetism of the iron(II) and cobalt(II) starting materials prevented successful use of NMR spectroscopy in identifying reaction products. Based on results of the diamagnetic Ni(II) study and the similar white crystalline products found in the three attempts, however, it was concluded that no reactions occurred between triphenylphosphine and the $[1,3\text{-}(SiMe_3)_2C_3H_3]_2M$ complexes of iron(II), cobalt(II), and nickel(II).

In Chapter 1, the reaction of $[1,3\text{-}(SiMe_3)_2C_3H_3]_2Ni$ and trimethylphosphine was described. Instead of forming a phosphine adduct, as observed in the case of $(C_3H_5)_2Ni$ and PMe_3 (eq 30),[5] a P–P coupling reaction occurs, resulting in $(MeP)_4$ (eq31). [108]

$$(C_3H_5)_2Ni + PMe_3 \xrightarrow{-78\ ^\circ C} (C_3H_5)_2Ni{\cdot}PMe_3 \quad (30)$$

$$[1,3\text{-}(SiMe_3)_2C_3H_3]_2Ni + 4\ PMe_3 \rightarrow [1,3\text{-}(SiMe_3)_2C_3H_3]_2Ni + (MeP)_4 \quad (31)$$

It was not known whether this reaction is unique to $[1,3\text{-}(SiMe_3)_2C_3H_3]_2Ni$, so similar reactions were studied using the iron(II) and cobalt(II) bis(allyl) analogs. In both cases, the addition of trimethylphosphine to solutions of the bis(allyl) complexes caused irreversible color changes in the reactions. An orange-red oil was collected from the reaction involving $[1,3\text{-}(SiMe_3)_2C_3H_3]_2Fe$, whereas a red oil was collected from the reaction involving $[1,3\text{-}(SiMe_3)_2C_3H_3]_2Co$. Over a period of days, crystals grew from the cobalt(II) product. These crystals had the same unit cell as that of staggered $[1,3\text{-}(SiMe_3)_2C_3H_3]_2Co$ itself. This fact alone does not help in determining if a P–P bond coupling reaction similar to the one in the Ni(II) case occurred, because the staggered form is both the preferred and structurally-observed form of $[1,3\text{-}(SiMe_3)_2C_3H_3]_2Co$, and the starting material may have already been in that conformation. No crystals grew from the oil of the iron(II) sample.

NMR spectroscopy cannot be used to identify the reaction products for either reaction, meaning that there is at least one paramagnetic component in the reaction product of each sample. The cobalt(II) species is the paramagnetic component in the case of $[1,3\text{-}(SiMe_3)_2C_3H_3]_2Co$ and PMe_3, as seen by the crystal structure determination. If $[1,3\text{-}(SiMe_3)_2C_3H_3]Co(PMe_3)_3$ were synthesized, it would be a diamagnetic species that could be dectected in an NMR experiment. In the case of $[1,3\text{-}(SiMe_3)_2C_3H_3]_2Fe$ and PMe_3, the paramagnetic component is most

likely the iron(II) starting material, but this fact has not been crystallographically substantiated; it is at least known that no phosphorus bis(adduct) is formed with $[1,3\text{-}(SiMe_3)_2C_3H_3]_2Fe$ because a diadduct species with η^3-allyls would be an 18-electron species and thus diamagnetic.

It is interesting to note that an $(\eta^3\text{-allyl}')_2Fe(PMe_3)_2$ species has been reported,[91,96] but it was synthesized via an allyl Grignard reaction from the iron(II) precursor $FeCl_2(PMe_3)_2$. It has also been reported that an (allyl)cobalt(I) phosphines species, $(C_3H_5)Co(PMe_3)_3$,[131] can be made from $Co(PMe_3)_3Cl$ and alkali metal allyl salt.

Conclusion

This work has shown that robust bis(allyl′)transition metal complexes can be used to form stabilized CO adducts. $[1,3\text{-}(SiMe_3)_2C_3H_3]_2Fe$ and $[1,3(SiMe_3)_2C_3H_3]_2Ni$ accept carbon monoxide as a donor ligand to form the 18-electron carbonyl adducts $[1,3(SiMe_3)_2C_3H_3]_2Fe(CO)_2$ and $[1,3\text{-}(SiMe_3)_2C_3H_3]_2NiCO$, respectively. The addition of CO to $[1,3\text{-}(SiMe_3)_2C_3H_3]_2Co$ results in the one-electron reduction of Co(II) to Co(I), forming the 18-electron $[1,3\text{-}(SiMe_3)_2C_3H_3]Co(CO)_3$, along with the formation of the oxidatively coupled 1,3,4,6-tetrakis(trimethylsilyl)-1,5-hexadiene.

The use of the sterically enhanced allyl ligand $[1,3\text{-}(SiMe_3)_2C_3H_3]^-$ instead of $C_3H_5^-$ offers two distinct advantages in the formation of allyl transition metal carbonyl complexes: the ease of synthesis and the stability of the resulting complexes. Since the trimethylsilyl-substituted bis(allyl)M (M = Fe,Co,Ni) complexes are thermally stable, the synthesis of corresponding carbonyl adducts

involves the direct addition of carbon monoxide to (allyl)metal solutions at room temperature (eq 32).

$$[1,3\text{-}(SiMe_3)_2C_3H_3]_2M\ (M = Fe,Co,Ni)\ + CO_{(xs)} \rightarrow [1,3\text{-}(SiMe_3)_2C_3H_3]_xM(CO)_y \quad (32)$$

As previously stated, there are no known homoleptic bis(allyl)iron or bis(allyl)cobalt species. Although $(C_3H_5)_2Fe(CO)_2$[102] and $(C_3H_5)Co(CO)_3$[132] have been synthesized, they are not generally formed by simple addition of CO to (allyl)metal complexes and prove to be more difficult to make than the trimethylsilyl-subsituted allyl analogs. The synthesis of $(C_3H_5)_2Fe(CO)_2$ is not straightforward. Allyl iodide can be oxidatively added to $Fe(CO)_5$ to form (allyl)$Fe(CO)_3$ iodide (eq 33), which can be further treated with sodium metal to produce an (allyl)irontricarbonyl sodium salt (eq 34); addition of allyl bromide to this salt yields $(C_3H_5)_2Fe(CO)_2$ (eq 35), which is thermally unstable.[102]

$$Fe(CO)_5 + C_3H_5I \rightarrow (C_3H_5)Fe(CO)_3I \quad (33)$$

$$(C_3H_5)Fe(CO)_3I + 2\ Na \rightarrow Na[(C_3H_5)Fe(CO)_3] \quad (34)$$

$$Na[(C_3H_5)Fe(CO)_3] + C_3H_5Br \rightarrow (C_3H_5)_2Fe(CO)_2 \quad (35)$$

The synthesis of $(C_3H_5)Co(CO)_3$ can be achieved by more than one method, but it usually involves the synthesis of a cobalt carbonyl starting material, followed

by subsequent reactions to isolate the desired (allyl)cobalt carbonyl product. As in the case with an allyl carbonyl iron, the synthesis of an (allyl)cobalt tricarbonyl makes use of a metal carbonyl starting material. A phase transfer reagent, which promotes the generation of $[Co(CO)_4]^-$ from $Co_2(CO)_8$, can be used in conjunction with allyl bromide and dicobalt octacarbonyl to form the desired $(C_3H_5)Co(CO)_3$ (eq 36).[133]

$$C_3H_5Br + Co_2(CO)_8 \xrightarrow[NaOH]{Et_3BzN^+Cl^-} (C_3H_5)Co(CO)_3 \qquad (36)$$

The product must be isolated from unreacted starting materials by distillation. Carbon monoxide can also be added to tris(allyl)cobalt[116] (see eq 26), but the difficulty in isolating and handling $(C_3H_5)_3Co$ renders this method tedious.

Besides the difficulty in synthesis, stability of the (allyl)transition metal carbonyl complexes is also an issue for the unsubstituted analogs. Although $(C_3H_5)_2Fe(CO)_2$ has a reported melting point of 57 °C, it can only be stored at low temperature under inert atmosphere or it decomposes.[102] This low thermal stabilty is in contrast to $[1,3(SiMe_3)_2C_3H_3]_2Fe(CO)_2$, which is stable at room temperature indefinitely. This difference is even more evident in the case of nickel.

The addition of CO to $(C_3H_5)_2Ni$ results in the oxidative coupling of the allyl ligands and the formation of $Ni(CO)_4$ (eq 37).[2]

$$(C_3H_5)_2Ni + 4\,CO \rightarrow \text{hexadiene} + Ni(CO)_4 \qquad (37)$$

Not only is [1,3-$(SiMe_3)_2C_3H_3]_2$Ni not degraded by an excess of carbon monoxide, the resulting carbonyl product [1,3-$(SiMe_3)_2C_3H_3]_2$NiCO is stable at room temperature. To date, the only reported homoleptic (allyl)Ni(II) carbonyl complex is an ansa-bridged species, that is proposed to exist as in intermediate at –78 °C; upon warming, a carbonyl insertion reaction occurs (eq 38).[92]

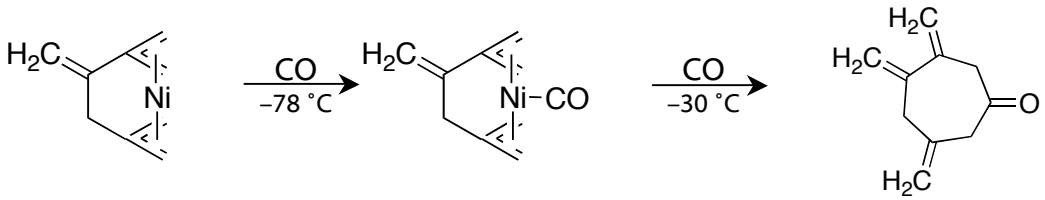

(38)

It has also been shown that DFT calculations using the PW91PW91 functional and 6-31+G(d,p) basis set can be used to compute C–O stretching frequencies with considerable accuracy, although the calculated values tend to be lower than experimental ones by ~20 cm^{-1}. With an average error of 1%, this method/basis set is a good choice for predicting molecular structures of (allyl)metal carbonyl complexes.

The steric bulk of the trimethylsilylated allyl ligands influences the reactivity of the bis(allyl′) complexes with small molecules. Although the addition of iodine to [1,3-$(SiMe_3)_2C_3H_3]_2$Ni results in the synthesis of an iodide-bridged Ni(II) species (see Chapter One), similar reactions with [1,3-$(SiMe_3)_2C_3H_3]_2$Fe and [1,3-$(SiMe_3)_2C_3H_3]_2$Co do not follow the same route. Instead, the iodine addition induces the formation of metal iodides, accompanied by the oxidative coupling of the allyl ligands (see eq 28). The bis(allyl) complexes of Fe(II) and Co(II), like that

of Ni(II), do not react with the bulky trimethylphosphine because of the steric hindrance of the species involved. It has not been established from this research whether $[1,3\text{-}(SiMe_3)_2C_3H_3]_2Fe$ or $[1,3\text{-}(SiMe_3)_2C_3H_3]_2Co$ reacts with trimethylphosphine to form adduct species or follows the reaction pathway of $[1,3\text{-}(SiMe_3)_2C_3H_3]_2Ni$, forming tetramethyltetraphosphane by a P–P coupling mechanism.

CHAPTER III

SYNTHESIS, CHARACTERIZATION, AND POLYMERIZATION STUDIES OF TRIMETHYLSILYL-SUBSTITUTED *s*-BLOCK ALLYL COMPLEXES

Introduction

There has been much interest in *s*-block organometallic chemistry in the last century.[134,135] The range of organometallic alkali metal complexes is broad, and many have long been used in chemical transformations;[136] reactions involving lithium compounds are the most prevalent. Organomagnesium compounds have been investigated as Grignard reagents since the early 1900s. Much of the interest in heavy alkaline-earth chemistry has been in the development of cyclopentadienyl derivatives.[104,105,137] Non-cyclopentadienyl organometallic complexes of heavy alkaline-earth metals[138] have been synthesized with π-delocalized ligands including fluorenyl,[139] indenyl,[140] and pentadienyl.[141]

The smallest π-delocalized ligand used in organometallic complexes is the allyl anion, $C_3H_5^-$.[142,143] Metal allyl complexes have been highly sought as reagents in organic reactions involving C–C bond formation.[144-146] Although many transition metal allyl complexes have been developed for their catalytic utility, *s*-block allyls have received little attention. Group1 allyl complexes of lithium (and to some extent sodium and potassium) have been used primarily as ligand transfer agents.

Recently, heterometallic lanthanide/alkali metal catalysts have been shown to be useful as polymerization catalysts.[28,87,149,150] Interestingly, the potassium allyl species polymerized methyl methacrylate more effectively when used as the sole catalyst rather than as part of a mixed metal species.[151] Even though the potential

uses of alkali metal allyl complexes are evident, most research has been confined to allyllithium complexes.[79,152-156] Detailed analysis of this type of Group 1 complex is lacking for the heavy alkali metal congeners. There are only two reports of structurally characterized potassium allyls,[28,151] and none reported for Rb and Cs allyls. Rubidium and cesium allyls have only been characterized in solution and have not been probed for their synthetic value.

Several Group 2 organometallic complexes have also shown catalytic activity,[157-159] but very few alkaline-earth allyls have been reported, much less studied for chemical reactivity. Some allylbarium compounds have been used in allylation reactions;[160,161] however, the barium complexes were synthesized in-situ and not characterized. There is only one structurally authenticated heavy alkaline-earth allyl complex.[80] Allyl complexes of the heavy alkaline-earth metals have not been pursued because they were thought to provide no advantage over Grignard reagents.[147,148]

Because the $C_3H_5^-$ anion is sterically compact, homoleptic organometallic complexes made with this ligand are often coordinatively unsaturated, and thus are highly reactive complexes. In first-row transition metal allyls, this unsaturation results in low thermal stabilities due to low-energy decomposition pathways of the complexes. The use of bulky substituents such as trimethylsilyl groups on the allyl ligand has allowed the synthesis and characterization of thermally stable, electron-deficient bis(allyl) compounds of Cr,[25] Fe,[25] Co,[26] and Ni.[108]

Due to the increased ionicity present in *s*-block organometallic complexes, the thermal stability of Group 1 and Group 2 allyls is not an issue, but the increased ionicity coupled with the use of sterically small ligands can make isolation of soluble

compounds difficult. Kinetic instability of organometallic *s*-block complexes can also be an issue, as steric effect, metal size, ligand basicity, and solubility equilibria all play a role in determining the isolability and reactivity of complexes.[162] The addition of steric bulk to cyclopentadienyl ligands has permitted the isolation of stabilized Group 2 metallocenes.[106,163] Steric stabilization was employed to synthesize organocalcium complexes using pentadienyl[141] and allyl ligands,[80] which were structurally authenticated. In this chapter, the synthesis and characterization of Group 1 and Group 2 complexes using the trimethylsilyl-substituted allyl ligand $[1,3\text{-}(SiMe_3)_2C_3H_3]^-$ will be discussed along with their potential use as polymerization catalysts of methyl methacrylate.

Experimental Section

General Considerations. All manipulations were performed with the rigorous exclusion of air and moisture using high vacuum, Schlenk, or glovebox techniques. Proton, and carbon (^{13}C) NMR spectra were obtained on a Bruker DPX–300 spectrometer at 300 and 75.5 MHz, respectively, and were referenced to the residual proton and ^{13}C resonances of C_6D_6 (d 7.15 and 128.0). All NMR data were processed using Bruker XWINNMR 3.5 software on an Octane workstation (Silicon Graphics, Mountain View, CA).

GC–MS data were obtained with a Hewlett–Packard 5890 Series II gas chromatograph/mass spectrometer with a 5971 Series mass selective detector. Melting points were determined on a Laboratory Devices Mel–Temp apparatus in sealed capillaries. Metal and combustion analyses were performed by Desert Analytics, Tuscon, AZ. Low C and H analyses are common for highly air-sensitive

organoalkaline-earth complexes, and may be due to incomplete combustion.[80,164,165]

Polymerization Reaction Considerations. Methylmethacrylate (4.00 mL, 37.4 mmol) was added via syringe to catalytic (allyl)metal solutions in toluene (~10 mL) at 0 °C. Polymerization reations were allowed to run the 30 seconds and then quenched with methanol. The precipitates were filtered and dried, prior to analysis. PMMA samples were studied at ambient temperatures unless otherwise noted. The tacticity of PMMA samples were determined by integration of the methyl regions in ^{1}H NMR spectra of the polymers.[166]

Materials. 1-$(SiMe_3)C_3H_5$ and *n*-BuLi (2.5 M in hexanes) were purchased from Acros; potassium, rubidium, and cesium metals were obtained from Strem, and SrI_2, BaI_2, and *t*-BuOK were purchased from Aldrich; all were used as received. 1,3-$(SiMe_3)_2C_3H_4$ and Li[1,3-$(SiMe_3)_2C_3H_3$] were synthesized according to literature procedures.[38] K[1,3-$(SiMe_3)_2C_3H_3$] was prepared by transmetallation of Li[1,3-$(SiMe_3)_2C_3H_3$] with potassium *t*-butoxide in hexanes solution. THF, toluene, and hexanes were distilled under nitrogen from potassium benzophenone ketyl.[39] Deuterated solvents were vacuum distilled from Na/K (22/78) alloy prior to use. Purification of methyl methcrylate involved stirring over CaH_2, followed by vacuum distillation and degassing using the freeze-pump-thaw method.

Synthesis of {[1,3-$(SiMe_3)_2C_3H_3$]Cs(thf)}$_\infty$. A 250 mL Erlenmeyer flask was fitted with a Schlenk adapter and a glass magnetic stir bar and charged with cesium metal (1.058 g; 7.960 mmol) and 50 mL of THF. A 125 mL Erlenmeyer flask was fitted with a septum and charged with 1,3-$(SiMe_3)_2C_3H_4$ (1.435 g; 7.699 mmol) and 40 mL of THF. The Schlenk-adapted flask was attached to a N_2 line, and both flasks were cooled to –78 °C using a dry ice/acetone bath. The

1,3-$(SiMe_3)_2C_3H_4$ solution was slowly cannulated into the flask containing cesium. The reaction was allowed to warm to room temperature overnight. The pale yellow solution was warmed to 40 °C for two hours. The solution was decanted from unreacted cesium, and THF was removed under vacuum, leaving an orange solid (0.913 g; 30% yield), mp 124–125 °C. Recrystallization from THF afforded colorless blocks. Anal. Acceptable elemental analysis could not be obtained for a solvated sample. A sample was heated under vacuum and analyzed as the base free product. Calcd for: $C_9H_{21}CsSi_2$: C, 33.96; H, 6.65. Found: C, 34.58; H, 6.58. ^{1}H NMR (300 MHz, THF-d_8, 298 K): δ –0.069 ppm (s, 18H, $Si(CH_3)_3$); 1.77 (mult, 4H, THF(β-CH_2)); 2.63 (d, J= 15.6 Hz, 2H, $C_{(1,3)}$–H); 3.62 (mult, 4H, THF(α-CH_2)); 6.32 (t, J= 15.6 Hz, 1H, $C_{(2)}$–H). ^{13}C NMR (75 MHz, THF-d_8, 298 K): δ 2.34 ppm ($Si(CH_3)_3$); 25.30 (THF(β-CH_2)); 67.37 (THF(α-CH_2)); 74.24 ($C_{(1,3)}$); 154.99 ($C_{(2)}$).

Synthesis of {[1,3-$(SiMe_3)_2C_3H_3$]Rb(thf)}$_\infty$. A 125 mL Erlenmeyer flask was fitted with a Schlenk adapter and a glass magnetic stir bar and charged with rubidium metal (0.300 g; 3.51 mmol) and 30 mL of THF. A 125 mL Erlenmeyer flask was fitted with a septum and charged with 1,3-$(SiMe_3)_2C_3H_4$ (0.645 g; 3.46 mmol) and 10 mL of THF. The Schlenk-adapted flask was attached to a N_2 line, and both flasks were cooled to 0 °C using an ice bath. The 1,3-$(SiMe_3)_2C_3H_4$ solution was slowly cannulated into the flask containing rubidium. The reaction was allowed to warm to room temperature overnight. The yellow solution was warmed to 50 °C for two hours. The solution was decanted from unreacted rubidium, and THF was removed under vacuum, leaving a yellow oil (0.120 g; 10% yield) from which micro-crystals grew that were unsuitable for X-ray crystallography. Anal.

Calcd for $C_{13}H_{29}RbOSi_2$: C, 45.52; H, 8.52; Rb, 24.92. Found: C, 46.67; H, 8.13; Rb, 24.92. ^{1}H NMR (300 MHz, THF-d_8, 298 K): δ –0.122 ppm (s, 18H, $Si(CH_3)_3$); 1.78 (mult, 4H, THF(β-CH_2)); 2.70 (d, J= 15.3 Hz, 2H, $C_{(1,3)}$–H); 3.62 (mult, 4H, THF(α-CH_2)); 6.52 (t, J= 15.3 Hz, 1H, $C_{(2)}$–H). ^{13}C NMR (75 MHz, THF-d_8, 298 K): δ 2.44 ppm ($Si(CH_3)_3$); 25.31 (THF(β-CH_2)); 67.40 (THF(α-CH_2)); 70.31 ($C_{(1,3)}$); 155.54 ($C_{(2)}$).

Synthesis of {[1,3-$(SiMe_3)_2C_3H_3$]$_5$$Ba_2K$(thf)}$_\infty$. A 125 mL Schlenk flask containing a magnetic stirring bar and fitted with an addition funnel was charged with BaI_2 (0.847 g; 2.24 mmol) in 20 mL of THF. K[1,3-$(SiMe_3)_2C_3H_3$] (1.010 g; 4.499 mmol), dissolved in 15 mL of THF, was added to the addition funnel. The apparatus was cooled to –78 °C using a dry ice/acetone bath. The THF solution of K[1,3-$(SiMe_3)_2C_3H_3$] was added dropwise with stirring over the course of 30 min. The solution was allowed to warm to room temperature overnight. THF was removed under vacuum, and the residue was extracted with hexanes. The extract was filtered over a medium porosity glass frit, and the hexanes was removed under vacuum to afford a yellow powder (1.091 g; 92% yield; mp 190 °C (dec.)). Rescrystallization from hexanes resulted in the growth of yellow blocks over a period of days. Anal. Calcd for $C_{49}H_{113}Ba_2KOSi_{10}$: C, 44.82; H, 8.67; Ba, 20.92. Found: C, 45.03; H, 9.01; Ba 20.70. ^{1}H NMR (300 MHz, THF-d_8, 298 K): δ –0.026 ppm (s, 36H, $Si(CH_3)_3$); 1.78 (mult, 4H, THF(β-CH_2)); 2.59 (d, J= 15.9 Hz, 4H, $C_{(1,3)}$–H); 3.61 (mult, 4H, THF(α-CH_2)); 6.53 (t, J= 15.9 Hz, 2H, $C_{(2)}$–H). ^{1}H NMR (300 MHz, C_6D_6, 298 K): δ 0.30 ppm (s, 36H, $Si(CH_3)_3$); 1.34 (mult, 4H, THF(β-CH_2)); 2.86 (d, J= 16.0 Hz, 4H, $C_{(1,3)}$–H); 3.48 (mult, 4H, THF(α-CH_2)); 6.80 (t, J=

16.0 Hz, 2H, $C_{(2)}$–H). ^{13}C NMR (75 MHz, C_6D_6, 298 K): δ 1.86 ppm ($Si(CH_3)_3$); 25.33 (THF(β-CH_2)); 68.76 (THF(α-CH_2)); 83.69 ($C_{(1,3)}$); 156.10 ($C_{(2)}$).

Synthesis of $\{[1,3\text{-}(SiMe_3)_2C_3H_3]_5Ba_2Li(thf)\}_\infty$. A 125 mL Schlenk flask containing a magnetic stirring bar and fitted with an addition funnel was charged with BaI_2 (0.128 g; 0.327 mmol) in 20 mL of toluene. Li[1,3-$(SiMe_3)_2C_3H_3$] (0.130 g; 0.676 mmol), dissolved in 15 mL of toluene, was added to the addition funnel. The apparatus was cooled to –78 °C using a dry ice/acetone bath. The toluene solution of Li[1,3-$(SiMe_3)_2C_3H_3$] was added dropwise with stirring over the course of 30 min. The solution was allowed to warm to room temperature overnight. Toluene was removed under vacuum, and the residue was extracted with hexanes. The extract was filtered over a medium porosity glass frit, and the hexanes was removed under vacuum, leaving very little product. The precipitate was dissolved in THF and stirred overnight. THF was removed under vaccum, and the residue was reconstituted in hexanes. The reaction was filtered, and hexanes was removed from the filtrate to afford to afford an orange-red oil. ^{1}H NMR (300 MHz, C_6D_6, 298 K): δ 0.37 ppm (s, 36H, $Si(CH_3)_3$); 1.31 (mult, 4H, THF(β-CH_2)); 3.14 (d, J= 16.0 Hz, 4H, $C_{(1,3)}$–H); 3.51 (mult, 4H, THF(α-CH_2)); 7.00 (t, J= 16.0 Hz, 2H, $C_{(2)}$–H). ^{13}C NMR (75 MHz, C_6D_6, 298 K): δ 2.04 ppm ($Si(CH_3)_3$); 25.34 (THF(β-CH_2)); 68.87 (THF(α-CH_2)); 85.53 ($C_{(1,3)}$); 155.06 ($C_{(2)}$).

Reaction of $\{[1,3\text{-}(SiMe_3)_2C_3H_3]_5Ba_2K(thf)\}_\infty$ and I_2. $\{[1,3\text{-}(SiMe_3)_2C_3H_3]_5Ba_2K(thf)\}_\infty$ (0.040 g, 0.030 mmol) was dissolved in THF (40 mL) in a 125 mL Erlenmeyer flask. Iodine (0.016 g, 0.061 mmol) was added to the $[1,3\text{-}(SiMe_3)_2C_3H_3]_5Ba_2K(thf)$ solution with stirring. Upon addition of iodine, the

solution turned purple and then quickly changed to colorless. THF was removed under vacuum, the residue was reconstituted in hexanes, and the reaction was filtered. Hexanes was removed from the decantate, leaving a yellow oil that was characterized by its ^{1}H NMR spectrum as 1,3,4,6-tetrakis(trimethylsilyl)-1,5-hexadiene, $[(SiMe_3)_2C_3H_3]_2$.

Synthesis of $[1,3\text{-}(SiMe_3)_2C_3H_3]_2Sr(thf)_2$. A 125 mL Schlenk flask containing a magnetic stirring bar and fitted with an addition funnel was charged with SrI_2 (0.775 g; 2.27 mmol) in 10 mL of THF. K[1,3-$(SiMe_3)_2C_3H_3$] (1.017 g; 4.530 mmol), dissolved in 15 mL of THF, was added to the addition funnel. The apparatus was cooled to –78 °C using a dry ice/acetone bath. The THF solution of K[1,3-$(SiMe_3)_2C_3H_3$] was added dropwise with stirring over the course of 30 min. The solution was allowed to warm to room temperature overnight. THF was removed under vacuum, and the residue was extracted with hexanes. The extract was filtered over a medium porosity glass frit, and the hexanes was removed from the pale yellow filtrate under vacuum to afford a pale yellow powder (0.828 g, 61% yield), mp 128–129 °C. Rescrystallization from hexanes resulted in the growth of transparent blocks over a period of days. Anal. Calcd for $C_{26}H_{58}O_2SrSi_4$: C, 51.81; H, 9.70; Sr, 14.54. Found: C, 49.71; H, 8.46; Sr 14.21. ^{1}H NMR (300 MHz, THF-d_8, 298 K): δ –0.032 ppm (s, 36H, $Si(CH_3)_3$); 1.77 (mult, 8H, THF(β-CH_2)); 2.83 (d, J= 16.0 Hz, 4H, $C_{(1,3)}$–H); 3.62 (mult, 8H, THF(α-CH_2)); 6.75 (t, J= 16.0 Hz, 2H, $C_{(2)}$–H). ^{1}H NMR (300 MHz, C_6D_6, 298 K): δ –0.30 ppm (s, 36H, $Si(CH_3)_3$); 1.30 (mult, 8H, THF(β-CH_2)) 3.19 (d, J= 16.0 Hz, 4H, $C_{(1,3)}$–H); 3.49 (mult, 8H, THF(α-CH_2)); 7.13 (t, J= 16.0 Hz, 2H, $C_{(2)}$–H). ^{13}C NMR (75 MHz, C_6D_6, 298 K): δ 2.12

ppm ($Si(CH_3)_3$); 25.22 (THF(β-CH_2)); 69.11 (THF(α-CH_2)); 78.40 ($C_{(1,3)}$); 158.88 ($C_{(2)}$).

Reaction of $[1,3\text{-}(SiMe_3)_2C_3H_3]_2Sr(thf)_2$. and I_2. $[1,3\text{-}(SiMe_3)_2C_3H_3]_2Sr(thf)_2$ (0.040 g, 0.066 mmol) was dissolved in THF (40 mL) in a 125 mL Erlenmeyer flask. Iodine (0.017 g, 0.066 mmol) was added to the $[1,3\text{-}(SiMe_3)_2C_3H_3]_2Sr(thf)_2$ solution with stirring. Upon addition of iodine, the solution turned purple and then quickly changed to colorless. THF was removed under vacuum, the residue was reconstituted in hexanes, and the reaction was filtered. Hexanes was removed from the decantate, leaving a yellow oil that was characterized by its ^1H NMR spectrum as 1,3,4,6-tetrakis(trimethylsilyl)-1,5-hexadiene, $[(SiMe_3)_2C_3H_3]_2$.

Reaction of $K[1,3\text{-}(SiMe_3)_2C_3H_3]$ and CaI_2: Synthesis of $[1,3\text{-}(SiMe_3)_2C_3H_3]_2Ca(thf)_2$ (1:1). A 125 mL Schlenk flask containing a magnetic stirring bar and fitted with an addition funnel was charged with CaI_2 (0.498 g; 1.69 mmol) in 15 mL of THF. $K[1,3\text{-}(SiMe_3)_2C_3H_3]$ (0.381 g; 1.70 mmol), dissolved in 15 mL of THF, was added to the addition funnel. The apparatus was cooled to –78 °C using a dry ice/acetone bath. The THF solution of $K[1,3\text{-}(SiMe_3)_2C_3H_3]$ was added dropwise with stirring over the course of 30 min. The solution was allowed to warm to room temperature overnight. THF was removed under vacuum, and the residue was extracted with hexanes. The extract was filtered over a medium porosity glass frit, and the hexanes was removed from the pale yellow filtrate under vacuum to afford a off-white powder (0.778 g, 85% yield). The product was characterized as $[1,3\text{-}(SiMe_3)_2C_3H_3]_2Ca(thf)_2$ by its ^1H NMR data. As this

compound has previously been synthesized,[80] no attempts to crystallize or obtain elemental analyses were made. ^{1}H NMR (300 MHz, THF-d_8, 298 K): δ –0.016 ppm (s, 36H, Si(CH_3)$_3$); 1.78 (mult, 8H, THF(β-CH_2)); 3.02 (d, J = 16.0 Hz, 4H, $C_{(1,3)}$–H); 3.62 (mult, 8H, THF(α-CH_2)); 6.90 (t, J = 16.0 Hz, 2H, $C_{(2)}$–H). ^{13}C NMR (75 MHz, THF-d_8, 298 K): δ 1.86 ppm (Si(CH_3)$_3$); 25.30 (THF(β-CH_2)); 67.40 (THF(α-CH_2)); 76.55 ($C_{(1,3)}$); 161.26 ($C_{(2)}$).

Reaction of [1,3-(SiMe$_3$)$_2$C$_3$H$_3$]$_2$Ca(thf)$_2$. and I$_2$. [1,3-(SiMe$_3$)$_2$C$_3$H$_3$]$_2$Ca(thf)$_2$ (0.161 g, 0.299 mmol) was dissolved in THF (40 mL) in a 125 mL Erlenmeyer flask. Iodine (0.074 g, 0.29 mmol) was added to the Ca^{2+} solution with stirring. Upon addition of iodine, the solution turned purple and then quickly changed to colorless. THF was removed under vacuum, the residue was reconstituted in hexanes, and the reaction was filtered. Hexanes was removed from the decantate, leaving a yellow oil that was characterized by its ^{1}H NMR spectrum as 1,3,4,6-tetrakis(trimethylsilyl)-1,5-hexadiene, [(SiMe$_3$)$_2$C$_3$H$_3$]$_2$.

Results and Discussion

Group 1 allyl complexes.

Although the trimethylsilyl-substituted allyl ligand, [1,3-(SiMe$_3$)$_2$C$_3$H$_3$]$^-$ has been used to synthesize a variety of *d*-block[25,26,88,108] and *f*-block[28,167-169] complexes, few alkali metal derivatives have been studied. Li[1,3-(SiMe$_3$)$_2$C$_3$H$_3$](TMEDA) was reported in 1990.[38] The usual bonding motif for allyllithium complexes is polymeric,[170,171] but the steric bulk of the ligands in Li[1,3-(SiMe$_3$)$_2$C$_3$H$_3$](TMEDA)

provides a monomeric structure (Figure 34).[79] The trimethylsilyl groups are arranged in a syn, syn conformation on the allyl carbon backbone.

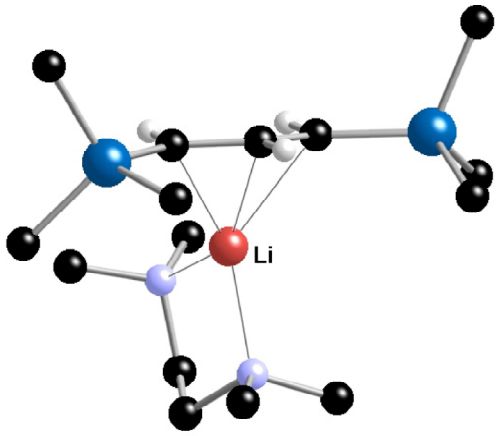

Figure 34. Solid-state structure of Li[1,3-$(SiMe_3)_2C_3H_3$](TMEDA), a monomeric complex.

Recently, the structure of {K[1,3-$(SiMe_3)_2C_3H_3$](DME)}$_\infty$ (Figure 35) was determined to be polymeric with the potassium ions forming a zigzag chain.[151] The trimethylsilyl arrangement is also syn, syn in this polymer. To date, no alkali metal allyl complexes have been structurally characterized for cesium and rubidium, so there is uncertainty about the coordination number of these metal centers.

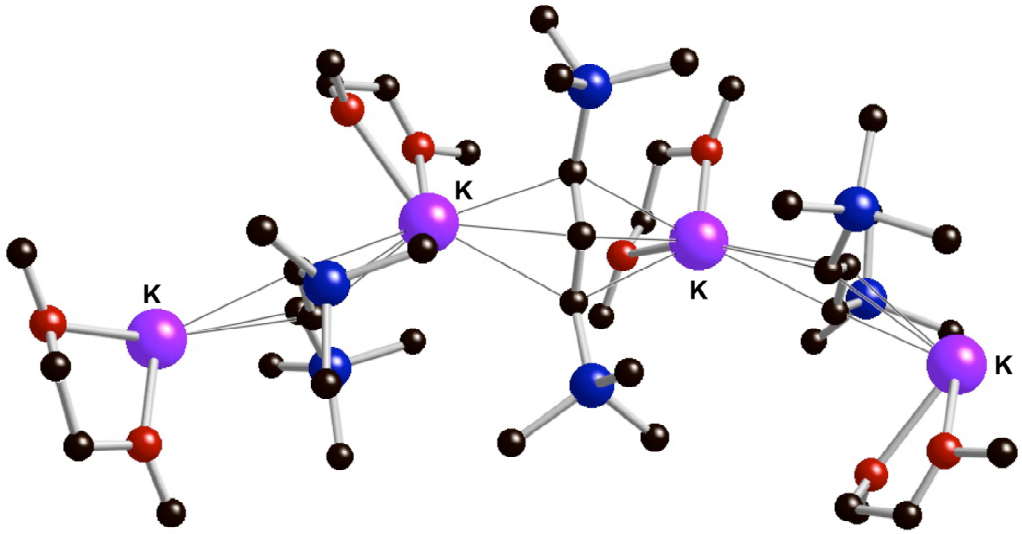

Figure 35. Solid-state structure of $\{K[1,3\text{-}(SiMe_3)_2C_3H_3](DME)\}_\infty$, showing potassium centers in zigzag chain.

Group 1 allyl complexes of cesium and rubidium were synthesized using the bulky 1,3-trimethylsilyl substituted propene in hopes of obtaining crystallographic data of the resulting complexes and determining the environment of these alkali metals in the complexes. Whereas deprotonation reactions run in toluene are used to synthesize the allyllithium species with $[1,3\text{-}(SiMe_3)_2C_3H_3]^-$ (eq 39), the alkali metal allyl complexes of rubidium and cesium were synthesized by direct addition of the trimethylsilyl-substituted propene hydrocarbon to the alkali metal in THF (eq40).

$$[1,3\text{-}(SiMe_3)_2C_3H_4] + n\text{-BuLi} \rightarrow Li[1,3\text{-}(SiMe_3)_2C_3H_3] + \text{butane} \quad (39)$$

$$[1,3\text{-}(SiMe_3)_2C_3H_4] + M\ (M = Rb, Cs) \rightarrow M[1,3\text{-}(SiMe_3)_2C_3H_3](thf)_x + H_2 \quad (40)$$

Although allyl reactions were run at low temperature (–78 °C) during the addition of the propene hydrocarbon to discourage ligand coupling, it was determined that warming the reactions above the melting points of the alkali metals (i.e., 28 °C for Cs; 39 °C for Rb) improved the modest yields without formation of the coupled allyl dimer $[1,3\text{-}(SiMe_3)_2C_3H_3]_2$.

Proton NMR spectra of the Cs and Rb allyl products have singlet, doublet, triplet patterns that are typical for π–bound allyls with syn, syn trimethylsilyl arrangements. Peak integrations were measured, and in both cases, the THF peaks were calculated to represent only one THF per metal atom. The elemental analysis of the allylrubidium species corroborates that there is one THF per Rb^+ center, but the allylcesium species consistently showed low carbon and hydrogen values. This fact probably reflects the lability of THF on the cesium center.

X-ray data were collected on crystals of $\{[1,3\text{-}(SiMe_3)_2C_3H_3]Cs(thf)\}_\infty$ and indicate a linear chain strucure with one THF molecule (disordered) per cesium atom, making it a formally five-coordinate complex (Figure 36); the trimethylsilyl substituents were found in a syn, syn conformation. This is the first structurally authenticated allylcesium. This structure has only one allyl per cesium and is linear (180°). Both $\{K[1,3\text{-}(SiMe_3)_2C_3H_3](DME)\}_\infty$ and the THF analog of the trimethylsilyl-substituted allylpotassium, $\{K[1,3\text{-}(SiMe_3)_2C_3H_3](THF)_{3/2}\}_\infty$,[172] have zigzag chain structures; the THF-coordinated potassium structure has alternating potassium metal centers, which coordinate one and two THF molecules (Figure 37).

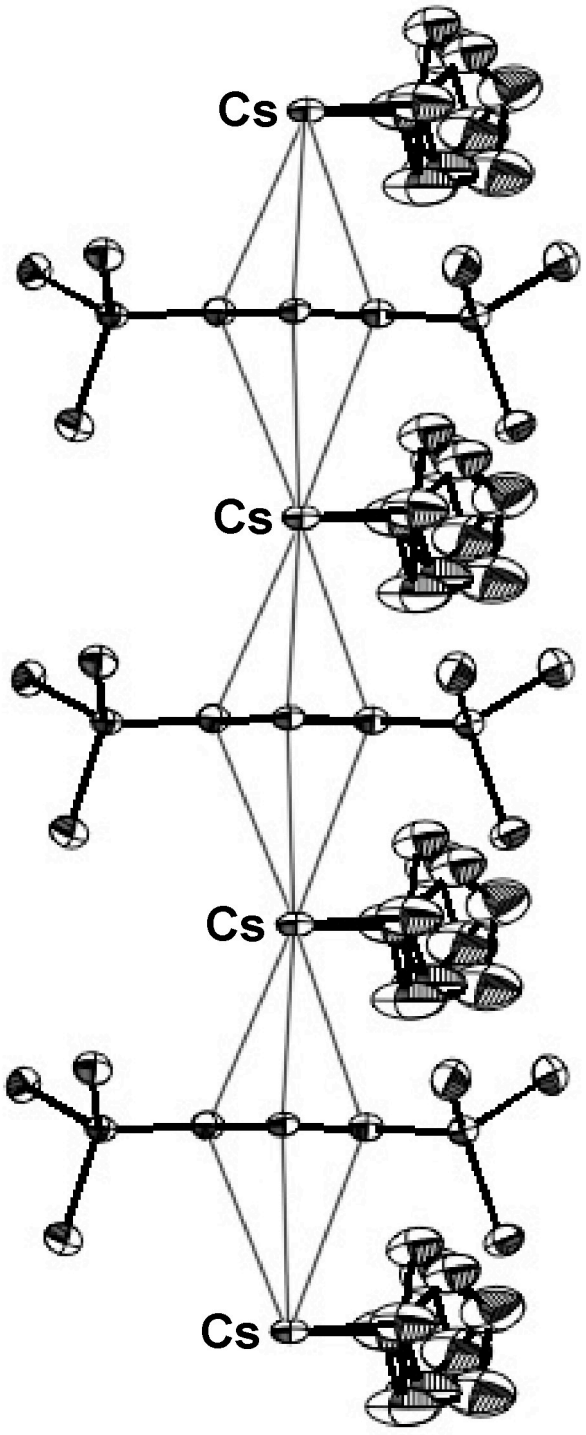

Figure 36. ORTEP of $\{[1,3\text{-}(SiMe_3)_2C_3H_3]Cs(thf)\}_\infty$ showing a linear polymeric structure and disordered THF ligands.

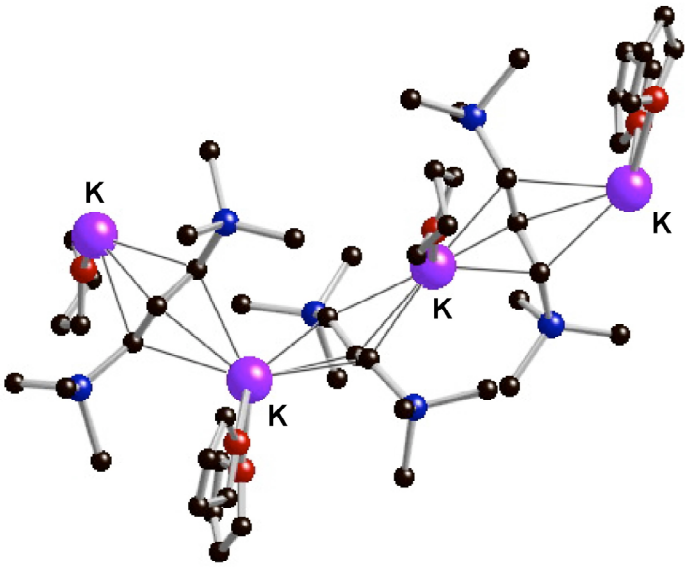

Figure 37. Solid-state structure of $\{K[1,3\text{-}(SiMe_3)_2C_3H_3](THF)_{3/2}\}_\infty$ with a zigzag polymeric structure.

The $Cs–C_{(allyl)}$ bond length range in $\{[1,3\text{-}(SiMe_3)_2C_3H_3]Cs(thf)\}_\infty$ is 3.331(6)–3.509(7) Å, and the Cs–O bond length is 3.060(16)Å. The cesium environment seems very unsaturated (Figure 38), but a closer look at the environment of the Cs^+ center (Figure 39) reveals several close contacts between the cesium center and hydrogen atoms on adjacent trimethylsilyl groups. There are three hydrogens on adjacent trimethylsilyl moieties that are within 3.21–3.38 Å of the cesium center (cf. Cs–H = 3.19 Å in CsH).[173] These values can be reasonably considered to represent energetically important contact distances in this complex.

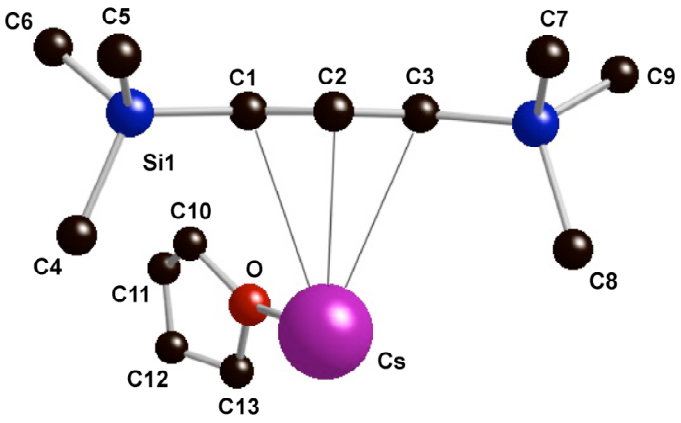

Figure 38. View of $\{[1,3\text{-}(SiMe_3)_2C_3H_3]Cs(thf)\}_\infty$ repeating unit.

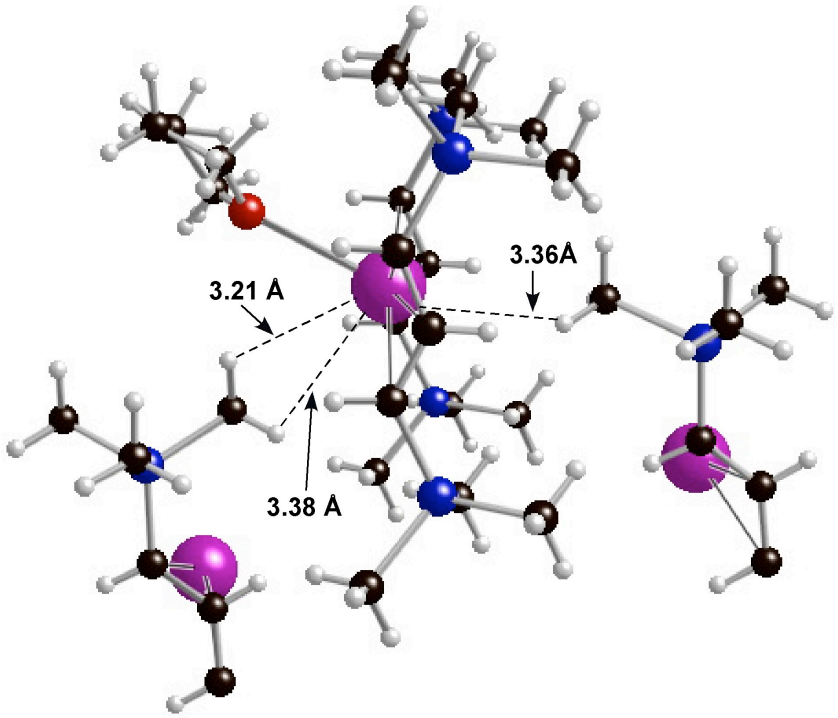

Figure 39. Close H–Cs contacts of $\{[1,3\text{-}(SiMe_3)_2C_3H_3]Cs(thf)\}_\infty$.

The true coordination number of Cs^+ in this complex is uncertain. As this complex is ionic in nature, the sum of the cation (adjusted for CN) and anion radii should equal the observed metal–ligand distances.[174] The ionic radius for five-coordinate Cs^+ is calculated as 1.60 Å.[174,175] Subtraction of this value from the average $Cs–C_{(allyl)}$ distance of 3.431 Å gives an allyl thickness (radius) value of 1.83 Å. This value is longer than the allyl thickness values calculated for the six-coordinate $\{K[1,3\text{-}(SiMe_3)_2C_3H_3](DME)\}_\infty$ ($r_{(allyl)}$ = 1.67 Å), the six-coordinate $Ca[1,3\text{-}(SiMe_3)_2C_3H_3](thf)_2$ ($r_{(allyl)}$ = 1.65 Å), and the six-coordinate $Sr[1,3\text{-}(SiMe_3)_2C_3H_3](thf)_2$ ($r_{(allyl)}$ = 1.62 Å) (see below).

However, the coordination number of Cs^+ in $\{[1,3\text{-}(SiMe_3)_2C_3H_3]Cs(thf)\}_\infty$ is eight if all three close-contact hydrogens are considered to be energetically important to the structure. The ionic radius of an eight-coordinate Cs^+ is 1.78 Å. Subtraction of this value from the average $Cs–C_{(allyl)}$ distance of 3.431 Å results in an allyl thickness value of 1.65 Å. This value falls within accepted limits for allyl complexes, lending credence to the fact that the close contacts present in $\{[1,3\text{-}(SiMe_3)_2C_3H_3]Cs(thf)\}_\infty$ are not just artifacts of crystal packing.

The $Cs–C_{(allyl)}$ distances in $\{[1,3\text{-}(SiMe_3)_2C_3H_3]Cs(thf)\}_\infty$ are similar to $Cs–C_{(Cp)}$ distaces found in the six-coordinate ($[(C_6H_5)_4P]^+[Cs_2(C_5H_5)_3]^-$)[176] ($Cs–C_{(Cp)}$ = 3.3295–3.386 Å), adjusting the values for the difference in coordination number of the two complexes. Likewise, the Cs–O distance in this allylcesium species is also within the expected range for cesium–THF bonding.[177-179] The allyl ligand C–C bonds are delocalized (1.380(10)–1.389(10) Å), as predicted for allylcesium by computation.[180] The allyl carbons form an angle of 131.2(7)°, which is

only slightly larger than the angle predicted for free $[1,3\text{-}(SiMe_3)_2C_3H_3]^-$ (130.3°)[80] and equivalent to that found in $\{K[1,3\text{-}(SiMe_3)_2C_3H_3](THF)_{3/2}\}_\infty$ (130.6(3)°). The terminal hydrogens and trimethylsilyl groups are bent out of the allyl plane by 2.9° and 4.3° for hydrogen and 2.9° and 4.3° for $SiMe_3$, repectively. This behavior has been documented in other allyl complexes.[25,169]

Although suitable crystals for X-ray crystallography were not obtained for the allylrubidium species, it is expected to be a polymer like the potassium and cesium counterparts. The elemental analysis indicates one THF molecule per rubidium atom. This thf/metal ratio is the same as that seen for the allylcesium analog; it is reasonable to propose a similar structure for the allylrubidium species.

Group 2 allyl complexes

Metathesis reactions are generally employed to make organometallic complexes of Group 2 metals, and this method was used to synthesize the heavy alkaline-earth allyl complex $[1,3\text{-}(SiMe_3)_2C_3H_3]_2Ca(thf)_2$, which was reported in 1999 (Figure 40).[80] It is a monomeric bis(allyl)calcium species with two THF molecules coordinated to the Ca^{2+} center and trimethylsilyl groups in a syn, syn conformation. This complex is soluble in both ethers and hydrocarbon solvents. This Group 2 allyl complex is the only reported complex to be structurally authenticated. Interestingly, the addition of one equivalent of $K[1,3\text{-}(SiMe_3)_2C_3H_3]$ to one equivalent of CaI_2 also forms the bis(allyl)calcium. This tendency to form a homoleptic calcium hydrocarbyl species is not seen in cyclopentadienyl calcium chemistry using 1:1 ratios although it has been reported in transition metal allyl chemistry (see Chapters 1 and 2).

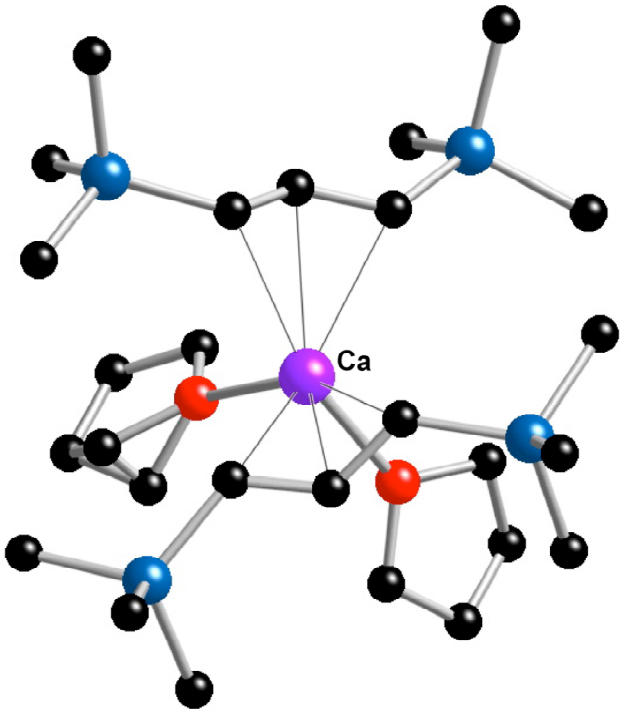

Figure 40. Solid-state structure of $[1,3\text{-}(SiMe_3)_2C_3H_3]_2Ca(thf)_2$, a monomeric species; one THF ligand displays disorder.

There is no mention of an allylstrontium species in the literature; a few allylbarium compounds have been synthesized for use in reactions, but not separately characterized.[160,161] It was expected that the trimethylsilyl-substituted allylbarium and allylstrontium species could be synthesized using two equivalents of $K[1,3\text{-}(SiMe_3)_2C_3H_3]$ and one equivalent of strontium iodide or barium iodide, respectively (eq 41).

$$2\ K[1,3\text{-}(SiMe_3)_2C_3H_3] + MI_2\ (M = Sr, Ba) \rightarrow [1,3\text{-}(SiMe_3)_2C_3H_3]_2M(thf)_x + 2\ KI\downarrow \quad (41)$$

Work-up of the reactions resulted in air-sensitive powders in good yields. Like the calcium confomer, these complexes are soluble in both ethers and hydrocarbon solvents. Proton NMR data of the allylbarium species show the characteristic singlet, doublet, triplet pattern of syn, syn trimethylsilyl arrangements on the allyl ligand. Curiously, integration of the NMR peaks results in the calculation of only THF peak per two allyl ligands. Based on this data, it was originally assumed that the structure of this allylbarium species is polymeric in form with one terminal and two shared allyl ligands on the barium center and one coordinated THF molecule per Ba^{2+} (Figure 41). The bridging and terminal allyl ligands must undergo fast exchange on the NMR timescale. Although the initially proposed allylbarium structure in Figure 41 was plausible, elemental analysis of the product indicated that this proposed structure did not reflect the true nature of the complex in the solid state.

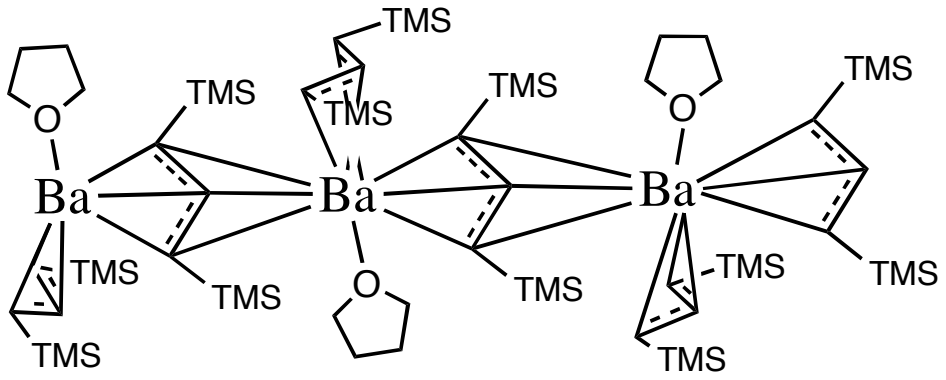

Figure 41. Initially proposed structure of the allylbarium species based on NMR data.

A crystal structure determination performed on this allylbarium species showed the solid state structure to be one of a heterometallic barium/potassium allyl polymeric chain (Figure 42). The repeating unit of this polymer contains one K^{+} and two Ba^{2+} cations. Each barium center is coordinated by one terminal and two bridging allyl ligands; the potassium metal center is coordinated by two bridging allyl ligands and one THF molecule. Elemental analysis data corroborate the crystal structure determination.

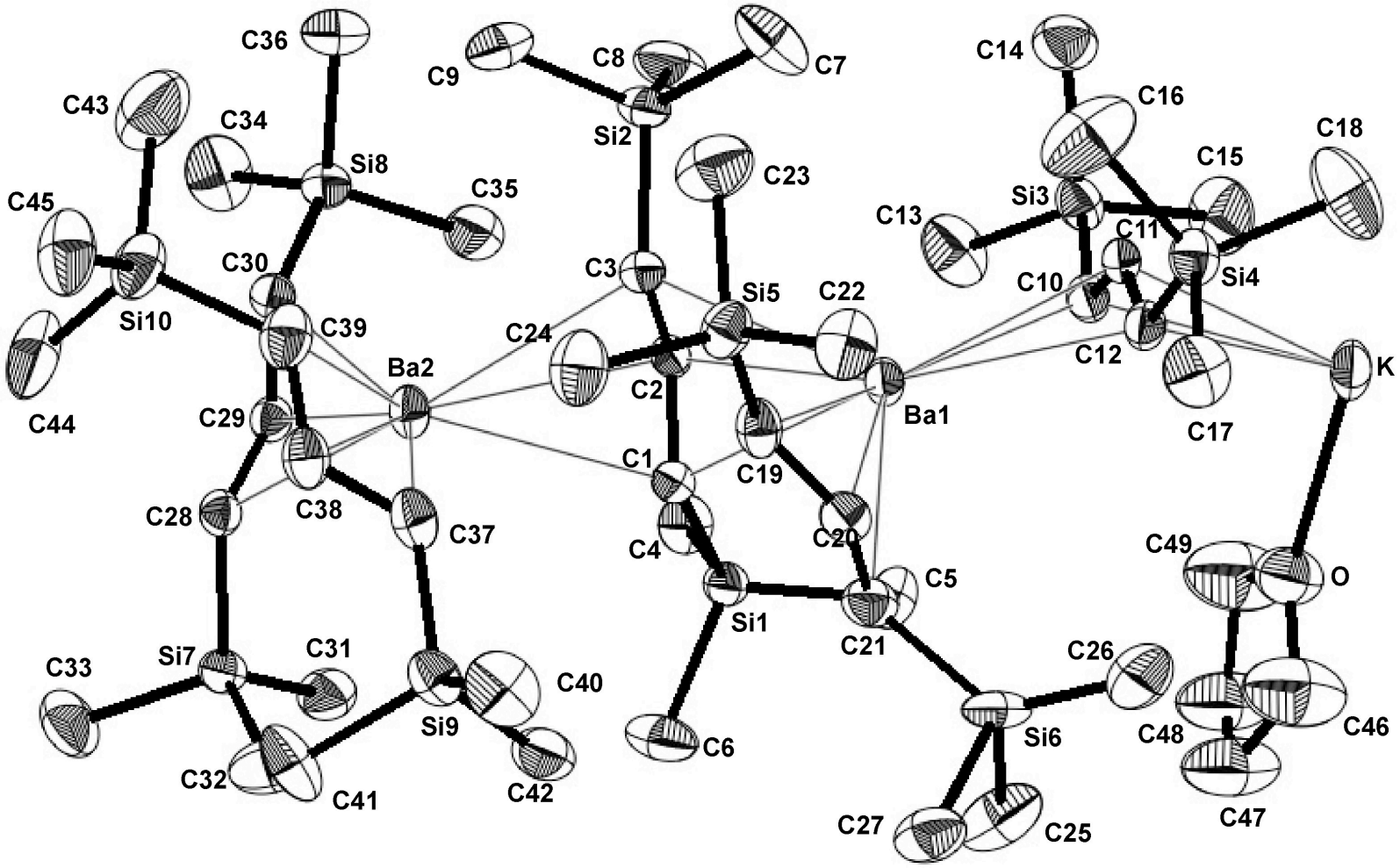

Figure 42. ORTEP of $\{[1,3\text{-}(SiMe_3)_2C_3H_3]_5Ba_2K(thf)\}_\infty$.

The heterometallic nature of this complex is not surprising, considering that the radii of six-coordinate K^+ (1.38 Å) and six-coordinate Ba^{2+} (1.35 Å) are similar.[130] Interestingly, the space group of $\{[1,3\text{-}(SiMe_3)_2C_3H_3]_5Ba_2K(thf)\}_\infty$ is chiral ($P2_12_12_1$).[181] The bridging allyl ligands in this helical Ba_2/K polymer rotate clockwise, making the polymer chiral (i.e., $\{P\text{-}[1,3\text{-}(SiMe_3)_2C_3H_3]_5Ba_2K(THF)\}_\infty$) (Figure 43). Presumably, crystals of the other isomer, $\{N\text{-}[1,3\text{-}(SiMe_3)_2C_3H_3]_5Ba_2K(THF)\}_\infty$, were formed, but not structurally characterized. The chirality imparted to this polymer by the orientation of the bridging allyl ligands is most likely a result of steric influence; it is possible that an ordered rotation of the bridging allyl ligands (clockwise or counterclockwise) results in reduced the steric hindrance among the polymeric chains. The crystal structure of $\{[1,3\text{-}(SiMe_3)_2C_3H_3]_5Ba_2K(thf)\}_\infty$ represents the first known heterometallic Ba/K organometallic complex to be crystallographically characterized and the first chiral polymeric structure of barium.

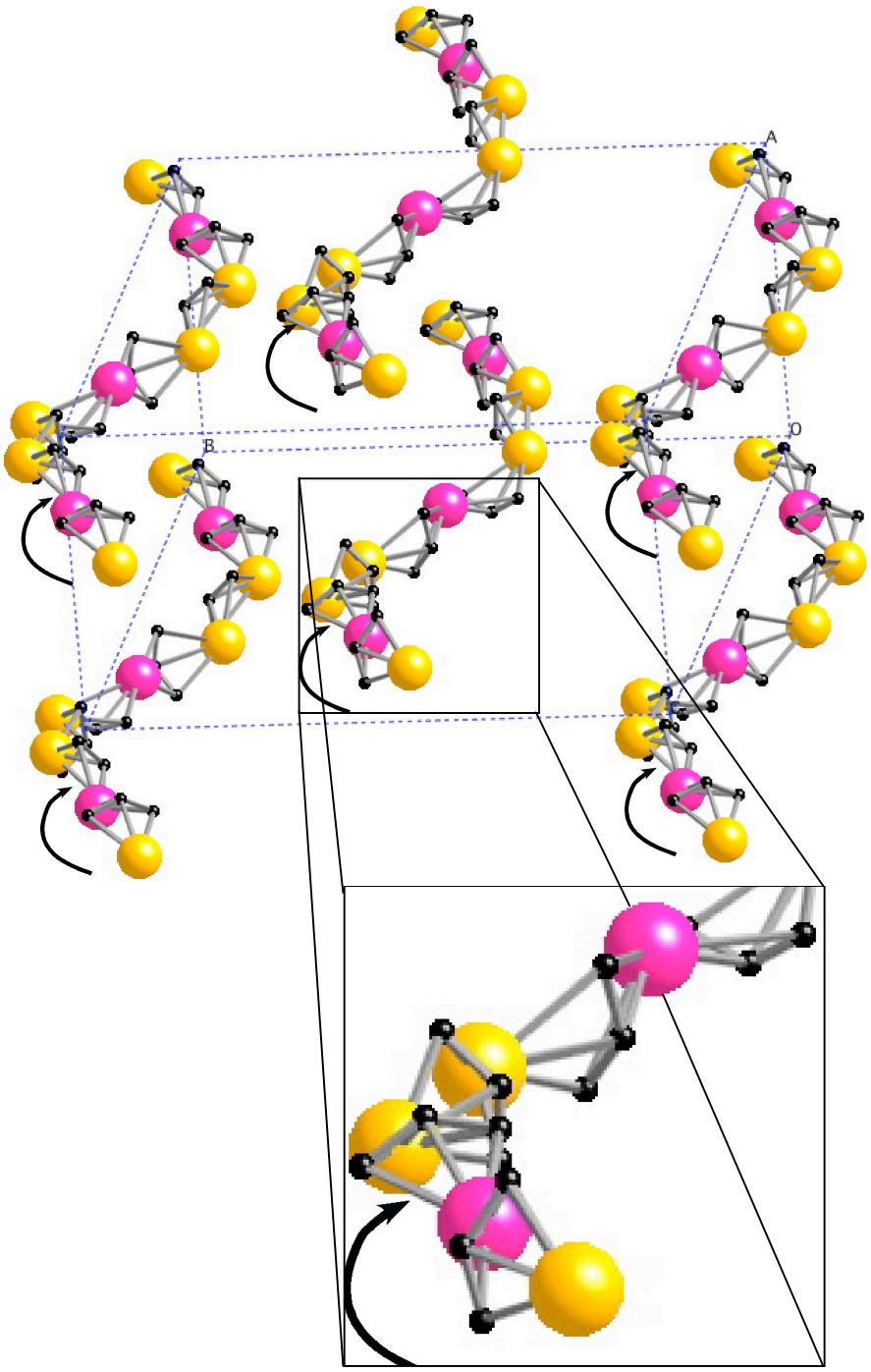

Figure 43. Solid-state structure of {P-[1,3-$(SiMe_3)_2C_3H_3]_5Ba_2K(THF)\}_\infty$, showing the clockwise rotation of bridging allyl ligands down the unit cell. Trimethylsilyl groups, terminal allyl ligands, and THF molecules are omitted for clarity. Inset shows close-up of allyl rotation.

Obviously, K[1,3-$(SiMe_3)_2C_3H_3$] and BaI_2 are not reacting in a 2:1 ratio in THF to form $\{[1,3\text{-}(SiMe_3)_2C_3H_3]_5Ba_2K(thf)\}_\infty$. The true ratio of the allylpotassium and BaI_2 for the balanced equation is 5:2, respectively (eq 42).

$$5\ K[1,3\text{-}(SiMe_3)_2C_3H_3] + 2\ BaI_2 \rightarrow \{[1,3\text{-}(SiMe_3)_2C_3H_3]_5Ba_2K(thf)\}_\infty + 4\ KI \quad (42)$$

Because of the discrepancy between the initially proposed structure and the experimentally determined structure, the NMR data for $\{[1,3\text{-}(SiMe_3)_2C_3H_3]_5Ba_2K(thf)\}_\infty$ was re-evaluated. Since there is only one set of resonances corresponding to allyl protons, all allyl ligands must be equivalent at room temperature, indicating fast exchange of any terminal and/or bridging allyls. In THF-$_{d8}$, the proton resonances on the allyl backbone for this sample (δ 2.59 (d); 6.53 (t)) are slightly upfield relative to those of K[1,3-$(SiMe_3)_2C_3H_3$] (δ 2.75 (d); 6.60 (t)).[182] This difference supports the hypothesis that allyl interacts with both potassium and barium metal centers in solution. Methyl methacrylate polymerization data also confirm that there is not free K[1,3-$(SiMe_3)_2C_3H_3$] in solution and some sort of interaction with Ba^{2+} must occur, as the turn-over-frequency is lower than that of the allylpotassium complex (see below).

The Ba–$C_{(terminal\ allyl)}$ bond lengths (2.876(4)–2.969(4) Å) are slightly shorter than both the Ba–$C_{(bridging\ allyl)}$ values (2.998(3)–3.141(4) Å) and those of K–$C_{(bridging\ allyl)}$ (2.980(4)–3.157(4) Å). However, the small range in M–C bond lengths show the allyl C–C bonds are delocalized. The allyl carbons form angles within the range of 128.7(3)°–131.0(4)°, which are similar to those seen in other

organometallic allyl complexes.[80,151,172] The K–$O_{(THF)}$ bond length (2.681(4) Å) is slightly longer than that seen for the five-coordinate K^+ in {K[1,3-$(SiMe_3)_2C_3H_3$](THF)$_{3/2}$}$_\infty$ (2.657 Å).

The K–C bond range is typical for π-bound organometallic ligands. For example, bond distances of 2.98–3.10 Å and 2.93–3.10 Å are observed in {K[1,3-$(SiMe_3)_2C_3H_3$](DME)}$_\infty$[151] and {K[1,3-$(SiMe_3)_2C_3H_3$](THF)$_{3/2}$}$_\infty$,[172] respectively. The K–C bond range found in potassium cyclopentadienides are similar (cf. 2.93–3.10 Å in [K($C_5(SiMe_3)_3H_2$)]$_\infty$[183] and 2.99–3.10 Å in [K($C_5(SiMe_3)H_4$)]$_\infty$).[184] The Ba–C bonding distances in {[1,3-$(SiMe_3)_2C_3H_3$]$_5$$Ba_2$K(thf)}$_\infty$ (terminal = 2.918 Å (av); bridging = 3.046 Å (av)) is similar to those found in other π-bound organometallic complexes of barium. For example, average Ba–C distances of 2.94(1) Å and 2.99(2)Å are found for ($C_5(C_3H_7)_4H)_2Ba$[36] and ($C_5Me_5)_2Ba$.[185] Even in the more sterically crowded (1,2,4-$(SiMe_3)_3C_5H_2)_2Ba$, the average Ba–C distance is 3.01(2)Å. [106]

There is a wide range of trimethylsilyl torsion angles in this polymeric complex. The Ba–K bridging allyl ligands exhibit the largest torsion range between the two trimethylsilyl moieties at 1.73°–9.61°. The trimethylsilyl torsion angle range on the Ba–Ba bridging allyls are smaller at 1.71°–5.82°, and the terminal allyl TMS torsion ranges on Ba1 and Ba2 are similar at 1.36°–5.69° and 3.01°–6.38°, respectively. These TMS torsion values are larger than those of {[1,3-$(SiMe_3)_2C_3H_3$]Cs(thf)}$_\infty$, but still within expected parameters.[25,80,169]

The closeness of K^+ and Ba^{2+} in size is likely responsible for the formation of the heterometallic {[1,3-$(SiMe_3)_2C_3H_3$]$_5$$Ba_2$K(thf)}$_\infty$ in preference to a

homometallic allylbarium species. The use of an allyllithium starting material may lead to a homometallic allylbarium species because of the large size difference in Ba^{2+} (1.35Å) and Li^{+} (0.76 Å). In a test of this hypothesis, a reaction was run with the trimethylsilyl-substituted allyllithium and BaI_2 in 2:1 ratio (eq 43).

$$2\ Li[1,3\text{-}(SiMe_3)_2C_3H_3]\ +\ BaI_2\ \rightarrow\ \text{(allyl)barium product}\ +\ 2\ LiI \qquad (43)$$

The NMR data for the product of this reaction was similar to that of $\{[1,3\text{-}(SiMe_3)_2C_3H_3]_5Ba_2K(thf)\}_\infty$. Proton NMR data of this allylbarium species (δ 0.37 (s); 3.14 (d); 7.00 (t)) has the characteristic singlet, doublet, triplet pattern of syn, syn trimethylsilyl arrangements on the allyl ligand, and the one set of resonances indicates equivalent allyl ligands due to fast exchange. The proton resonances however are shifted downfield with respect to those of $\{[1,3\text{-}(SiMe_3)_2C_3H_3]_5Ba_2K(thf)\}_\infty$ (δ –0.026 (s); 2.59 (d); 6.53(t)). This downfield shift could be a result of less electron density in the allyl environment in this species relative to the Ba_2/K polymer.

It cannot be determined from the NMR data whether this product is homo- or heterometallic in nature, but like the Ba_2/K polymer, there is only one THF molecule per two allyl molecules. It is likely that the structure of this (allyl)barium species is isostructural with $\{[1,3\text{-}(SiMe_3)_2C_3H_3]_5Ba_2K(thf)\}_\infty$, with an expected 5:2 reaction ratio (eq 44).

$$5\ Li[1,3\text{-}(SiMe_3)_2C_3H_3]\ +\ 2\ BaI_2\ \rightarrow\ \{[1,3\text{-}(SiMe_3)_2C_3H_3]_5Ba_2Li(thf)\}_\infty\ +\ 4\ LiI \qquad (44)$$

The reaction of two equivalents of K[1,3-$(SiMe_3)_2C_3H_3$] with SrI_2 is more straightforward. Like the previously mentioned (allyl)calcium and (allyl)barium species, the proton NMR spectrum of the (allyl)strontium species exhibits the singlet, doublet, triplet pattern that is associated with a syn, syn trimethylsilyl configuration on the allyl ligands. Integration of the proton peak resonances shows that two THF molecules are present on the Sr^{2+} metal center, which is corroborated by elemental analysis data.

X-ray analysis data collected on crystals of this sample show that [1,3-$(SiMe_3)_2C_3H_3]_2Sr(thf)_2$ is isostructural with [1,3-$(SiMe_3)_2C_3H_3]_2Ca(thf)_2$ (Figure44). Like its calcium congener, this allylstrontium complex crystallizes in a tetragonal space group ($P4_2/n$), and only half of this molecule is unique. The $Sr–C_{(allyl)}$ bond distance range is 2.797(3)–2.805(3) Å, which is similar to other six-coordinate Sr–C distances for organometallic Sr^{2+} complexes. For example, the $Sr–C_{(Cp)}$ bond distance range in (1,2,4-$(SiMe_3)_3C_5H_2)_2Sr$ is 2.773(4)–2.850(4) Å.[106] The $Sr–C_{(Cp)}$ bond lengths in seven-coordinate complexes such as $(C_5(C_3H_7)_4H)_2Sr(thf)$[186] (2.785(3)–2.889(3) Å) and (1,2,4-$(Me_3C)_3C_5H_2)_2Sr(thf)$[187] (2.841(3)–2.902(3) Å) are slightly longer than the $Sr–C_{(allyl)}$ values, but that is expected since the cyclopentadienyl ligands are more sterically crowded than the allyl ligand and the radii of six- and seven-coordinate Sr^{2+} differs, both of which results in longer Sr–C distances.

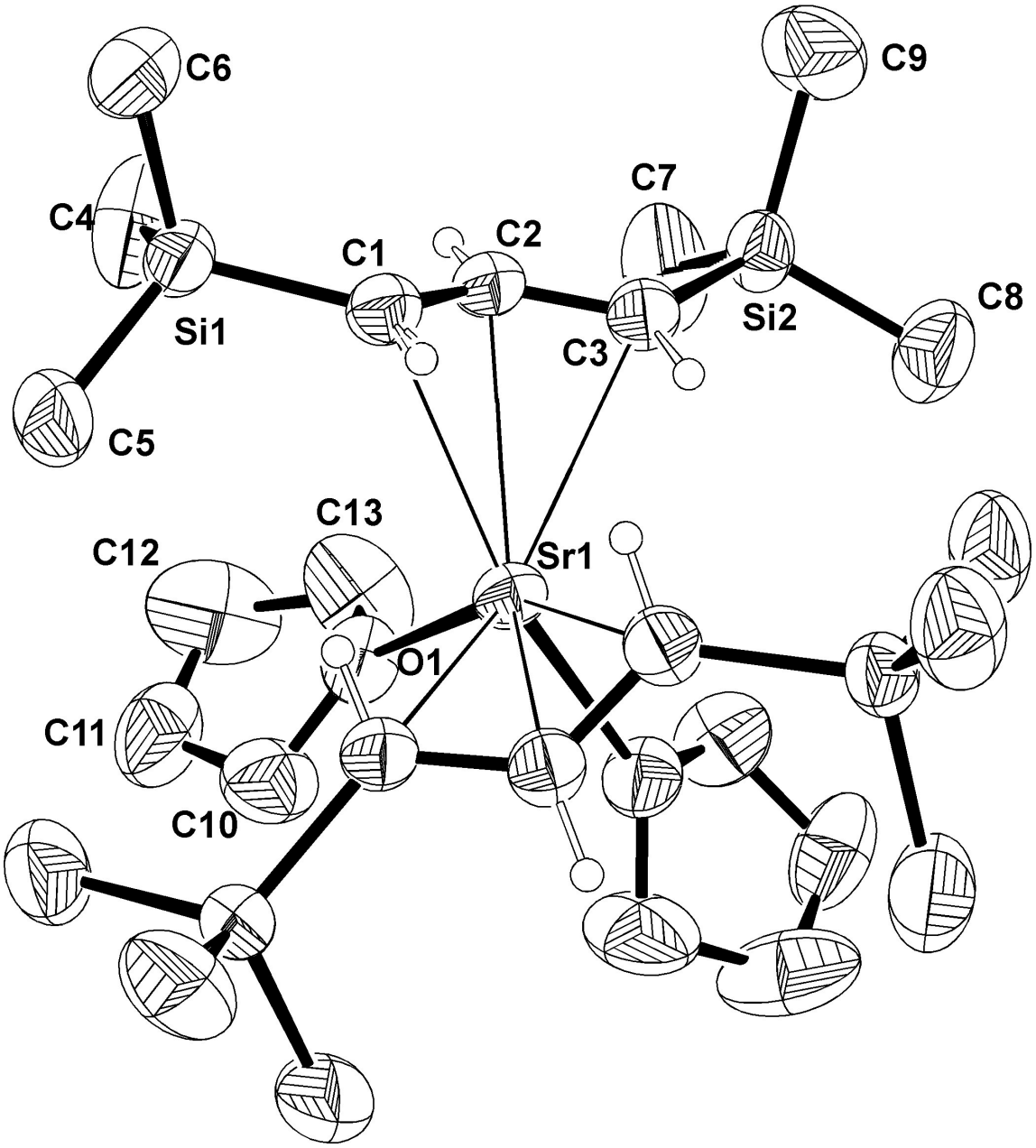

Figure 44. ORTEP of $[1,3\text{-}(SiMe_3)_2C_3H_3]_2Sr(thf)_2$, a monomeric species.

The average Sr–$O_{(THF)}$ distance of 2.514(10) is typical for THF-coordinated organostrontium complexes.[140,162,164,187] The angle between the allyl planes for $[1,3\text{-}(SiMe_3)_2C_3H_3]_2Sr(thf)_2$ (115.1°) is equivalent to that of $[1,3\text{-}(SiMe_3)_2C_3H_3]_2Ca(thf)_2$ (115.5°).[80] Even though the average bond length in the allylstrontium species (2.801(5) Å) is longer than that of the allylcalcium analog (cf.av. Ca–$C_{(allyl)}$ = 2.654(5) Å), the allyl plane angle is most likely determined by the steric bulk of the trimethylsilyl substituents.

The C–C–C angle within the allyl carbon ligand (129.4(3)°) is within the range seen in other organometallic allyl complexes,[80,151,172] and the narrow C–C(allyl) bond range of 1.398(5)–1.406(5) Å is a function of the delocalization of the bonds. The terminal hydrogens on the allyl carbon backbone are displaced from the allyl plane by 10.2° for C1–C2–C3–H3 and 2.4° for C3–C2–C1–H1. The difference in these values is not readily understood, as the torsion values for $[1,3\text{-}(SiMe_3)_2C_3H_3]_2Ca(thf)_2$ are nearly equal (cf. 16.9° and 16.2°). It is thought that this type of bending promotes rehybridization of the allyl carbon atoms to improve metal–ligand bonding.[80]

In an attempt to synthesize heteroleptic (allyl)alkaline-earth complexes, iodine was added to the homoleptic $[1,3\text{-}(SiMe_3)_2C_3H_3]_2M(thf)_2$ (M = Ca, Sr) in a 1:1 ratio and to the polymeric $\{[1,3\text{-}(SiMe_3)_2C_3H_3]_5Ba_2K(thf)\}_\infty$ in a 2:1 ratio. Instead of isolating (allyl)alkaline-earth iodides, work-up of the reactions yielded the coupled allyl dimer $[1,3\text{-}(SiMe_3)_2C_3H_3]_2$, as characterized by proton NMR spectroscopy. The formation of $[1,3\text{-}(SiMe_3)_2C_3H_3]_2$ upon addition of iodine has also been noted for $[1,3\text{-}(SiMe_3)_2C_3H_3]_2M$ (M= Fe, Co) (see Chapter 2).

Initial polymerization studies

A common monomer used in determining the activity of potential polymerization catalysts is methyl methacrylate. It has been shown that heterometallic trimethylsilyl-substituted allyl complexes of lanthanide/alkali metals can be used to polymerize methyl methacrylate.[28,87,149,150] Furthermore, K[1,3-$(SiMe_3)_2C_3H_3$] polymerizes methyl methacrylate more effectively when used as the sole catalyst rather than as part of a mixed metal species.[151] In an effort to determine if other *s*-block allyl complexes exhibit this catalytic activity, methyl methacrylate polymerization reactions were run with the as-synthesized allylcesium, allyl strontium, and Ba_2/K allyl polymer species. Initial studies have shown all three species to be active as catalysts for methyl methacrylate polymerization, with a conversion percent range of 72–94% and a TOF range of 18,600–21,100 hr^{-1}. The polymer produced by the allylcesium catalyst was atactic, whereas the polymer produced by the allylstrontium catalyst was slightly isotactic (71%). The Ba_2/K catalyst produced polymer that was less isotactic than in the allylstrontium case, but more so than in the case of the allylcesium (i.e., 61%). These complexes appear to have similar conversions to that of K[1,3-$(SiMe_3)_2C_3H_3$] (83%) for the polymerization of methyl methacrylate; however, the allylpotassium species has a much higher TOF (104,000 hr^{-1}). More studies need to be run before thorough comparisons to known methyl methacrylate polymerization catalysts can be made.

Conclusion

The bulky trimethylsilylated allyl $[1,3\text{-}(SiMe_3)_2C_3H_3]^-$ can be used to synthesize *s*-block allyl complexes of Cs^+, Rb^+, Sr^{2+}, and Ba^{2+}. Whereas $[1,3\text{-}(SiMe_3)_2C_3H_3]_2Sr(thf)_2$ is a monomeric species isostructural with its Ca^{2+} analog, $\{[1,3\text{-}(SiMe_3)_2C_3H_3]Cs(thf)\}_\infty$ is a linear chain polymer. The metathesis reaction of the allylpotassium and BaI_2 results in the formation of the chiral heterometallic polymer $\{[1,3\text{-}(SiMe_3)_2C_3H_3]_5Ba_2K(thf)\}_\infty$. These allyl complexes have been shown to be active polymerization catalysts of methyl methacrylate.

CHAPTER IV

ISOMERIZATION AND THERMAL DECOUPLING OF GROUP 2 AZULENIDES

Introduction

Inter-annular bridges between cyclopentadienyl ligands of metallocenes result in the formation of *ansa*-metallocenes. The incorporation of a bridging moiety can change the geometry of the complex, thus altering its electronic behavior[188] and affecting its reactivity.[189] These geometry-restricted species have found much use as stereospecific catalysts.[190,191] For example, *ansa*-metallocenes of the group IV transition metals are known polymerization catalysts for isotactic polypropylene.[192,193] Stereoselectivity and regioselectivity of the catalyst can be influenced by the sterics of the ligands.[194-196]

The reductive coupling of fulvenes with metals is a facile procedure for synthesizing *ansa*-metallocenes.[197-199] *s*-Block examples have been sought as ligand transfer agents to produce chiral transition metal catalysts[197,200] and have usually been made *in situ*. The first *ansa*-calcocene was reported by Edelmann in 1993; it was made by the addition of 6,6-dimethylfulvene to activated calcium granules (eq 45).[201]

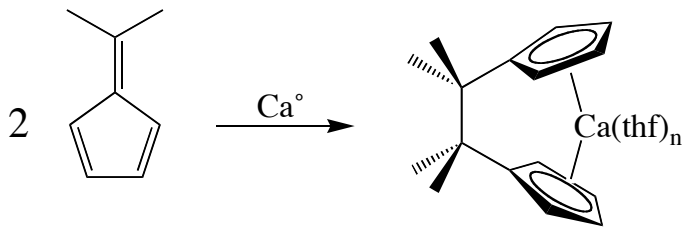

(45)

One problem with this synthesis is the formation of the unbridged isopropyl-substituted metallocene. In addition, there appears to be little selectivity for the *rac* over the *meso ansa*-calcocene isomer when bulky substituents are present on the cyclopentadienyl ring.[202] In contrast, polycyclic fulvenes in which the double bond of the fulvene is part of an annulated ring system consistently afford *rac ansa*-metallocenes in high selectivity.[202] For example, *ansa*-acenaphthylenide complexes have been synthesized with several metal centers including Sm, Yb, and Ca.[203 204]

Azulene, an isomer of naphthalene ($C_{10}H_8$), (Figure 45) and its derivatives are used as anti-inflammatory, anti-allergy, and anti-irritation agents.[205,206] These non-alternant hydrocarbons are natural products and can be found in chamomile oil. Although azulene is expensive as a reagent, the azulene derivative 1,4-dimethyl-7-isopropyl-azulene (guaiazulene) is a natural product of the guaiac tree and is a much cheaper reagent for study than azulene. The structure of azulene accounts for many of its interesting properties such as its dipole moment, its intense blue color, and its reactivity at the five-membered ring.[207] Much research has been conducted on the electronic properties of azulenes.[205,208-210]

Figure 45. Structures of azulene (left) and naphthalene (right).

Azulenes, because of their polycyclic aromatic structures, can be viewed as substituted fulvenes (Figure46). Therefore, *ansa*-bridged biazulenide complexes can be synthesized using azulenes as ligands, as reductive coupling occurs between two

azulenyl ligands in the presence of activated metals.[211] [212] Several transition metal biaiazulenide and biguaiazulenide complexes have been synthesized and studied.

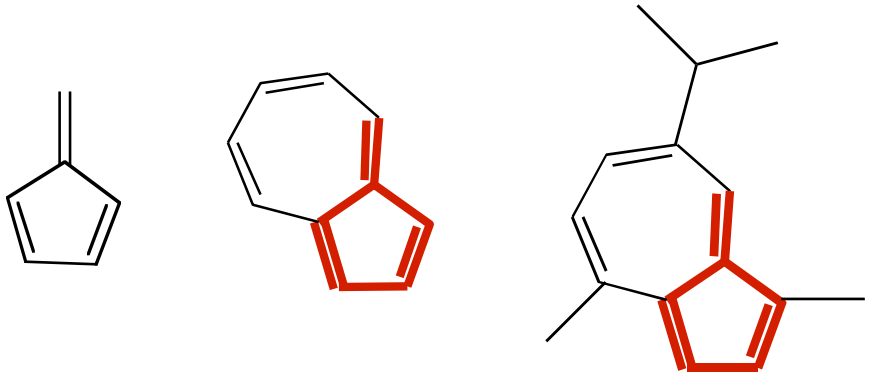

Figure 46. Structures of fulvene (left), azulene (center), and guaiazulene (right), highlighting the fulvene backbone in each.

For example, bis-(azulenyl)iron(II)[213] was first reported by Fisher in 1964. It was later structurally determined that the two azulenyl ligands were coupled in the complex.[211,212] Other metal centers have been used to form similar complexes including Ti,[214] Zr,[215] Hf,[194] and Yb.[216] Curiously, no Group 2 biazulenides have been studied in detail. At the start of this research, only (biguaiazulenyl)magnesium was reported in the literature, and it was synthesized *in situ* for use as a transmetallation agent; it was not fully characterized [214]

The synthesis and study of *s*-block biazulenide complexes may prove valuable in ways other than for use as ligand transfer agents. In addition to their potential catalytic uses, if the reductive coupling of the ligands could be reversed, these complexes could provide new sources of zero-valent metals.[134] In this research, a series of *s*-block biazulenyl complexes were synthesized and characterized. (Biguaiazulenyl)calcium(thf)$_2$ was used as a model for this group of

compounds in thermal decoupling reactions and will be the only complex described here. DFT calculations were run to help understand the energetics of the decoupling process. As this research was being conducted, the crystal structure of (biguaiazulenyl)calcium(thf)$_2$ was reported,[202,216] which allowed direct comparisons of calculated and experimental geometries.

Experimental Section

General Considerations. All manipulations were performed with the rigorous exclusion of air and moisture using high vacuum, Schlenk, or glovebox techniques. Proton and carbon (^{13}C) NMR spectra were obtained on a Bruker DPX–300 spectrometer at 300 and 75.5 MHz, respectively, and were referenced to the residual proton and ^{13}C resonances of C_6D_6 (δ 7.15 and 128.0). HMQC NMR spectra were recorded on a Bruker DPX–400 spectrometer and were similarly referenced. All NMR data were processed using Bruker XWINNMR 3.5 software on an Octane workstation (Silicon Graphics, Mountain View, CA).

Melting points were determined on a Laboratory Devices Mel–Temp apparatus in sealed capillaries. Metal and combustion analyses were performed by Desert Analytics, Tuscon, AZ. Themogravimetric analyses were performed on a TA Instruments Hi-Res TGA 2950 Thermogravimetric Analyzer. The analyzer was enclosed in a glove-bag that was purged with nitrogen (2h). The scans were collected under a flow of N_2 while heating from 25 °C to 600 °C at a rate of 10 °C/min, unless otherwise noted.

Materials. Azulene and guaiazulene were purchased from Acros, potassium metal was purchased from Strem, and $MgBr_2$, CaI_2, and SrI_2 were purchased from

Aldrich; all were used as received. THF, toluene, and hexanes were distilled under nitrogen from potassium benzophenone ketyl.[39] Deuterated solvents were vacuum distilled from Na/K (22/78) alloy prior to use.

Synthesis of reduced Group 2 metals. Zero-valent Group 2 (Reike) metals were obtained by literature procedure. [217,218] Alkaline earth di-iodides were reduced in the presence of potassium metal in THF at reflux temperatures or for longer periods of time at 25 °C. Excess metal halide was used to ensure complete oxidation of potassium metal. The reduced alkaline-earth metal suspensions were black, and the activated metals were used in situ in subsequent reactions.

Reaction of potassium and guaiazulene. Guaiazulene (1.503 g, 7.579 mmol) was dissolved in THF (40 mL) in a 125 Erlenmeyer flask. Potassium metal (0.996 g, 25.5 mmol) was added to the guaiazulene solution, and the reaction was stirred overnight. The reaction was filtered to remove any unreacted potassium metal. THF was removed from the filtrate, leaving a brown solid (2.04 g).

Reaction of potassium and azulene. Azulene (0.138 g, 1.08 mmol) was dissolved in THF (40 mL) in a 125 Erlenmeyer flask. Potassium metal (0.090 g, 2.3 mmol) was added to the azulene solution, and the reaction was stirred overnight. The reaction was filtered to remove any unreacted potassium metal. THF was removed from the filtrate, leaving a brown solid (0.18 g; 35% yield). Although NMR data confirm one THF molecule per potassium metal center, elemental analysis data show one-half THF molecule per potassium. Anal. Calcd for $C_{24}H_{24}K_2O$: C, 70.88; H, 5.95; K,19.22. Found: C, 72.03; H, 5.92; K 19.22.

Reaction of activated magnesium and guaiazulene: synthesis of (diguaiazulenide)bis(tetrahydrofuran)magnesium. Guaiazulene (5.00g, 25.2

mmol) was added to a suspension of activated magnesium (0.457 g, 18.8 mmol) in THF (40 mL) in a 125 Erlenmeyer flask. The reaction was stirred overnight and then filtered. THF was removed under vacuum from the filtrate, leaving a precipitate and unreacted guaiazulene. Small portions of hexanes were used to rinse the guaiazulene from the gray-green precipitate (2.495 g; 35% yield). Partial loss of THF was noted in elemental analysis data. Anal. Calcd for $C_{34}H_{44}MgO$: Mg, 4.93. Found: Mg 5.38.

Reaction of activated calcium and guaiazulene: synthesis of (diguaiazulenide)bis(tetrahydrofuran)calcium. Guaiazulene (1.599 g, 8.022 mmol) was added to a suspension of activated calcium (0.1608 g, 4.011 mmol) in THF (40 mL) in a 125 Erlenmeyer flask. The reaction was stirred overnight and then filtered. THF was removed under vacuum from the filtrate, leaving a precipitate and unreacted guaiazulene. Small portions of hexanes were used to rinse the guaiazulene from the off-white precipitate (0.688g; 40% yield). Anal. Calcd for $C_{38}H_{52}CaO_2$: C, 78.57; H, 9.02; Ca, 6.90. Found: C, 78.22; H, 9.36; Ca 6.85. Proton and carbon signals in the NMR data are labeled according to Figure 47. ^{1}H NMR (300 MHz, THF-d_8, 298 K): δ 0.89 (d, J = 6.7 Hz, 6H, CH(CH_3)$_2$); 1.03, (d, J = 6.7 Hz, 6H, CH(CH_3)$_2$); 1.75 (m, 8H, THF); 2.00 (s, 6H, H(1/16)); 2.17 (s, 6H, H(12/27)); 2.55 (hept, J = 6.7 Hz, 2H, H(13/28); 3.62 (m, 8H, THF); 4.16 (s, 2H, H(7/22); 5.57 (d, J = 6.6 Hz, 2H, H(9/24)); 5.61 (d, J = 3.2 Hz, 2H, H(3/18)); 5.67 (d, J = 3.2 Hz, 2H, H(4/19)); 5.73 (d, J = 6.6 Hz, 2H, H(10/25)). ^{13}C NMR (75 MHz, C_6D_6, 298 K): δ 12.61 (C(1/16)); 24.34 (C(12/27); 21.71, 24.54 (C(14/15/29/30)); 25.30 (THF); 38.00 (C(13/28)); 44.89 (C(7/22)); 67.70 (THF); 102.91 (C(4/19));

110.30 (C(3/18)); 111.75 (C(8/23)); 117.40 (C(9/24)); 117.91 (C(10/25)); 123.76 (C(11/26)); 134.85 (C(6/21)); 149.81 (C(5/20)).

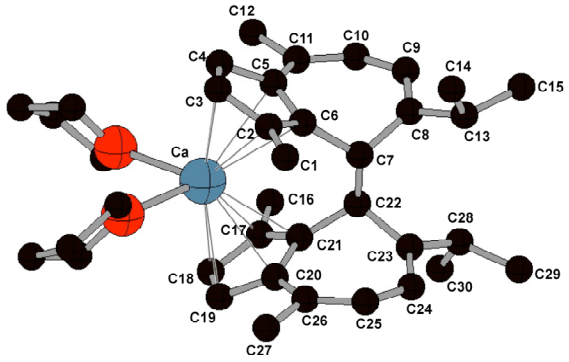

Figure 47. Labelled solid-state structure of (diguaiazulenide)bis(tetrahydrofuran)calcium.

Reaction of activated calcium and azulene: synthesis of (diazulenide)bis(tetrahydrofuran)calcium. Azulene (0.472g, 3.68 mmol) was added to a suspension of activated calcium (0.0724 g, 1.81 mmol) in THF (40 mL) in a 125 Erlenmeyer flask. The reaction was stirred overnight and then filtered. THF was removed under vacuum from the filtrate, leaving a precipitate and unreacted azulene. Small portions of hexanes were used to rinse the azulene from the off-white precipitate (0.241 g; 30% yield). Partial loss of THF was noted in elemental analysis data. Anal. Calcd for $C_{24}H_{24}CaO$: C, 78.22; H, 6.56; Ca, 10.87. Found: C, 77.39; H, 6.51; Ca 10.37. ^{1}H NMR (300 MHz, THF-d_8, 298 K): δ 1.77 (m, 8H, THF); 3.60 (m, 8H, THF); 4.05 (s, 2H); 5.24 (dd, 2H); 5.67 (dd, 2H); 5.73 (dd, 2H); 5.81 (mult, 6H); 6.74 (d, 2H). ^{13}C NMR (75 MHz, C_6D_6, 298 K): δ 25.45 (THF); 46.35; 67.69 (THF); 105.19; 107.52; 110.00; 119.27; 122.33; 125.59; 126.78; 130.09; 132.58.

Computational Details. Geometry optimization calculations were performed using the GAUSSIAN 03W suite of programs.[42] The B3LYP functional, which incorporates Becke's three–parameter exchange functional[43] and the correlation functional of Lee, Yang, and Parr,[44,45] was used.[46] The DFT-optimized triple zeta polarized basis set (TZV) (Ahlrichs) with 5d diffuse functions was used for the Ca^{2+} metal center[219] and the standard Pople basis set 6-31G(d,p) was used for the other elements for geometry optimizations and energy calculations.[48] Stationary points were characterized by the calculation of vibrational frequencies, and unless otherwise noted, all geometries were found to be minima (N_{imag}=0).

Results and Disscussion

The use of finely divided metal powders in organic synthesis has received much study over the years since their original discovery by Rieke.[220-223] Activated alkaline-earth metals used for this research were prepared following the method of reduction of metal halides with alkali metal.[217,224] Excess calcium iodide was used to ensure that no potassium was present in the resulting calcium metal suspension. Guaiazulene was added to the suspension, and the reaction was allowed to stir overnight prior to workup. The product, collected as a precipitate, was washed with hexanes to remove unreacted guaiazulene. The other reactions described in the experimental section were similarly conducted.

The reaction of activated calcium and guaiazulene yields two isomer products: (8,8´-biguaizulenide)calcium$(thf)_2$ and (8,6´-biguaizulenide)calcium$(thf)_2$, as detected by their different solubilities in THF and DME (Figure 48). For this research, a (8,8´-biguaizulenide)calcium$(thf)_2$ sample was used for thermal

decoupling studies. The (8,8´-biguaizulenide)calcium(thf)$_2$ isomer has been structurally authenticated by another group.[202,216] As such, NMR data from this research will not be discussed because it confirms the interpretation by Shapiro etal.

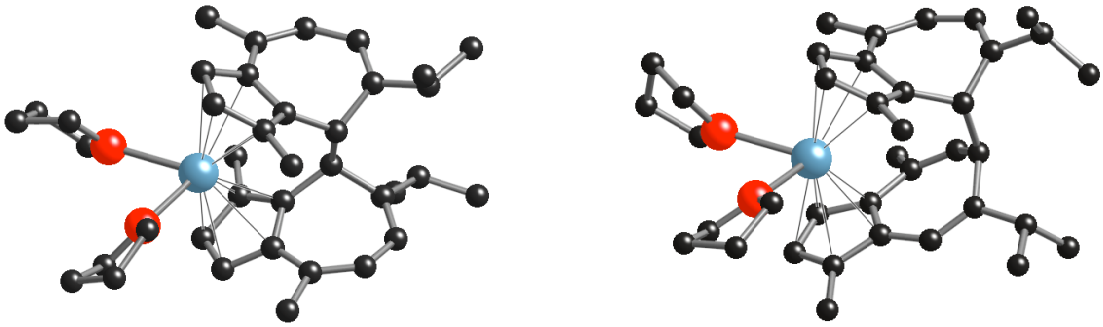

Figure 48. Calculated structures of *rac*-8,8´-isomer (left) and *meso*-8,6´-isomer (right) of (biguaizulenide)calcium(thf)$_2$.

The 8,8´-isomer has a *rac*-structure, where the two guaiazulenyl ligands are bound with methyl groups pointing in opposite directions, but the 8,6´-isomer has a meso-structure, where the two guaiazulenyl ligands are bound with methyl groups pointing in the same direction. Of the two isomers, the 8,8´-isomer is the thermodynamically favored one; as seen in a solution thermolysis study (Figure 49), the 8,6´-isomer converts to the 8,8´-isomer in solution at ~95°C (1 day).[202] For the *meso*-structure to convert to a *rac*-structure, the C–C bridge must be broken and reformed.

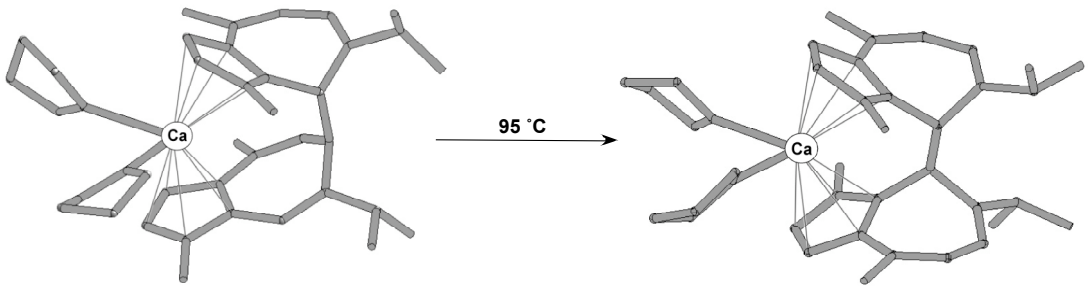

Figure 49. Conversion of *meso*-8,6´-isomer (left) to *rac*-8,8´-isomer (right) at 95 °C.

DFT calculations were employed to better understand the energetics of this reaction. The thermodynamic change associated with the conversion of *meso*-(8,6´-biguaizulenide)calcium(thf)$_2$ to *rac*-(8,8´-biguaiazulenide)calcium(thf)$_2$ was investigated using B3LYP and two different basis sets, TZV (Ahlrichs) + 5d (on Ca) and 6-31G(d) on (C, H, O). The Alhrichs TZV basis set puts highly contracted d functions on the calcium center to more accurately approximate the bending seen in calcocene complexes. Equilibrium geometries were calculated for both the *meso*-(8,6´-biguaizulenide)calcium(thf)$_2$ and *rac*-(8,8´-biguaiazulenide)calcium(thf)$_2$ for comparison of their ΔG° and ΔH° values.

As a measure of the accuracy of the DFT calculations, calculated structural parameters of the *rac*-8,8´-isomer were compared with experimental ones of the structurally authenticated *rac*-8,8´-isomer. In the calculated *rac*-(8,8´-biguaiazulenide)Ca(thf)$_2$ structure, the Ca–C$_{(ring)}$ bond length range is 2.680–2.717 Å (Ca–centroid = 2.405 Å) and the bridging C–C bond is 1.595 Å. These values are close to those reported for the crystal structure of the *rac*-8,8´-isomer (c.f. Ca–C$_{(ring)}$ = 2.668(3)–2.758(3), Ca–centroid = 2.412(9) Å, and C–C$_{(bridging)}$ = 1.577(4)Å). [202] Other parameters such as centroid–Ca–centroid angle, O–Ca–O angle, and the

angle between Cp planes are similar in both the calculated and experimental *rac*-8,8′-isomer structures (122.24° (calc) / 120.2° (exp), 80.49° (calc) / 84.30(9)° (exp), and 58.0° (calc) / 59.3° (exp), respectively).

The *meso*-8,6′-isomer is higher in energy than the *rac*-8,8′-isomer by 6.9 kcal/mole in ΔG° and 6.7 kcal/mole in ΔH°. This fact is reflected in the differences in their structures. The *meso*-8,6′-isomer, with its two guaiazulenyl ligands bound in the same orientation, has a larger centroid–Ca–centroid angle (134.10°), but a smaller angle between Cp planes (44.62°) than those of the *rac*-8,8′-isomer. These parameters show that the two Cp moieties are more centered over the calcium in the 8,6′-isomer than in the 8,8′-isomer, where the calcium center displays greater displacement from a metallocene-like arrangement. As a result, the Ca–C(ring) bonding range (2.642–2.849 Å) in the 8,6′-isomer is larger to compensate for the steric strain of the complex, and both the Ca–centroid (2.440 Å (av)) and the bridging C–C bond (1.604 Å) are longer in the 8,6′-isomer. The elongated bridging C–C bond (c.f. C–C ≈ 1.52 Å in ethano-bridged *ansa*-calcocenes)[189,201] accounts for the ease with which it is broken during thermolysis.

In an effort to gauge the steric role of the methyl and isopropyl moieties in the thermodynamic values of the thermolyic conversion, DFT calculations were run on the unsubstituted (4,6′-biazulenide)calcium(thf)$_2$ and (4,4′-biazulenide)calcium(thf)$_2$ (Figure 50). This hypothetical reaction follows the same trend as the substituted case does in that the symmetrically-bridged species (4,4′-isomer) is thermodynamically more stable than the asymmetrically-bridged species (4,6′-isomer); (4,6′-biazulenide)calcium(thf)$_2$ is higher in energy than (4,4′-biazulenide)calcium(thf)$_2$ by 3.1 kcal/mole in ΔG° and 4.1 kcal/mole in ΔH°.

The difference in energetics of the two isomers mimics that of the two biguaiazulenide species. As such, the same structural trends are also present in this system.

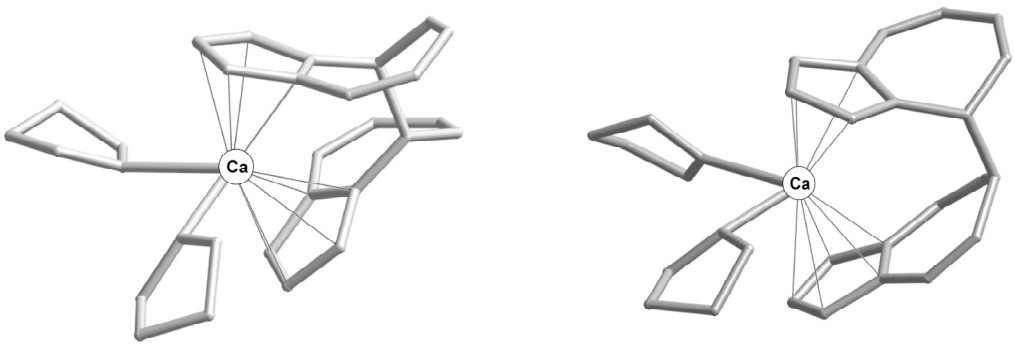

Figure 50. Calculated structures of 4,4′-isomer (left) and 4,6′-isomer (right) of (biaizulenide)calcium(thf)$_2$.

The 4,6′-isomer has a larger centroid–Ca–centroid angle (137.48°), but a smaller angle between Cp planes (43.15°) than those of the 4,4′-isomer (122.54° and 58.67°, respectively). Similar to the biguaiazulenide case, the Ca–C(ring) bonding range (2.631–2.850 Å) is larger in the 4,6′-isomer than in the 4,4′-isomer (2.646–2.743 Å), and both the Ca–centroid (2.451 Å (av)) and the bridging C–C bond (1.602 Å) are slightly longer in the 4,6′-isomer than in the 4,4′-isomer (2.409 Å and 1.591 Å, respectively). The methyl and isopropyl moieties do not seem to affect the structures of this type of ansa-calcocenes, as seen in the similarities of the structural parameters between 4,6′-biazulenide species and its 6,8′-biguaiazulenide analog and 4,4′-biazulenide species and its 8,8′-biguaiazulenide analog.

Cleavage of the C–C bridging bond also occurs for (biguaizulenide)calcium(thf)$_2$ in the solid state. As a sample was heated in a sealed capillary to ~234 °C, the off-white sample took on a greenish hue and free guaiazulene was released and collected near the top of the capillary; the decomposition product residue was discerned to have a metallic appearance (Figure51). A similar behavior was also seen for (biazulenide)calcium(thf)$_2$ when a sample is heated to ~220 °C.

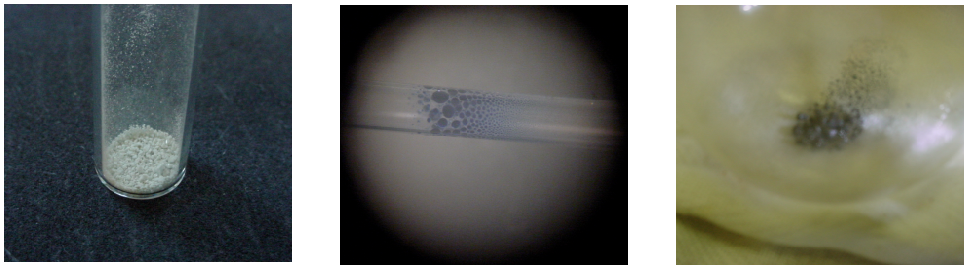

Figure 51. Sample of (biguaizulenide)calcium(thf)$_2$ before heating (left), release of guaiazulene after heating (234 °C) (center), and product residue (metallic appearance) obtained after heating treatment (right).

In order to obtain guaiazulene as a decomposition product upon heating a sample of (biguaizulenide)calcium(thf)$_2$ in the solid state, scission of the bridging C–C bond must occur. Conversion of the 8,6´-isomer to the 8,8´-isomer in solution has already attributed the to this bond breakage.[202] In the solid state, the disruption of the bridging C–C bond in the complex is a result of oxidative decoupling of the guaiazulene ligands; as a result,the calcium metal center must be reduced to account for the loss of two electrons from the [biaguaiazulenide]$^{2-}$ ligand.

DFT methods were used to model the thermal decomposition of (4,4´-biazulenide)calcium(thf)$_2$. The smaller biazulenide complex was used for this computational study because the extra bulk of the guaiazulenyl ligands was more computationally expensive and similar outcomes are expected for the two analogs based on the earlier DFT results. Like the previous DFT study, this system was investigated using B3LYP and two different basis sets, TZV (Ahlrichs) + 5d (on Ca) and 6-31G(d) on (C, H, O). The thermal decomposition of the (4,4´-biazulenide) species to calcium metal and azulene was described via a mechanism that involved scission of the bridging bond and the formation of a slipped metallocene-like intermediate (Figure 52).

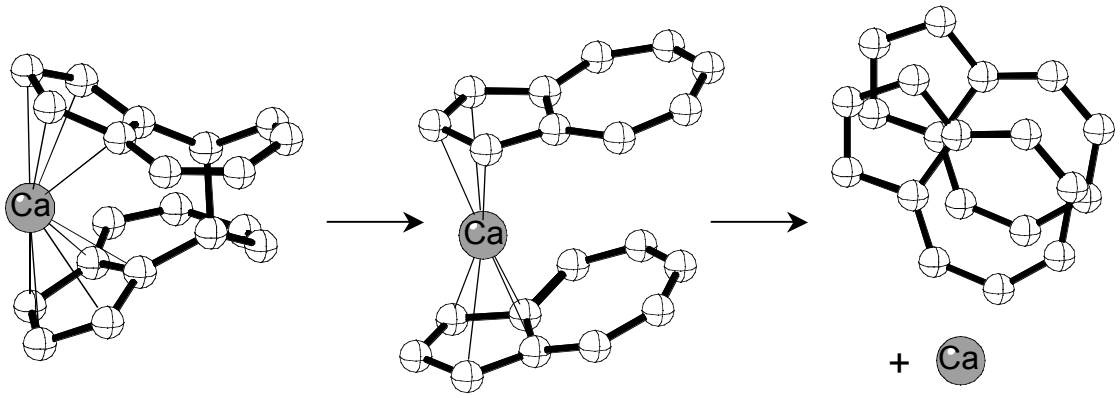

Figure 52. Proposed decomposition of (4,4´-biazulenide)calcium(thf)$_2$ via metallocene-like intermediate.

DFT calculations showed that the proposed decomposition mechanism is plausible. The metallocene-like intermediate is higher in energy than the 4,4´-isomer by 19 kcal/mole in ΔG°. The energetic sum of the decomposition products, two molecules of azulene and a zero-valent calcium center, is in turn lower in value than the intermediate by 13 kcal/mole in ΔG°. The metallocene-like intermediate is

bound η^3 to one azulenide and η^4 to the other one. The Ca–$C_{(\eta^3\text{-ring})}$ bond lengths (2.596–2.722 Å) are slightly longer than the Ca–$C_{(\eta^4\text{-ring})}$ values (2.448–2.681 Å). These values are actually somewhat shorter than those calculated for (4,4´-biazulenide)calcium$(thf)_2$ and the Ca–$C_{(\eta^5\text{-ring})}$ values found in (8,8´-biguaiazulenide)calcium$(thf)_2$.

When comparing this intermediate species (with its shorter Ca–C bonds) to the calculated (and experimental) C–C bridged species, it is understandable that the C–C bridge reforms in the case of the solution thermolysis of (8,6´-biguaiazulenide)calcium$(thf)_2$ to (8,8´-biguaiazulenide)calcium$(thf)_2$. Calculations have shown increased electron density at the carbon position 4, 6, and 8 on the back of the azulenyl ring system.[205,208,209] However, the extra energy supplied by heating a sample in the solid state to decomposition, could result in a separation of ligands and metal center, as electron transfer occurs to the metal center.

Thermogravimetric analysis was used to determine the identity of the decomposition products of (8,8´-biguaiazulenide)calcium$(thf)_2$ upon heating under nitrogen. The thermogravimetric analyzer and sealed samples were enclosed in a glove-bag that was purged with nitrogen for ~2 hours. The atmosphere was tested for the presence of oxygen with a 1M solution of diethylzinc in hexanes; the was no detectable formation of zinc oxide upon opening the vial of diethylzinc in the glove-bag.

The sample decomposed upon heating as the weight loss was measured. A plot of sample weight (mg) vs temperature (°C) was constructed (Figure 53) and a derivative of that plot was calculated to determine the percentage weight loss over time. The rate of heating is important in the decomposition product formation.

Whereas a heating rate of 5 °C/min resulted in a decomposition product corresponding to about 30% of initial weight, a heating rate of 10–20 °C/min resulted in a 10% of initial weight product. The following table provides the theoretical percent weight change data in comparison with the experimental percent weight change data of a heated sample (20 °C/min) of (8,8´-biguaiazulenide)calcium(thf)$_2$ (Table 9).

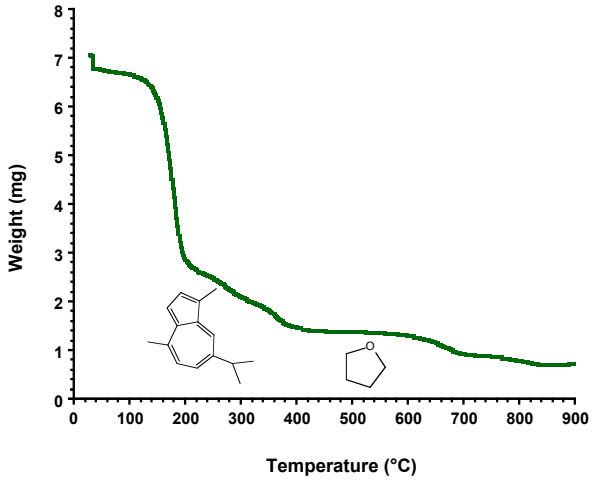

Figure 53. Plot of weight loss (mg) vs. temperature (°C), indicating loss of guaiazulene and tetrahydrofuran.

Table 9. Theoretical percent weight change vs. experimental percent weight change for (8,8´-biguaiazulenide)calcium(thf)$_2$.

Theoretical % Wt Change	**Experimental % Wt Change**
Guaiazulene (loss of two): –68%	Guaiazulene: –67%
Tetrahydrofuran (loss of two): –25%	Tetrahydrofuran: –18%
Calcium residue (Ca: 7%; CaO: 10%)	Calcium residue: 10%

The thermogravimetric data point to the formation of calcium oxide and not metallic calcium as a decomposition product of (8,8´-biguaiazulenide)calcium(thf)$_2$. Since the glove-bag atmosphere was tested for the presence of oxygen before and after the heat cycle, the logical oxygen source is tetrahydrofuran. This hypothesis is also substantiated by the experimental loss of THF at 18%, corresponding to only partial loss of two THF molecules per complex. Because the rate of heating affected the formation of the decomposition product, it is still possible that metallic calcium was formed in the capillary tube during initial heating experiments; it is likely that tetrahydrofuran may be removed intact under certain conditions. Other calcium products (including metallic calcium) may be obtained from varying the Lewis bases on the calcium center or removing them entirely from the biguaiazulenide complex.

Conclusion

The differences in both the orientation of the guaiazulenyl ligands and position of the C–C bridge in the structures of *meso*-(8,6´-biguaizulenide)calcium(thf)$_2$ and *rac*-(8,8´-biguaiazulenide)calcium(thf)$_2$ affect the relative stabilities of the complexes. In contrast to the *rac*-8,8´-isomer with guaiazulenyl ligands facing in opposite directions, the *meso*-8,6´-isomer, with its two guaiazulenyl ligands oriented in the same direction, experiences greater strain on the bridging C–C bond, which explains the conversion of the *meso*-8,6´-isomer and *rac*-8,8´-isomer in solution at 95 °C. In the solid state, (8,8´-biguaiazulenide)bis(tetrahydrofuran)calcium thermally decouples to yield free guaiazulene and calcium oxide. Substitution or removal of the adducted base may

alter the identity of the decomposition product residue. The thermal isomerization in solution and the decomposition in the solid state can be interpreted via the intermediacy of a metallocene-like species with slipped rings, as studied computationally with DFT methods.

CHAPTER V

THE CASE OF BULKY BERYLLOCENES: ATTEMPTED SYNTHESIS OF $[1,2,4\text{-}(SiMe_3)_3C_5H_2]_2Be$

Introduction

There has been much interest in the development of cyclopentadienyl derivatives of alkaline-earth metals over the last two decades.[104,105,137,225] A characteristic feature of nearly all base-free metallocenes of the heavy alkaline-earth (Ca, Sr, Ba) and lanthanide (Sm, Eu, Yb) elements is a distinctly "bent" geometry, with ring centroid–metal–ring centroid angles as small as 131°.[104,105,185,226-230] For example, bis[1,2,4-tris(trimethylsilyl)cyclopentadienyl] complexes $[1,2,4\text{-}(SiMe_3)_3C_5H_2]_2Ae$ ($(Cp^{3Si})_2Ae$; Ae = Ca, Sr, Ba) have been isolated and structurally characterized as bent metallocenes.[106] The non-linear structures of decamethylmetallocenes are found in both the solid state and the gas phase.[231,232] The origin of nonlinear structures in Group 2 metallocenes is not easily explained on steric or electrostatic grounds alone. One analysis of the bending phenomenon found that a strongly linear correlation existed between metal–ring distances and the ring–metal–ring bending angles in decamethylmetallocenes of the alkaline-earth, lanthanide, and *p*-block elements;[230] larger metals (with longer M–C distances) were associated with greater bending angles.

In contrast, almost all crystallographically characterized magnesocenes, including Cp_2Mg,[233] $(C_5Me_5)_2Mg$,[234] $[(t\text{-}Bu)C_5H_4]_2Mg$,[235] $[(CHCH_3Ph)C_5H_4]_2Mg$,[236] and $(Me_4C_5H)_2Mg$[237] have parallel rings. As Mg^{2+} is considerably smaller than the heavier alkaline-earth metals (i.e., $r_{Mg^{2+}} = 0.72$ Å;

$r_{Ca^{2+}}$ = 1.00 Å){Shannon, 1976 #88}, this observation fits the above-mentioned metal–ring distances vs. ring–metal–ring bending angles trend. The slight tilting of the rings observed in $(Cp^{3Si})_2Mg$ (7.8°) has been ascribed to the large amount of steric encumbrance around the Mg^{2+} center generated by the two Cp^{3Si} rings.[238]

Although numerous half-sandwich complexes are known for beryllium,[239] very few beryllocene complexes have been reported.[240-242] The hapticity of the cyclopentadienyl rings in $(C_5H_5)_2Be$ has been disputed since it was first synthesized by Fischer and Hoffmann in 1959.[243] However, X-ray studies[244-246]and theoretical calculations[247,248] have lent support to an η^5/η^1 slip-sandwich structure for beryllocene (Figure 54). The cyclopentadienyl rings undergo rearrangements via 1,5-sigmatropic shifts, which change the $(\eta^5\text{-}C_5H_5)Be^+$ point of attachment to the η^1-ring, and molecular inversions, which interchange the η^5- and η^1-rings.[249]

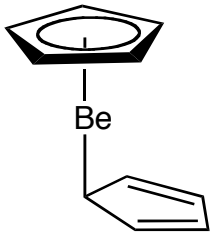

Figure 54. Diagram of $(C_5H_5)_2Be$, showing η^5/η^1 bonding of Cp rings.

Recently, several substituted beryllocenes have been structurally characterized.[249] As expected for this type of organometallic species, these complexes are air- and moisture-sensitive. The octamethylated $(C_5Me_4H)_2Be$ is prepared from a facile reaction of $BeCl_2$ and $K(C_5Me_4H)$ in ether (eq 46).

$$2\ K(C_5Me_4H)\ +\ BeCl_2 \xrightarrow{Et_2O} (C_5Me_4H)_2Be + 2\ KCl\downarrow \qquad (46)$$

This complex, like the parent beryllocene, exhibits η^5/η^1 cyclopentadienyl bonding, and the Cp rings are fluxional in solution. The bulkier permethylated beryllocene was synthesized under more forcing conditions (refluxing in toluene/ether for 3 days). The solid-state structure of $(C_5Me_5)_2Be$ shows both cyclopentadienyl ligands bound in an η^5 manner and in parallel fashion, like $(C_5Me_5)_2Mg$.[234] However, $(C_5Me_5)_2Be$ reacts with $CNC_6H_3Me_2$ to form a half-sandwich complex.[250] This reaction is thought to occur via insertion into a Be–C(σ) bond, thus suggesting that an η^5/η^1 cyclopentadienyl arrangement exists for $(C_5Me_5)_2Be$ in solution.

The steric pressure on a beryllocene with the bulkier Cp^{3Si} rings might be even greater, and could conceivably prevent the formation of the complex through the operation of "steric oversaturation."[251] This principle was also thought to be the reason that a permethylated beryllocene could not be synthesized due to ligand bulk. The synthesis of $(C_5Me_5)_2Be$[242] in 2000 demonstrated that steric oversaturation may not always apply. In this chapter, an attempt to synthesize a substituted beryllocene using the bulky [1,2,4-tris(trimethylsilyl)cyclopentadienyl]$^-$ ligand is discussed along with DFT calculations that support the possibility of forming such a bulky complex.

Experimental Section

General Remarks: All manipulations were performed with the rigorous exclusion of air and moisture using high vacuum, Schlenk, or drybox techniques. Anhydrous beryllium chloride (Strem Chemicals) was used as received. K[1,2,4-$(SiMe_3)_3C_5H_2$] was prepared as previously described.[162] Solvents for reactions were distilled under nitrogen from sodium or potassium benzophenone ketyl. NMR solvents were vacuum distilled from Na/K (22/78) alloy and stored over 4A molecular sieves. Proton and carbon (^{13}C) NMR spectra were obtained on a Bruker NR-300 spectrometer at 300 and 75.5 MHz, respectively, and were referenced to the residual resonances of C_6D_6 (δ 7.15 and 128.0) or [D_8]THF (δ 3.58 and 67.4).

Attempted Syntheses of [1,2,4-$(SiMe_3)_3C_5H_2]_2Be$: $BeCl_2$ (0.031 g, 0.39 mmol) and K[1,2,4-$C_5H_2(SiMe_3)_3$] (0.252 g, 0.79 mmol) were added to a flask under nitrogen at room temperature. Diethyl ether (20 mL) was added to the flask, and the reaction mixture was stirred for 3 days at room temperature, evaporated to dryness under vacuum, and the residue extracted with hexanes. ^1H NMR analysis of the extract indicated that only starting materials were present. The reaction was repeated in a 1:1 diethylether/toluene mixture, and refluxed under nitrogen for 3 days. A black residue was left at the completion of the reaction, and no metallocene was isolated on workup of the reaction mixture.

Computational Details. Calculations on $(Cp^{3Si})_2Be$ were performed using the *Gaussian* 03 *W* suite of programs.[42] A full geometry optimization using even the relatively modest 6-31G(d,p) basis set would have involved a computationally expensive set of 839 basis functions. An ONIOM calculation[252] was performed instead, using the 6-31G(d,p) basis set on Be, the ten carbon atoms of the

cyclopentadienyl rings, and the directly attached atoms (hydrogen or silicon). The semi-empirical PM3 method was used for the 18 methyl groups. The B3PW91 functional, which incorporates Becke's three-parameter exchange functional[46] with the 1991 gradient-corrected correlation functional of Perdew and Wang,[253] was used; this hybrid functional has previously been shown to provide realistic geometries for organometallic species.[254,255] Frequency calculations were used to establish that all optimized geometries were local minima ($N_{imag} = 0$).

Results and Discussion

The bis[(tris(trimethylsilyl)cyclopentadienyl]alkaline-earth metallocenes, $(Cp^{3Si})_2Ae$ (Ae = Ca, Sr, Ba), can be isolated from the 2:1 reaction of $K[Cp^{3Si}]$ and AeI_2 in ether (eq47). [106]

$$2\ K[Cp^{3Si}] + AeI_2 \xrightarrow{Et_2O} (Cp^{3Si})_2Ae + 2\ KI\downarrow \qquad (47)$$

(Ae = Ca, Sr, Ba)

The complexes are thermally stable and begin to sublime at temperatures ranging from 125 to 140 °C at between 10^{-5} to 10^{-7} torr. These complexes must be formed in ether, since in the presence of even small amounts of THF, the mono(ring) complexes $(Cp^{3Si})AeI(thf)_n$ are isolated as the exclusive products.[162] Once formed, however, the complexes can be recrystallized as base-free metallocenes from THF solution. The hexakis(trimethylsilyl)metallocenes visibly decompose upon exposure to air after only a few seconds, turning from white to

dark brown. In contrast, enhanced air-stability has been reported for both the octa- and decaisopropylated alkaline-earth metallocenes.[36,256] The magnesium compound $(Cp^{3Si})_2Mg$ was reported some time ago by Jutzi and coworkers.[238] Of the remaining Group 2 elements, only the radium and beryllium analogues remain unknown.

We attempted to synthesize $(Cp^{3Si})_2Be$ with a method similar to that used to prepare $(Me_4C_5H)_2Be$ and $(C_5Me_5)_2Be$;[242] viz., the reaction of $BeCl_2$ and $K[Cp^{3Si}]$ in diethyl ether (3 days at room temperature) or in a 1:1 diethyl ether/toluene mixture at reflux for 3 days. The reaction at room temperature yielded only starting materials; refluxing the reaction produced a black residue from which no metallocene was isolated. Although we were not successful in isolating a beryllocene containing two Cp^{3Si} rings, combination DFT/semiempirical (ONIOM) calculations were performed on several possible conformations of $(Cp^{3Si})_2Be$, including η^1/η^1, η^1/η^5, and η^5/η^5, to try to establish the steric feasibility of such a structure.

The η^1/η^1 geometry shown in Figure 55 (a) was used as a starting geometry in optimization. The unsubstituted position on the rings was chosen as the site of ligation, both to minimize steric interactions between the rings and from the fact that in $(\eta^5\text{-}C_5Me_4H)(\eta^1\text{-}C_5Me_4H)Be$, the beryllium is attached to the un-substituted carbon atom in the η^1-bonded ring. Nevertheless, during optimization one ring rotated relative to the other, and the structure collapsed to an η^1/η^5 geometry (Figure 55 (b)). The beryllium is now attached to a carbon bearing a trimethylsilyl group; the Be–C(η^1) distance is 1.781 Å (cf. 1.827 Å in Cp_2Be[246]), and Si3 is bent out of the C_5 plane by 1.03 Å (32.8°).

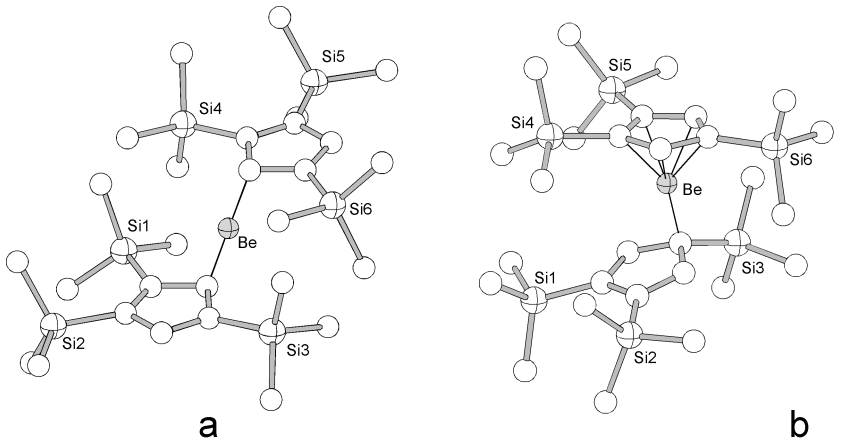

Figure 55. Calculated structures of $[1,2,4\text{-}(SiMe_3)_3C_5H_2]_2Be$ with η^1/η^1 Cp ligands (a) and η^1/η^5 Cp ligands (b). During optimization (a) converted to (b).

Such a rearrangement can be rationalized on electronic grounds, as silicon atoms help stabilize negative charges on adjacent atoms; the bending distortion also serves to increase the negative charge on the carbon atom.[257] The Be–C(η^5) bonds are in the narrow range from 1.901 Å to 1.934 Å, and average 1.923 Å, nearly matching the the average Be–C (η^5-Cp) bond length in the parent molecule (1.93 Å[246]). The structure is a local minimum on the potential energy surface (PES) (no imaginary frequencies), but a similar η^1/η^5 structure can be obtained that is formally related to the first by a ring rotation (Figure 56 (c)). The latter geometry is also a minimum on the PES, and has nearly identical geometric parameters (Be–C(η^1) = 1.780 Å; Be– C(η^5) = 1.921 Å (av)). Structure (b) is 1.9 kcal mol^{-1} higher in enthalpy (ΔH°) than (c), a difference that is not meaningful at this level of theory. The height of the energy barrier that might separate the two forms, however, is not known.

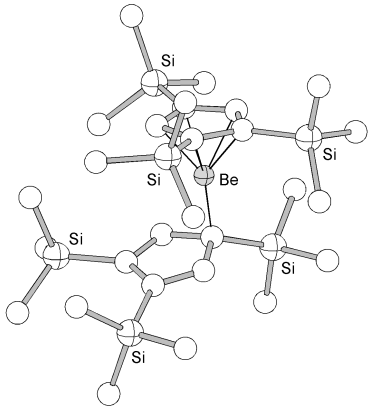

Figure 56. Another calculated η^1/η^5 configuration of $[1,2,4\text{-}(SiMe_3)_3C_5H_2]_2Be$ (c) with Be bound to a substituted carbon position.

The stability of an η^5/η^5 configuration was evaluated by starting from an eclipsed conformation similar to that in $[1,2,4\text{-}(SiMe_3)_3C_5H_2]_2Ca$.[106] The sandwich geometry was retained during optimization (Figure 57 (d)); a frequency calculation indicated that it was a local minimum ($N_{imag} = 0$). The angle between the ring planes is 6.9°, and the metallocene is somewhat slipped, with Be–C bonds ranging from 2.04 Å to 2.14 Å; the latter distance is slightly longer than the maximum distance observed in $(C_5Me_5)_2Be$ (2.11 Å), which is already long compared to the Be–C bond length in the parent molecule.[246] Even so, there are no intermolecular methyl···methyl′ contacts closer than 3.64 Å; the closest analogous contact in $(C_5Me_5)_2Be$ is at 3.63 Å. The η^5/η^5 structure is 3.3 kcal mol^{-1} higher in enthalpy ($\Delta H°$) than (c); the height of the energy barrier that separates the η^1/η^5 and η^5/η^5 forms is not known.

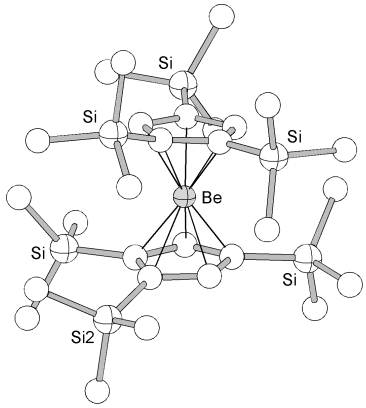

d

Figure 57. Proposed η^5/η^5 $[1,2,4\text{-}(SiMe_3)_3C_5H_2]_2Be$ structure based on Ca^{2+} analog.

Conclusion

Under the same reaction conditions used for the synthesis of permethylated beryllocene,[241,258] the corresponding $[1,2,4\text{-}(SiMe_3)_3C_5H_2]_2Be$ compound was not formed. However, ONIOM calculations suggest that the trimethylsilyl-substituted beryllocene would be sterically feasible. In any case, the failure of the reactions designed to produce $[1,2,4\text{-}(SiMe_3)_3C_5H_2]_2Be$ is probably best ascribed to kinetic difficulties, rather than to fundamental steric limitations on the geometry of the beryllocene. The inability to isolate certain sterically-enhanced complexes may indeed be a consequence of kinetics in many cases and not sterics, as suggested by the principle of steric oversaturation.

APPENDIX A:

OTHER X-RAY STRUCTURAL DETERMINATIONS

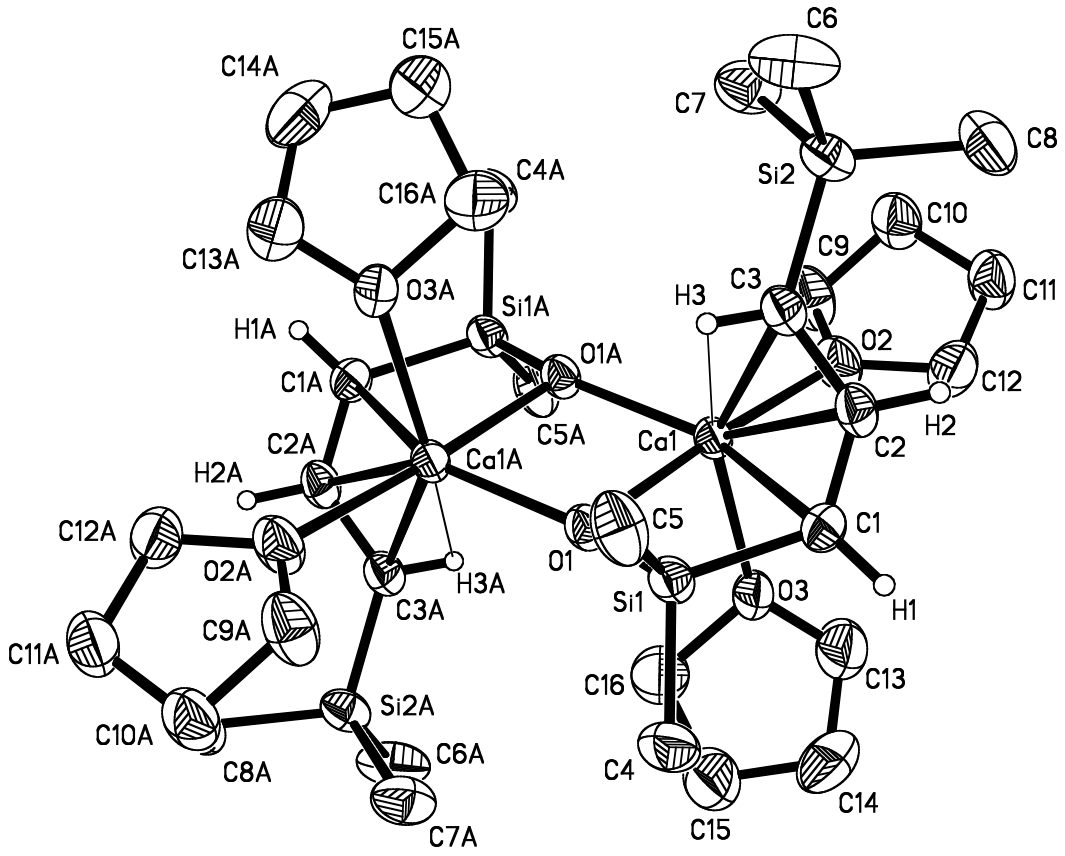

Figure 58. ORTEP of {[1-($SiMe_3$)-3-μ-($OSiMe_2$)C_3H_5]Ca(thf)$_2$}$_2$.

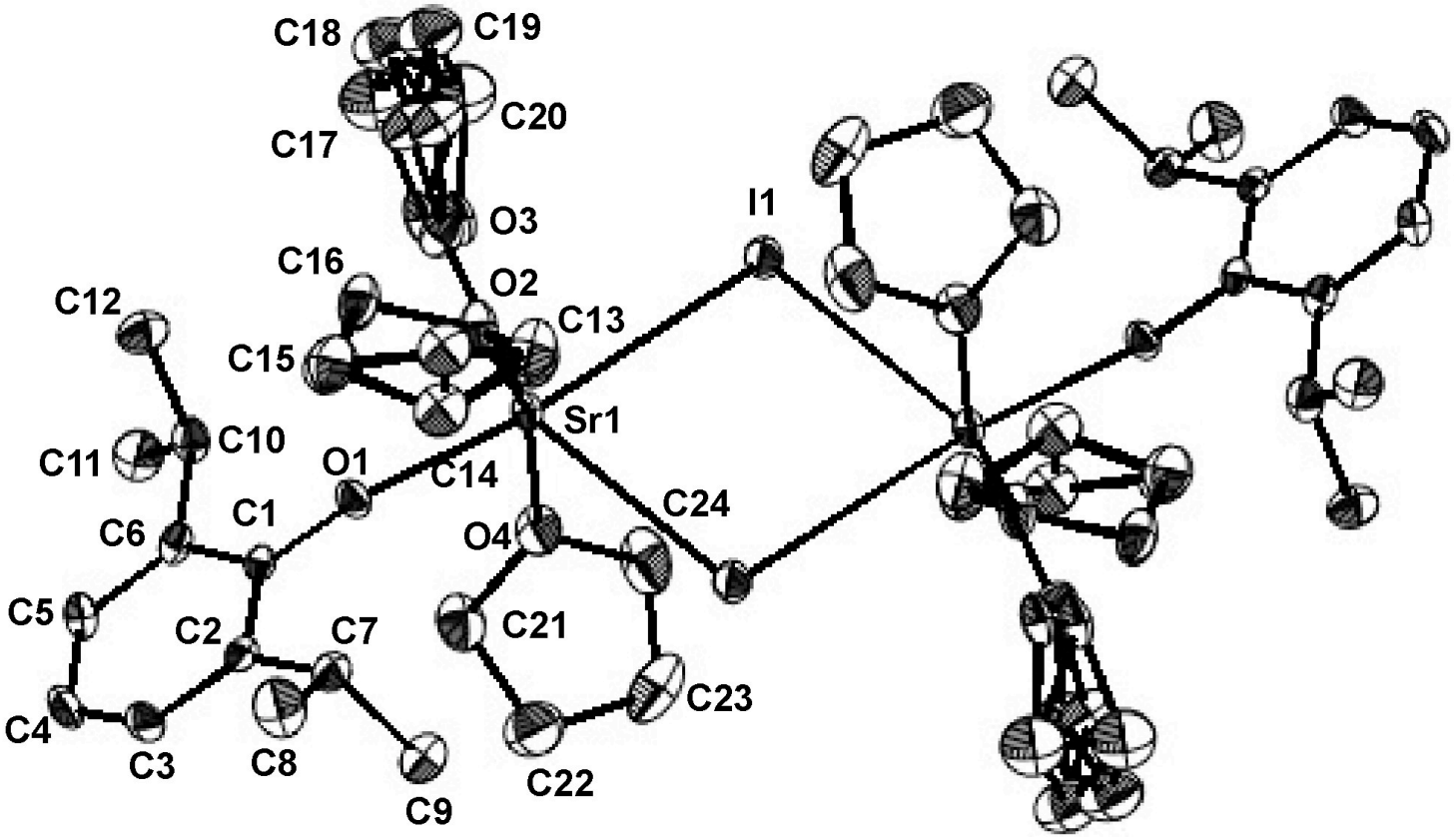

Figure 59. ORTEP of $[2,6\text{-}(C_3H_7)_2C_6H_3O]SrI(thf)_3$, showing disordered THF ligands.

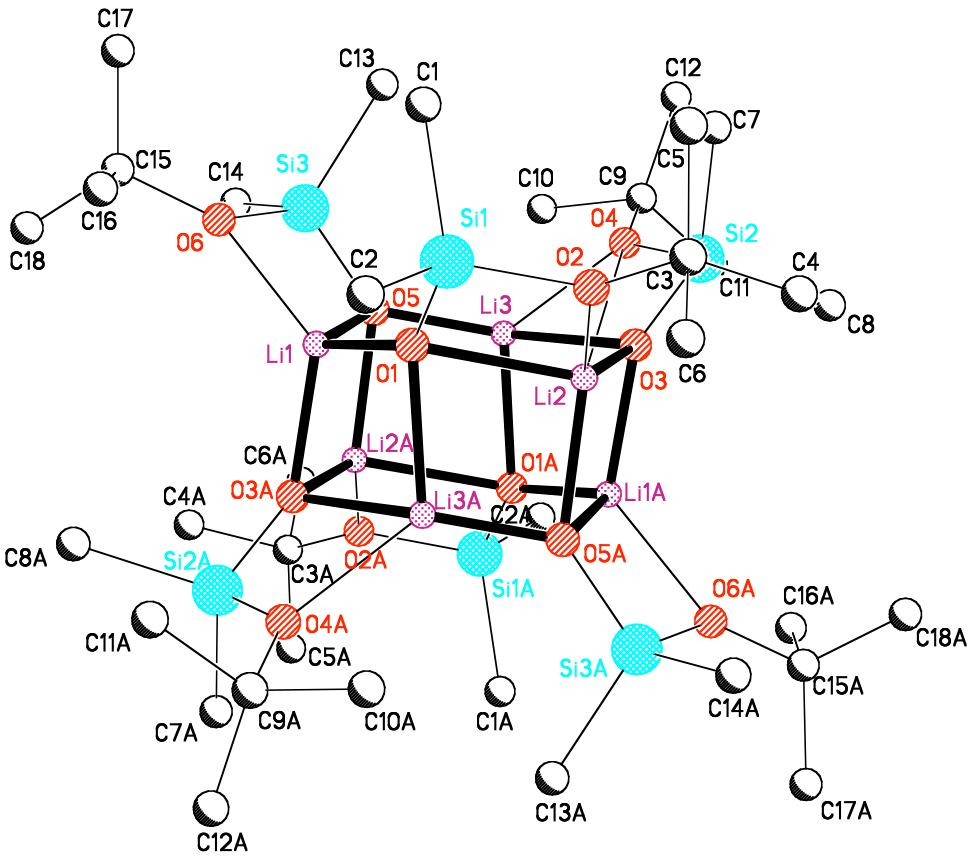

Figure 60. PLUTO of Li–O pseudo-hexagonal prism.

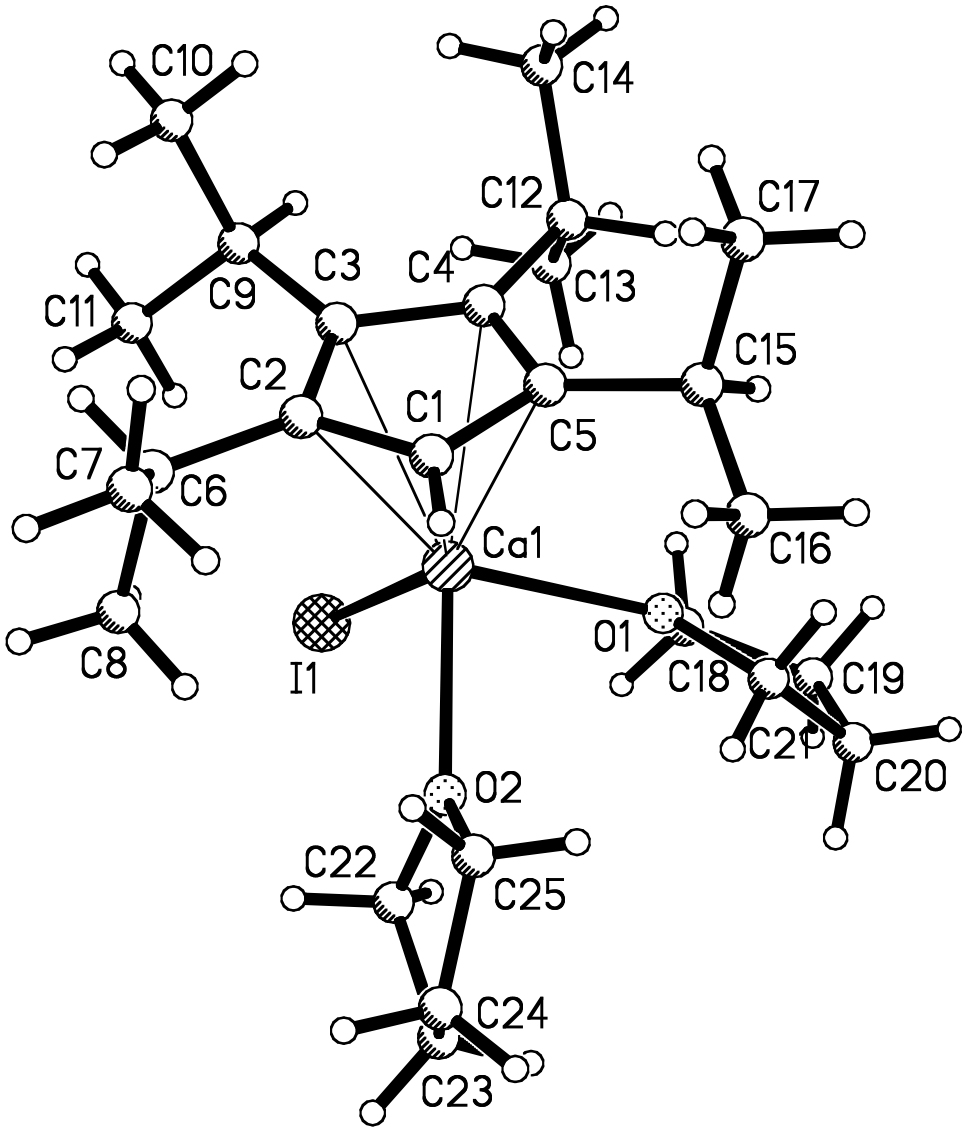

Figure 61. Solid-state structure of $[(C_3H_7)_4C_5H]CaI(thf)_2$.

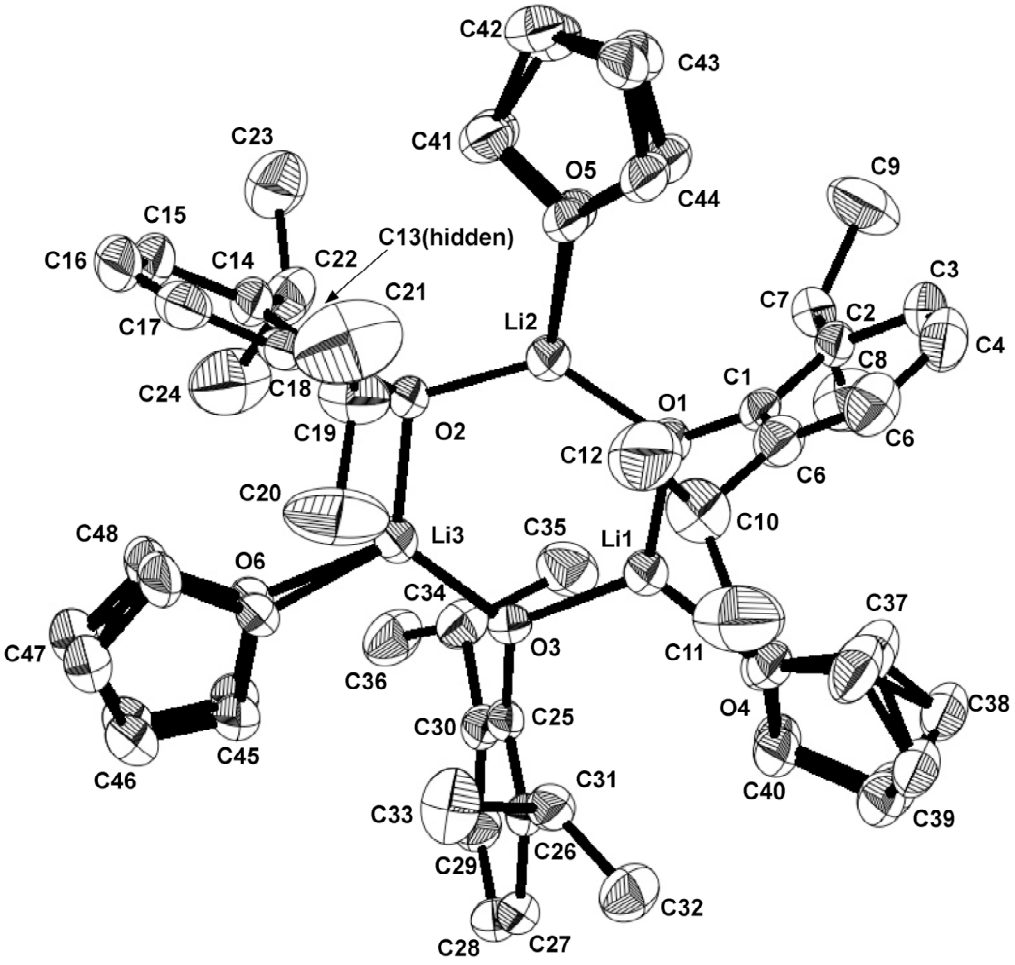

Figure 62. ORTEP of {[2,6-$(C_3H_7)_2C_6H_3O$]Li(thf)}$_3$, showing disordered THF ligands.

APPENDIX B:

CRYSTAL DATA AND ATOMIC FRACTIONAL COORDINATES FOR X-RAY STRUCTURAL DETERMINATIONS

Table 10. Crystal data and structure refinement for *cis*-[1,3-$(SiMe_3)_2C_3H_3]_2Ni$.

Identification code	04148	
Empirical formula	C18 H42 Ni Si4	
Formula weight	429.59	
Temperature	173(2) K	
Wavelength	0.71073 Å	
Crystal system	Monoclinic	
Space group	*C*2/*c*	
Unit cell dimensions	*a* = 16.537(5) Å	α = 90°
	b = 12.438(4) Å	β = 90.155(5)°
	c = 12.723(4) Å	γ = 90°
Volume	2617.0(14) $Å^3$	
Z	4	
Density (calculated)	1.090 Mg/m^3	
Absorption coefficient	0.924 mm^{-1}	
F(000)	936	
Crystal color, morphology	orange, needle	
Crystal size	0.32 x 0.12 x 0.08 mm^3	
Theta range for data collection	1.60 to 25.06°	
Index ranges	$-19 \le h \le 19$, $-13 \le k \le 14$, $-15 \le l \le 15$	
Reflections collected	8667	
Independent reflections	2315 [*R*(int) = 0.0311]	
Observed reflections	2208	
Completeness to theta = 25.06°	99.7%	
Absorption correction	Multi-scan	
Max. and min. transmission	1.000000 and 0.786877	
Refinement method	Full-matrix least-squares on F^2	
Data / restraints / parameters	2315 / 10 / 136	
Goodness-of-fit on F^2	1.033	
Final *R* indices [$I>2\sigma(I)$]	*R*1 = 0.0285, *wR*2 = 0.0727	
R indices (all data)	*R*1 = 0.0307, *wR*2 = 0.0738	
Largest diff. peak and hole	0.463 and -0.263 e $Å^{-3}$	

Table 11. Atomic coordinates (x 10^4) and equivalent isotropic displacement parameters (Å^{2}x10 ^{3}) for *cis*-[1,3-$(SiMe_3)_2C_3H_3]_2Ni$. U_{eq} is defined as one third of the trace of the orthogonalized U_{ij} tensor.

	x	y	z	U_{eq}
Ni1	5000	1161(1)	2500	28(1)
Si1	4924(1)	2703(1)	418(1)	38(1)
C4	5275(3)	2636(3)	-978(3)	68(1)
C5	5655(2)	3586(2)	1125(3)	56(1)
C6	3901(2)	3341(3)	471(3)	63(1)
C1	4887(2)	1282(2)	916(2)	34(1)
C2	4225(2)	770(2)	1414(2)	36(1)
C3	3785(2)	1246(2)	2247(2)	33(1)
Si2	2949(10)	472(13)	2916(13)	37(1)
C7	1977(13)	830(30)	2290(30)	58(2)
C8	2914(12)	817(16)	4343(13)	57(2)
C9	3110(12)	-1018(12)	2756(18)	70(3)
C3'	3785(2)	1246(2)	2247(2)	33(1)
Si2'	2987(5)	546(7)	3023(7)	37(1)
C7'	2028(7)	628(13)	2265(13)	58(2)
C8'	2785(6)	1228(10)	4317(6)	57(2)
C9'	3292(6)	-881(7)	3246(11)	70(3)

Table 12. Crystal data and structure refinement for $\{[1,3\text{-}(SiMe_3)_2C_3H_3]NiI\}_2$.

Identification code	03197	
Empirical formula	C18 H42 I2 Ni2 Si4	
Formula weight	742.10	
Temperature	173(2) K	
Wavelength	0.71073 Å	
Crystal system	Orthorhombic	
Space group	$C222_1$	
Unit cell dimensions	$a = 16.448(4)$ Å	$\alpha = 90°$
	$b = 19.038(4)$ Å	$\beta = 90°$
	$c = 19.669(4)$ Å	$\gamma = 90°$
Volume	6159(2) Å^3	
Z	8	
Density (calculated)	1.601 Mg/m^3	
Absorption coefficient	3.387 mm^{-1}	
$F(000)$	2944	
Crystal color, morphology	dark red, block	
Crystal size	0.24 x 0.16 x 0.12 mm^3	
Theta range for data collection	1.94 to 25.05°	
Index ranges	$-19 \le h \le 19$, $-15 \le k \le 22$, $-22 \le l \le 23$	
Reflections collected	15491	
Independent reflections	5389 [$R(\text{int}) = 0.0597$]	
Observed reflections	4470	
Completeness to theta = 25.05°	99.4%	
Absorption correction	Semi-empirical from equivalents	
Max. and min. transmission	1.000000 and 0.599781	
Refinement method	Full-matrix least-squares on F^2	
Data / restraints / parameters	5389 / 0 / 248	
Goodness-of-fit on F^2	1.027	
Final R indices [$I>2\text{sigma}(I)$]	$R1 = 0.0485$, $wR2 = 0.1222$	
R indices (all data)	$R1 = 0.0594$, $wR2 = 0.1274$	
Absolute structure parameter	0.16(3)	
Largest diff. peak and hole	2.046 and -0.447 e Å^{-3}	

Table 13. Atomic coordinates (x 10^4) and equivalent isotropic displacement parameters ($Å^2$x10 ^{3}) for {[1,3-$(SiMe_3)_2C_3H_3$]NiI}$_2$. U_{eq} is defined as one third of the trace of the orthogonalized U_{ij} tensor.

	x	y	z	U_{eq}
Ni1	10185(1)	2297(1)	8375(1)	35(1)
I1	10000	1337(1)	7500	52(1)
I2	10000	3252(1)	7500	55(1)
Si1	9045(2)	1539(1)	9416(1)	44(1)
Si2	10893(1)	3764(1)	9276(1)	40(1)
C1	10141(5)	1646(4)	9198(4)	37(2)
C2	10645(5)	2253(4)	9303(3)	33(2)
C3	10310(5)	2924(4)	9208(4)	34(2)
C4	8324(6)	2154(6)	8976(6)	64(3)
C5	8930(8)	1706(8)	10347(6)	88(4)
C6	8769(7)	623(5)	9178(6)	69(3)
C7	11273(6)	3810(6)	10179(5)	64(3)
C8	10185(6)	4487(5)	9085(5)	60(3)
C9	11779(6)	3792(6)	8692(5)	62(3)
Ni2	7714(1)	4872(1)	9122(1)	38(1)
I3	7686(1)	4049(1)	10121(1)	54(1)
Si3	6441(1)	3958(1)	8310(1)	39(1)
Si4	8257(2)	6166(1)	7931(1)	41(1)
C10	7564(5)	4110(4)	8418(4)	40(2)
C11	7998(5)	4699(4)	8162(4)	38(2)
C12	7661(6)	5374(4)	8202(4)	40(2)
C13	6246(6)	3069(6)	8637(6)	69(3)
C14	5768(6)	4585(5)	8777(6)	64(3)
C15	6212(6)	4002(7)	7393(5)	67(3)
C16	8385(7)	6038(6)	7009(5)	64(3)
C17	7619(7)	6951(5)	8093(5)	63(3)
C18	9258(6)	6248(6)	8357(6)	68(3)

Table 14. Crystal data and structure refinement for $\{[1,3\text{-}(SiMe_3)_2C_3H_3]Cs(thf)\}_\infty$.

Identification code	04168	
Empirical formula	C13 H29 Cs O Si2	
Formula weight	390.45	
Temperature	173(2) K	
Wavelength	0.71073 Å	
Crystal system	Monoclinic	
Space group	$P2_1/n$	
Unit cell dimensions	$a = 6.4496(8)$ Å	$\alpha = 90°$
	$b = 10.1112(13)$ Å	$\beta = 90.587(2)°$
	$c = 30.041(4)$ Å	$\gamma = 90°$
Volume	1959.0(4) Å^3	
Z	4	
Density (calculated)	1.324 Mg/m^3	
Absorption coefficient	2.001 mm^{-1}	
$F(000)$	792	
Crystal color, morphology	colorless, block	
Crystal size	0.28 x 0.24 x 0.14 mm^3	
Theta range for data collection	2.13 to 25.03°	
Index ranges	$-7 \le h \le 7$, $-11 \le k \le 12$, $-35 \le l \le 35$	
Reflections collected	18362	
Independent reflections	3461 [R(int) = 0.0367]	
Observed reflections	3053	
Completeness to theta = 25.03°	99.9%	
Absorption correction	Multi-scan	
Max. and min. transmission	1.000000 and 0.867632	
Refinement method	Full-matrix least-squares on F^2	
Data / restraints / parameters	3461 / 46 / 176	
Goodness-of-fit on F^2	1.043	
Final R indices [I>2sigma(I)]	$R1 = 0.0574$, $wR2 = 0.1161$	
R indices (all data)	$R1 = 0.0672$, $wR2 = 0.1198$	
Largest diff. peak and hole	1.318 and -2.483 e Å^{-3}	

Table 15. Atomic coordinates (x 10^4) and equivalent isotropic displacement parameters ($Å^2$x10 ^{3}) for {[1,3-$(SiMe_3)_2C_3H_3$]Cs(thf)}$_\infty$. U_{eq} is defined as one third of the trace of the orthogonalized U_{ij} tensor.

	x	y	z	U_{eq}
Cs1	4121(1)	2053(1)	3350(1)	41(1)
Si1	9095(3)	3718(3)	4164(1)	43(1)
Si2	8948(3)	2217(2)	2315(1)	35(1)
C1	9162(11)	2517(8)	3715(3)	40(2)
C2	9155(10)	2725(7)	3258(2)	33(2)
C3	9123(11)	1845(8)	2907(2)	38(2)
C4	6405(13)	4082(11)	4367(3)	62(3)
C5	10250(15)	5356(10)	3993(3)	65(3)
C6	10553(15)	3059(12)	4662(3)	70(3)
C7	10336(13)	3793(8)	2172(3)	48(2)
C8	6200(12)	2472(9)	2107(3)	50(2)
C9	10034(13)	794(8)	1981(3)	45(2)
O1	4310(110)	-120(120)	3990(30)	112(5)
C10	5760(80)	-250(60)	4350(20)	91(5)
C11	4960(90)	-1270(70)	4630(20)	122(7)
C12	2890(90)	-1230(80)	4570(20)	133(8)
C13	2480(80)	-780(110)	4130(30)	145(7)
O1'	4510(30)	-30(30)	4084(8)	112(5)
C10'	6410(20)	-701(17)	4177(7)	91(5)
C11'	5890(30)	-1954(18)	4344(8)	122(7)
C12'	3930(30)	-1920(20)	4478(9)	133(8)
C13'	2900(30)	-870(30)	4243(10)	145(7)

Table 16. Crystal data and structure refinement for {[1,3-$(SiMe_3)_2C_3H_3]_5Ba_2K(thf)\}_\infty$.

Identification code	04357	
Empirical formula	C49 H113 Ba2 K O Si10	
Formula weight	1313.07	
Temperature	173(2) K	
Wavelength	0.71073 Å	
Crystal system	Orthorhombic	
Space group	$P2_12_12_1$	
Unit cell dimensions	$a = 11.4705(14)$ Å	$\alpha = 90°$
	$b = 21.891(3)$ Å	$\beta = 90°$
	$c = 30.387(4)$ Å	$\gamma = 90°$
Volume	7630.2(16) $Å^3$	
Z	4	
Density (calculated)	1.143 Mg/m^3	
Absorption coefficient	1.264 mm^{-1}	
$F(000)$	2744	
Crystal color, morphology	yellow, block	
Crystal size	0.45 x 0.32 x 0.26 mm^3	
Theta range for data collection	1.63 to 27.51°	
Index ranges	$-14 \le h \le 14$, $-28 \le k \le 28$, $-39 \le l \le 39$	
Reflections collected	91768	
Independent reflections	17485 [R(int) = 0.0464]	
Observed reflections	15246	
Completeness to theta = 27.51°	99.8%	
Absorption correction	Multi-scan	
Max. and min. transmission	0.7346 and 0.6000	
Refinement method	Full-matrix least-squares on F^2	
Data / restraints / parameters	17485 / 40 / 610	
Goodness-of-fit on F^2	1.031	
Final R indices [I>2sigma(I)]	$R1 = 0.0349$, $wR2 = 0.0819$	
R indices (all data)	$R1 = 0.0450$, $wR2 = 0.0882$	
Absolute structure parameter	-0.005(10)	
Largest diff. peak and hole	0.841 and -0.305 e $Å^{-3}$	

Table 17. Atomic coordinates (x 10^4) and equivalent isotropic displacement parameters ($Å^2$x10 ^{3}) for {[1,3-$(SiMe_3)_2C_3H_3]_5Ba_2K(thf)\}_\infty$. U_{eq} is defined as one third of the trace of the orthogonalized U_{ij} tensor.

	x	y	z	U_{eq}
Ba1	2577(1)	3798(1)	3100(1)	41(1)
Ba2	3034(1)	4075(1)	1308(1)	45(1)
K1	2346(1)	4841(1)	4708(1)	63(1)
C1	3641(3)	4410(2)	2256(1)	39(1)
C2	2424(3)	4464(2)	2225(1)	39(1)
C3	1598(3)	4007(2)	2164(1)	42(1)
Si1	4635(1)	5045(1)	2388(1)	42(1)
C4	4093(4)	5776(2)	2144(2)	59(1)
C5	4717(5)	5135(2)	2996(2)	63(1)
C6	6143(4)	4887(2)	2185(2)	74(2)
Si2	2(1)	4103(1)	2141(1)	55(1)
C7	-704(6)	3778(3)	2646(2)	99(2)
C8	-388(4)	4932(3)	2133(2)	81(2)
C9	-555(5)	3693(4)	1645(2)	112(3)
C10	1736(3)	4787(2)	3730(1)	43(1)
C11	1340(3)	4240(2)	3914(1)	41(1)
C12	1944(4)	3736(2)	4070(1)	44(1)
Si3	841(1)	5457(1)	3608(1)	52(1)
C13	1351(5)	5857(3)	3101(2)	84(2)
C14	-719(5)	5246(3)	3561(2)	77(2)
C15	932(6)	6031(3)	4068(2)	96(2)
Si4	1245(1)	3070(1)	4324(1)	55(1)
C16	100(7)	2781(3)	3951(3)	131(3)
C17	2327(6)	2451(2)	4420(2)	87(2)
C18	580(8)	3259(3)	4860(2)	118(3)
C19	3026(4)	2563(2)	2787(1)	53(1)
C20	3865(3)	2640(2)	3109(2)	50(1)
C21	4701(4)	3104(2)	3155(2)	59(1)

Table 17 Continued.

	x	y	z	U_{eq}
C21'	4701(4)	3104(2)	3155(2)	59(1)
C21"	4701(4)	3104(2)	3155(2)	59(1)
Si5	2059(1)	1901(1)	2733(1)	58(1)
C23	501(6)	2125(3)	2644(3)	103(2)
C24	2465(6)	1424(2)	2248(2)	85(2)
Si6	5820(9)	3141(7)	3598(3)	65(1)
C25	6640(30)	3872(8)	3511(10)	104(4)
C26	5330(20)	3050(14)	4172(5)	97(3)
C27	6919(19)	2528(9)	3474(9)	84(3)
Si6'	5701(7)	3086(7)	3640(2)	65(1)
C25'	6971(19)	3543(11)	3435(9)	104(4)
C26'	6130(20)	2306(8)	3808(8)	97(3)
C27'	5210(20)	3508(11)	4147(6)	84(3)
Si6"	6056(3)	3008(2)	3473(2)	65(1)
C25"	6764(12)	3765(5)	3585(5)	104(4)
C26"	5688(11)	2596(6)	3985(4)	97(3)
C27"	7203(9)	2558(5)	3173(4)	84(3)
C28	4100(3)	4740(2)	538(1)	41(1)
C29	3185(3)	5114(2)	672(1)	40(1)
C30	1987(4)	5010(2)	675(1)	42(1)
Si7	5644(1)	4950(1)	540(1)	45(1)
C31	5859(4)	5682(2)	842(2)	65(1)
C32	6527(5)	4326(3)	797(2)	88(2)
C33	6203(5)	5041(3)	-35(2)	87(2)
Si8	918(1)	5615(1)	788(1)	52(1)
C34	850(6)	6177(3)	322(2)	92(2)
C35	1341(4)	6054(2)	1291(2)	75(1)
C36	-583(4)	5287(3)	845(2)	88(2)
C37	4032(4)	2848(2)	1483(1)	57(1)

Table 17. Continued.

	x	y	z	U_{eq}
C38	3473(4)	2799(2)	1081(2)	56(1)
C39	2305(5)	2896(2)	981(2)	67(1)
Si9	5559(1)	2640(1)	1604(1)	56(1)
C40	5623(6)	1935(3)	1938(2)	94(2)
C41	6427(6)	2536(3)	1091(2)	90(2)
C42	6284(4)	3240(3)	1943(2)	75(1)
Si10	1665(2)	2781(1)	438(1)	75(1)
C43	159(7)	3112(4)	433(3)	131(3)
C44	2573(8)	3168(3)	15(2)	107(2)
C45	1530(7)	1970(3)	267(2)	100(2)
O1	4381(3)	5318(2)	4443(2)	86(1)
C46	4421(8)	5867(4)	4183(4)	148(3)
C47	5644(6)	6047(4)	4136(3)	133(2)
C48	6258(6)	5504(4)	4228(3)	133(2)
C49	5501(8)	5137(4)	4499(4)	148(3)

Table 18. Crystal data and structure refinement for $[1,3\text{-}(SiMe_3)_2C_3H_3]_2Sr(thf)_2$.

Identification code	04227	
Empirical formula	C26 H58 O2 Si4 Sr	
Formula weight	602.70	
Temperature	173(2) K	
Wavelength	0.71073 Å	
Crystal system	Tetragonal	
Space group	$P4_2/n$	
Unit cell dimensions	$a = 14.9010(8)$ Å	$\alpha = 90°$
	$b = 14.9010(8)$ Å	$\beta = 90°$
	$c = 16.825(2)$ Å	$\gamma = 90°$
Volume	3735.7(5) $Å^3$	
Z	4	
Density (calculated)	1.072 Mg/m^3	
Absorption coefficient	1.589 mm^{-1}	
$F(000)$	1296	
Crystal color, morphology	colorless, block	
Crystal size	0.36 x 0.28 x 0.16 mm^3	
Theta range for data collection	1.83 to 25.03°	
Index ranges	$-17 \le h \le 17$, $-17 \le k \le 17$, $-20 \le l \le 20$	
Reflections collected	36801	
Independent reflections	3303 [$R(\text{int}) = 0.0574$]	
Observed reflections	2380	
Completeness to theta = 25.03°	100.0%	
Absorption correction	Multi-scan	
Max. and min. transmission	0.7851 and 0.5985	
Refinement method	Full-matrix least-squares on F^2	
Data / restraints / parameters	3303 / 45 / 185	
Goodness-of-fit on F^2	1.031	
Final R indices [$I>2\text{sigma}(I)$]	$R1 = 0.0419$, $wR2 = 0.1067$	
R indices (all data)	$R1 = 0.0660$, $wR2 = 0.1243$	
Largest diff. peak and hole	0.451 and -0.276 e $Å^{-3}$	

Table 19. Atomic coordinates (x 10^4) and equivalent isotropic displacement parameters ($Å^2$x10 ^{3}) for $[1,3\text{-}(SiMe_3)_2C_3H_3]_2Sr(thf)_2$. U_{eq} is defined as one third of the trace of the orthogonalized U_{ij} tensor.

	x	y	z	U_{eq}
Sr1	7500	2500	801(1)	51(1)
C1	7800(2)	1145(2)	1923(2)	58(1)
C2	8621(2)	1240(2)	1531(2)	56(1)
C3	9164(2)	2006(2)	1445(2)	58(1)
Si1	7160(1)	105(1)	2035(1)	62(1)
C4	7600(20)	-750(20)	1307(15)	123(5)
C5	5958(9)	282(16)	1838(17)	109(4)
C6	7304(16)	-370(17)	3049(9)	99(3)
Si1'	7160(1)	105(1)	2035(1)	62(1)
C4'	7202(13)	-599(13)	1135(8)	123(5)
C5'	5992(6)	369(9)	2358(11)	109(4)
C6'	7618(9)	-622(10)	2870(7)	99(3)
Si2	10306(1)	1997(1)	1055(1)	64(1)
C7	10394(4)	1226(4)	200(4)	121(2)
C8	10692(3)	3128(3)	755(4)	109(2)
C9	11135(3)	1614(4)	1826(3)	110(2)
O1	7202(11)	1585(11)	-420(7)	73(3)
C10	6394(9)	1583(9)	-864(8)	99(3)
C11	6320(20)	670(30)	-1220(30)	118(5)
C12	7200(20)	290(30)	-1170(30)	148(10)
C13	7791(14)	1020(30)	-860(20)	126(8)
O1'	7051(11)	1391(11)	-261(8)	73(3)
C10'	6239(9)	1066(10)	-592(8)	99(3)
C11'	6460(20)	620(30)	-1360(20)	118(5)
C12'	7400(20)	440(30)	-1330(30)	148(10)
C13'	7765(14)	910(30)	-620(20)	126(8)

Table 20. Crystal data and structure refinement for {[1-($SiMe_3$)-3-μ-($OSiMe_2$)C_3H_5]Ca(thf)$_2$}$_2$.

Identification code	03036	
Empirical formula	C32 H68 Ca2 O6 Si4	
Formula weight	741.38	
Temperature	173(2) K	
Wavelength	0.71073 Å	
Crystal system	Monoclinic	
Space group	$P2_1/n$	
Unit cell dimensions	$a = 10.405(2)$ Å	$\alpha = 90°$
	$b = 17.476(4)$ Å	$\beta = 97.777(4)°$
	$c = 12.022(2)$ Å	$\gamma = 90°$
Volume	2165.9(8) Å^3	
Z	2	
Density (calculated)	1.137 Mg/m^3	
Absorption coefficient	0.409 mm^{-1}	
$F(000)$	808	
Crystal color, morphology	colorless, needle	
Crystal size	0.43 x 0.24 x 0.16 mm^3	
Theta range for data collection	2.07 to 25.06°.	
Index ranges	$-11 \le h \le 12$, $-20 \le k \le 20$, $-14 \le l \le 12$	
Reflections collected	12148	
Independent reflections	3834 [R(int) = 0.0386]	
Observed reflections	3090	
Completeness to theta = 25.06°	99.7%	
Absorption correction	Semi-empirical from equivalents	
Max. and min. transmission	1.000000 and 0.908318	
Refinement method	Full-matrix least-squares on F^2	
Data / restraints / parameters	3834 / 27 / 229	
Goodness-of-fit on F^2	1.008	
Final R indices [I>2sigma(I)]	$R1 = 0.0401$, $wR2 = 0.0999$	
R indices (all data)	$R1 = 0.0539$, $wR2 = 0.1097$	
Largest diff. peak and hole	0.503 and -0.272 e Å^{-3}	

Table 21. Atomic coordinates (x 10^4) and equivalent isotropic displacement parameters ($Å^2$x10^{3}) for {[1-($SiMe_3$)-3-μ-($OSiMe_2$)C_3H_5]Ca(thf)$_2$}$_2$. U_{eq} is defined as one third of the trace of the orthogonalized U_{ij} tensor.

	x	y	z	U_{eq}
Ca1	9285(1)	865(1)	4594(1)	27(1)
O1	10221(2)	-199(1)	3846(1)	30(1)
C1	9851(3)	1110(1)	2459(2)	34(1)
C2	10436(2)	1703(1)	3112(2)	32(1)
C3	11320(2)	1655(1)	4104(2)	32(1)
Si1	10377(1)	98(1)	2588(1)	31(1)
C4	9371(3)	-489(2)	1493(2)	52(1)
C5	12101(3)	3(2)	2334(2)	47(1)
Si2	12149(1)	2433(1)	4916(1)	35(1)
C6	13922(3)	2460(2)	4793(3)	60(1)
C7	12058(3)	2327(2)	6459(2)	51(1)
C8	11431(3)	3381(2)	4457(3)	62(1)
O2	8209(2)	1952(1)	5284(2)	45(1)
C9	8048(3)	2098(2)	6432(2)	53(1)
C10	8254(3)	2944(2)	6582(2)	51(1)
C11	7695(3)	3265(2)	5473(2)	53(1)
C12	7753(3)	2619(2)	4647(2)	52(1)
O3	7121(4)	434(3)	3945(5)	42(1)
C13	6131(5)	860(3)	3189(5)	67(2)
C14	5762(6)	335(4)	2237(5)	76(2)
C15	5861(6)	-439(3)	2798(6)	81(2)
C16	6822(5)	-352(3)	3801(4)	65(1)
O3'	7096(9)	619(9)	3807(11)	42(1)
C13'	6540(11)	510(6)	2668(10)	67(2)
C14'	5640(13)	-145(8)	2657(11)	76(2)
C15'	5427(10)	-243(6)	3875(10)	81(2)
C16'	6219(10)	345(6)	4520(8)	65(1)

Table 22. Crystal data and structure refinement for Li–O pseudo-hexagonal prism.

Identification code	03006	
Empirical formula	C36 H90 Li6 O12 Si6	
Formula weight	925.26	
Temperature	173(2) K	
Wavelength	0.71073 Å	
Crystal system	Monoclinic	
Space group	$P2_1/n$	
Unit cell dimensions	$a = 12.736(3)$ Å	$\alpha = 90°$
	$b = 20.161(5)$ Å	$\beta = 118.065(4)°$
	$c = 13.338(4)$ Å	$\gamma = 90°$
Volume	3022(1) $Å^3$	
Z	2	
Density (calculated)	1.017 Mg/m^3	
Absorption coefficient	0.181 mm^{-1}	
$F(000)$	1008	
Crystal color, morphology	colorless, block	
Crystal size	0.39 x 0.38 x 0.29 mm^3	
Theta range for data collection	1.82 to 25.11°.	
Index ranges	$-14 \le h \le 15$, $-23 \le k \le 23$, $-15 \le l \le 15$	
Reflections collected	19315	
Independent reflections	5326 [$R(\text{int}) = 0.0453$]	
Observed reflections	3063	
Completeness to theta = 25.11°	99.2%	
Absorption correction	Semi-empirical from equivalents	
Max. and min. transmission	1.000000 and 0.759633	
Refinement method	Full-matrix least-squares on F^2	
Data / restraints / parameters	5326 / 0 / 299	
Goodness-of-fit on F^2	1.012	
Final R indices [$I>2\text{sigma}(I)$]	$R1 = 0.1192$, $wR2 = 0.2806$	
R indices (all data)	$R1 = 0.1704$, $wR2 = 0.3187$	
Largest diff. peak and hole	1.370 and -0.438 e $Å^{-3}$	

Table 23. Atomic coordinates (x 10^4) and equivalent isotropic displacement parameters ($Å^2$x10^{3}) for Li–O pseudo-hexagonal prism. U_{eq} is defined as one third of the trace of the orthogonalized U_{ij} tensor.

	x	y	z	U_{eq}
Si1	-2727(2)	-164(1)	2300(2)	81(1)
Si2	-1695(2)	1044(1)	6071(2)	67(1)
Si3	520(2)	1533(1)	3783(2)	86(1)
Si1'	-3144(19)	30(12)	4430(20)	96(7)
Si2'	-1120(20)	466(12)	1976(18)	93(7)
Si3'	90(20)	1769(11)	5500(20)	100(8)
Li1	24(11)	249(6)	3471(9)	78(3)
Li2	-1788(9)	-234(6)	4563(10)	81(3)
Li3	205(10)	871(5)	5667(13)	83(4)
O1	-1362(4)	-187(2)	3200(4)	89(2)
O2	-3363(4)	-335(2)	3112(4)	82(1)
O3	-1253(4)	398(2)	5697(4)	77(1)
O4	-565(4)	1565(2)	6378(4)	70(1)
O5	718(4)	982(2)	4702(4)	92(2)
O6	214(5)	1065(2)	2618(4)	87(1)
C1	-3180(8)	698(5)	1690(8)	127(3)
C2	-3143(9)	-779(5)	1138(7)	133(4)
C3	-4546(7)	-504(5)	2891(8)	98(2)
C4	-4491(10)	-468(8)	4066(11)	181(6)
C5	-5412(9)	-41(7)	2095(12)	182(6)
C6	-4804(10)	-1208(6)	2517(13)	182(6)
C7	-3080(7)	1398(5)	4896(9)	127(3)
C8	-1937(9)	891(5)	7301(8)	119(3)
C9	-232(9)	2188(4)	6971(9)	116(3)
C10	894(9)	2398(5)	6870(10)	149(4)
C11	183(14)	2046(7)	8243(10)	208(8)
C12	-1187(12)	2671(5)	6507(16)	224(9)

Table 23. Continued.

	x	y	z	U_{eq}
C13	-774(9)	2092(4)	3480(9)	128(3)
C14	1832(10)	2048(6)	4145(11)	159(5)
C15	192(10)	1191(5)	1566(9)	114(3)
C16	-609(11)	608(7)	781(8)	169(6)
C17	-378(15)	1837(6)	1057(10)	203(7)
C18	1376(12)	1092(6)	1621(11)	164(5)

Table 24. Crystal data and structure refinement for $[2,6\text{-}(C_3H_7)_2C_6H_3O]SrI(thf)_3$.

Identification code	03122	
Empirical formula	C48 H82 I2 O8 Sr2	
Formula weight	1216.18	
Temperature	173(2) K	
Wavelength	0.71073 Å	
Crystal system	Monoclinic	
Space group	$P2_1/c$	
Unit cell dimensions	$a = 14.676(7)$ Å	$\alpha = 90°$
	$b = 10.824(5)$ Å	$\beta = 99.421(6)°$
	$c = 17.816(8)$ Å	$\gamma = 90°$
Volume	2792(2) Å^3	
Z	2	
Density (calculated)	1.447 Mg/m^3	
Absorption coefficient	3.060 mm^{-1}	
$F(000)$	1232	
Crystal color, morphology	colorless, block	
Crystal size	0.30 x 0.24 x 0.22 mm^3	
Theta range for data collection	1.41 to 25.13°	
Index ranges	$-17 \le h \le 17$, $0 \le k \le 12$, $0 \le l \le 21$	
Reflections collected	45758	
Independent reflections	4930 [R(int) = 0.0712]	
Observed reflections	4038	
Completeness to theta = 25.13°	98.7%	
Absorption correction	Semi-empirical from equivalents	
Max. and min. transmission	1.000000 and 0.603866	
Refinement method	Full-matrix least-squares on F^2	
Data / restraints / parameters	4930 / 52 / 302	
Goodness-of-fit on F^2	1.024	
Final R indices [I>2sigma(I)]	$R1 = 0.0445$, $wR2 = 0.1102$	
R indices (all data)	$R1 = 0.0576$, $wR2 = 0.1181$	
Largest diff. peak and hole	1.618 and -0.852 e Å^{-3}	

Table 25. Atomic coordinates (x 10^4) and equivalent isotropic displacement parameters ($Å^2$x10 ^{3}) for [2,6-$(C_3H_7)_2C_6H_3O$]SrI$(thf)_3$. U_{eq} is defined as one third of the trace of the orthogonalized U_{ij} tensor.

	x	y	z	U_{eq}
Sr1	1486(1)	882(1)	9617(1)	27(1)
I1	-264(1)	1723(1)	10540(1)	39(1)
O1	2668(2)	706(3)	8943(2)	31(1)
C1	3220(3)	623(4)	8432(3)	28(1)
C2	3546(3)	-544(4)	8223(3)	30(1)
C3	4102(3)	-605(5)	7670(3)	35(1)
C4	4338(4)	432(5)	7296(3)	38(1)
C5	4037(3)	1588(5)	7510(3)	35(1)
C6	3494(3)	1707(4)	8074(3)	32(1)
C7	3258(4)	-1678(4)	8620(3)	37(1)
C8	4024(5)	-2664(6)	8772(4)	62(2)
C9	2364(5)	-2225(6)	8181(4)	62(2)
C10	3212(4)	2955(4)	8351(3)	36(1)
C11	3098(4)	3969(5)	7741(4)	50(2)
C12	3893(4)	3362(5)	9041(3)	49(2)
O2	2682(2)	28(4)	10690(2)	44(1)
C13	2663(14)	-1180(20)	11020(30)	54(3)
C14	3656(12)	-1574(16)	11253(11)	55(3)
C15	4180(30)	-800(50)	10770(60)	61(3)
C16	3632(11)	390(30)	10700(60)	45(2)
O2'	2682(2)	28(4)	10690(2)	44(1)
C13'	2706(14)	-1140(20)	11080(20)	54(3)
C14'	3537(10)	-1807(12)	10865(10)	55(3)
C15'	4190(20)	-790(40)	10720(50)	61(3)
C16'	3641(10)	390(30)	10730(50)	45(2)
O3	1922(3)	3077(3)	10033(2)	40(1)
C17	1621(11)	4223(11)	9645(8)	40(4)
C18	2030(13)	5261(10)	10122(9)	78(4)

Table 25. Continued.

	x	y	z	U_{eq}
C19	2110(20)	4713(18)	10938(11)	75(9)
C20	2300(30)	3391(19)	10821(12)	54(7)
O3'	1922(3)	3077(3)	10033(2)	40(1)
C17'	1348(12)	4091(13)	9701(9)	40(4)
C18'	1409(13)	5020(13)	10303(11)	78(4)
C19'	2380(20)	4820(20)	10786(15)	75(9)
C20'	2480(30)	3470(20)	10747(16)	54(7)
O4	559(3)	1516(4)	8342(2)	47(1)
C21	871(5)	1396(7)	7619(3)	60(2)
C22	246(5)	442(7)	7198(4)	73(2)
C23	-598(5)	423(7)	7568(5)	77(2)
C24	-432(4)	1389(8)	8163(4)	72(2)

Table 26. Crystal data and structure refinement for $[(C_3H_7)_4C_5H]CaI(thf)_2$.

Identification code	01259	
Empirical formula	C25 H45 Ca I O2	
Formula weight	544.59	
Temperature	173(2) K	
Wavelength	0.71073 Å	
Crystal system	Triclinic	
Space group	P-1	
Unit cell dimensions	$a = 8.983(1)$ Å	$\alpha = 87.130(3)°$
	$b = 9.783(2)$ Å	$\beta = 75.649(3)°$
	$c = 17.179(3)$ Å	$\gamma = 68.540(3)°$
Volume	1359.7(4) $Å^3$	
Z	2	
Density (calculated)	1.330 Mg/m^3	
Absorption coefficient	1.383 mm^{-1}	
$F(000)$	568	
Crystal color, morphology	red-brown, block	
Crystal size	0.21 x 0.20 x 0.16 mm^3	
Theta range for data collection	2.24 to 25.06°.	
Index ranges	$-10 \le h \le 10$, $-11 \le k \le 11$, $-20 \le l \le 12$	
Reflections collected	8205	
Independent reflections	4754 [$R(\text{int}) = 0.0390$]	
Observed reflections	3295	
Completeness to theta = 25.06°	98.6%	
Absorption correction	Multiscans	
Max. and min. transmission	1.000000 and 0.769755	
Refinement method	Full-matrix least-squares on F^2	
Data / restraints / parameters	4754 / 0 / 270	
Goodness-of-fit on F^2	0.994	
Final R indices [$I>2\text{sigma}(I)$]	$R1 = 0.0492$, $wR2 = 0.1059$	
R indices (all data)	$R1 = 0.0765$, $wR2 = 0.1134$	
Largest diff. peak and hole	1.104 and -1.197 e $Å^{-3}$	

Table 27. Atomic coordinates (x 10^4) and equivalent isotropic displacement parameters ($Å^2$x10 ^{3}) for $[(C_3H_7)_4C_5H]CaI(thf)_2$. U_{eq} is defined as one third of the trace of the orthogonalized U_{ij} tensor.

	x	y	z	U_{eq}
Ca1	11931(1)	10232(1)	2735(1)	30(1)
I1	8788(1)	9679(1)	3447(1)	47(1)
C1	13550(6)	12064(5)	2508(3)	31(1)
C2	11906(6)	12974(5)	2873(3)	30(1)
C3	10935(6)	13063(5)	2312(3)	28(1)
C4	12013(6)	12199(5)	1608(3)	29(1)
C5	13643(6)	11590(5)	1730(3)	27(1)
C6	11358(6)	13698(6)	3709(3)	38(1)
C7	12656(8)	14205(7)	3893(4)	52(2)
C8	10910(8)	12705(7)	4368(4)	52(2)
C9	9155(6)	14078(5)	2383(3)	38(1)
C10	9057(7)	15678(6)	2247(4)	50(2)
C11	7892(7)	14017(6)	3140(4)	50(2)
C12	11603(6)	11954(5)	827(3)	33(1)
C13	10333(7)	11209(6)	938(4)	42(1)
C14	11091(7)	13357(6)	359(4)	48(2)
C15	15220(6)	10751(5)	1114(3)	31(1)
C16	16654(6)	9911(6)	1484(4)	45(2)
C17	15722(7)	11807(6)	500(4)	50(2)
O1	13092(4)	8000(4)	1911(2)	44(1)
C18	12181(8)	7110(7)	1771(5)	70(2)
C19	13409(8)	5728(7)	1374(5)	73(2)
C20	14955(9)	5557(7)	1557(5)	72(2)
C21	14788(8)	7114(7)	1753(5)	61(2)
O2	13367(4)	8909(4)	3665(2)	38(1)
C22	12677(7)	8124(7)	4301(4)	53(2)
C23	14090(7)	7152(6)	4634(4)	50(2)
C24	15182(8)	8051(7)	4510(4)	55(2)
C25	14913(7)	8885(7)	3804(4)	52(2)

Table 28. Crystal data and structure refinement for {[2,6-$(C_3H_7)_2C_6H_3O$]Li(thf)}$_3$.

Identification code	00237	
Empirical formula	C48 H75 Li3 O6	
Formula weight	768.90	
Temperature	293(2) K	
Wavelength	0.71073 Å	
Crystal system	Monoclinic	
Space group	$P2_1/n$	
Unit cell dimensions	$a = 13.294(2)$ Å	$\alpha = 90°$
	$b = 16.149(2)$ Å	$\beta = 90.079(2)°$
	$c = 22.392(3)$ Å	$\gamma = 90°$
Volume	4807(1) Å^3	
Z	4	
Density (calculated)	1.062 Mg/m^3	
Absorption coefficient	0.067 mm^{-1}	
$F(000)$	1680	
Crystal color, morphology	colorless, block	
Crystal size	0.24 x 0.17 x 0.12 mm^3	
Theta range for data collection	1.55 to 23.84°.	
Index ranges	$-15 \le h \le 13$, $-18 \le k \le 15$, $-25 \le l \le 25$	
Reflections collected	22629	
Independent reflections	7381 [R(int) = 0.0308]	
Completeness to theta = 23.84°	99.7%	
Absorption correction	SADABS, R. Blessling, 1995	
Max. and min. transmission	1.000000 and 0.884002	
Refinement method	Full-matrix least-squares on F^2	
Data / restraints / parameters	7381 / 222 / 572	
Goodness-of-fit on F^2	1.076	
Final R indices [I>2sigma(I)]	$R1 = 0.0602$, $wR2 = 0.1776$	
R indices (all data)	$R1 = 0.0947$, $wR2 = 0.1993$	
Largest diff. peak and hole	0.385 and -0.331 e Å^{-3}	

Table 29. Atomic coordinates (x 10^4) and equivalent isotropic displacement parameters ($Å^2$x10^{3}) for {[2,6-$(C_3H_7)_2C_6H_3O$]Li(thf)}$_3$. U_{eq} is defined as one third of the trace of the orthogonalized U_{ij} tensor.

	x	y	z	U_{eq}
Li(1)	8553(3)	2207(3)	5507(2)	60(1)
Li(2)	6324(3)	2354(3)	5180(2)	62(1)
Li(3)	6838(3)	1869(3)	6452(2)	60(1)
O(1)	7642(1)	2538(1)	4958(1)	56(1)
O(2)	5829(1)	2030(1)	5901(1)	52(1)
O(3)	8165(1)	1894(1)	6258(1)	52(1)
C(1)	7828(2)	3045(2)	4492(1)	54(1)
C(2)	7914(2)	2707(2)	3911(1)	56(1)
C(3)	8078(2)	3249(2)	3437(1)	72(1)
C(4)	8169(2)	4088(2)	3522(2)	86(1)
C(5)	8099(2)	4410(2)	4087(2)	84(1)
C(6)	7931(2)	3900(2)	4582(1)	68(1)
C(7)	7818(2)	1787(2)	3824(1)	63(1)
C(8)	8801(3)	1339(2)	3959(2)	100(1)
C(9)	7426(4)	1530(3)	3215(2)	122(2)
C(10)	7831(3)	4262(2)	5207(2)	94(1)
C(11)	8756(4)	4670(4)	5443(3)	164(2)
C(12)	6938(4)	4800(4)	5280(2)	159(2)
C(13)	4902(2)	2038(2)	6133(1)	54(1)
C(14)	4355(2)	1298(2)	6192(1)	70(1)
C(15)	3423(2)	1323(3)	6478(2)	96(1)
C(16)	3023(3)	2029(4)	6685(2)	110(2)
C(17)	3528(3)	2764(3)	6604(1)	95(1)
C(18)	4468(2)	2792(2)	6330(1)	71(1)
C(19)	5030(3)	3590(2)	6245(2)	94(1)
C(20)	5736(5)	3784(3)	6763(3)	171(3)
C(21)	4369(5)	4342(3)	6134(4)	195(3)
C(22)	4782(3)	492(2)	5962(2)	87(1)

Table 29. Continued.

	x	y	z	U_{eq}
C(23)	4021(3)	12(3)	5578(2)	114(1)
C(24)	5192(4)	-46(3)	6473(2)	134(2)
C(25)	8922(2)	1615(2)	6599(1)	46(1)
C(26)	9573(2)	2172(2)	6891(1)	48(1)
C(27)	10345(2)	1856(2)	7244(1)	56(1)
C(28)	10493(2)	1015(2)	7308(1)	63(1)
C(29)	9865(2)	471(2)	7017(1)	59(1)
C(30)	9074(2)	749(2)	6664(1)	51(1)
C(31)	9417(2)	3098(2)	6815(1)	59(1)
C(32)	10387(3)	3604(2)	6814(2)	86(1)
C(33)	8680(3)	3436(2)	7270(2)	100(1)
C(34)	8367(2)	161(2)	6340(1)	64(1)
C(35)	8656(3)	70(2)	5683(1)	85(1)
C(36)	8279(3)	-693(2)	6630(2)	85(1)
O(4)	9992(18)	2250(30)	5300(20)	71(1)
C(37)	10395(10)	2795(18)	4859(13)	112(4)
C(38)	11471(5)	2936(5)	5080(4)	82(1)
C(39)	11736(18)	2043(14)	5201(13)	79(2)
C(40)	10810(30)	1764(17)	5544(14)	67(3)
O(4')	9969(18)	2230(30)	5330(20)	71(1)
C(37')	10377(10)	2891(17)	4988(13)	112(4)
C(38')	11354(5)	2525(5)	4730(3)	82(1)
C(39')	11726(18)	2082(14)	5280(12)	79(2)
C(40')	10760(30)	1661(17)	5487(14)	67(3)
O(5)	5310(20)	2740(20)	4641(13)	69(5)
C(41)	4300(20)	2457(17)	4681(10)	84(4)
C(42)	3975(13)	2414(16)	4032(11)	90(4)
C(43)	4428(14)	3182(16)	3779(10)	86(3)
C(44)	5309(8)	3364(8)	4190(6)	83(3)
O(5')	5343(19)	2580(20)	4564(13)	69(5)
C(41')	4350(20)	2264(17)	4619(10)	84(4)

Table 29. Continued.

	x	y	z	U_{eq}
C(42')	3757(13)	2579(16)	4086(12)	90(4)
C(43')	4362(13)	3303(16)	3882(11)	86(3)
C(44')	5424(8)	3001(8)	4009(6)	83(3)
O(6)	6469(11)	1513(10)	7260(5)	67(3)
C(45)	7247(11)	1484(17)	7746(7)	96(6)
C(46)	6769(9)	1453(7)	8278(5)	93(3)
C(47)	5829(6)	1815(6)	8223(3)	89(2)
C(48)	5632(12)	1909(18)	7618(6)	113(7)
O(6')	6544(11)	1787(10)	7312(5)	67(3)
C(45')	7177(11)	1182(16)	7658(7)	96(6)
C(46')	6745(9)	1015(7)	8196(5)	93(3)
C(47')	5717(6)	1215(6)	8145(3)	89(2)
C(48')	5538(11)	1571(18)	7598(6)	113(7)

REFERENCES AND NOTES

(1) Wilke, G.; Bogdanovic, B. *Angew. Chem.* **1961**, *73*, 756.

(2) Jolly, P. W.; Wilke, G. *The Organic Chemistry of Nickel*; Academic: New York, 1974; Vol. 1.

(3) Wilke, G.; Bogdanovic, B.; Hardt, P.; Heimbach, P.; Keim, W.; Kroner, M.; Oberkirch, W.; Tanaka, K.; Walter, D. *Angew. Chem., Int. Ed. Engl.* **1966**, *5*, 151-164.

(4) Walter, D.; Wilke, G. *Angew. Chem., Int. Ed. Engl.* **1966**, *5*, 897-8.

(5) Henc, B.; Jolly, P. W.; Salz, R.; Stobbe, S.; Wilke, G.; Benn, R.; Mynott, R.; Seevogel, K.; Goddard, R.; Krueger, C. *J. Organomet. Chem.* **1980**, *191*, 449-75.

(6) Jolly, P. W. In *Comprehensive Organometallic Chemistry*; Wilkinson, G., Stone, F. G. A., Abel, E., Eds.; Pergamon: Oxford, 1982; Vol. 6, p 145-182.

(7) Hegedus, L. S.; Varaprath, S. *Organometallics* **1982**, *1*, 259-63.

(8) Billington, D. C. *Chem. Soc. Rev.* **1985**, *14*, 93-120.

(9) Hegedus, L. S.; Thompson, D. H. P. *J. Am. Chem. Soc.* **1985**, *107*, 5663-9.

(10) Consiglio, G.; Waymouth, R. M. *Chem. Rev.* **1989**, *89*, 257-276.

(11) Wilke, G.; π-Allyl Transition Metal Adducts with Lewis Acids and/or Lewis Bases. U.S. Patent 3,468,921, Sept 23, 1969.

(12) Jolly, P. W.; Stobbe, S.; Wilke, G.; Goddard, R.; Krueger, C.; Sekutowski, J. C.; Tsay, Y. H. *Angew. Chem.* **1978**, *90*, 144-5.

(13) Corey, E. J.; Semmelhack, M. F. *J. Am. Chem. Soc.* **1967**, *89*, 2755-7.

(14) Boennemann, H.; Bogdanovic, B.; Wilke, G. *Angew. Chem., Int. Ed. Engl.* **1967**, *6*, 804.

(15) Decleva, P.; Fronzoni, G.; Lisini, A. *Chem. Phys.* **1989**, *134*, 307-15.

(16) Decleva, P.; Fronzoni, G.; Lisini, A. *Chem. Phys.* **1992**, *168*, 51-60.

(17) Casarin, M.; Pandolfo, L.; Vittadini, A. *Organometallics* **2001**, *20*, 754-762.

(18) Li, X.; Tse, J. S.; Bancroft, G. M.; Puddephatt, R. J.; Tan, K. H. *Organometallics* **1995**, *14*, 4513-20.

(19) Goddard, R.; Krueger, C.; Mark, F.; Stansfield, R.; Zhang, X. *Organometallics* **1985**, *4*, 285-90.

(20) Hitchcock, P. B.; Kerton, F. M.; Lawless, G. A. *J. Am. Chem. Soc.* **1998**, *120*, 10264-10265.

(21) Jutzi, P.; Holtmann, U.; Kanne, D.; Kruger, C.; Blom, R.; Gleiter, R.; Hylakryspin, I. *Chem. Ber.* **1989**, *122*, 1629-1639.

(22) Bandy, J. A.; Cloke, F. G. N.; Cooper, G.; Day, J. P.; Girling, R. B.; Graham, R. G.; Green, J. C.; Grinter, R.; Perutz, R. N. *J. Am. Chem. Soc.* **1988**, *110*, 5039-5050.

(23) Ray, B.; Neyroud, T. G.; Kapon, M.; Eichen, Y.; Eisen, M. S. *Organometallics* **2001**, *20*, 3044-3055.

(24) Carlson, C. N.; Smith, J. D.; Hanusa, T. P.; Brennessel, W. W.; Young, V. G., Jr. *J. Organomet. Chem.* **2003**, *683*, 191-199.

(25) Smith, J. D.; Hanusa, T. P.; Young, V. G., Jr. *J. Am. Chem. Soc.* **2001**, *123*, 6455-6456.

(26) Smith, J. D.; Quisenberry, K. T.; Hanusa, T. P.; Brennessel, W. W. *Acta Crystallogr., Sect. C.* **2004**, *60*, m507-m508.

(27) Kuehl, C. J.; Simpson, C. K.; John, K. D.; Sattelberger, A. P.; Carlson, C. N.; Hanusa, T. P. *J. Organomet. Chem.* **2003**, *683*, 149-154.

(28) Woodman, T. J.; Schormann, M.; Hughes, D. L.; Bochmann, M. *Organometallics* **2003**, *22*, 3028-3030.

(29) Carlson, C. N.; Hanusa, T. P.; Brennessel, W. W. *J. Am. Chem. Soc.* **2004**, *126*, 10550–10551.

(30) Batich, C. D. *J. Am. Chem. Soc.* **1976**, *98*, 7585-90.

(31) Tinyakova, E. I.; Alferov, A. V.; Golenko, T. G.; Dolgoplosk, B. A.; Oreshkin, I. A.; Sharaev, O. K.; Chernenko, G. N.; Yakovlev, V. A. *J. Polym. Sci., Polym. Symp.* **1967**, *16*, 2625-34.

(32) Alferov, A. V., Babitsky, B. D., Vydrina, T. K., Dolgoplosk, B. A., Kormer, V. A., Krol, V. A., Lobach, M. I., Mushina, E. A., Parfenova, G. A., Romanova, S. T., Sakharova, E. V., Tinyakova, E. I., Sharaev, O. K. Polymerizing Butadiene in the Presence of Reaction Products of π-Allylic Complexes of Transition Metal and Organic Electron Acceptors. U.S Patent 3,468,866, Sept 23, 1969.

(33) Kormer, V. A.; Churlyaeva, L. A.; Yufa, T. L. *Vysokomol. Soedin., Ser. B* **1970**, *12*, 483-4.

(34) Schott, A.; Schott, H.; Wilke, G.; Brandt, J.; Hoberg, H.; Hoffmann, E. G. *Liebigs Ann. Chem.* **1973**, 508-30.

(35) Hanusa, T. P.; Smith, J. D.; Carlson, C. N.; Young, V. G., Jr.; Brennessel, W. In *Abstracts of Papers, 224th ACS National Meeting, Boston, MA, United States, August 18-22, 2002*; Presented in part at the 224th Meeting of the American Chemical Society, Boston, MA, August, 2002; paper INOR-076.: Boston, MA, 2002, p INOR-076.

(36) Williams, R. A.; Tesh, K. F.; Hanusa, T. P. *J. Am. Chem. Soc.* **1991**, *113*, 4843-4851.

(37) Schwarzenbach, G.; Flaschka, H. *Complexometric Titrations*; 2nd. ed.; Methuen: London, 1969.

(38) Fraenkel, G.; Chow, A.; Winchester, W. R. *J. Am. Chem. Soc.* **1990**, *112*, 1382-1386.

(39) Perrin, D. D.; Armarego, W. L. F. *Purification of Laboratory Chemicals*; 3rd ed.; Pergamon: Oxford, 1988.

(40) Tolman, C. A. *J. Am. Chem. Soc.* **1970**, *92*, 2956.

(41) SHELXTL; 6.1 ed.; Bruker Analytical X-Ray Systems, Madison, WI.: 2000.

(42) Gaussian **2003**, Gaussian 03, Revision K.02, M. J. Frisch, G. W. Trucks, H. B. Schlegel, G. E. Scuseria, M. A. Robb, J. R. Cheeseman, J. A. Montgomery, Jr., T. Vreven, K. N. Kudin, J. C. Burant, J. M. Millam, S. S. Iyengar, J. Tomasi, V. Barone, B. Mennucci, M. Cossi, G. Scalmani, N. Rega, G. A. Petersson, H. Nakatsuji, M. Hada, M. Ehara, K. Toyota, R. Fukuda, J. Hasegawa, M. Ishida, T. Nakajima, Y. Honda, O. Kitao, H. Nakai, M. Klene, X. Li, J. E. Knox, H. P. Hratchian, J. B. Cross, C. Adamo, J. Jaramillo, R. Gomperts, R. E. Stratmann, O. Yazyev, A. J. Austin, R. Cammi, C. Pomelli, J. W. Ochterski, P. Y. Ayala, K. Morokuma, G. A. Voth, P. Salvador, J. J. Dannenberg, V. G. Zakrzewski, S. Dapprich, A. D. Daniels, M. C. Strain, O. Farkas, D. K. Malick, A. D. Rabuck, K. Raghavachari, J. B. Foresman, J. V. Ortiz, Q. Cui, A. G. Baboul, S. Clifford, J. Cioslowski, B. B. Stefanov, G. Liu, A. Liashenko, P. Piskorz, I. Komaromi, R. L. Martin, D. J. Fox, T. Keith, M. A. Al-Laham, C. Y. Peng, A. Nanayakkara, M. Challacombe, P. M. W. Gill, B. Johnson, W. Chen, M. W. Wong, C. Gonzalez, and J. A. Pople, Gaussian, Inc., Pittsburgh PA, 2003.

(43) Becke, A. D. *Phys. Rev. A* **1988**, *38*, 3098-3100.

(44) Lee, C.; Yang, W.; Parr, R. G. *Phys. Rev. B* **1988**, *37*, 785-789.

(45) Miehlich, B.; Savin, A.; Stoll, H.; Preuss, H. *Chem. Phys. Lett.* **1989**, *157*, 200-206.

(46) Becke, A. D. *J. Chem. Phys.* **1993**, *98*, 5648-5652.

(47) Godbout, N.; Salahub, D. R.; Andzelm, J.; Wimmers, E. *Can. J. Chem.* **1992**, *50*, 560-.

(48) Krishnan, R.; Binkley, J. S.; Seeger, R.; Pople, J. A. *J. Chem. Phys.* **1980**, *72*, 650-4.

(49) Crystals of $C_{18}H_{42}Si_4$ are monoclinic, space group C_2, with $a = 18.400(10)$ Å, $b = 6.521(4)$ Å, $c = 13.294(9)$ Å, $\beta = 125.879(11)°$, $V = 1292.4(14)$ Å3, $Z = 2$, and $\rho_{calc} = 0.953$ g cm^{-3} for fw = 370.88. Refinement of 1516 reflections collected at the University of Minnesota at 173±2 K led to residuals of $R(F^2) = 0.1158$ and $Rw(F^2) = 0.26044$ (for $I > 2.0\sigma(I)$).

(50) Quisenberry, K. T.; Hanusa, T. P. Unpublished NMR results.

(51) Curiously, in the substituted $(2\text{-}MeC_3H_4)_2Ni$, the eclipsed form predominates 2:1 at low (–75 °C) temperatures, but the staggered form is preferred over the eclipsed by 2.3:1 at room temperature.13.

(52) Davis, A. L.; Keeler, J.; Laue, E. D.; Moskau, D. *J. Magn. Reson.* **1992**, *98*, 207-16.

(53) Breen, T. L.; Stephan, D. W. *Organometallics* **1997**, *16*, 365-369.

(54) Steinicke, A.; Thiele, K. H.; Haaland, A.; Sokolov, V. I.; Volden, H. V. *Z. Anorg. Allg. Chem.* **1997**, *623*, 1925-1930.

(55) Baudler, M.; Hahn, J.; Clef, E. *Z. Naturforsch., B: Chem. Sci.* **1984**, *39B*, 438-444.

(56) Albrand, J. P.; Cogne, A.; Robert, J. B. *J. Am. Chem. Soc.* **1978**, *100*, 2600-4.

(57) Smith, L. R.; Mills, J. L. *J. Am. Chem. Soc.* **1976**, *98*, 3852-7.

(58) Jutzi, P.; Meyer, U. *J. Organomet. Chem.* **1987**, *333*, C18-C20.

(59) Schmitz, M.; Leininger, S.; Bergstrasser, U.; Regitz, M. *Heteroatom Chem.* **1998**, *9*, 453-460.

(60) Hersh, W. H. *J. Chem. Educ.* **1997**, *74*, 1485-1489.

(61) Musher, J. I.; Corey, E. J. *Tetrahedron* **1962**, *18*, 791-809.

(62) Avent, A. G.; Cloke, F. G. N.; Day, J. P.; Seddon, E. A.; Seddon, K. R.; Smedley, S. M. *J. Organomet. Chem.* **1988**, *341*, 535-41.

(63) Behringer, K. D.; Bluemel, J. *Mag. Res. Chem.* **1995**, *33*, 729-33.

(64) Stransky, N.; Herzschuh, R.; Gehrke, J. P.; Taube, R. *J. Organomet. Chem.* **1984**, *270*, 353-6.

(65) Greenwood, F. L.; Kellert, M. D. *Org. Synth. Coll. Vol.* **1963**, *4*, 108-110.

(66) Wells, A. F. *Structural Inorganic Chemistry*; 5th ed.; Clarendon: Oxford, 1984.

(67) Churchill, M. R.; O'Brien, T. A. *Inorg. Chem.* **1967**, *6*, 1386-90.

(68) Massa, W.; Faza, N.; Kang, H.-C.; Focke, C.; Heitz, W. *Acta Polym.* **1997**, *48*, 432-437.

(69) Johnson, J. R.; Tully, P. S.; Mackenzie, P. B.; Sabat, M. *J. Am. Chem. Soc.* **1991**, *113*, 6172-7.

(70) McMullen, A. K.; Tilley, T. D.; Rheingold, A. L.; Geib, S. J. *Inorg. Chem.* **1990**, *29*, 2228-32.

(71) Goddard, R.; Krueger, C.; Mynott, R.; Neumann, M.; Wilke, G. *J. Organomet. Chem.* **1993**, *454*, C20-C25.

(72) Krueger, C.; Sekutowski, J. C.; Berke, H.; Hoffmann, R. *Z. Naturforsch., B: Chem. Sci.* **1978**, *33B*, 1110-15.

(73) Lee, B. Y.; Kim, Y. H.; Shin, H. J.; Lee, C. H. *Organometallics* **2002**, *21*, 3481-3484.

(74) Hoberg, H.; Fananas, F. J.; Angermund, K.; Krueger, C.; Romao, M. J. *J. Organomet. Chem.* **1985**, *281*, 379-88.

(75) Tobisch, S.; Boegel, H. *Int. J. Quantum Chem.* **1995**, *56*, 575-87.

(76) Gugelchuk, M. M. *Theochem* **1995**, *357*, 263-73.

(77) Pauling, L. *The Nature of the Chemical Bond*; 3rd. ed.; Cornell University Press: Ithaca, 1960.

(78) Rohmer, M. M.; Demuynck, J.; Veillard, A. *Theor. Chim. Acta* **1974**, *36*, 93-102.

(79) Boche, G.; Fraenkel, G.; Cabral, J.; Harms, K.; Van Eikema Hommes, N. J. R.; Lohrenz, J.; Marsch, M.; Schleyer, P. v. R. *J. Am. Chem. Soc.* **1992**, *114*, 1562-5.

(80) Harvey, M. J.; Hanusa, T. P.; Young, V. G., Jr. *Angew. Chem. Int. Ed.* **1999**, *38*, 217-219.

(81) Chance, J. M.; Linebarrier, D. L.; Nile, T. A. *Transition Met. Chem. (London)* **1987**, *12*, 276-7.

(82) Wilke, G. *Angew. Chem., Int. Edit. Engl.* **1988**, *27*, 185-206.

(83) Franks, R. J.; Nicholas, K. M. *Organometallics* **2000**, *19*, 1458-1460.

(84) Sneeden, R. P. A.; Zeiss, H. H. *J. Organomet. Chem.* **1971**, *28*, 259-63.

(85) Karol, F. J.; Johnson, R. N. *J. Polym. Sci., Polym. Chem. Ed.* **1975**, *13*, 1607-17.

(86) Bade, O. M.; Blom, R.; Ystenes, M. *Organometallics* **1998**, *17*, 2524-2533.

(87) Woodman, T. J.; Sarazin, Y.; Garratt, S.; Fink, G.; Bochmann, M. *J. Mol. Catal. A: Chemical* **2005**, *235*, 88-97.

(88) Schormann, M.; Garratt, S.; Bochmann, M. *Organometallics* **2005**, *24*, 1718-1724.

(89) Wilke, G.; Catalysts for the Oligomerization and Polymerization of Olefins. German patent DE 19630810, February 8, 1965.

(90) Alberti, D.; Goddard, R.; Poerschke, K.-R. *Organometallics* **2005**, *24*, 3907-3915.

(91) Grosselin, J. M.; Dixneuf, P. H. *J. Organomet. Chem.* **1986**, *314*, C76-C80.

(92) Baker, R.; Copeland, A. H. *Tetrahedron Lett.* **1976**, 4535-8.

(93) Chatani, N.; Yamasaki, Y.; Murai, S.; Sonoda, N. *Tetrahedron Lett.* **1983**, *24*, 5649-52.

(94) Lautens, M.; Editor *Science of Synthesis, Volume 1, Houben-Weyl Methods of Molecular Transformations; Organometallics: Compounds with Transition Metal-Carbon p-Bonds and Compounds of Groups 10-8 (Ni, Pd, Pt, Co, Rh, Ir, Fe, Ru, Os)*, 2002.

(95) Abel, E. W.; Stone, F. G. A.; Wilkinson, G.; Editors *Comprehensive Organometallic Chemistry II: A Review of the Literature 1982-1994, 14 Volume Set*, 1995.

(96) Gabor, B.; Holle, S.; Jolly, P. W.; Mynott, R. *J. Organomet. Chem.* **1994**, *466*, 201-9.

(97) Crabtree, R. H. *The Organometallic Chemistry of the Transition Metals*; Second ed.; John Wiley & Sons: New York, 1994.

(98) Bitterwolf, T. E. *Inorg. Chem. Commun.* **2004**, *7*, 956-959.

(99) Loubser, C.; Roos, H. M.; Lotz, S. *J. Organomet. Chem.* **1991**, *402*, 393-412.

(100) Cann, K.; Riley, P. E.; Davis, R. E.; Pettit, R. *Inorganic Chemistry* **1978**, *17*, 1421-8.

(101) Nesmeyanov, A. N.; Ustynyuk, Y. A.; Kritskaya, I. I.; Shchembelov, G. A. *J. Organomet. Chem.* **1968**, *14*, 395-403.

(102) Nesmeyanov, A. N.; Kritskaya, I. I. *J. Organomet. Chem.* **1968**, *14*, 387-94.

(103) Wilke, G.; (Studiengesellschaft Kohle m.b.H.). NL, 1965, p 13 pp.

(104) Hanusa, T. P. *Organometallics* **2002**, *21*, 2559-2571.

(105) Jutzi, P.; Burford, N. *Chem. Rev.* **1999**, *99*, 969-990.

(106) Harvey, M. J.; Quisenberry, K. T.; Hanusa, T. P.; Young, V., G., Jr. *Eur. J. Inorg. Chem.* **2003**, 3383-3390.

(107) Grosselin, J. M.; Dixneuf, P. H. *J. Organomet. Chem.* **1986**, *314*, C76-C80.

(108) Quisenberry, K. T.; Smith, J. D.; Voehler, M.; Stec, D. F.; Hanusa, T. P.; Brennessel, W. W. *J. Am. Chem. Soc.* **2005**, *127*, 4376-4387.

(109) Kurras, E.; Klimsch, P. *Monatsh. Chem.* **1964**, *6*, 735-6.

(110) Evans, D. F. *J. Chem. Soc.* **1959**, 2003-2005.

(111) Schubert, E. M. *J. Chem. Educ.* **1992**, *69*, 62.

(112) Grant, D. H. *J. Chem. Educ.* **1995**, *72*, 39-40.

(113) Smith, J. D., Ph.D. Thesis, Vanderbilt University, 2002.

(114) Bertani, R.; Scrivanti, A.; Carturan, G. *Inorg. Chim. Acta* **1985**, *98*, L9-L10.

(115) Jolly, P. W. In *Comprehensive Organometallic Chemistry*; Wilkinson, G., Stone, F. G. A., Abel, E., Eds.; Pergamon: Oxford, 1982; Vol. 8, p Chapter 37.6.

(116) Boennemann, H.; Grard, C.; Kopp, W.; Pump, W.; Tanaka, K.; Wilke, G. *Angew. Chem.* **1973**, *85*, 1024-35.

(117) Hehre, W. J.; Yu, J.; Klunzinger, P. E.; Lou, L. *A Brief Guide to Molecular Mechanics and Quantum Chemical Calculations*; Wavefunction, Inc: Irvine, 1998.

(118) Elschenbroich, C.; Salzer, A. *Organometallics: A Concise Introduction*; 2nd ed.; VCH Publishers: New York, 1992.

(119) Simon, F. E.; Lauher, J. W. *Inorg. Chem.* **1980**, *19*, 2338-43.

(120) Wilke, G.; Cooligimerization of Diolefins. German Patent DE 19620326, March 26, 1962.

(121) Otsuka, S.; Taketomi, K. *Eur. Polym. J.* **1966**, *2*, 280-97.

(122) Tanaka, K. Japanese Patent 40015661, 1965; *Chem. Abstr.* 63:99682.

(123) Tanaka, K.; Uchiyama, M.; Takeshita, Y.; Japanese Patent 44021106, 1969; *Chem. Abstr.* 72:22449.

(124) Quisenberry, K. T.; Hanusa, T. P. Unpublished results.

(125) Andrews, D. C.; Davidson, G. *J. Chem. Soc., Dalton Trans.* **1972**, 1381-4.

(126) Leung, P. C.; Coppens, P. *Acta Crystallogr., Sect. B* **1983**, *B39*, 535-42.

(127) Albright, T. A.; Hofmann, P.; Hoffmann, R. *J. Am. Chem. Soc.* **1977**, *99*, 7546-57.

(128) Clarke, H. L. *J. Organomet. Chem.* **1974**, *80*, 155-73.

(129) Quisenberry, K. T.; Hanusa, T. P. In *Encyclopedia of Inorganic Chemistry* 2nd ed.; King, R. B. Ed. Wiley: Indianapolis, **2005**,. in press.

(130) Shannon, R. D. *Acta Crystallogr., Sect A.* **1976**, *32*, 751-767.

(131) Rakowski, M. C.; Hirsekorn, F. J.; Stuhl, L. S.; Muetterties, E. L. *Inorganic Chemistry* **1976**, *15*, 2379-82.

(132) Heck, R. F.; Breslow, D. S. *J. Am. Chem. Soc.* **1961**, *83*, 1097-102.

(133) In *Comprehensive Organometallic Chemistry* 1st ed.; Wilkinson, G., Stone, F. G. A., Abel, E. W., Eds.; Pergamon Press: New York, 1982; Vol. 5.

(134) Hanusa *Adv. Organomet. Chem.* **2001**, *40*, 215-340.

(135) Hanusa, T. P. In *Comprehensive Coordination Chemistry, 2nd ed.*; McCleverty, J. A., Meyer, T. B., Eds.; Elsevier: San Diego, CA, 2004; Vol. 3, p 1–92 .

(136) Wardell, J. L. *Organometallic Chemistry* **1985**, *13*, 1-11.

(137) Hays, M. L.; Hanusa, T. P. *Adv. Organomet. Chem.* **1996**, *40*, 117-170.

(138) Hanusa, T. P. *Coord. Chem. Rev.* **2000**, *210*, 329-367.

(139) Mösges, G.; Hampel, F.; Kaupp, M.; Schleyer, P. v. R. *J. Am. Chem. Soc.* **1992**, *114*, 10880-10889.

(140) Overby, J. S.; Hanusa, T. P. *Organometallics* **1996**, *15*, 2205-2212.

(141) Overby, J. S.; Hanusa, T. P. *Angew. Chem. Int. Ed. Engl.* **1994**, *33*, 2191-2193.

(142) Hunt, H. D.; Peterson, D. L.; Simpson, W. T. *J. Chem. Phys.* **1957**, *27*, 20-3.

(143) Chandrasekhar, J.; Andrade, J. G.; Schleyer, P. v. R. *J. Am. Chem. Soc.* **1981**, *103*, 5609-12.

(144) Yamamoto, Y.; Asao, N. *Chem. Rev.* **1993**, *93*, 2207-93.

(145) Schlosser, M. *Pure Appl. Chem.* **1988**, *60*, 1627-34.

(146) Biellmann, J. F.; Ducep, J. B. *Organic Reactions* **1982**, *27*, 1-344.

(147) Ioffe, S. T.; Nesmeyanov, A. *The Organic Compounds of Magnesium, Beryllium, Calcium, Strontium, and Barium*; North-Holland: Amsterdam, 1967.

(148) Gowenlock, B. G.; Lindsell, W. E. In *J. Organomet. Chem. Library, Organomet. Chem. Rev.*; Elsevier: Amsterdam, 1977; Vol. 3, p 1-.

(149) Maiwald, S.; Weissenborn, H.; Sommer, C.; Muller, G.; Taube, R. *J. Organomet. Chem.* **2001**, *640*, 1-9.

(150) Woodman, T. J.; Schormann, M.; Bochmann, M. *Organometallics* **2003**, *22*, 2938-2943.

(151) Simpson, C. K.; White, R. E.; Carlson, C. N.; Wrobleski, D. A.; Kuehl, C. J.; Croce, T. A.; Steele, I. M.; Scott, B. L.; Young, V. G., Jr.; Hanusa, T. P.; Sattelberger, A. P.; John, K. D. *Organometallics* **2005**, *24*, 3685-3691.

(152) Hitchcock, P. B.; Lappert, M. F.; Leung, W.-P.; Liu, D.-S.; Mak, T. C. W.; Wang, Z.-X. *J. Chem. Soc., Dalton Trans.* **1999**, 1257-1262.

(153) Hitchcock, P. B.; Lappert, M. F.; Wang, Z.-X. *Chem. Commun.* **1996**, 1647-1648.

(154) Schuemann, U.; Weiss, E.; Dietrich, H.; Mahdi, W. *J. Organomet. Chem.* **1987**, *322*, 299-307.

(155) Praesang, C.; Sahin, Y.; Hofmann, M.; Geiseler, G.; Massa, W.; Berndt, A. *Eur. J. Inorg.c Chem.* **2004**, 3063-3073.

(156) Marr, F.; Frohlich, R.; Hoppe, D. *Tetrahedron: Asymmetry* **2002**, *13*, 2587-2592.

(157) Harder, S. *Angew. Chem., Int. Ed.* **2004**, *43*, 2714-2718.

(158) Harder, S.; Feil, F. *Organometallics* **2002**, *21*, 2268-2274.

(159) Harder, S.; Feil, F. *Polymeric Materials Science and Engineering* **2002**, *87*, 53.

(160) Yanagisawa, A.; Habaue, S.; Yamamoto, H. *J. Am. Chem. Soc.* **1991**, *113*, 8955-8956.

(161) Yanagisawa, A.; Habaue, S.; Yasue, K.; Yamamoto, H. *J. Am. Chem. Soc.* **1994**, *116*, 6130-6141.

(162) Harvey, M. J.; Hanusa, T. P. *Organometallics* **2000**, *19*, 1556-1566.

(163) Burkey, D. J.; Alexander, E. K.; Hanusa, T. P. *Organometallics* **1994**, *13*, 2773-2786.

(164) Sitzmann, H.; Weber, F.; Walter, M. D.; Wolmershaeuser, G. *Organometallics* **2003**, *22*, 1931-1936.

(165) Tang, Y.; Zakharov, L. N.; Rheingold, A. L.; Kemp, R. A. *Organometallics* **2005**, *24*, 836-841.

(166) Strauch, J. W.; Faure, J.-L.; Bredeau, S.; Wang, C.; Kehr, G.; Froehlich, R.; Luftmann, H.; Erker, G. *J. Am. Chem. Soc.* **2004**, *126*, 2089-2104.

(167) Kuehl, C. J.; Simpson, C. K.; John, K. D.; Sattelberger, A. P.; Carlson, C. N.; Hanusa, T. P. *J. Organomet. Chem.* **2003**, *683*, 149-154.

(168) Woodman, T. J.; Schormann, M.; Hughes, D. L.; Bochmann, M. *Organometallics* **2004**, *23*, 2972-2979.

(169) Carlson, C. N.; Hanusa, T. P.; Brennessel, W. W. *J. Am. Chem. Soc.* **2004**, *126*, 10550-10551.

(170) Koester, H.; Weiss, E. *Chem. Ber.* **1982**, *115*, 3422-6.

(171) Boche, G.; Marsch, M.; Massa, W.; Baum, G.; Klebe, G.; Boehn, K. H.; Harms, K.; Sheldrick, G. M. *Stud. Org. Chem. (Amsterdam)* **1986**.

(172) Gren, C. Unpublished Results.

(173) Gibb, T. R. P., Jr.; Schumacher, D. P. *J. Phys. Chem.* **1960**, *64*, 1407-10.

(174) Raymond, K. N.; Eigenbrot, C. W. *Acc. Chem. Res.* **1980**, *13*, 276-283.

(175) Sockwell, S. C.; Hanusa, T. P. *Inorg. Chem.* **1990**, *29*, 76-80.

(176) Harder, S.; Prosenc, M. H. *Angew. Chem. Int. Ed. Engl.* **1996**, *35*, 97-99.

(177) Pauer, F.; Stalke, D. *J. Organomet. Chem.* **1991**, *418*, 127-45.

(178) Englich, U.; Hassler, K.; Ruhlandt-Senge, K.; Uhlig, F. *Inorganic Chemistry* **1998**, *37*, 3532-3537.

(179) Pauls, J.; Neumuller, B. *Z. Anorg. Allg. Chem.* **2001**, *627*, 2127-2132.

(180) Hommes, N. v. E.; Bühl, M.; Schleyer, P. v. R.; Wu, Y.-D. *J. Organomet. Chem.* **1991**, *409*, 307-320.

(181) Stout, G. H.; Jensen, L. H. *X-ray Structure Determination: A Practical Guide*; 2nd ed.; John Wiley & Sons: New York, 1989.

(182) Quisenberry, K. T. Unpublished Results.

(183) Harvey, M. J.; Hanusa, T. P.; Pink, M. *J. Chem. Soc., Dalton Trans.* **2001**, 1128-1130.

(184) Jutzi, P.; Leffers, W.; Hampel, B.; Pohl, S.; Saak, W. *Angew. Chem.* **1987**, *99*, 563-4.

(185) Williams, R. A.; Hanusa, T. P.; Huffman, J. C. *Organometallics* **1990**, *9*, 1128-1134.

(186) Burkey, D. J.; Hanusa, T. P. *Acta Crystallogr., Sect. C* **1996**, *52*, 2452-2454.

(187) Weber, F.; Sitzmann, H.; Schultz, M.; Sofield, C. D.; Andersen, R. A. *Organometallics* **2002**, *21*, 3139-3146.

(188) Lauher, J. W.; Hoffmann, R. *J. Am. Chem. Soc.* **1976**, *98*, 1729-1742.

(189) Kane, K. M.; Shapiro, P. J.; Vij, A.; Cubbon, R.; Rheingold, A. L. *Organometallics* **1997**, *21*, 4567-4571.

(190) Erker, G.; Kehr, G.; Frohlich, R. *J. Organomet. Chem.* **2004**, *689*, 1402-1412.

(191) Schweier, G.; Brintzinger, H.-H. *Macromol. Symp.* **2001**, *173*, 89-103.

(192) Brintzinger, H.-H.; Fischer, D.; Mülhaupt, R.; Rieger, B.; Waymouth, R. M. *Angew. Chem., Int. Ed. Engl.* **1995**, *34*, 1143-1170.

(193) Resconi, L.; Cavallo, L.; Fait, A.; Piemontesi, F. *Chem. Rev.* **2000**, *100*, 1253-1345.

(194) Iwama, N.; Osano, Y. T. *Organometallics* **2005**, *24*, 132-135.

(195) Spaleck, W.; Kueber, F.; Winter, A.; Rohrmann, J.; Bachmann, B.; Antberg, M.; Dolle, V.; Paulus, E. F. *Organometallics* **1994**, *13*, 954-63.

(196) Ewen, J. A.; Elder, M. J. *Makromol. Chem., Macromol. Symp.* **1993**, *66*, 179-190.

(197) Schwemlein, H.; Brintzinger, H. H. *J. Organomet. Chem.* **1983**, *254*, 69-73.

(198) Shapiro, P. J.; Kane, K. M.; Vij, A.; Stelck, D.; Matare, G. J.; Hubbard, R. L.; Caron, B. *Organometallics* **1999**, *18*, 3468-3473.

(199) Eisch, J. J.; Shi, X.; Owuor, F. A. *Organometallics* **1998**, *17*, 5219-5221.

(200) Rinehart, K. L., Jr.; Frerichs, A. K.; Kittle, P. A.; Westman, L. F.; Gustafson, D. H.; Pruett, R. L.; McMahon, J. E. *J. Am. Chem. Soc.* **1960**, *82*, 4111-12.

(201) Rieckhoff, M.; Pieper, U.; Stalke, D.; Edelmann, F. T. *Angew. Chem., Int. Ed. Engl.* **1993**, *32*, 1079-1081.

(202) Sinnema, P.-J.; Shapiro, P. J.; Hohn, B.; Twamley, B. *J. Organomet. Chem.* **2003**, *676*, 73-79.

(203) Fedushkin, I. L.; Dechert, S.; Schumann, H. *Angew. Chem., Int. Ed.* **2001**, *40*, 561-563.

(204) Fedushkin, I. L.; Petrovskaya, T. V.; Bochkarev, M. N.; Dechert, S.; Schumann, H. *Angew. Chem. Int. Ed.* **2001**, *40*, 2474-2477.

(205) Waltman, R. J.; Bargon, J. *Magnetic Resonance in Chemistry* **1995**, *33*, 679-85.

(206) Koller, J.; Baumer, U.; Kaup, Y.; Schmid, M.; Weser, U. *Z. Naturforsc., B: Chem. Sci.* **2003**, *58*, 462-480.

(207) Salter, C.; Foresman, J. B. *J. Chem. Educ.* **1998**, *75*, 1341-1345.

(208) Bachmann, R.; Burda, C.; Gerson, F.; Scholz, M.; Hansen, H.-J. *Helv. Chim. Acta* **1994**, *77*, 1458-65.

(209) Pariser, R. *J. Chem. Phys.* **1956**, *25*, 1112-16.

(210) Kozlowski, P. M.; Rauhut, G.; Pulay, P. *J. Chem. Phys.* **1995**, *103*, 5650-62.

(211) Churchill, M. R.; Wormald, J. *Chem. Commun.* **1968**, 1033-4.

(212) Churchill, M. R.; Wormald, J. *Inorg. Chem.* **1969**, *8*, 716-24.

(213) Fischer, E. O.; Mueller, J. *J. Organomet. Chem.* **1964**, *1*, 464.

(214) Burger, P.; Hund, H. U.; Evertz, K.; Brintzinger, H. H. *J. Organomet. Chem.* **1989**, *378*, 153-61.

(215) Iwama, N.; Uchino, H.; Osano, Y. T.; Sugano, T. *Organometallics* **2004**, *23*, 3267-3269.

(216) Fedushkin, I. L.; Kurskii, Y. A.; Balashova, T. V.; Bochkarev, M. N.; Dechert, S.; Muehle, S.; Schumann, H. *Russ. Chem. Bull.* **2003**, *52*, 1363-1371.

(217) Rieke, R. D.; Hudnall, P. M. *J. Am. Chem. Soc.* **1972**, *94*, 7178-7179.

(218) McCormick, M. J.; Moon, K. B.; Jones, S. R.; Hanusa, T. P. *J. Chem. Soc., Chem. Commun.* **1990**, 778-779.

(219) Schafer, A.; Huber, C.; Ahlrichs, R. *J. Chem. Phys.* **1994**, *100*, 5829-5835.

(220) Park, M. J.; Lee, S. J.; Park, M. K.; Han, B. H. *Bull. Korean Chem. Soc.* **2000**, *21*, 336-338.

(221) Rieke, R. D.; Chao, L.-C. *Synthesis and Reactivity in Inorganic and Metal-Organic Chemistry* **1974**, *4*, 101-5.

(222) Rieke, R. D.; Uhm, S. J.; Hudnall, P. M. *J. of the Chem. Soc., Chem. Commun.* **1973**, 269-70.

(223) Rieke, R. D.; Burns, T. P.; Wehmeyer, R. M.; Kahn, B. E. *ACS Symp. Ser.* **1987**, *333*, 223-245.

(224) McCormick, M. J.; Williams, R. A.; Levine, L. J.; Hanusa, T. P. *Polyhedron* **1988**, *7*, 725-730.

(225) Stalke, D. *Angew. Chem , Int. Ed. Engl.*, **1994**, *33*, 2168-2171.

(226) Evans, W. J.; Hughes, L. A.; Hanusa, T. P.; Doedens, R. J. *Organometallics* **1986**, *5*, 1285-1291.

(227) Kaupp, M. *Angew. Chem. Int. Ed.* **2001**, *40*, 3535-3565.

(228) Kaupp, M.; Schleyer, P. v. R.; Dolg, M.; Stoll, H. *J. Am. Chem. Soc.* **1992**, *114*, 8202-8208.

(229) Hollis, T. K.; Burdett, J. K.; Bosnich, B. *Organometallics* **1993**, *12*, 3385-3386.

(230) Burkey, D. J.; Hanusa, T. P. *Comments Inorg. Chem.* **1995**, *17*, 41-77.

(231) Andersen, R. A.; Boncella, J. M.; Burns, C. J.; Blom, R.; Haaland, A.; Volden, H. V. *J. Organomet. Chem.* **1986**, *312*, C49-C52.

(232) Andersen, R. A.; Blom, R.; Burns, C. J.; Volden, H. V. *J. Chem. Soc., Chem. Commun.* **1987**, 768-769.

(233) Bünder, W.; Weiss, E. *J. Organomet. Chem.* **1975**, *92*, 1-6.

(234) Vollet, J.; Baum, E.; Schnoeckel, H. *Organometallics* **2003**, *22*, 2525-2527.

(235) Gardiner, M. G.; Raston, C. L.; Kennard, C. H. L. *Organometallics* **1991**, *10*, 3680-3686.

(236) Westerhausen, M.; Makropoulos, N.; Wieneke, B.; Karaghiosoff, K.; Noeth, H.; Schwenk-Kircher, H.; Knizek, J.; Seifert, T. *Eur. J. Inorg. Chem.* **1998**, 965-971.

(237) Schumann, H.; Gottfriedsen, J.; Glanz, M.; Dechert, S.; Demtschuk, J. *J. Organomet. Chem.* **2001**, *617-618*, 588-600.

(238) Morley, C. P.; Jutzi, P.; Krüger, C.; Wallis, J. M. *Organometallics* **1987**, *6*, 1084-1090.

(239) Schmidbaur, H. *Gmelin Handbook of Inorganic Chemistry*; 8 ed.; Springer: Berlin, 1987.

(240) Wong, C.-H.; Wang, S.-M. *Inorg. Nucl. Chem. Lett.* **1975**, *11*, 677-678.

(241) Pratten, S. J.; Cooper, M. K.; Aroney, M. J. *J. Organomet. Chem.* **1990**, *381*, 147-153.

(242) Del Mar Conejo, M.; Fernandez, R.; Gutierrez-Puebla, E.; Monge, A.; Ruiz, C.; Carmona, E. *Angew. Chem., Int. Ed.* **2000**, *39*, 1949-1951.

(243) Fischer, E. O.; Hofmann, H. P. *Chem. Ber.* **1959**, *92*, 482-486.

(244) Wong, C.-H.; Lee, T.-Y.; Chao, K.-J.; Lee, S. *Acta Crystallogr., Sect. B* **1972**, B*28*, 1662-1665.

(245) Wong, C.; Lee, T. Y.; Lee, T. J.; Chang, T. W.; Liu, C. S. *Inorg. Nucl. Chem. Lett.* **1973**, *9*, 667-673.

(246) Nugent, K. W.; Beattie, J. K.; Hambley, T. W.; Snow, M. R. *Aust. J. Chem.* **1984**, *37*, 1601-1606.

(247) Margl, P.; Schwarz, K.; Blochl, P. E. *J. Chem. Phys.* **1995**, *103*, 683-690.

(248) Rayon, V. M.; Frenking, G. *Chem–Eur. J.* **2002**, *8*, 4693-4707.

(249) del Mar Conejo, M.; Fernandez, R.; del Rio, D.; Carmona, E.; Monge, A.; Ruiz, C.; Marquez, A. M.; Sanz, F. J. *Chem–Eur. J.* **2003**, *9*, 4452-4461.

(250) del Mar Conejo, M.; Fernandez, R.; Carmona, E.; Andersen, R. A.; Gutierrez-Puebla, E.; Monge, M. A. *Chem–Eur. J.* **2003**, *9*, 4462-4471.

(251) Hanusa, T. P. *Chem. Rev.* **1993**, *93*, 1023-1036.

(252) Dapprich, S.; Komaromi, I.; Byun, K. S.; Morokuma, K.; Frisch, M. J. *J. Molec. Struct.-THEOCHEM* **1999**, *462*, 1-21.

(253) Perdew, J. P.; Wang, Y. *Phys. Rev. B* **1992**, *45*, 13244-13249.

(254) Ziegler, T. *Chem. Rev.* **1991**, *91*, 651-667.

(255) Smith, J. D.; Hanusa, T. P. *Organometallics* **2001**, *20*, 3056-3062.

(256) Sitzmann, H.; Dezember, T.; Ruck, M. *Angew. Chem. Int. Ed.* **1998**, *37*, 3114-3115.

(257) Harder, S.; Lutz, M.; Straub, A. W. G. *Organometallics* **1997**, *16*, 107-113.

(258) Burns, C. J.; Andersen, R. A. *J. Organomet. Chem.* **1987**, *325*, 31-37.